



João Miguel Ribeiro Avó

Mestre em Bioorgânica

Photochemical Control of Rheology

Dissertação para obtenção do Grau de Doutor em
Química

Orientador: Professor Doutor A. Jorge Parola, Professor
Associado, FCT-UNL

Co-orientador: Professor Doutor João C. Lima, Professor
Associado, FCT-UNL

Júri:

Presidente: Professora Doutora Maria Luísa Dias de Carvalho de Sousa Leonardo

Arguentes: Professor Doutor Francisco Galindo Honrubia
Doutor Carlos Miguel Calisto Baleizão

Vogais: Professor Doutor Carlos Alberto Mateus Afonso
Professora Doutora Paula Cristina de Sérgio Branco



Novembro de 2014

João Miguel Ribeiro Avó

Mestre em Bioorgânica

Photochemical Control of Rheology

Dissertação para obtenção do Grau de Doutor em
Química

Supervisor: Professor Doutor A. Jorge Parola, Professor
Associado, FCT-UNL

Co-supervisor: Professor Doutor João C. Lima, Professor
Associado, FCT-UNL

“The respect of those you respect is worth more than the applause of the multitude.”

— *Arnold Glasow*

Copyright

A Faculdade de Ciências e Tecnologia e a Universidade Nova de Lisboa têm o direito, perpétuo e sem limites geográficos, de arquivar e publicar esta dissertação através de exemplares impressos reproduzidos em papel ou de forma digital, ou por qualquer outro meio conhecido ou que venha a ser inventado, e de divulgar através de repositórios científicos e de admitir a sua cópia e distribuição com objectivos educacionais ou de investigação, não comerciais, desde que seja dado crédito ao autor e editor.

Agradecimentos

E eis que chega ao fim esta jornada. Talvez mais do que o conhecimento adquirido durante estes 4+ anos, fica toda uma evolução psicológica que resulta do aglomerado de sucessos e fracassos, da montanha russa emocional que acompanha um doutoramento. Assim, quero agradecer a todos os que me acompanharam neste pedaço de vida.

Em primeiro lugar os meus orientadores. Ao Jorge Parola pela confiança que depositou em mim e que me permitiu realizar uma investigação que me interessava, e que me obrigou a ir mais além para resolver os inúmeros problemas que surgiram. Ao João Lima, que com o seu sempre presente “tough-love” me proporcionou momentos de extrema miséria intelectual, mas que foram essenciais para aperfeiçoar o meu espírito crítico e pensar mais além, características essenciais de um bom cientista.

A todo o grupo de fotoquímica, por terem criado um bom (ainda que por vezes demasiado barulhento) ambiente de trabalho, tão necessário para manter a criatividade. Em especial ao Artur e à Ana Marta, que para além das discussões científicas, me deram um importante apoio nos maus momentos.

À minha família, pelo apoio que me deram “fora das 4 linhas”. Ao meu Pai, que sempre foi o meu porto seguro e me deu segurança para chegar até aqui e à Linda por toda a paciência para nos aturar. À minha Mãe, que me fez ser como sou hoje e que estou certo que ficaria orgulhosa por ter chegado até aqui.

E por fim, à Carina, o meu tudo. Foste a minha âncora emocional e sem ti teria certamente desistido disto a dada altura. Obrigado por toda a confiança que tiveste em mim mesmo quando eu já não tinha. Obrigado por tudo.

Resumo

O trabalho de investigação elaborado no âmbito desta tese de Doutoramento teve como objectivo a preparação de novos fluídos fotorreológicos. Para isso, foram seguidas duas estratégias distintas. A primeira baseou-se na síntese de compostos tripodais funcionalizados com unidades fotodimerizáveis derivadas de ácido cinâmico, coumarina e antraceno. Foram sintetizados dois conjuntos de compostos variando as unidades centrais bem como os espaçadores, obtendo-se moléculas de diferente peso molecular e solubilidade. Os compostos sintetizados foram caracterizados quanto às suas propriedades fotoquímicas e todos exibiram reactividade quando irradiados com luz ultravioleta. Em particular, ambos os compostos derivados de coumarina apresentaram a maior reactividade quanto à fotopolimerização, resultando na formação de nanopartículas dendriméricas ou no aumento da viscosidade de soluções orgânicas. A segunda estratégia focou-se no desenho cuidadoso de líquidos iónicos fotossensíveis, baseado em resultados de diversos estudos quantitativos de relação estrutura-propriedade. Desta forma, foram sintetizados líquidos iónicos com catiões funcionalizados com unidades de ácido cinâmico ou coumarina. Aquando da sua irradiação, todos os compostos apresentaram reactividade, resultando na alteração das suas propriedades físicas, tais como o ponto de fusão ou viscosidade. Para além disso, foram desenvolvidos novos derivados de coumarina com diferentes propriedades fotofísicas e fotoquímicas com possível aplicação na síntese de novos líquidos iónicos fotossensíveis.

Palavras-Chave: *Fotoquímica, Fotopolimerização, Fotorreologia, Líquidos Iónicos, Coumarinas*

Abstract

The main objective of the research work developed in the framework of this PhD thesis was the preparation and development of novel photorheological fluids. This was pursued following two distinct strategies. The first one focused on the synthesis of tripodal compounds functionalized with photodimerizable moieties of cinnamic acid, coumarin and anthracene. Two sets of compounds were prepared, varying the central unit as well as spacers resulting in molecules with different solubilities and molecular weight. All compounds were characterized towards their photochemical properties and all exhibited photoreactivity upon irradiation with ultra-violet light. In particular, both coumarin derivatives exhibited the greatest photopolymerization reactivity, resulting in the formation of dendrimeric nanoparticles or in the increase of viscosity of organic solutions. The second strategy was focused on the careful design of photosensitive ionic liquids, based on the results of several quantitative structure-property relationship studies. Thus, photosensitive ionic liquids were synthesized bearing cinnamic acid or coumarin moieties in the organic cation. Upon irradiation, all compounds exhibited reactivity, which resulted in changes in their physical properties, such as melting point or viscosity. In addition, novel coumarin chromophores with different photophysical and photochemical properties were developed. It is expected that these compounds may find application in the preparation of new photosensitive ionic liquids.

Keywords: *Photochemistry, Photopolymerization, Photorheology, Ionic Liquids, Coumarins*

Contents

I.	Introduction	3
	Stimuli-responsive materials	3
	Stimuli-responsive rheological fluids.....	4
	Photorheological fluids.....	6
	Thesis Overview.....	17
II.	Photopolymerizable compounds for photochemical control of rheology.....	21
	II.1 – Low molecular-weight photopolymerizable molecules.....	23
	Conclusions	33
	II.2 – High-molecular weight photopolymerizable compounds.....	34
	Conclusions	48
III.	Photoactive ionic liquids	53
	III.1 – Introduction	53
	Ionic liquids in smart material systems	54
	Viscosity of ionic liquids.....	60
	III.2 – Cinnamic acid based ionic liquids.....	62
	III.3 – Coumarin based ionic liquids	80
	III.3.1 – Novel coumarin chromophores for the preparation of photoresponsive ionic liquids	91
	III.4 – Conclusions	104
IV.	Conclusions and Future Perspectives	105
V.	Experimental Part.....	106
	Synthesis.....	107
	Procedures	107
	Photochemistry.....	122
	Dynamic Light Scattering	123
	Atomic Force Microscopy.....	123
	Viscometry	123
	Photophysics.....	123

Computational calculations	124
VI. References	125

Figure index

Figure I.1 – Schematic representation of suspended particle alignment induced by an electric or magnetic field (adapted from [5])	5
Figure I.2 – Microscopic photographs of paraffin-based ER fluid before (left) and after (right) application of an electric field (adapted from [13]).....	6
Figure I.3 – Schematic representation of different micellar aggregate morphology upon increase in concentration.	8
Figure I.4 – Schematic representation of different effective head group sizes of anionic surfactant and corresponding micellar aggregation morphologies (adapted from [29]).....	9
Figure I.5 – Schematic representation of isomerization induced changes in aggregation behaviour of azobenzene-based cationic surfactant micelles (adapted from [42]).....	11
Figure I.6 – Light-induced gelation of aqueous laponite suspensions: initially (left) particles are stabilized by pluronic surfactant and unconnect; upon UV irradiation (right), the particles assemble into a network, causing the fluid to turn into a gel (adapted from [])	12
Figure I.7 – Schematic representation of branched PEG polymer modified with 9-anthracene carboxylic acid used in the formulation of a PR fluid (adapted from [62]).	13
Figure I.8 – Schematic representation of light-induced crosslinking between polymer chains due to anthracene dimerization used in the photochemical controlled release of bioactive molecules (adapted from [66]).....	14
Figure I.9 – Schematic representation of light-induced crosslinking between polymer chains due to coumarin dimerization used in the photochemical control of fluid viscosity (adapted from [68]).	15
Figure I.10 – (a) Schematic representation of the photoresponse of cinnamate monomer 11 and dimer 12; (b) Photographic images representing the photorheological effect of acetone solutions of 11 (adapted from [76]).	16
Figure II.1 – Schematic representation of photocontrolled reversible polymerization of tripodal molecules bearing photosensitive moieties.	21
Figure II. 2 – Representation of orbital symmetry of frontier orbitals of generic alkene (left) and symmetry forbidden orbital interaction in a thermal [2+2] cycloaddition (right)	22
Figure II. 3 – Frontier orbitals of generic alkene in the excited state (left) and symmetry allowed orbital interactions in a photochemical induced [2+2]-cycloaddition (right).....	22
Figure II. 4 – Symmetry allowed frontier orbital interactions between one coumarin molecule in the ground state and one molecule in the excited state	23
Figure II.5 – Molecular structure of tris(2-aminoethyl)amine 13	23

Figure II.6 – (a) UV-Vis spectral modifications of 1.1×10^{-5} M 16 in chloroform upon irradiation at 300 nm. Total irradiation time is 20 min; (b) Photochemical quantum yield dependence on concentration of 16.....	25
Figure II. 7 – ^1H NMR spectra of 16 in chloroform acquired before and after irradiation at 300 nm. .	26
Figure II. 8 – (a) UV-Vis spectral modifications of chloroform solution of 22 at 1.0×10^{-5} M upon irradiation at 330 nm. Total irradiation time is 60 min; (b) Photochemical quantum yield variation with increasing concentration of 22; (c) Precipitation-induced UV-Vis spectral modifications of a 2.0×10^{-3} M solution of 22 in chloroform upon irradiation at 330 nm. Total irradiation time is 40 min.....	29
Figure II. 9 – ^1H NMR spectra of 22 acquired before and after irradiation at 330 nm in chloroform. .	30
Figure II. 10 – (a) Correlation curve variation upon irradiation at 330 nm of a solution of 22 at 8.3×10^{-3} M in chloroform; (b) Time and concentration dependence of photoinduced growth of dendrimeric nanoparticles of 22 in chloroform; (c) and (d) AFM images of a suspension of dendrimeric nanoparticles of 22 obtained after 10 and 400 minutes of irradiation at 330 nm, respectively.....	32
Figure II. 11 – Schematic representation of the proposed photoinduced dendrimeric growth of nanoparticles of 22 due to dimerization of coumarin moieties.	32
Figure II.12 – Molecular structures of backbones used for the preparation of photopolymerizable tripodal compounds: tris(2-aminoethyl)amine and tris(tetraethyleneglycol)phloroglucinol 23.....	35
Figure II. 13 – (a) UV-Vis spectral modification of a solution of 1.4×10^{-5} M 31 in chloroform upon irradiation at 300 nm. Total irradiation time is 20 min; (b) Photochemical quantum yield dependence on concentration of 31.....	37
Figure II. 14 – ^1H NMR spectra of 31 in chloroform before and after irradiation at 300 nm.	37
Figure II. 15 – (a) UV-Vis spectral modification of a chloroform deaerated solution of 36 at 3.0×10^{-5} M upon irradiation at 360 nm. Total irradiation time is 10 min; (b) Photochemical quantum yield dependence on the concentration of 39	39
Figure II. 16 – ^1H NMR spectra of 36 in chloroform obtained before and after irradiation at 360nm. Total irradiation time is 60 min.....	40
Figure II. 17 – Viscosity of binary mixtures of water and acetonitrile at different ratios, determined by direct measurement with conventional viscometer (black dots) and calculated indirectly from DLS data (red dots).....	41
Figure II.18 - (a) UV-Vis spectral modification of a solution of 39 at 1.1×10^{-5} M in chloroform upon irradiation at 320 nm. Total irradiation time is 60 min; (b) Photochemical quantum yield dependence on concentration of 39.....	43
Figure II. 19 – ^1H NMR spectra of 39 in chloroform obtained before and after irradiation.	44
Figure II. 20 – Representation of the three main rheological behaviors exhibited by fluids	45
Figure II. 21 – Schematic representation of the typical components of a rotational rheometer.....	46
Figure II. 22 – Viscosity curve of a DMF solution of 39 at 10% (w/v) before (black dots) and after (red dots) irradiation at 320 nm. Total irradiation time is 120 min.	47

Figure III.1 - Molecular structure of the first synthesized ionic liquids; a) ethanolammonium nitrate 40; b) ethylammonium nitrate 41	53
Figure III. 2 - Representative ionic liquid components	54
Figure III. 3 - Molecular structure of ionic liquids used as electrolytes; (a) methylpropylpyrrolidinium bis(trifluoromethyl-sulfonyl)imide 42; (b) polymerizable 2-(dimethylethylamino)ethylmethacrylate bromide 43.....	55
Figure III. 4 – Ionogel based wearable pH sensor for the analysis of human sweat [141].....	56
Figure III. 5 – Reversible color switching between three oxidation states of pure ethylmethylimidazolium vanadium (V) oxide IL upon electrolysis (adapted from [146])	57
Figure III. 6 – Increased selectivity of methylred based IL over conventional sodium salt from pH 1 to 7 (adapted from [147])	57
Figure III. 7 – Molecular structures of azobenzene based photochromic ionic liquids (from [148] and [149]).....	58
Figure III. 8 – Cinnamate-based photoresponsive ionic liquids (from [154]).....	59
Figure III. 9 – Effect of cation alkyl chain length and counterion on hexafluorophosphate (red dots) and bis(trifluoromethyl-sulfonyl)imide (black dots) alkylmethylimidazolium ILs (from [161]).....	61
Figure III. 10 - Crystal structures of the compounds 5a (top) and 5b (bottom), showing the label scheme for all non-H-atoms which are represented as thermal ellipsoids drawn at the 50% probability	66
Figure III. 11 - Representation of the diverse C–H•••O (yellow dashed lines), C–H•••N (blue dashed lines) and C–H•••F (green dashed lines) weak hydrogen bonds found in the crystal structures of the compounds 55 and 58: (a) highlight of the interactions between adjacent cationic and anionic species in 55; (b) crystal packing of 55 viewed in the [1 0 0] direction of the unit cell; (c) crystal packing of 58 viewed in the [1 0 0] direction of the unit cell	67
Figure III. 12 - Spectral modifications of 55 at 5.4×10^{-5} M in acetonitrile upon irradiation at 300 nm (a) and 240 nm (b). Under the used experimental setup, PSS was reached after 10 min irradiation at 300 nm while the recovery by irradiating at 240 nm required ca. 600 min.....	69
Figure III. 13 – ^1H NMR spectrum of irradiated solution of ionic liquid 55 at the photostationary state	69
Figure III. 14 - ^1H NMR spectrum of irradiated solution of ionic liquid 58 at the photostationary state	69
Figure III. 15 - ^1H NMR spectrum of a solution of ionic liquid 55 after irradiation at 240 nm (55_{rec}). 70	70
Figure III. 16 – DSC thermograms of ionic liquids 55 (a) and 58 (b) before irradiation (i), at the PSS (PSS) and after photochemical recovery (rec).....	70
Figure III. 17 – ^1H NMR spectrum of 55 in chloroform after irradiation at 300 nm in neat conditions. Total irradiation time is 120 min.	71

Figure III. 18 - ^1H NMR spectrum of 55 in chloroform after irradiation at 300 nm in neat conditions under inert atmosphere. Total irradiation time is 120 min.	72
Figure III. 19 - Isomer fraction dependency of melting temperature depression of irradiated neat samples (black dots) and acetonitrile solution (red dot) of 55.	73
Figure III. 20 - Spectral modifications of 60 at 1.2×10^{-5} M in acetonitrile upon irradiation at 300 nm (a) and 240 nm (b). Under the used experimental setup, PSS was reached after 15 min irradiation at 300 nm while the recovery by irradiating at 240 nm required ca. 600 min.....	75
Figure III. 21 – ^1H NMR spectrum of 60 irradiated in chloroform at 300 nm. Total irradiation time is 120 min.....	75
Figure III. 22 – ^1H NMR spectrum of 60 in chloroform after irradiated at 300 nm in neat conditions. Total irradiation time is 120 min.	76
Figure III. 23 - ^1H NMR spectrum of 60 in chloroform after irradiated at 300 nm in neat conditions under inert atmosphere. Total irradiation time is 120 min.	76
Figure III. 24 - Viscosity curve of pure 60 before (black dots) and after (red dots) irradiation at 300 nm. Total irradiation time is 120 min.	77
Figure III. 25 – Quadratic dependence of the scattered intensity in IL 60 before (black circles) and after (red circles) irradiation compared with that obtained in the reference solvent (chloroform, blue squares).....	79
Figure III. 26 – (a) Spectral modifications of 62 at 1.7×10^{-5} M in acetonitrile upon irradiation at 300 nm. Total irradiation time is 60 min. (b) Photochemical quantum yield dependence with concentration of 62.....	82
Figure III. 27 - ^1H NMR spectrum of 62 in chloroform before and after irradiation at 330 nm. Total irradiation time is 120 min.	83
Figure III. 28 – ^1H NMR spectra of 4-methyl-7-alkoxy coumarin derivative in chloroform before and after photoinduced dimerization.....	83
Figure III. 29 - ^1H NMR spectrum of 62 in chloroform after irradiation at 330 nm in neat conditions. Total irradiation time is 120 min.	85
Figure III. 30 - ^1H NMR spectrum of 62 in chloroform after irradiation at 330 nm in neat conditions under inert atmosphere. Total irradiation time is 120 min.	85
Figure III. 31 - DSC thermograms of ionic liquid 62 before (i) and after (PSS) irradiation at 330 nm. 86	86
Figure III. 32 - (a) Spectral modifications of 64 at 1.1×10^{-5} M in acetonitrile upon irradiation at 330 nm. Total irradiation time is 60 min. (b) Photochemical quantum yield dependence with concentration of 64.....	87
Figure III. 33 - ^1H NMR spectrum of 64 in chloroform obtained after irradiation at 330 nm. Total irradiation time is 120 min.	87
Figure III. 34 - Viscosity curve of pure 64 before (black dots) and after (red dots) irradiation at 330 nm. Total irradiation time is 120 min.....	88

Figure III. 35 - Quadratic dependence of the scattered intensity in IL 64 before (black circles) and after (red circles) irradiation compared with that obtained in the reference solvent (chloroform, blue squares).....	90
Figure III. 36 – (a) Fluorescence lifetime decays of 3-vinyl coumarins 72b (black) and 72c (red) and their respective 3-styryl counterparts 73b (green) and 73c (blue); Fluorescence lifetime of 3-styryl coumarins 73b (green) and 73c (blue) and their respective nitro derivatives 73f (brown) and 73g (orange).	94
Figure III. 37 – UV-Vis spectral transformation of a solution of 72a at 2.3 mM in acetonitrile upon irradiation at 313 nm. Total irradiation time is 30 min.	94
Figure III. 38 - ^1H NMR spectra (400 MHz, CDCl_3) of a solution of coumarin 77 before (red) and after (blue) irradiation for 60 min. $\lambda_{\text{irrad}} = 275$ nm.....	97
Figure III. 39 - ^1H NMR spectra (400 MHz, CDCl_3) of a solution of coumarin 80a irradiated at different times: 0 min (red); 5 min (yellow); 10 min (green); 20 min (blue); 120 min (purple). $\lambda_{\text{irrad}} = 360$ nm.....	98
Figure III. 40 - ^1H NMR spectra (400 MHz, CDCl_3) of a solution of coumarin 80b irradiated at different times: 0 min (red); 5 min (yellow); 10 min (green); 20 min (blue); 120 min (purple). $\lambda_{\text{irrad}} = 370$ nm.....	99
Figure III. 41 - ^1H NMR spectra (400 MHz, CDCl_3) of a solution of coumarin 80c irradiated at different times: 0 min (red); 5 min (yellow); 10 min (green); 20 min (blue); 120 min (purple). $\lambda_{\text{irrad}} = 333$ nm.....	99
Figure III. 42 - Frontier orbitals for compound 79 obtained from density functional theory (DFT) calculations.....	100
Figure III. 43- Frontier orbitals for compound 80a obtained from density functional theory (DFT) calculations.....	100
Figure III. 44 – UV-Vis spectral modification of coumarins 80a (a), 80b (b) and 80c (c) in acetonitrile upon irradiation at the longest wavelength transition.....	102
Figure III. 45 - Calculated spectra for the <i>Z</i> and <i>E</i> isomers of 80a and the combined spectra of the mixture of isomers with experimental molar fractions.....	103
Figure III. 46 – Fluorescence variation of coumarin 80b adsorbed into hydroxyethylacrylamide/poly(ethyleneglycol).....	103

Scheme Index

Scheme I.1 – Photochemical dimerization of 9-methyanthracene 1	7
Scheme I.2 – Photochemical dimerization reaction of coumarin 4	9
Scheme I.3 – General network of reactions of flavylum compounds in acidic and neutral aqueous media, exemplified for 4',7-dihydroxyflavylium 10	10
Scheme II. 1 - Synthetic pathway for the preparation of tripodal cinnamic acid derivative 16: i) thionyl chloride, chloroform, 89%; ii) tris(2-aminoethyl)amine, K ₂ CO ₃ or NEt ₃ , dichloromethane, 91% or 34%, respectively	24
Scheme II.2 – Synthetic pathway for the preparation of tripodal anthracene derivative 19: i) thionyl chloride, chloroform; ii) tris(2-aminoethyl)amine, K ₂ CO ₃ or NEt ₃ , dichloromethane	27
Scheme II. 3 - Synthetic pathway for the preparation of tripodal coumarin derivative 22: i) thionyl chloride, chloroform, 90%; ii) tris(2-aminoethyl)amine, K ₂ CO ₃ or NEt ₃ , dichloromethane, 95%	27
Scheme II. 4 – Synthetic pathway for the preparation of tripodal cinnamate derivative 31: i) K ₂ CO ₃ , acetone, 72%; ii) phloroglucinol, K ₂ CO ₃ , acetonitrile, 8.6% (for precursor 30)	36
Scheme II. 5 – Synthetic pathway for the preparation of anthracene precursor 34: i) NaNO ₂ , NaOH, water, 53%; ii) NaBH ₄ , methanol, 24%	38
Scheme II. 6 – Synthetic pathway for the preparation of tripodal anthracene derivative 36: i) K ₂ CO ₃ , acetone, 76%; ii) phloroglucinol, K ₂ CO ₃ , acetonitrile, 61%	38
Scheme II. 7 – Synthetic pathway for the preparation of tripodal coumarin derivative 39: i) K ₂ CO ₃ , acetone, 60%; ii) phloroglucinol, K ₂ CO ₃ , acetonitrile, 63%	42
Scheme III. 1 – Photochemical reaction of generic spiropyran compounds	56
Scheme III. 2 - Ring-closing and ring-opening of photosensitive diarylethene-containing ionic liquids 153	59
Scheme III. 3 – Synthetic pathway for the preparation of cinnamate organic cations: i) methanol/H ₂ SO ₄ , 94%; ii) 1,3-dibromopropane, K ₂ CO ₃ , acetone, 94%; iii) <i>N</i> -methylimidazole, acetonitrile, 76%; iv) trimethylamine, acetonitrile, 66%	63
Scheme III. 4 - Synthetic pathway for the preparation of cinnamate photoresponsive ionic liquids: i) 1,3-dibromopropane, K ₂ CO ₃ , acetone, 94%; ii) 1,6-dibromohexane, K ₂ CO ₃ , acetone, 89%; iii) <i>N</i> -methylimidazole, acetonitrile, 76%; iv) LiNTf ₂ , dichloromethane, 70-76%	65
Scheme III. 5 – Synthetic pathway for the preparation of room temperature cinnamate ionic liquids: i) triphenylphosphine, Br ₂ , acetonitrile, 87%; ii) K ₂ CO ₃ , acetone, 91%; iii) <i>N</i> -methylimidazole, acetonitrile, 91%	74
Scheme III. 6 - Synthetic pathway for the preparation of coumarin photoresponsive ionic liquids: i) 1,3-dibromopropane, K ₂ CO ₃ , acetone, 92%; ii) 1,13-dibromotetraethyleneglycol, K ₂ CO ₃ , acetone, 86%; iii) <i>N</i> -methylimidazole, acetonitrile, 75-91%	81

Scheme III. 7 –Alternative photochemical reactions taken by coumarin derivatives	84
Scheme III. 8 – Suggested alternative photochemical reactions taken by compounds 62	84
Scheme III. 9 – Synthetic pathway for the preparation of 3-styryl coumarins 73: i) Pd(OAc) ₂ , DMF, 9-98%.....	92
Scheme III. 10 – Suggested photochemical reactions of hypothetical coumarin-based stilbene analog 74.....	95
Scheme III. 11 – Synthetic pathway for the preparation of 5-styryl coumarins 80a-c: i) OXONE®, HBr, dichloromethane, 91%; ii) [PdCl ₂ (dppf)].CH ₂ Cl ₂ , CH ₂ CHBF ₃ K, NEt ₃ , <i>n</i> -propanol, 92%; iii) Pd(PPh ₃) ₄ , AgOAc, Ar-I, DMF, 50-90%.....	95

Table Index

Table III. 1 – Melting points of ionic cinnamate derivatives 53 and 54.....	64
Table III. 2 - Melting points of ionic cinnamate derivative 53 with different counterions	64
Table III. 3 - Absorption Maxima (λ_{max}), Photochemical Quantum Yields (Φ_{R}), and Cis Isomer Fraction before Irradiation and at the Photostationary State (PSS) of Ionic Liquids 55 and 58 in Acetonitrile.....	68
Table III. 4 - Melting (T_{m}) and Peak (T_{p}) Temperatures and Melting Enthalpies (ΔH_{m}) of ILs 55 and 58 before Irradiation at 300 nm ($_{\text{i}}$), after the PSS Has Been Reached ($_{\text{PSS}}$) and after Recovery upon Irradiation at 240 nm ($_{\text{rec}}$)	71
Table III. 5 - Time dependent <i>cis</i> isomer ratio and melting point depression (ΔT_{m}) of irradiated neat samples of ionic liquids 55 and 58	73
Table III. 6 - Absorption Maxima (λ_{max}), Photochemical Quantum Yields (Φ_{R}), and Cis Isomer Fraction before Irradiation and at the Photostationary State (PSS) of IL 60.....	75
Table III. 7 - β HRS, $\beta J=1$ (dipolar) and $\beta J=3$ (octupolar) values (in atomic units*, using Convention T) and depolar-ization ratios, DR, and anisotropies, ρ , deduced from HRS measurements at 1064 nm for compound 60, before and after irradiation	78
Table III. 8 - Melting (T_{m}) and Peak (T_{p}) Temperatures and Melting Enthalpies (ΔH_{m}) of IL 62 before ($_{\text{i}}$) and after ($_{\text{PSS}}$) irradiation at 330 nm.....	86
Table III. 9 - β HRS, $\beta J=1$ (dipolar) and $\beta J=3$ (octupolar) values (in atomic units*, using Convention T) and depolar-ization ratios, DR, and anisotropies, ρ , deduced from HRS measurements at 1064 nm for compound 64, before and after irradiation	89
Table III. 10 - Absorption and Emission Maxima, Fluorescence Quantum Yield and Average Fluorescent Lifetime of Selected Coumarins in Acetonitrile Solutions	93
Table III. 11 – Synthetic yields and <i>Z/E</i> ratio of coumarins 80a-c.....	96
Table III. 12 - Absorption and Emission Maxima, Molecular Absorptivity, Fluorescence Quantum Yield, Average Fluorescent Lifetime and radiative and apparent nonradiative rate constants of selected coumarins	96
Table III. 13 - Fluorescence and Reaction Quantum Yield, Average Fluorescent Lifetime and radiative, nonradiative and reactive rate constants of selected coumarins	101

Abbreviation List

A	Absorbance
AFM	Atomic force microscopy
CA	Cinnamic acid
CMC	Critical micelle concentration
Compd	Compound
Conc.	Concentration
CTAB	Cetyltrimethylammonium bromide
DFT	Density functional theory
D_h	Hydrodynamic diameter
DLS	Dynamic light scattering
DMF	Dimethylformamide
DSC	Differential scanning calorimetry
D_t	Diffusion coefficient
EDTA	Ethylenediaminetetraacetate
ER	Electrorheological
HOMO	Highest occupied molecular orbital
HRS	Hyper-Rayleigh scattering
Hz	Hertz
IL	Ionic liquid
k	Boltzmann constant
k_{nr}	Non-radiative rate constant
k_{nr}^*	Apparent non-radiative rate constant
k_r	Radiative rate constant
LED	Light-emitting diode
LMWGs	Low-molecular weight gelator
LUMO	Lowest unoccupied molecular orbital
M	Molar
MALDI-MS	Matrix-assisted laser desorption/ionization-mass spectrometry
MR	Magnetorheological
NEt_3	Triethylamine
nm	Nanometer
NMR	Nuclear magnetic resonance
OMCA	<i>o</i> -methylcinnamic acid
PCA	<i>p</i> -Coumarin acid

PEG	Polyethyleneglycol
ppm	Parts per million
PR	Photorheological
PSS	Photostationary state
QSPR	Quantitative structure-property relationship
SMA _s	Shape-memory alloys
SN	Nucleophilic substitution
SOMO	Single occupied molecular orbital
SRIL	Stimuli-responsive ionic liquid
SRM	Stimuli responsive materials
T	Temperature
TDDFT	Time-dependent density functional theory
TEG	Tetraethylene glycol
Tf	Triflyl
UV	Ultra-violet
Vis	Visible
B	Hyperpolarizability
ϵ	Molar absorptivity
η	Viscosity
λ	Wavelength
λ_{abs}	Wavelength of absorption maximum
λ_{em}	Wavelength of emission maximum
τ	Delay time
τ_{m}	Average excited state lifetime
Φ_{F}	Fluorescence quantum yield
Φ_{R}	Photochemical quantum yield

Chapter I

I. Introduction

Stimuli-responsive materials

Throughout human history, technological development has been closely linked to the nature of the materials used for creating tools and other devices. In fact, pre-historic periods were named after these materials, i.e. Stone, Bronze and Iron Ages, evidencing their crucial role in human evolution. In Modern Age, the discovery of the first synthetic polymer by Baekeland, in the first decade of the twentieth century, marked the beginning of a technological period that lasts until today, the Age of Polymers. Over the past one hundred years, polymers have grown in popularity and can be found ubiquitously, progressively replacing wood and metals in a wide variety of applications. However, in more recent years, the driving force for technological change in many respects has shifted towards information technology. Instead of traditional structural functions, new materials are required to have sensibility or actuation capabilities. The increasing need for highly autonomous systems and devices that require less human control led to pursuit for materials that can intelligently interact with their environment and structures that assess their own health. Such systems could have a tremendous impact in advancing many fields including medicine, microelectronics, and robotics, among others. Therefore, the increasing interest in materials that respond to external stimuli, such as fluctuations in temperature, pressure or light intensity and change their physico-chemical properties accordingly led to the beginning of the Smart Material Age.

Smart, or stimuli-responsive material (SRM) is currently defined as “a system or material which has built-in or intrinsic sensors, actuators and control mechanisms whereby it is capable of sensing a stimulus, responding to it in a predetermined manner and extent, in an appropriate time, and reverting to its original state as soon as the stimulus is removed”.¹ The first material to evidence a smart behavior was potassium sodium tartrate, commonly known as Rochelle salt. This compound displays both pyroelectric and piezoelectric effects, becoming electrically polarized upon an applied temperature change or mechanical stress. This property led to its extensive use in gramophones, microphones and earpieces.² However, the properties of Rochelle salt are only representative of a small fraction of smart materials, which can produce a variety of responses to a wide range of stimuli. Depending on the external stimuli they respond to, or the transformation that is generated, smart materials can be divided in different classes. For example, pyroelectrics are materials that become electrically polarized upon a temperature variation.³ They are particularly used for infrared detection in surveillance and targeting applications. The infrared radiation is absorbed and induces an increase in temperature of the pyroelectric component, changing its polarization and, thus, generating an electric signal. Analogously, piezoelectrics are another class of smart materials that exhibit electric polarization with an external stimulus. In this case, this effect occurs when mechanical stress is

induced.⁴ The converse effect can be exhibited, i.e., when an electric field is applied, a dimensional change takes place. Since the discovery of this effect in the end of the 19th century, piezoelectrics gathered great attention from the scientific community and became the most representative class of smart materials. They find application in a wide variety of devices in fields ranging from automotive industry and telecommunications to medical instruments or military weaponry.⁵ Shape-memory alloys (SMAs) are another class of smart materials that respond to external-stimuli with dimensional changes. These materials, upon proper thermal and mechanical treatment, have the ability to remember up to two shapes which they had previously occupied. When subjected to a mechanical load below a certain temperature, SMAs can be plastically deformed beyond their elastic limit, but then are capable of regaining their original shape if they are then heated above a certain temperature. SMAs are employed as actuators in systems used in very different fields, from spacecraft and aircraft to medicine, robotics or even household appliances.⁵ There are also smart materials that generate visual responses to external stimuli. For example, luminescent materials display the property of emitting energy in the form of light after excitation by an external stimulus. This excitation can be achieved by irradiation of light of different wavelength, heating or application of an electric field. Light-emitting diodes (LED) are the most common type of luminescent materials, which are composed by an electroluminescent material comprised between two electrodes. Instead of emission of light, chromogenic materials respond essentially to the same stimuli by changing their color. Electrochromic materials are the most common type of chromogenics, and the majority of them are composed by metal oxides that undergo a redox reaction when an electric field is applied, although organic compounds have recently been employed. Chromogenic and luminescent materials find use in sensor devices, paints, smart windows, household appliances or automotive industry.⁶

Stimuli-responsive rheological fluids

One particular type of SRM is the class of rheological fluids. These materials are developed and used in their liquid state and respond to external stimuli by varying properties such as viscosity and viscoelasticity. This change is optimally fast and reversible and can be quite substantial, turning a low viscosity fluid into an almost-solid substance. This phenomenon has a longstanding fundamental and practical interest, with possible applications in clutches, brakes, vibration damping, valves and other devices. The vast majority of smart rheological materials currently used are sensitive to application of magnetic or electric fields. These fluids typically consist of a dispersed, polarizable particulate phase suspended in a non-conductive carrier fluid (hydrocarbon or silicone oil).⁷ Upon application of an electric or magnetic field, the dispersed particles become polarized and begin to interact with each other, forming chain-like structures which increase fluid viscosity (Figure I.1).

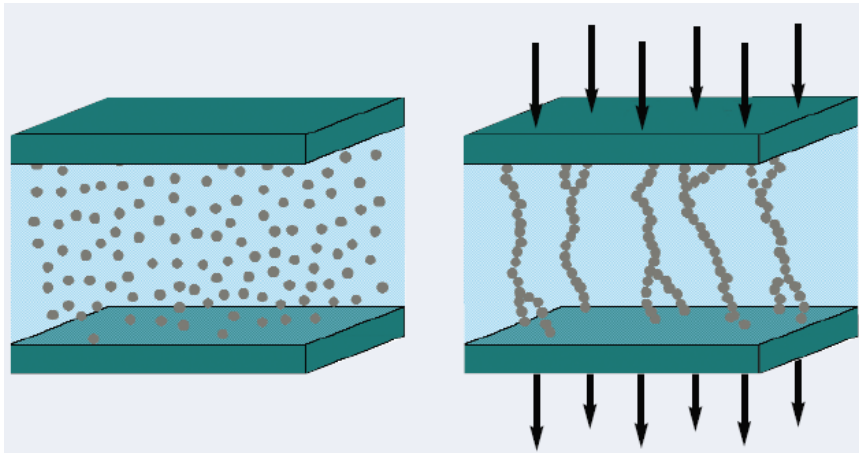


Figure I.1 – Schematic representation of suspended particle alignment induced by an electric or magnetic field (adapted from [5])

Such particulate suspensions are usually composed by metal oxides, aluminosilicates, silica or polymers, for electrorheological fluids, or ferromagnetic and paramagnetic solid particles for magnetorheological fluids. For example, Dürschmidt and Hoffmann prepared an electrorheological fluid composed of hydrophobically modified saponite particles suspended in *n*-hexadecane.⁸ Although the fluid exhibited a significant electrorheological effect, sedimentation of clay particles occurred, reducing its durability. This is a common problem with ER fluids and typically a stabilizer is required.⁹ An usual strategy to overcome this drawback involves coating charged particles with surfactants of opposite charge, significantly increasing ER fluid durability.¹⁰

In the case of magnetorheological fluids, coating agents are particularly important due to magnetic nature and high density of particles used.¹¹ Jang and co-workers evidenced this importance in magnetorheological fluids composed of carbonyl iron microparticles suspended in mineral oil. By using polyvinyl butyral as a coating agent, the sedimentation, abrasion and oxidation rate of metal particles were reduced without compromising the magnetorheological effect.¹² Instead of using coating agents to prevent aggregation of solid particles, different formulations with high durability can be prepared from liquid-liquid emulsions.¹³ Pan and McKinley were pioneers in developing emulsion systems that exhibit electrorheological effect, by suspending conductive polychlorinated paraffin in silicon oil.¹³ After application of an electric field, the paraffin droplets align forming microscopic fiber-like structures (Figure I.2), increasing viscosity of the emulsion.

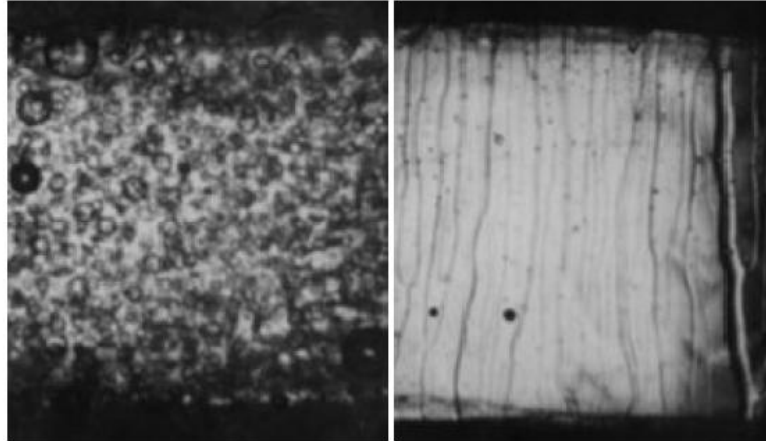


Figure I.2 – Microscopic photographs of paraffin-based ER fluid before (left) and after (right) application of an electric field (adapted from [13])

Photorheological fluids

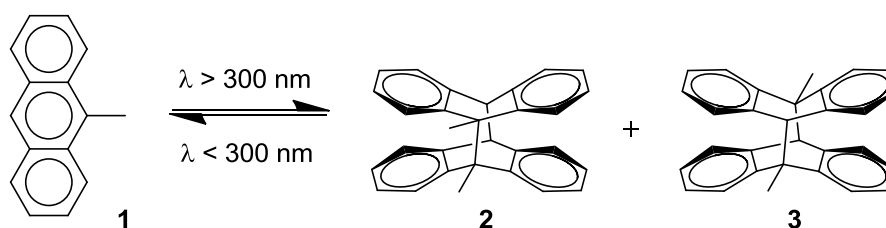
Photorheological (PR) fluids are systems that generate similar rheological changes to those of ER and MR fluids, although in response to light stimuli. These changes usually occur at the molecular level and therefore, the majority of PR fluids are single phase solutions where aggregation and sedimentation do not pose durability problems.¹⁴ Besides, these systems present other advantages over conventional rheological stimuli-responsive fluids. For instance, whereas ER and MR fluids must often be comprised between two plates, PR fluids do not require a specific apparatus, allowing switching by a light source at a single location, even physically removed from the fluid.¹⁵ In addition, light presents the ability to be directed to a precise spot with micron-level resolution and allows rheology control at the microscopic scale, which expands the applicability of stimuli-responsive rheological materials as microvalves or flow sensors for microfluidic systems or as nanocarriers for controlled drug delivery systems.^{16,17} Finally, due to the chemical nature of the rheological effect, PR fluids tend to retain property changes after the stimulus is removed. However, this property often gives rise to reversibility issues in these type of fluids, with the recovery to the initial state often being slow.^{14,15}

Depending on the system originating the rheological effect, PR fluids can essentially be classified into four classes: surfactant-, nanoparticle-, polymer- or gelator-based PR fluids.

Surfactant-based photorheological fluids

One of the first occurrences of photorheological effect was reported by Wolff and co-workers during the 1980s.^{18,19} Their studies concerned the selective production of the unstable head-to-head

dimer of 9-methylanthracene by preorganization in micellar solutions of cetyltrimethylammonium bromide (CTAB) and subsequent irradiation with light (Scheme I.1). As a side effect, they observed that addition of 9-methylanthracene to the CTAB led to a strong enhancement of viscosity, which was reduced upon irradiation.^{18,19} The authors attributed this rheological effect to the shrinkage of CTAB micelle size and a decrease of aggregation stability upon photodimerization of anthracene derivatives.²⁰



Scheme I.1 – Photochemical dimerization of 9-methylanthracene 1

After this first report, the strategy of applying a well-characterized photochemical reaction to induce structural changes in surfactant self-assembled aggregates became prevalent in the development of several PR fluids. Surfactant-based PR fluids rely on the aggregation behavior of surfactant molecules and on the fact that several aggregate structures may form in solution. Surfactant molecules contain hydrophobic and hydrophilic moieties, i.e. one or two alkyl chains and an ionic or non-ionic polar head group. Being amphiphilic they generally concentrate at borders of phases differing in dielectric constant, such as the air/water interface. When a critical surfactant concentration in water is exceeded (critical micelle concentration, CMC) surfactant molecules in the bulk phase aggregate to form spherical micelles consisting of 60 to 120 monomers depending on the specific surfactant. In addition, at a concentration some orders of magnitude above the CMC, micelles change their morphology to yield rod-like or thread-like aggregates, which can entangle into dense networks and cause viscoelastic behavior of the solution (Figure I.3).²¹

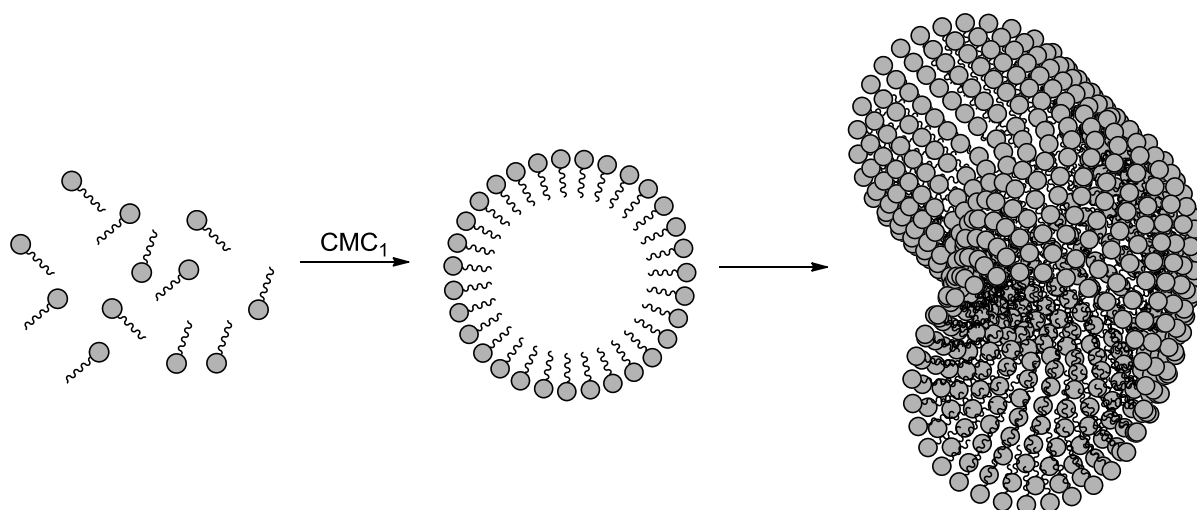
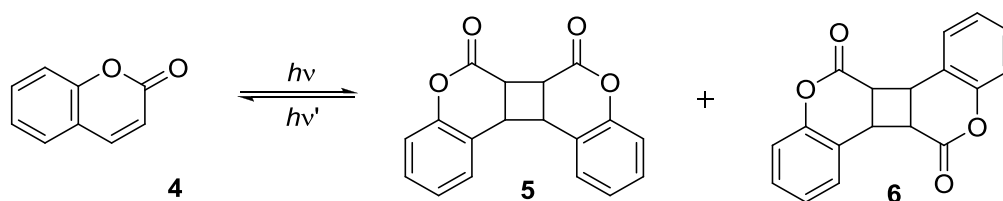


Figure I.3 – Schematic representation of different micellar aggregate morphology upon increase in concentration.

Furthermore, when present at small concentrations, certain aromatic solutes may affect the aggregation state of surfactant molecules and increase viscosity by up to two orders of magnitude. For instance, 2,2,2-trifluoro-1-(9-anthryl)-ethanol when solubilized in dilute CTAB solutions produced a highly viscous fluid due to the formation of rod-like micelles.²² The same effect was obtained in CTAB solutions containing 9-antracencarboxylic acid and ionene polyelectrolytes.²³ However, it was shown that upon irradiation with UV light and concomitant dimerization of anthracene derivatives, the viscosity was reduced significantly, which was attributed to the disruption of interactions between aromatic solute and surfactant molecules and shrinkage in micelle size. Similar results have been obtained for other anthracene analogs and different surfactants. Lehnberger and Wolff used acridizinium bromide, which is known to undergo [4+4] photocycloaddition identically to anthracene, in tetramethylammoniumhydrogen-2-dodecyl malonate (TMHM) aqueous solution obtaining a PR fluid whose viscosity was greatly reduced after irradiation.^{24,25}

Other photoresponsive molecules that undergo photochemical dimerization have shown to have similar interaction with surfactant aggregates and gained importance for the development of novel PR fluids. For instance, coumarins are a natural class of organic compounds and have been extensively investigated mainly due to their outstanding optical properties, i.e., high extinction coefficient and fluorescence quantum yield.²⁶ However, coumarins are also known to yield dimers of different geometries upon irradiation (Scheme I.2) and this reaction was explored as a way to induce viscosity changes in surfactant solutions. Yu and Wolff were among the first to report the preparation of PR fluids with coumarins as photosensitive moieties.²⁷ Their systems were composed by 6-alkylcoumarins and surfactant (CTAB or Triton X-100) solutions. Depending on the size of the alkyl substituent, the observed photorheological effects were different. Short substituents yielded direct PR effect, i.e. an increase in viscosity upon irradiation, whilst long alkyl substituents had an opposite effect. Despite the relatively high number of reports on surfactant-based PR fluids, the mechanism of action of the aromatic solutes was unclear until Raghavan and co-workers made a series of reports

where several cinnamic acid derivatives were employed in surfactant solutions to prepare PR fluids. In their first report, *o*-methylcinnamic acid (OMCA) was dissolved in aqueous solutions of CTAB and found to induce the formation of long entangled worm-like micelles, resulting in highly viscous mixtures.²⁸ Photoisomerization of the photosensitive molecule led to a drastic reduction in micellar length, with consequent reduction of viscosity. Using the same cinnamic acid (CA) derivative, but with a zwitterionic surfactant (erucyl dimethyl amidopropyl betaine, EDAB), the same group formulated a system that displayed the opposite effect of the previous one, i.e., photoisomerization of *trans*-OMCA to *cis*-OMCA resulted in the formation of long wormlike micelles and increased viscosity.²⁹ These experiments shed light on the mechanism behind light-induced variations of micelle structures. The interactions between aromatic compounds and surfactant molecules give rise to changes in effective sizes of head and tail groups, giving rise to two effective geometries, cone and cylinder (Figure I.4). Micellar aggregates shape, and consequently size, are governed by the effective shape of surfactant molecules: conic geometries give rise to rather spherical micelles, whereas cylinder-shaped surfactant molecules aggregate as long, entangled wormlike micelles.



Scheme I.2 – Photochemical dimerization reaction of coumarin 4

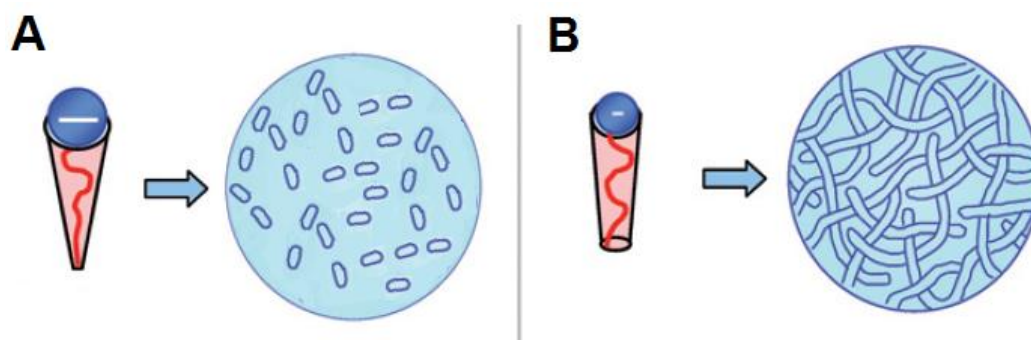
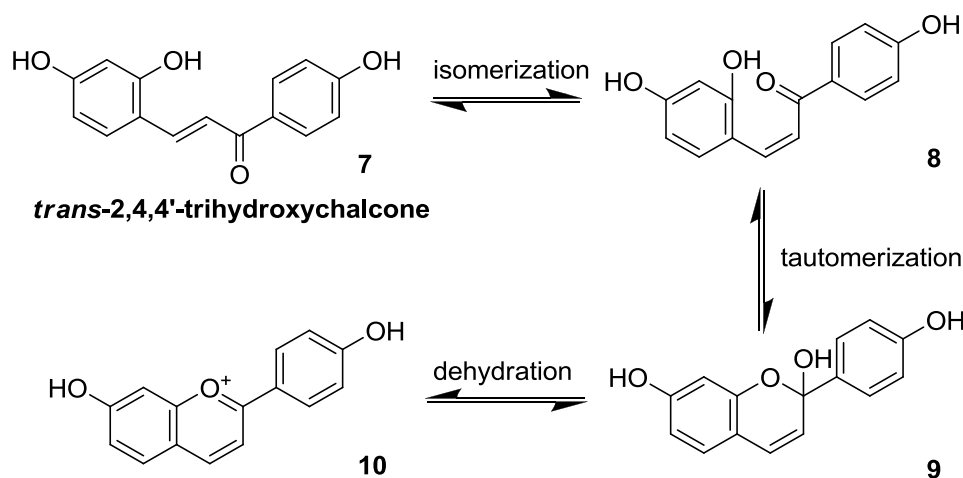


Figure I.4 – Schematic representation of different effective head group sizes of anionic surfactant and corresponding micellar aggregation morphologies (adapted from [29])

This same principle was applied in the development of nonaqueous fluids, using *p*-coumaric acid (PCA) as photoresponsive molecule and lecithin as surfactant.³⁰ Usually, this lipid forms short reverse micelles in apolar organic solvents, but when PCA is added to the solution, micelles grow into

long chains, forming an organogel. Upon irradiation with UV light, PCA isomerized and interactions with lecithin molecules were disrupted, leading to a free-flowing liquid with low viscoelasticity.

Although the majority of PR fluids displayed significant viscosity changes (factors of 1000 to 10000), reversibility is usually low due to much lower absorptivity of photoproducts over the entire wavelength spectrum. To overcome this problem, Pereira *et al.* applied a different photoisomerizable compound, *trans*-2,4,4'-trihydroxychalcone in CTAB and salicylic acid solutions.³¹ Chalcones are aromatic ketones that are structurally similar to cinnamic acids, and therefore, also undergo photoisomerization reactions. However, depending on substituents and conditions, irradiation of chalcones gives rise to a multiequilibrium system involving several chemical species interconvertible by light and pH (Scheme I.3).



Scheme I.3 – General network of reactions of flavylium compounds in acidic and neutral aqueous media, exemplified for 4',7-dihydroxyflavylium 10.

Because *trans*-chalcone species interacts with the head groups of surfactant molecules, this equilibrium allowed switching from long wormlike to short spherical micelles, with a consequent 10-fold decrease in viscosity. By controlling the pH values of the solution, flavylium cation was allowed to hydrate and revert slowly to *trans*-chalcone species, rendering this PR fluid completely reversible. The salicylic acid used in this work is known to intercalate with CTAB molecules and form worm-like micelles yielding solutions with viscoelastic properties.^{32,33} For this reason, Sakai and co-workers used it to elongate mixed micelles of CTAB and an azobenzene-modified cationic surfactant.³⁴ Irradiation with UV light led to a decrease in viscosity due to isomerization of azobenzene surfactant and consequent micelle structure disruption. Further irradiation with visible light returned the system to its original state. In effect, appending azobenzene structural units in the lipophilic tail of surfactants offers the ability to control uniquely aggregation properties through irradiation with appropriate wavelengths with high reversibility.^{35,36,37,38,39} The planar *trans* form of such surfactants is more hydrophobic than the nonplanar *cis* (UV light) form, and hence the CMC, which typically correlates with the hydrophobicity of the surfactant tails, is lower for the *trans* than the *cis* isomer of the surfactant.^{40,41}

Therefore, several reports on PR fluids based on intrinsically photosensitive surfactants containing azobenzene moieties were made.^{42, 43} Worth mentioning is a photocontrolable gel developed by Lee and co-workers, where an azobenzene-based cationic surfactant was mixed with modified poly(acrylic acid).⁴² In this system, irradiation of UV-light allowed switching of aggregation behavior of surfactant micelles, which acted as crosslinkers for polymer chains resulting in the formation of a gel (Figure I.5).

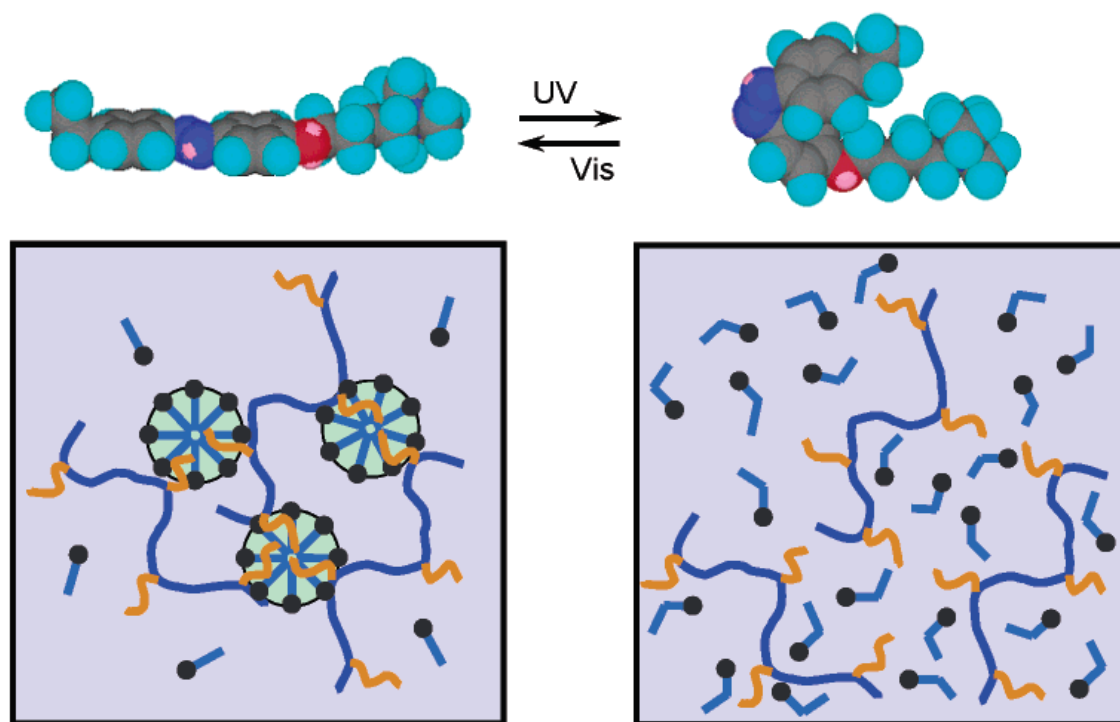


Figure I.5 – Schematic representation of isomerization induced changes in aggregation behaviour of azobenzene-based cationic surfactant micelles (adapted from [42]).

Nanoparticle-based photorheological fluids

There are innumerable reports on the viscosity control of fluids by the addition of solid nanoparticles.⁵⁻⁸⁻¹² PR fluids based on the aggregation of nanoparticles rely on the same principles as most MR and ER fluids, i.e., the rheological effect is caused by the self-assembly of anisotropic nanoparticles into a complex network.⁵⁻⁸⁻¹² However, whereas the aggregation is caused by temporary polarization of nanoparticles in MR or ER fluids, a different strategy is required when using light stimuli. Therefore, nanoparticles with intrinsically anisotropic charge distribution are usually required for the formulation of this type of PR fluids. Laponite is a synthetic hydrous sodium lithium magnesium silicate clay composed of anisotropic disc-shaped nanoparticles whose surface is negatively charged. However, the edge of the laponite particles are composed of hydrous oxide and become positively charged in acidic medium.^{44,45} For these interesting properties, laponite has been

applied extensively in cosmetics, paints, foods and pharmaceuticals as a thickening agent.⁴⁶ Recently, it has been applied in the formulation of PR fluids in which nanoparticle aggregation and consequent viscosity increase were controlled with UV-light irradiation.^{47,48} Besides laponite, these systems were composed by Pluronic F-127, a nonionic surfactant known to stabilize laponite suspensions,⁴⁹ and diphenyliodonium-2-carboxylate monohydrate as a photoresponsive molecule. This latter compound belongs to the class of photo-acid generators, a group of molecules that undergo photolysis and generate a photoproduct with an acidic moiety.^{50,51,52} Therefore, irradiation of these PR fluids leads a decrease in pH and, in turn, laponite particle edges become positively charged. This causes the surfactant to desorb and form micelles in solution and laponite particles to assemble into a three-dimensional network, resulting in a significant increase in fluid viscosity, as depicted in Figure I.6.^{47,48}

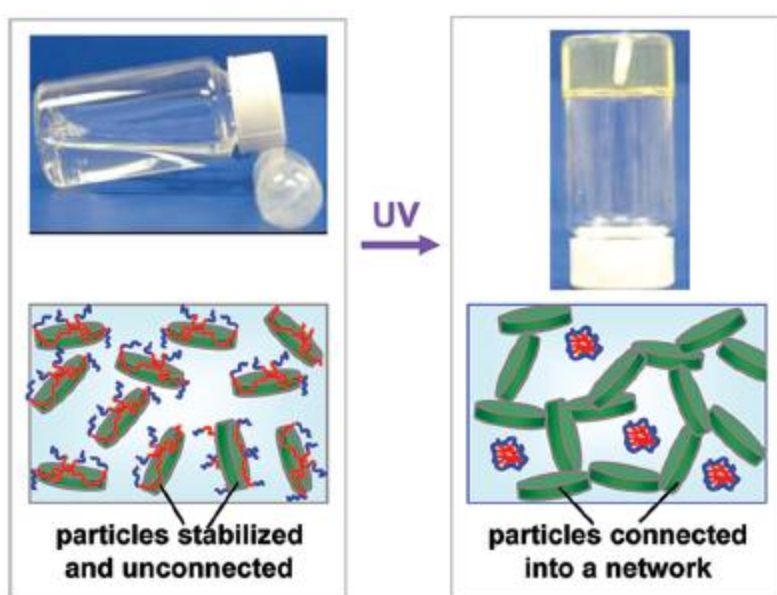


Figure I.6 – Light-induced gelation of aqueous laponite suspensions: initially (left) particles are stabilized by pluronic surfactant and unconnect; upon UV irradiation (right), the particles assemble into a network, causing the fluid to turn into a gel (adapted from [47])

Unlike MR or ER fluids, these systems do not revert to the initial state after removal of the stimulus, requiring an increase in pH to disassemble laponite nanoparticles and obtain a liquid suspension. However, the aggregation of nanoparticles can be reversibly controlled with light stimuli as evidenced by Yuan and co-workers in a report involving polyorganosiloxane nanoparticles functionalized with *p*-nitrocinnamate.⁵³ Upon irradiation, cinnamate moieties dimerize causing aggregation of nanoparticles, which in turn results in increased viscosity.

Polymer-based photorheological fluids

One of the most widespread fluids evidencing photorheological effect in technological applications are light-activated resins. These materials undergo photopolymerization when exposed to UV or visible light, which results in a quick transition from liquid to solid state. Light-activated resins are typically composed of reactive oligomers, reactive diluents and photoinitiators, which are responsive for generating free radicals and starting polymerization. Their photochemical nature brings advantages over traditional polymerization processes because no mixing is required allowing for denser and clearer resins.⁵⁴ Therefore, they find application in a wide variety of fields from electronics to medicine.⁵⁵ For example, Chen-Yang *et al.* developed a UV curable resin based on photopolymerizable modified cyclotriphosphazenes for fire-retarding wood coatings.⁵⁶ In dentistry, UV curing resins are constantly evolving and play a crucial role replacing traditional metal amalgams as restorative materials.⁵⁷ One common characteristic among light-activated resins is the fact that the photochemical polymerization is irreversible. Nonetheless, photopolymerization and other photochemical reactions occurring in polymer systems can also be explored for the development of PR fluids that give rise to reversible sol-gel transitions. For instance, Zheng and co-workers, synthesized a branched polyethylene glycol (PEG) polymer modified with 9-anthracene carboxylic acid (Figure I.7) that underwent reversible photo-cross-linking when exposed to alternating wavelengths of irradiation. The system exhibited sol-to-gel transition and its properties such as viscosity, topography and swellability were tunable with light.⁵⁸ The same group applied the same strategy on an eight-branched PEG-based hydrogel, modified with *p*-nitrocinnamic acid. This molecule exhibited high photoreactivity,^{59,60,61} allowing the formulation of a PR fluid that underwent rapid photogelation and photoscission.⁶² The system was further studied as a light-controlled drug delivery system for skin regeneration applications.⁶³

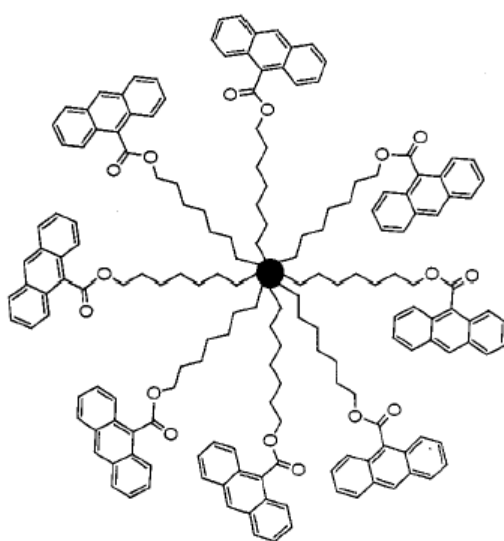


Figure I.7 – Schematic representation of branched PEG polymer modified with 9-anthracene carboxylic acid used in the formulation of a PR fluid (adapted from [62]).

A similar system was obtained through photopolymerization of cinnamylidene acetyl grafted onto PEG-based polymers. Irradiation with UV-light induced growth of polymer chains, which in turn led to the formation of a gel.⁶⁴ In a different report, six polyurethanes containing coumarin dimer components in the polymer backbone were prepared.⁶⁵ It was shown that upon irradiation with UV light coumarin dimers undergo photocleavage of cyclobutane rings to yield dicoumarins, breaking polymer backbone and reducing system viscosity. Re-polymerization was achieved after irradiation at longer wavelengths due to photodimerization of coumarin moieties. In addition to appending photodimerizable moieties in polymer backbone, it is also possible to incorporate them as side groups to obtain photorheological fluids. This way, it is possible to control cross-linking between polymer chains with light stimuli. This strategy was employed by several groups in the preparation of PR fluids with varied composition and applicability. For example, Wells and co-workers synthesized a graftable anthracene-based cross-linker for the modification of a potential variety of polymers.⁶⁶ This molecule was used on alginate and hyaluronic acid to obtain photogels whose properties were reversibly altered with UV-light exposure. In addition, the modified hydrogels exhibited controlled release of bioactive molecules through irradiation due to disruption of polymer backbone by photocrosslinking (Figure I.8).⁶⁶ Coumarins have also been grafted onto polymer backbones to induce photo-crosslinking and change rheological properties. Bergmann and co-workers demonstrated this effect on a polymer films that expand due to the formation of free-volume between polymer chains by photodimerization of coumarins.⁶⁷ A similar strategy was employed by Dai and Kim in the preparation of a β -cyclodextrin polymer that increases viscosity upon irradiation.⁶⁸ In this system, coumarin derivatives were allowed to form complexes with polymer β -cyclodextrin residues and dimers formed by exposure to UV-light acted as cross-linkers (Figure I.9).

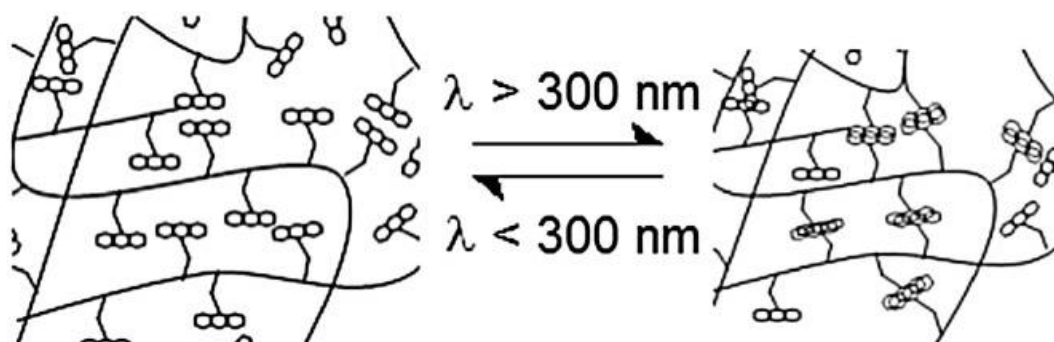


Figure I.8 – Schematic representation of light-induced crosslinking between polymer chains due to anthracene dimerization used in the photochemical controlled release of bioactive molecules (adapted from [66]).

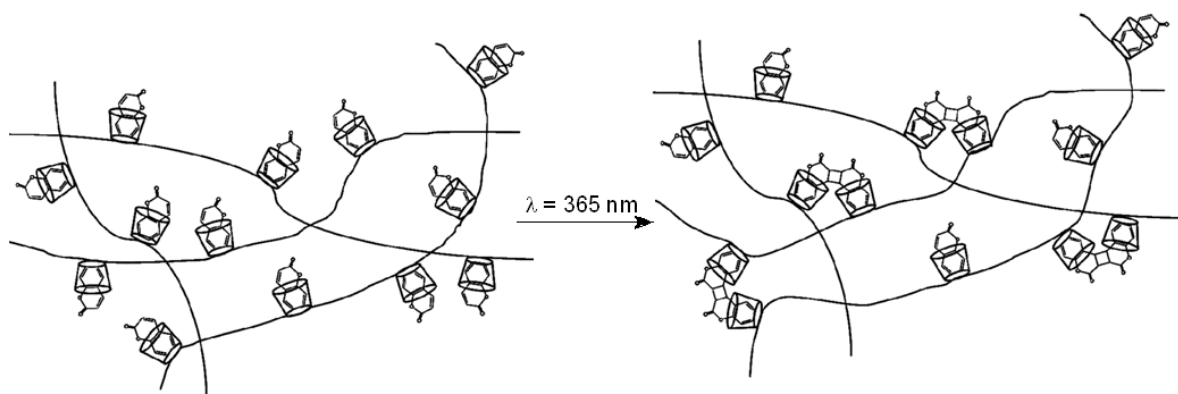


Figure I.9 – Schematic representation of light-induced crosslinking between polymer chains due to coumarin dimerization used in the photochemical control of fluid viscosity (adapted from [68]).

Crosslinking of polymer chains through dimerization of cinnamate derivatives has also been reported. By functionalizing phospholipid polymers randomly with cinnamoyl groups, a photoresponsive hydrogel was obtained, with potential applicability in drug delivery systems due to their biocompatibility.⁶⁹ *p*-Nitrocinnamate was also used for the preparation of a photosensitive gelatin, yielding a smart hydrogel with great biocompatibility, whose swelling properties were addressable with light.⁷⁰

PR fluids based on low-molecular-weight gelators

Low-molecular-weight gelators (LMWGs) have been synthesized based on a wide variety of compounds, from ionic amphiphiles to small biomolecules.^{71,72} These compounds form fibril structures in solution due to intermolecular interactions, such as hydrogen bonding, which may entangle and lead to solutions with high viscosity and elasticity, in a similar fashion to certain polymer solutions. Therefore, in parallel to systems previously described, by introducing photoresponsive moieties into LMWGs molecular structure, it is possible to control intermolecular interaction responsible for gelation with light stimuli, and obtain fluids with photorheological effect.⁷³

Oligopeptides and other amino-acid derivatives are commonly used as gelators due to a combination of interactions such as van der Waals and ionic interactions, π - π stacking and hydrogen bonding that leads to the formation of fibrils. Expectedly, several reports on PR fluids based on LMWGs involve modification of this class of molecules. For instance, two units of phenylalanine were connected by photoresponsive maleic–fumaric acid amides and showed sol-to-gel transition upon UV irradiation. The effect was attributed to morphological transformation at the supramolecular level due to isomerization of the gelator.⁷⁴ In a different work, dialanine functionalized with photoisomerizable spiropyran was applied to obtain a PR fluid with sol-to-gel transition. In this

system, non-planar spiropyran moieties prevent interactions among dipeptide LMWGs while the isomerized merocyanine moieties have a strong tendency to form π - π stacking that can support dipeptide interactions.⁷⁵

Kuang *et al.* functionalized an oligopeptide with *p*-nitrocinnamate to obtain a dendron capable of self-assemble into fibrous network in common organic solvents at low concentrations and form a gel.⁷⁶ Upon irradiation gel to sol transition occurred due to the photodimerization of cinnamate groups which disrupted gel structure (Figure I.10)

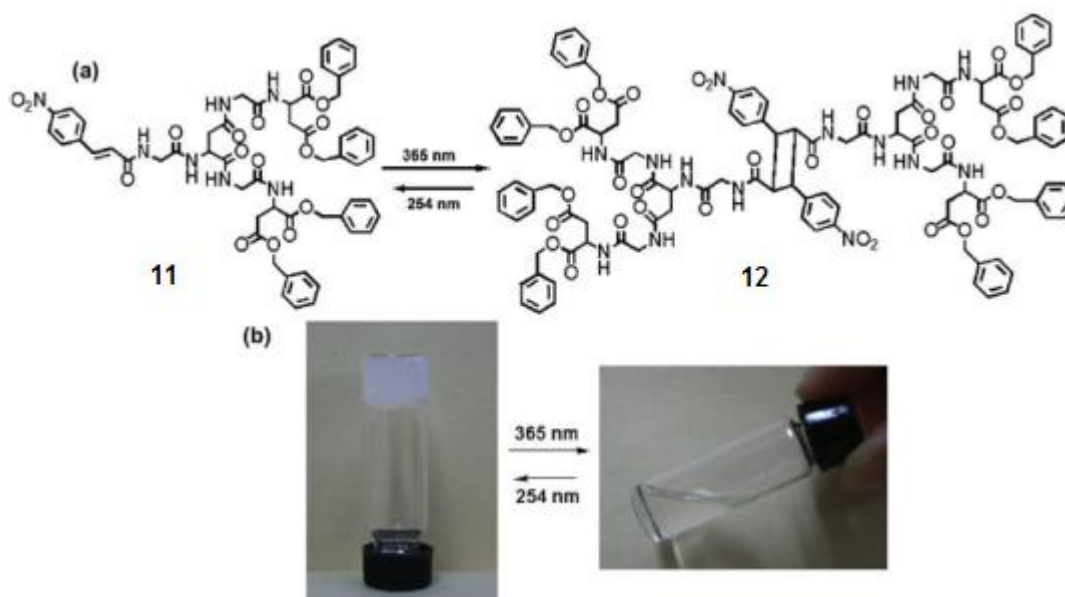


Figure I.10 – (a) Schematic representation of the photoresponse of cinnamate monomer 11 and dimer 12; (b) Photographic images representing the photorheological effect of acetone solutions of 11 (adapted from [76]).

In summary, photorheological fluids have been developed based on a variety of systems, from surfactant solutions to nanoparticle suspensions. In general, these materials give rise to a photorheological effect through the control of molecular aggregation phenomena through irradiation of light. Surfactant-based fluids are currently the most widespread type of PR materials due to their availability and simplicity to prepare, often giving rise to strong viscosity changes upon irradiation. However, the ever-growing need for drug delivery systems *in vivo*, had led to shift in scientific interest towards biocompatible polymers and gels as the basis for the development of novel PR fluids. These systems, while providing strong PR effects, require long preparation processes due to the need for polymer derivatization. Finally, nanoparticle-based PR fluids have shown to give rise to significant viscosity changes, although lacking the reversibility exhibited by surfactant- or polymer-based systems. Therefore, research in PR fluids is still required to develop systems that give rise to strong viscosity changes with good reversibility, while being readily available and biocompatible.

Thesis Overview

The main objective of this thesis research is to develop new photorheological systems based on a variety of photoresponsive moieties that undergo dimerization and/or isomerization reactions.

On Chapter II, the syntheses of tripodal photopolymerizable compounds bearing cinnamate, anthracene and coumarin moieties are described. The photochemical properties are characterized and their capability to undergo photopolymerization is evaluated. The resulting effect on their rheological properties is also investigated.

On Chapter III, the design and synthesis of photoactive ionic liquids bearing cinnamate or coumarin derivatives is described. These compounds are characterized towards physical properties such as melting point and viscosity. In addition, their photochemical reactivity is investigated, and the effect of irradiation of their physical properties is evaluated. In addition, the preparation and photophysical and photochemical characterization of novel coumarin chromophores are also described.

On Chapter IV, the methodology followed for the synthesis and characterization of the compounds presented throughout the thesis is described.

Chapter II

II. Photopolymerizable compounds for photochemical control of rheology

In this chapter, the preparation of photopolymerizable molecules is presented. These compounds were designed as three-branched molecules bearing photodimerizable moieties as chain ends. Through photochemical dimerization/cleavage reactions of these functional groups, it was anticipated that the synthesized tripodal molecules would undergo light-controlled polymerization (Figure II.1) and allow modulation of crosslinking density or molecular weight of the photoreactive polymer.

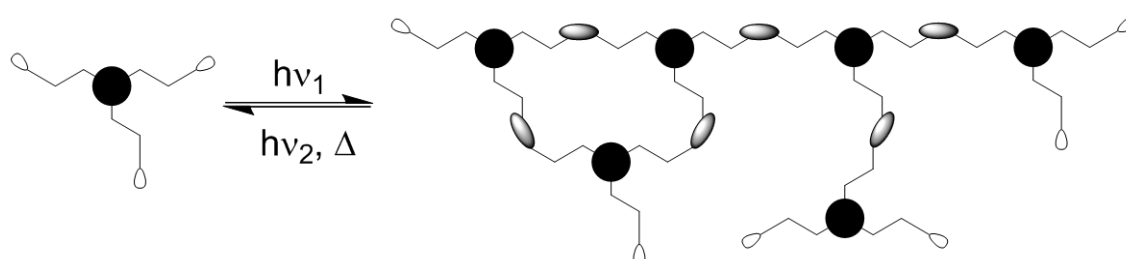


Figure II.1 – Schematic representation of photocontrolled reversible polymerization of tripodal molecules bearing photosensitive moieties.

The formation of polymers by photoinitiated polymerization is the basis of a large variety of commercial applications.⁷⁷ Its use dates back ca. 4000 years to when Egyptians and Babylonians used sunlight to photocrosslink linens during mummification and to waterproof papyrus boats via the photopolymerization of an asphalt oil.⁷⁸ Nowadays, most of these systems rely on free radical polymerization reactions, and are usually composed of acrylate or methacrylate monomers and a free-radical generating photoinitiator. These reactions begin with the formation of a free-radical species through the absorption of light and result in a typical chain growth mechanism.^{79,80} Due to the high speed of this process, photoinitiated free radical polymerization has been used extensively in medical applications, microfluidics or materials engineering.^{79,81} However, although these systems are widely applicable, some disadvantages concerning reversibility and rate control are often presented. Thus, great scientific interest has recently been directed towards thermally reversible photopolymerizable composites in order to expand the range of potential applications. In addition, significant effort to study and control radical termination has been made in the past decades.^{82,83} On the other hand, photodimerization reactions have been used as an alternative to modulate polymerization reactions with great control.⁸⁴ Although significantly slower than free radical generation, photodimerization often presents the advantage of allowing photochemical and thermal reversibility. In addition, they offer the possibility to carry out photopolymerization in the presence of oxygen, which is known to quench radical formation.⁸⁵ Photodimerization reactions occur through [2+2] or [4+4] cycloaddition

mechanism. They belong to the group of pericyclic reactions which usually take place in a concerted way. The most relevant reactions in this group are 4+2-cycloadditions, also known as Diels-Alder reactions.^{86,87,88,89} These thermally initiated reactions are relevant in many biological systems for the formation of six-membered ring structures⁹⁰, besides their widespread use in natural material synthesis⁹¹. On the contrary, [2+2]- and [4+4]-cycloadditions are mostly photochemically induced and form a four-membered cyclobutane ring from two π -bonds or an eight-membered cyclooctane ring from four π -bonds with the formation of new σ -bonds. The differences between thermal and photochemical processes are justified by the molecular orbitals involved in these pericyclic reactions. According to the Woodward-Hoffmann rules, the cycloaddition reactions take place between the highest occupied molecular orbital (HOMO) of one molecule and the lowest unoccupied molecular orbital (LUMO) of another molecule (Figure II. 2). Moreover, the formation of a new binding interaction must be symmetry allowed, i.e., the lobes of the involved orbitals must have the same sign. For example, in a [2+2]-cycloaddition, interaction between HOMO and LUMO is symmetry forbidden and therefore the reaction cannot be thermally initiated.

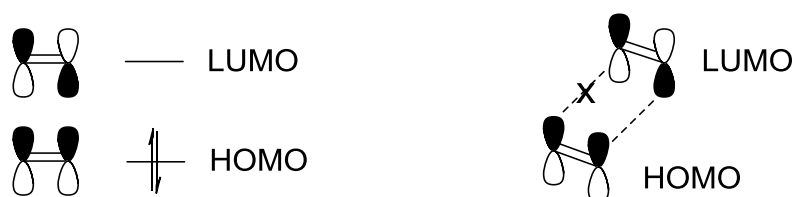


Figure II. 2 – Representation of orbital symmetry of frontier orbitals of generic alkene (left) and symmetry forbidden orbital interaction in a thermal [2+2] cycloaddition (right)

However, the opposite occurs if the reaction is photochemically induced. When an electron is promoted from HOMO to the LUMO by absorption of a photon with the correct energy, two single occupied molecular orbitals (SOMO) are formed (Figure II. 3). Thus, when a molecule in the excited state approaches a molecule in the ground state, two binding interactions can be established between the two SOMO of the excited molecule and the LUMO and HOMO of the ground state molecule, resulting in the formation of two new σ -bonds. (Figure II. 3)

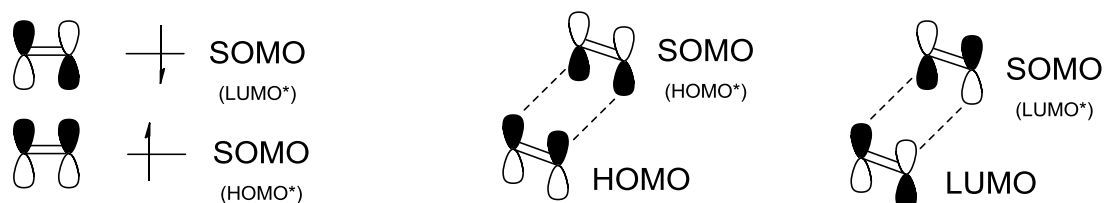


Figure II. 3 – Frontier orbitals of generic alkene in the excited state (left) and symmetry allowed orbital interactions in a photochemical induced [2+2]-cycloaddition (right)

The change in molecular orbital symmetry can be demonstrated by computational studies (Figure II. 4) on unsubstituted coumarin **4**, which is one of the most applied photosensitive moieties in

a variety of smart materials due to its well characterized photodimerization reactions. In particular, several photorheological fluids based on the photoinduced dimerization of such molecules has been previously described.^{27,65,67}

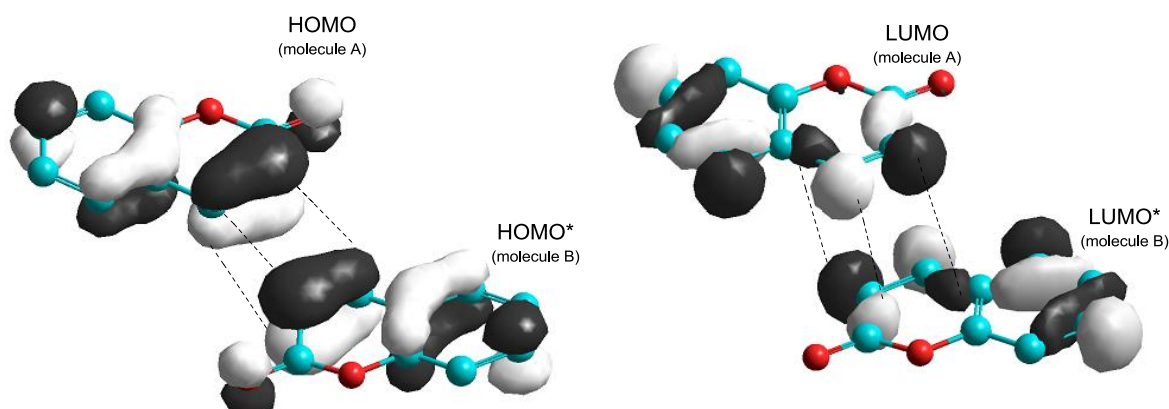


Figure II. 4 – Symmetry allowed frontier orbital interactions between one coumarin molecule in the ground state and one molecule in the excited state

II.1 – Low molecular-weight photopolymerizable molecules

The first set of tripodal photopolymerizable molecules described in this chapter were synthesized using tris(2-aminoethyl)amine, **13** (Figure II.5), as triple-branched backbone, which was functionalized with photoresponsive moieties through nucleophilic addition/elimination reaction with acyl chlorides, obtained from the corresponding carboxylic acid derivatives as described in schemes Scheme II. 1-3.

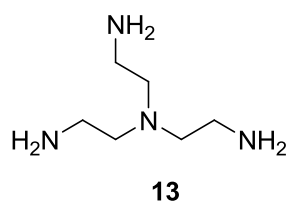
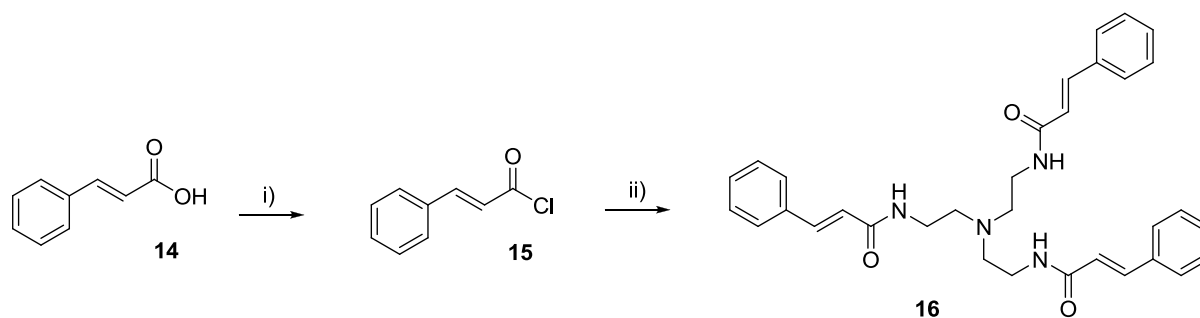


Figure II.5 – Molecular structure of tris(2-aminoethyl)amine 13

This synthetic strategy allowed for the preparation of molecules bearing three amide moieties, which are important functions in the establishment of intermolecular hydrogen-bond type interactions, necessary for the formation of several organogels.^{92,93}



Scheme II. 1 - Synthetic pathway for the preparation of tripodal cinnamic acid derivative 16: i) thionyl chloride, chloroform, 89%; ii) tris(2-aminoethyl)amine, K_2CO_3 or NEt_3 , dichloromethane, 91% or 34%, respectively

Compound **16** was prepared through condensation of cinnamoyl chloride **15** and **13** in dichloromethane. Initially, this reaction was carried out in the presence of triethylamine in order to remove the hydrogen chloride byproduct and prevent ester hydrolysis. After formation of **16**, removal of the base catalyst was achieved through flash chromatography. However, when triethylamine was replaced with potassium carbonate, the reaction yield improved significantly (34 to 91%). In addition, the base catalyst could be removed by filtration, and chromatography purification was not necessary. The photochemical properties of **16** were investigated in chloroform solution. The UV-Vis spectrum is in agreement with the expected spectra for unsubstituted *trans*-cinnamic acid derivatives, with the characteristic strong charge transfer $\pi_{\text{styryl}}-\pi^*_{\text{carbonyl}}$ band at ca. 270 nm, the weak $\pi_{\text{styryl}}-\pi^*_{\text{styryl}}$ band at ca. 300 nm and an additional band at lower wavelengths (Figure II.6a).⁹⁴ Upon irradiation at 300 nm, spectral transformations were detected, which suggest that a photochemical process takes place. As previously mentioned, cinnamic acid derivatives are known to undergo two main photochemical reactions upon irradiation, *trans*-to-*cis* photoisomerization and [2+2] photocycloaddition. Both reactions give rise to similar spectral transformations characterized by a decrease in absorbance around the absorption maximum and an increase at shorter wavelengths. However, UV-Vis spectra obtained for irradiated solutions of **16** show that the variations are not in accordance with isomerization nor dimerization reactions. Whilst a decrease in absorbance at ca. 270 nm is detected, an increase at lower wavelengths was not observed, suggesting that *trans*-cinnamate moieties in **16** do not undergo dimerization or isomerization (Figure II.6a). Moreover, the absence of isosbestic points in these spectra indicates that a photodegradation process may occur upon irradiation. In addition, determination of the reaction quantum yield shows that the reaction rate is not affected by concentration of **16** (Figure II.6b), thus, evidencing that a bimolecular process such as photodimerization does not occur upon irradiation.

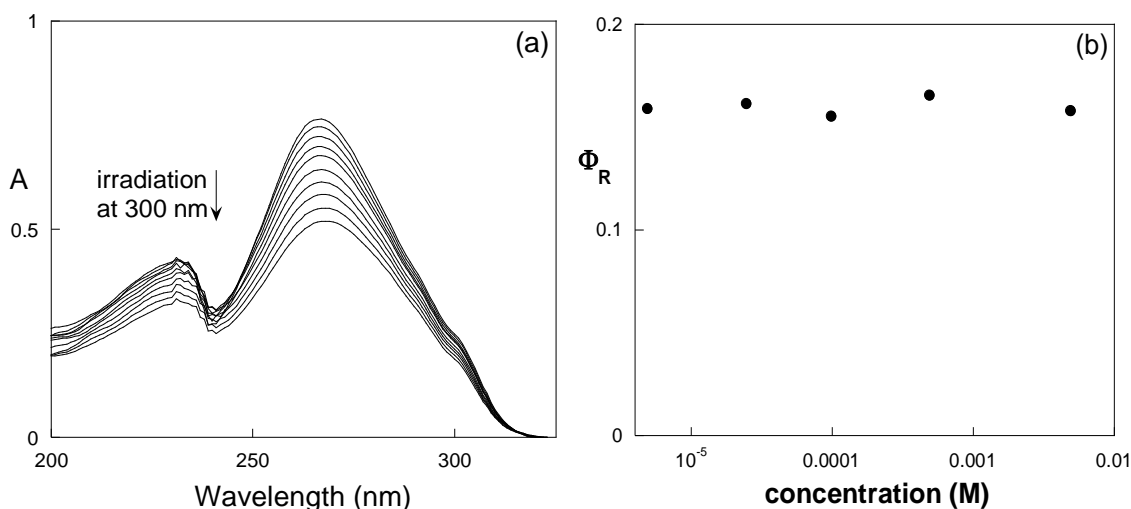


Figure II.6 – (a) UV-Vis spectral modifications of 1.1×10^{-5} M **16 in chloroform upon irradiation at 300 nm. Total irradiation time is 20 min; (b) Photochemical quantum yield dependence on concentration of **16**.**

To shed light on the nature of the photochemical process taken by compound **16**, irradiated solutions were analyzed by NMR spectroscopy. Both isomerization and dimerization photoproducts could, in principle, be detected by the presence of characteristic peaks, such as doublet at ca. 6.0 ppm with a coupling constant of ca. 12 Hz corresponding to the α -protons of the *cis*-cinnamate moieties or multiplets with lower chemical shifts (3.5–4.5 ppm) corresponding to the cyclobutane protons arising from photodimerization. However, the complexity of the ^1H NMR spectrum obtained for irradiated chloroform solutions of **16** suggests that multiple photoproducts are formed upon irradiation (Figure II. 7). Whilst the peaks corresponding to unreacted *trans*-**16** are still discernible, in particular the doublets at 6.6 and 7.6 ppm corresponding to the α - and β - protons of the cinnamate moieties, respectively, a large variety of peaks with undefined multiplicity are present in both the aliphatic and aromatic regions of the spectrum. Moreover, the characteristic peaks of the expected photoproducts are absent, which is in accordance with the spectral changes previously observed in the UV spectrum upon irradiation (Figure II.6a). Thus, through spectroscopic analysis of irradiated solutions of **16**, it was evidenced that its cinnamate moieties do not undergo the expected photochemical reactions of *trans*-to-*cis* irradiation or [2+2] cycloaddition. Instead, photodegradation into a variety of compounds seems to be the apparent photochemical pathway. It is proposed that photo-oxidation of the tertiary amine moiety is the main photodegradation pathway.⁹⁵

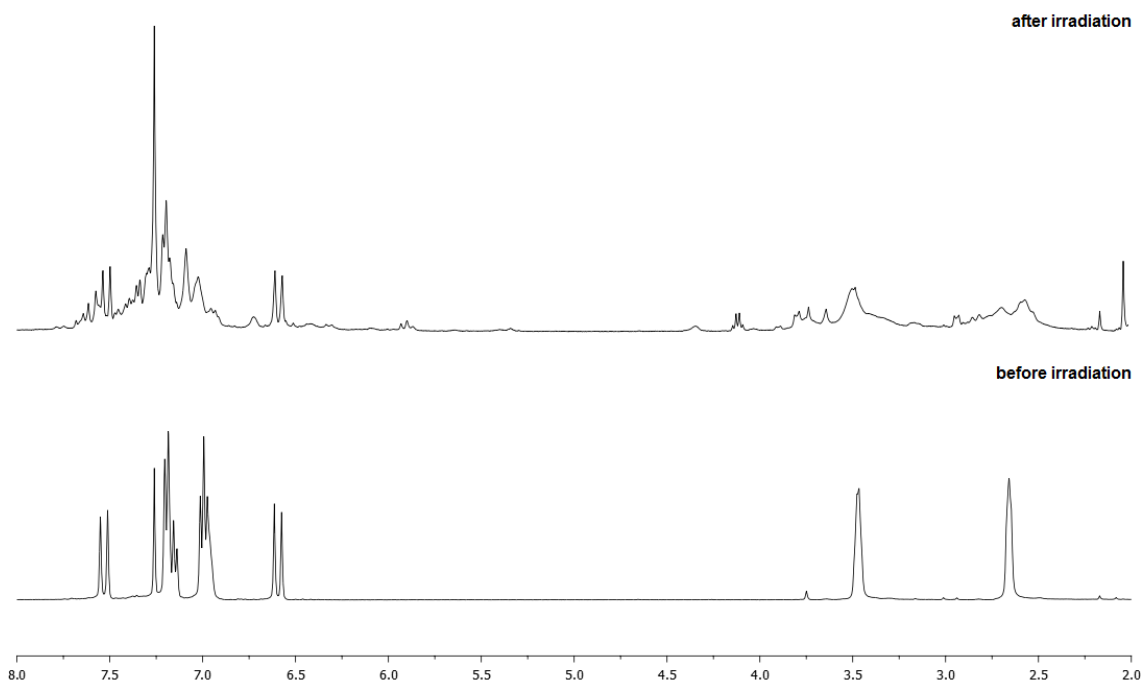
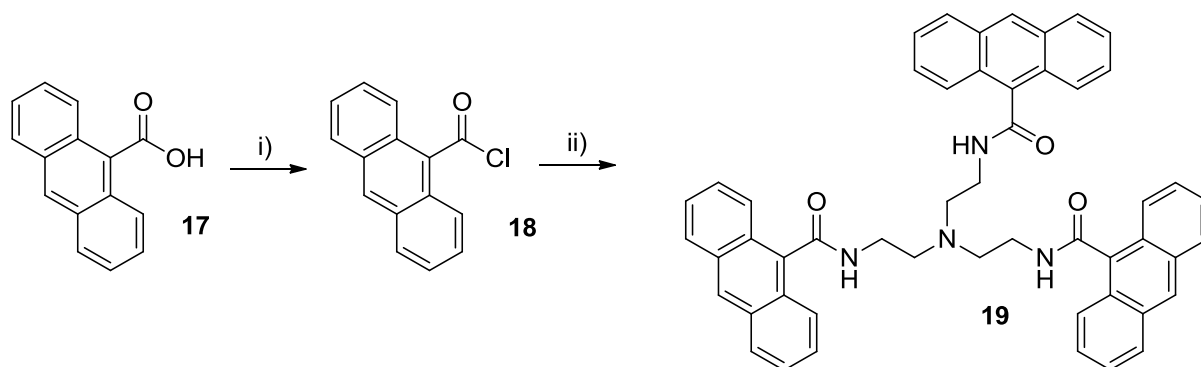


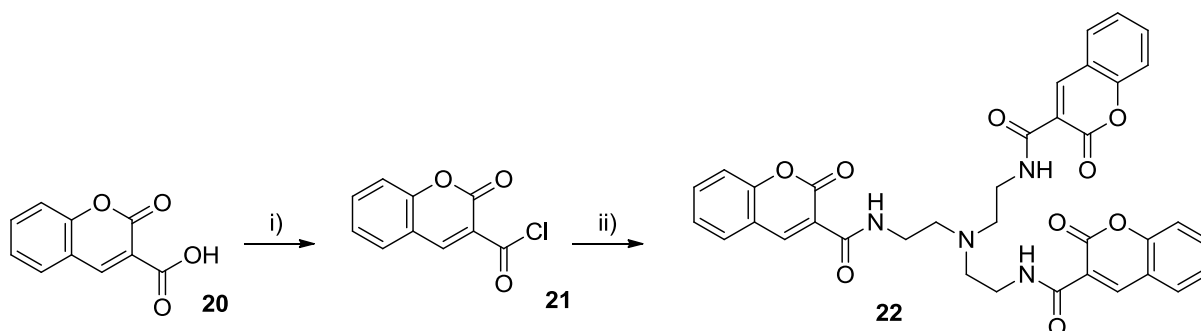
Figure II. 7 – ^1H NMR spectra of **16** in chloroform acquired before and after irradiation at 300 nm.

It was demonstrated that the selected cinnamate moiety was inadequate to induce the anticipated photopolymerization of low molecular-weight tripodal molecules. Therefore, it was replaced with an anthracene moiety in the design of a different tripodal compound. As previously mentioned, anthracene derivatives undergo photochemical dimerization through [4+4] cycloaddition. In addition, unlike cinnamic acid derivatives, the photodimerization quantum yield of anthracene derivatives is usually rather high.^{96,97} This is due to the fact that the excited state lifetime of anthracene derivatives is usually long lived (10-20 ns).⁹⁸ For this reason, anthracenes have been widely used in photorheological systems, as shown in the previous chapter.^{22,23,62,66} Thus, tripodal compound **19** was designed, and its synthetic pathway followed the same strategy used for the preparation of compound **16** (Scheme II.2). Anthracene-9-carboxyl chloride, **18**, was readily prepared from anthracene-9-carboxylic acid **17** in the presence of thionyl chloride in chloroform solution. However, the condensation reaction with **13** in the presence of triethylamine did not yield the envisioned trianthracene derivative **19**. In fact, NMR spectroscopic data collected after purification of the reaction mixture evidenced that only the mono-anthracene derivative was prepared. It is expected that the large size of the anthracene moiety gives rise to significant sterical hindrance, thus, inhibiting the condensation reaction on the primary amine moieties of compound **13**. The same results were obtained when triethylamine base catalyst was replaced with potassium carbonate.



Scheme II.2 – Synthetic pathway for the preparation of tripodal anthracene derivative **19**: i) thionyl chloride, chloroform; ii) tris(2-aminoethyl)amine, K_2CO_3 or NEt_3 , dichloromethane

It was envisioned that the sterically hindered anthracene moiety could be replaced with a less bulky chromophore that also undergoes photochemical dimerization. In the previous chapter, it was demonstrated that coumarin moieties give rise to dimerization reactions in a variety of systems. In particular, these reactions have been explored in the control of viscosity in photorheological fluids. Although the photodimerization quantum yield for these compounds is generally lower than for anthracene derivatives, it is still significantly higher than those exhibited by cinnamic acid moieties due to the difference in their excited state lifetimes.^{99,100,101,102} Thus, coumarin-3-carboxylic acid **20** was selected as the photosensitive precursor allowing derivatization into a tripodal molecule with the same synthetic strategy used for the preparation of **16**. In this case, replacing the triethylamine base catalyst with potassium carbonate also resulted in better reaction yields and a more simplified purification process. Thus, compound **22** was obtained from coumarin-3-carboxylic acid in a two-step reaction in good yield (Scheme II. 3).



Scheme II. 3 - Synthetic pathway for the preparation of tripodal coumarin derivative **22**: i) thionyl chloride, chloroform, 90%; ii) tris(2-aminoethyl)amine, K_2CO_3 or NEt_3 , dichloromethane, 95%

The photochemical properties of **22** were investigated in chloroform solution with UV-Vis spectroscopy. The absorption spectrum **22** exhibits two bands without vibrational structure in the UV region at approximately 300 and 350 nm, corresponding to the typical π - π^* transitions associated to the charge transfer from the benzenic cycle to the pyranone moiety of basic coumarin skeletons

(Figure II. 8a).¹⁰³ These transitions are associated to an excitation from the HOMO and the HOMO-1 orbital, respectively, to the LUMO. Due to the presence of an electron-withdrawing amide moiety group at position 3, the absorption maxima of **22** are shifted bathochromically (~30–40 nm) in comparison with unsubstituted coumarin.¹⁰⁴ In addition, the calculated molar absorptivity value ϵ of 38893 M⁻¹ cm⁻¹ is approximately three times higher than that of unsubstituted coumarin (ca. 9000-12500 M⁻¹ cm⁻¹, depending on solvent polarity), due to the presence of three independent chromophores.¹⁰⁴

In order to evaluate the photochemical properties of compound **22**, irradiation at the longest wavelength transition (330 nm) was carried out and the transformations were followed by UV-Vis spectroscopy. Absorption spectra of chloroform solutions of **22** show that upon irradiation a photochemical reaction takes place, indicated by the spectral transformations depicted in Figure II. 8a. These changes are in agreement with the expected photodimerization reaction described for coumarin derivatives. However, these results are insufficient to determine whether the photodimerization occurs between two coumarin units from the same three-branched molecule or from different molecules. Therefore, Φ_R values were calculated for irradiated chloroform solutions at different concentrations of **22**. It was evidenced that the photochemical reaction quantum yield increased with increasing concentration, suggesting that dimerization process of **22** under the studied conditions is intermolecular (Figure II. 8b). NMR spectra obtained for chloroform solutions of **22** before and after irradiation are also in agreement with a photodimerization reaction pathway (Figure II. 9). This is evidenced by the low intensity peaks that become visible in the ¹H NMR spectrum after irradiation. The peaks at low field correspond to the amide and aromatic protons of the coumarin dimers and therefore, the chemical shifts are close to those of unreacted **22**. At high field, the singlet at ca. 3.5 ppm corresponds to protons of the cyclobutane moiety formed upon dimerization. The fact that only one signal corresponding to cyclobutane moieties is present may be indicative that only one isomer is formed upon dimerization.

By UV-Vis spectroscopy, it was also observed that, at higher concentrations, irradiation led to increased light-scattering due to the formation of small particles, evidenced by the absorbance spectra depicted in Figure II. 8c.

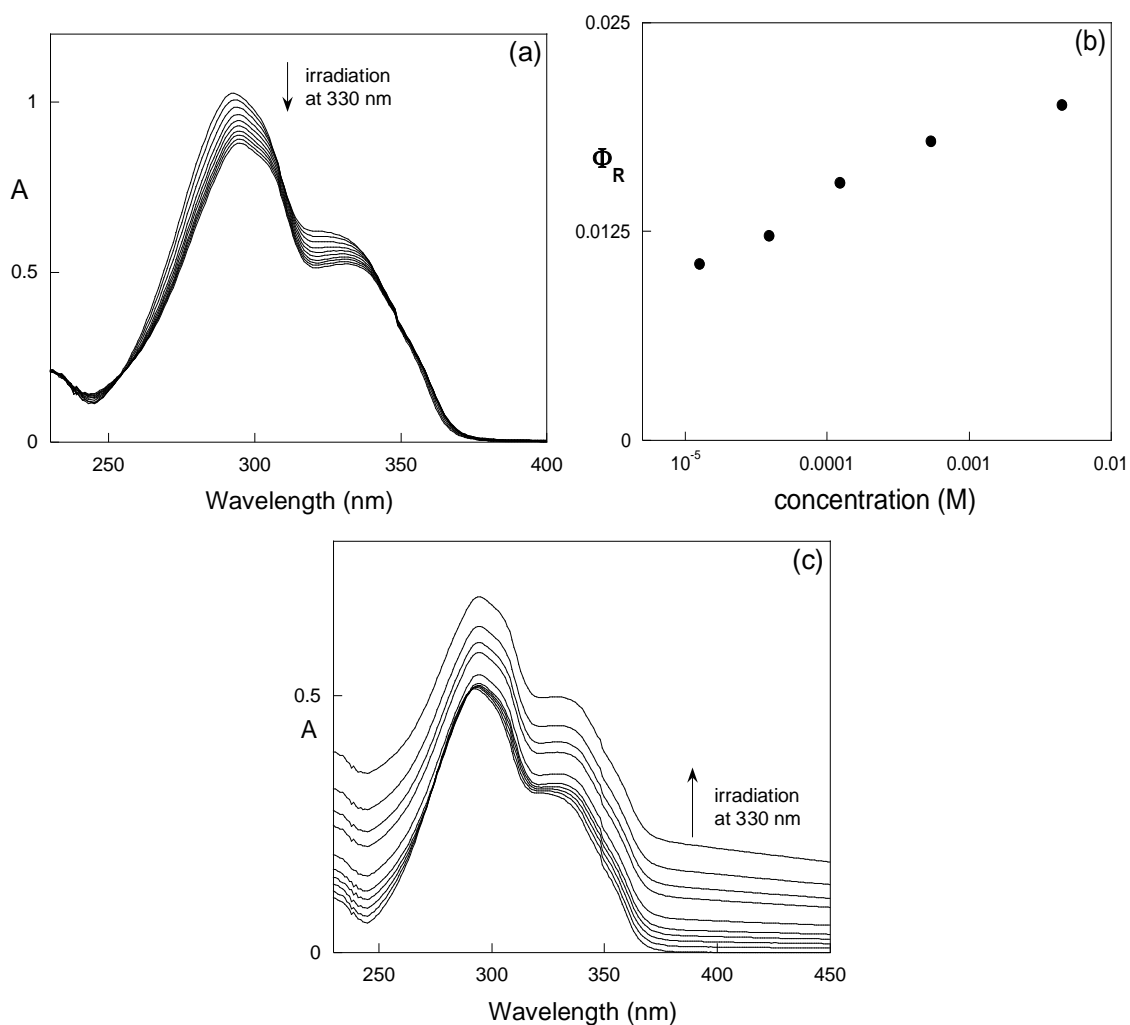


Figure II. 8 – (a) UV-Vis spectral modifications of chloroform solution of 22 at 1.0×10^{-5} M upon irradiation at 330 nm. Total irradiation time is 60 min; (b) Photochemical quantum yield variation with increasing concentration of 22; (c) Precipitation-induced UV-Vis spectral modifications of a 2.0×10^{-3} M solution of 22 in chloroform upon irradiation at 330 nm. Total irradiation time is 40 min.

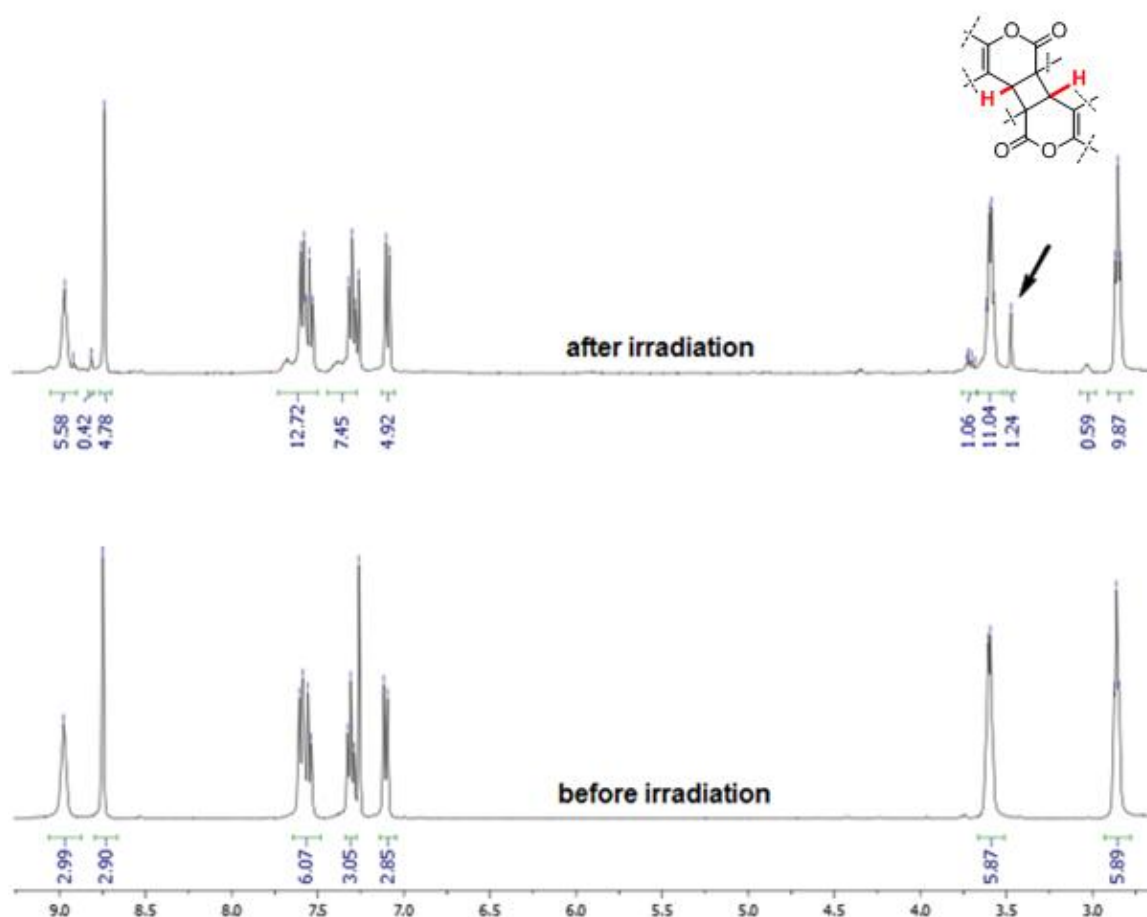


Figure II. 9 – ^1H NMR spectra of **22** acquired before and after irradiation at 330 nm in chloroform.

Therefore, it was hypothesized that irradiation of concentrated solutions of **22** led to the formation of oligomers that precipitated due to low solubility in the selected solvent, giving rise to small particle suspensions. This effect was monitored with Dynamic Light Scattering (DLS) spectroscopy. This technique measures the random thermal motion of suspended particles, known as Brownian motion, which arises from collisions between the particles and solvent molecules. This random motion is modeled by the Stokes-Einstein equation (II.1), where D_h is the hydrodynamic diameter, D_t is the diffusion coefficient, k is the Boltzmann constant, T the temperature and η the dispersant liquid viscosity:

$$D_h = \frac{kT}{3\pi\eta D_t} \quad \text{II.1}$$

When light is shined in a suspension, it is scattered in all directions and the Brownian motion of the particles generates a fluctuation in the scattered light intensity. The fluctuating signal is measured across very short time intervals, τ , to produce a correlation curve, C , with an exponential decay function (equation II.2), where q is an instrumental factor dependent on the solvent refractive

index, laser wavelength and scatter angle, and from which the diffusional coefficient, D_t is extracted. From equation II.1, particle size can be calculated.

$$C = \exp(-2D_t q^2 \tau) \quad \text{II.2}$$

Figure II. 10a depicts the correlation curves obtained for chloroform solutions of **22** with increasing irradiation time lengths. It is shown that irradiation leads to correlation curves with longer decay times, which is caused by a reduction of diffusional motion of particles. From Stokes-Einstein equation, it is demonstrated that this effect can be derived by either an increase in system viscosity, η , or an increase in particle size, D_h . In order to determine whether the changes observed in DLS spectroscopic measurements were caused by the growth of the detected nanoparticles, samples irradiated for different time lengths were analyzed with atomic-force microscopy (AFM). This technique belongs to the class of scanning probe microscopies, which can measure local properties such as height, friction or conductivity with an appropriate probe. Atomic-force microscopes operate measuring force between sample and a probe with a sharp, nanometric tip. Thus, topographical images with high resolution at the nanoscopic scale can be obtained.¹⁰⁵ Figure II. 10c-d depicts two AFM images obtained for irradiated solutions of **22** collected at different irradiation time lengths. In both samples, spherical shaped particles were detected. However, particle size varies significantly with irradiation length. It is shown that after 10 minutes of irradiation, i.e., the time at which the first particles are detected by DLS spectroscopy, particles with diameters of ca. 100 nm are observed (Figure II. 10c), whereas longer irradiation yielded larger particles, with particles with ca. 400 nm being observed after irradiating for 400 minutes (Figure II. 10d). Thus, it was evidenced through AFM imaging that the reduction of diffusion coefficient D_t detected by DLS spectroscopy was caused by an increase in particle size induced by irradiation rather than an increase in viscosity. With the Stokes-Einstein equation II.1, it is possible to calculate the mean size of suspended particles and it is evidenced that they show a virtually linearly dependence with irradiation time length, as depicted in Figure II. 10b. Repeating the irradiation experiments at different concentrations of **22** shows that the growth rate of these particles is significantly affected by concentration, which is in accordance with the results obtained for Φ_R measurements (Figure II. 8).

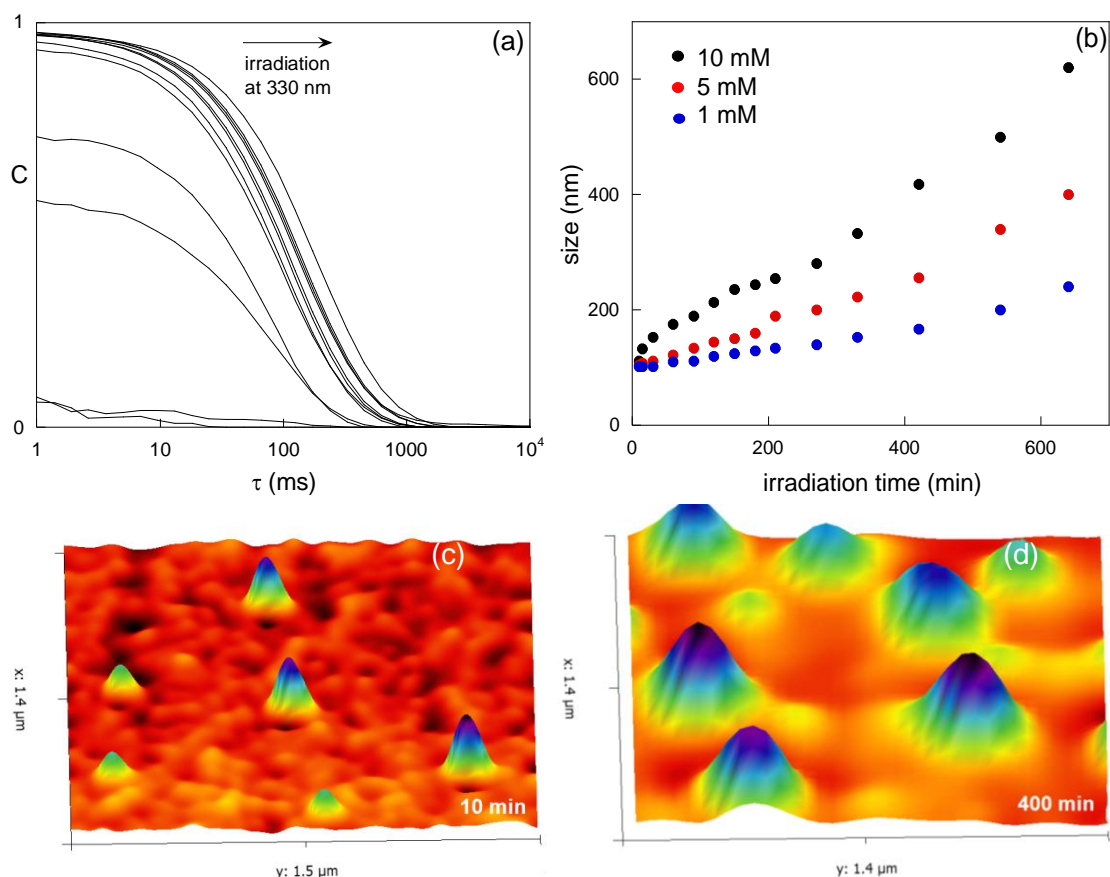


Figure II. 10 – (a) Correlation curve variation upon irradiation at 330 nm of a solution of **22** at 8.3×10^{-3} M in chloroform; (b) Time and concentration dependence of photoinduced growth of dendrimeric nanoparticles of **22** in chloroform; (c) and (d) AFM images of a suspension of dendrimeric nanoparticles of **22** obtained after 10 and 400 minutes of irradiation at 330 nm, respectively.

It was hypothesized that intermolecular photochemical dimerization of coumarin moieties of **22** results in photopolymerization into insoluble oligomers that grow dendrimERICALLY with continuous irradiation through photochemical dimerization of terminal coumarin moieties with solvated **22** monomers (Figure II. 11).

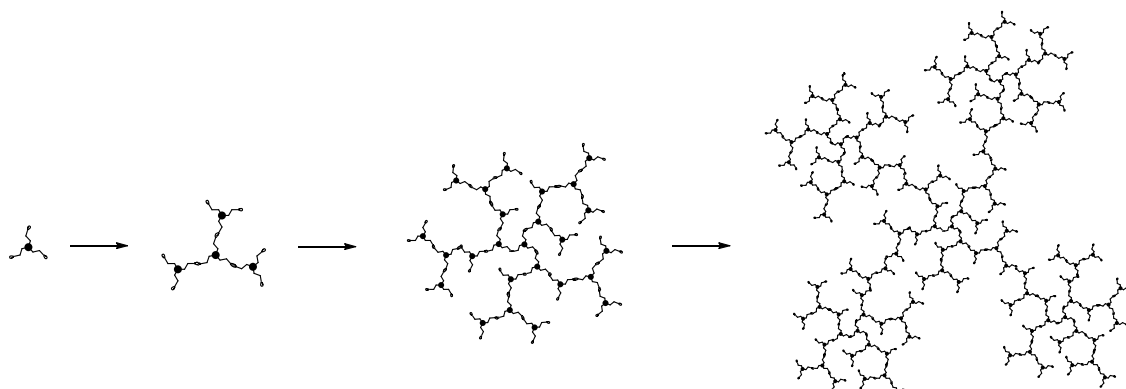


Figure II. 11 – Schematic representation of the proposed photoinduced dendrimERIC growth of nanoparticles of **22** due to dimerization of coumarin moieties.

Conclusions

In conclusion, photopolymerizable compounds based on coumarin and cinnamic acid were designed and prepared from readily available photosensitive precursors in good yields. Their photochemistry in organic solution was characterized and it was evidenced that intermolecular photodimerization reaction occurred upon irradiation in the case of coumarin derivatives. Photochemical quantum yields were determined and the obtained values were low, resulting in low conversion levels after long irradiation periods. Therefore, no photorheological effect was determined. In addition, it was demonstrated that coumarin derivative gave rise to insoluble aggregates of nanometric size upon irradiation, which were analyzed by DLS spectroscopy and atomic force microscopy. It was evidenced that photopolymerization of **22** lead to the formation of oligomers that grow dendrimERICALLY into spherical nanoparticles during irradiation at absorption maximum. In order to increase the quantum yield for the photopolymerization of three-branched compounds, synthesis of an anthracene derivative was attempted. Due to high sterical hindrance by anthracene moieties, tri-functionalized compound was not obtained. Therefore, it is necessary to review the design of such compounds in order to increase the solubility of the resulting photoproducts and also the photochemical quantum yield.

II.2 – High-molecular weight photopolymerizable compounds

In this chapter, the preparation of high molecular-weight photopolymerizable compounds is presented. Similarly to the compounds described in the previous chapter, these molecules were designed as three-branched structures bearing photodimerizable units. However, in order to increase solubility and prevent precipitation of the final photoproducts, tris(2-aminoethyl)amine **13** was replaced with tris(tetraethyleneglycol)phloroglucinol **23** (Figure II.12). In addition, different photosensitive derivatives were used in order to increase chemical reactivity and prevent the formation of byproducts. The followed synthetic pathways are summarized in Scheme II. 4-7.

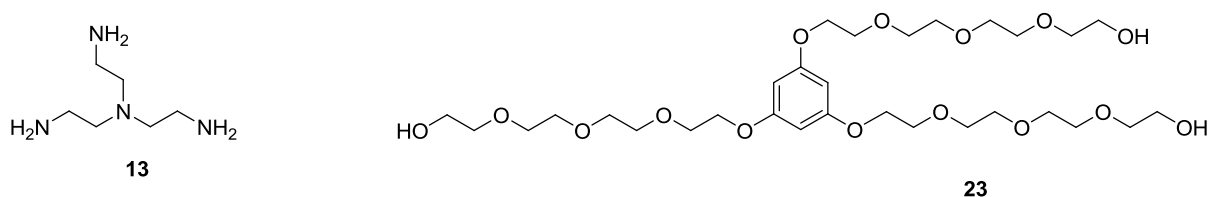
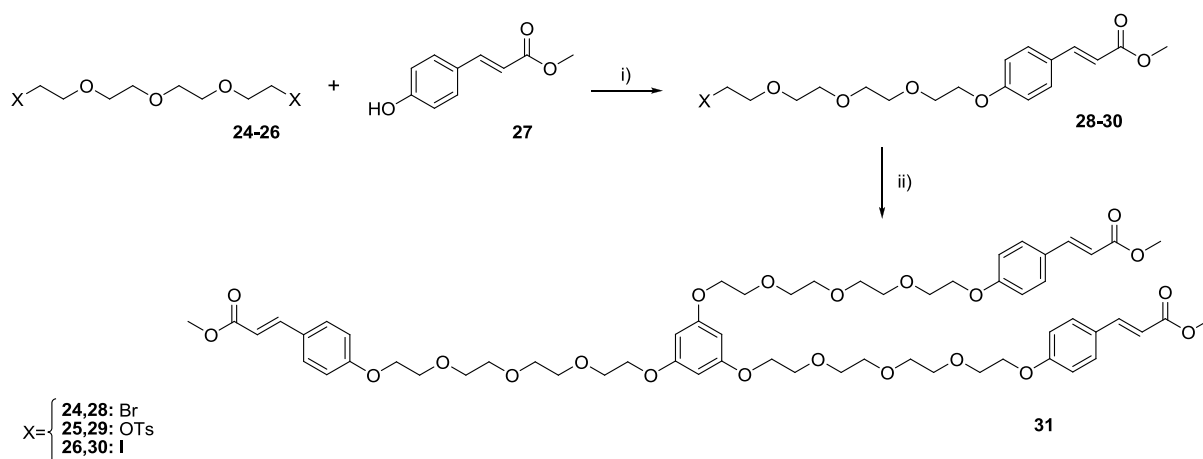


Figure II.12 – Molecular structures of backbones used for the preparation of photopolymerizable tripodal compounds: tris(2-aminoethyl)amine and tris(tetraethyleneglycol)phloroglucinol **23**.

Compound **31** was prepared in four steps from tetraethyleneglycol, TEG, and *p*-coumaric acid. TEG was derivatized into 1,13-dibromotetraethyleneglycol **24** in the presence of triphenylphosphine and bromine in acetonitrile providing two leaving groups suitable for S_N-type reactions. *p*-Coumaric acid was derivatized into its methyl ester **27**, through an acid-catalyzed esterification in methanol in order to allow the phenolic moiety to be used as a nucleophile in S_N-type reaction with **24** to yield cinnamate-tetraethyleneglycol-bromide conjugate **28**. This compound was reacted with phloroglucinol to obtain the desired final product **31**. The final step yield was considerably low (<10%), which was attributed to the low reactivity of bromide as a leaving group. Thus, compound **24** was replaced with 1,13-ditosyltetraethylene glycol **25** due to the higher reactivity of tosylate as a leaving group. However, this strategy failed to improve the overall reaction yield. It was observed that the polarity of conjugate **29** and its precursor **25** was very similar, rendering impossible the purification through common chromatographic techniques. Therefore, the process was repeated replacing **25** with 1,13-diiodotetraethylene glycol **26**. In principle, iodide has reactivity lower than tosylate but higher than bromide, which should lead to better reaction yields in the synthesis of **31**. However, although this strategy allowed resolution of reaction mixture in the preparation of **30**, final step yield was not significantly improved (8.6%).



Scheme II. 4 – Synthetic pathway for the preparation of tripodal cinnamate derivative **31**: i) K_2CO_3 , acetone, 72%; ii) phloroglucinol, K_2CO_3 , acetonitrile, 8.6% (for precursor **30**).

The photochemical properties of **31** were investigated in solution, and its ability to undergo photopolymerization was tested. The obtained UV spectrum and molar absorptivity ϵ values are in agreement with the expected results for *p*-coumaric acid derivatives.⁸⁴ The band centered at ca. 300 nm corresponds to π - π^* transitions of the cinnamate moieties and is bathochromic shifted, when compared to the spectra of native cinnamate esters, due to the substituent at *para* position of the coumarate moiety (Figure II. 13). Therefore, the weak band related with $\pi_{\text{styryl}}-\pi^*_{\text{styryl}}$ could not be detected. In addition, the strong absorption band below 250 nm corresponds to electronic transitions in benzene rings of both coumarate and phloroglucinol moieties. Upon irradiation at 300 nm, changes in the UV spectrum of **31** were detected. In fact, there is a decrease in absorbance in the low energy band, with a minor hypsochromic shift in absorption maximum and a concomitant increase in absorbance at lower wavelengths (Figure II. 13). These spectral transformation are consistent with *trans*-to-*cis* isomerization and [2+2]-cycloaddition that can occur in coumarate moieties. The photochemical quantum yield Φ_R was determined at different concentrations in order to determine the nature of the process. Figure II. 13b shows that varying concentration did not yield changes in Φ_R , suggesting that an intramolecular reaction takes place upon irradiation. These results could arise from both *trans*-to-*cis* isomerization or [2+2]-cycloaddition between two coumarate moieties in the same molecule. Therefore, ^1H NMR spectra of irradiated solution were collected to shed light on the photochemical reactivity of **31**. The spectrum depicted in Figure II. 14, obtained after photostationary state was achieved, evidences that only photoisomerization takes place upon irradiation. This conclusion is supported by the appearance of a doublet at 5.8 ppm with coupling constant of 12 Hz, corresponding to the α -protons of *cis*-coumarate moieties and the lack of new signals at 3.5-4.5 ppm, which would indicate the presence of cyclobutane moieties resulting from photodimerization.

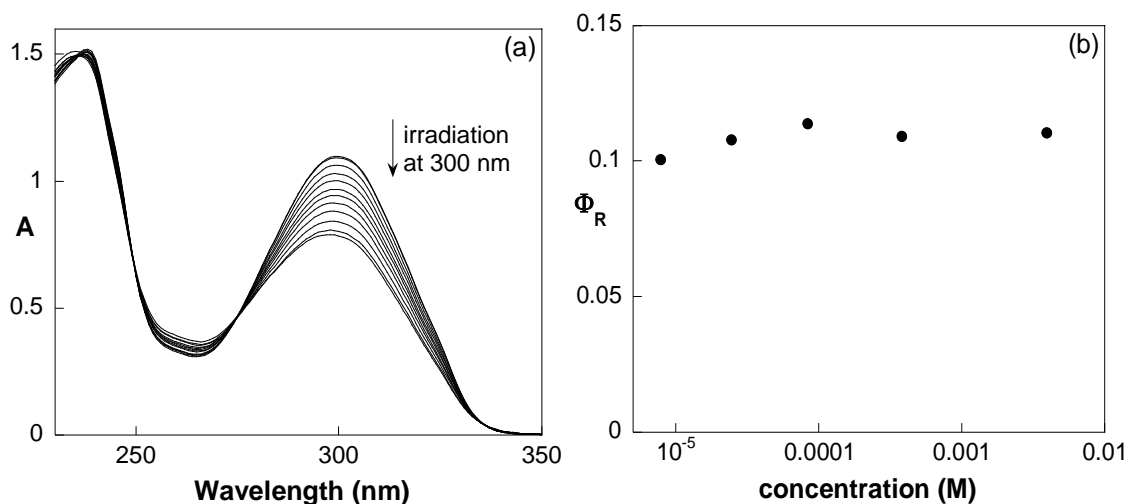


Figure II. 13 – (a) UV-Vis spectral modification of a solution of 1.4×10^{-5} M **31** in chloroform upon irradiation at 300 nm. Total irradiation time is 20 min; (b) Photochemical quantum yield dependence on concentration of **31**.

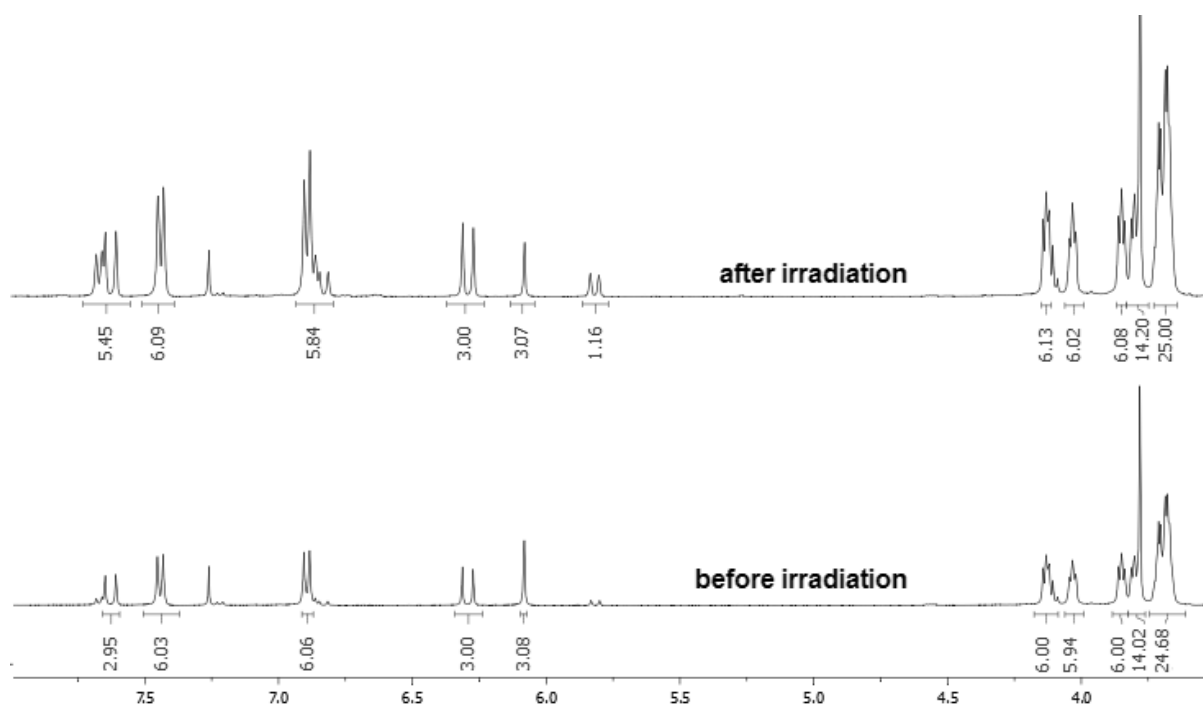
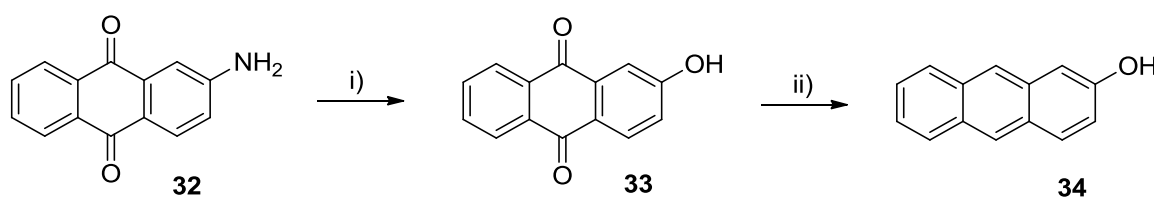


Figure II. 14 – ^1H NMR spectra of **31** in chloroform before and after irradiation at 300 nm.

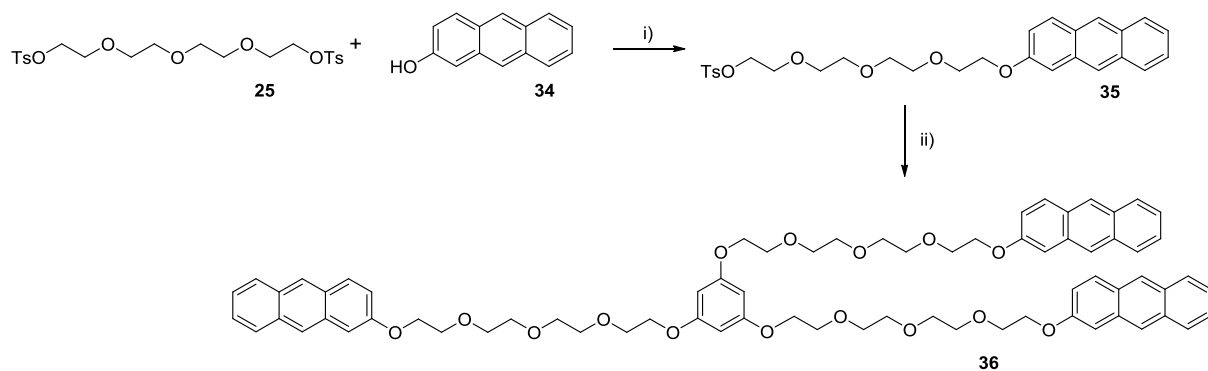
These results show that cinnamate derivatives were not adequate to give rise to photopolymerization in molecules with tripodal backbones through photoinduced [2+2]-cycloaddition. The fact that cinnamate derivatives may undergo an additional photochemical process, i.e., photoisomerization, in addition to the typically low excited state lifetime of these moieties lead to low dimerization quantum yields and justify why it did not occur upon irradiation of **31**.

Following the same strategy described previously for low molecular weight tripodal compounds (chapter II.1), the cinnamate moieties were replaced with anthracene derivatives. Due to the higher excited state lifetime, and, consequently the higher photodimerization quantum yield of anthracenes it was envisioned that the synthesized compound would undergo photopolymerization upon irradiation and allow the anticipated photochemical control of viscosity of its organic solutions. Therefore, the synthesis of a tripodal anthracene derivative was attempted. 2-hydroxy-anthracene **34** was selected as the photoresponsive moiety and prepared from 2-amino-anthraquinone **32** in a two-step reaction (Scheme II. 5) with an overall low reaction yield for the synthesis of **34** (13%).



Scheme II. 5 – Synthetic pathway for the preparation of anthracene precursor **34**: i) NaNO₂, NaOH, water, 53%; ii) NaBH₄, methanol, 24%

Nonetheless, compound **34** was used as a nucleophile in the synthesis of compound **35**, which was reacted with phloroglucinol in the presence of potassium carbonate to obtain **36** in good yield (Scheme II. 6).



Scheme II. 6 – Synthetic pathway for the preparation of tripodal anthracene derivative **36**: i) K₂CO₃, acetone, 76%; ii) phloroglucinol, K₂CO₃, acetonitrile, 61%.

The photochemical properties of **36** were investigated by UV-Vis spectroscopy. The obtained UV spectrum is in agreement with the expected results for anthracene derivatives, with a strong absorption band centered at 350 nm with several maxima, corresponding to vibrational sub-levels.¹⁰⁶ In addition, the absorption bands are bathochromically shifted when compared to native anthracene derivative, due to the electron donating effects of the alkoxy moiety at position 2. Upon irradiation of chloroform solutions of **36** at 360 nm, transformations in the UV spectrum were observed (Figure II. 15a). The decrease in absorbance at absorption maxima is consistent with the anticipated

photodimerization reaction of anthracene derivatives. In addition, determination of Φ_R values in solutions of **36** showed that the reaction photochemical reaction rate increases on the concentration of **36**, which suggests that intermolecular [4+4]-cycloaddition occurs upon irradiation (Figure II. 15b). To corroborate this hypothesis, ^1H NMR spectrum of a solution of **36** was collected before and after irradiation at 360 nm (Figure II. 16).

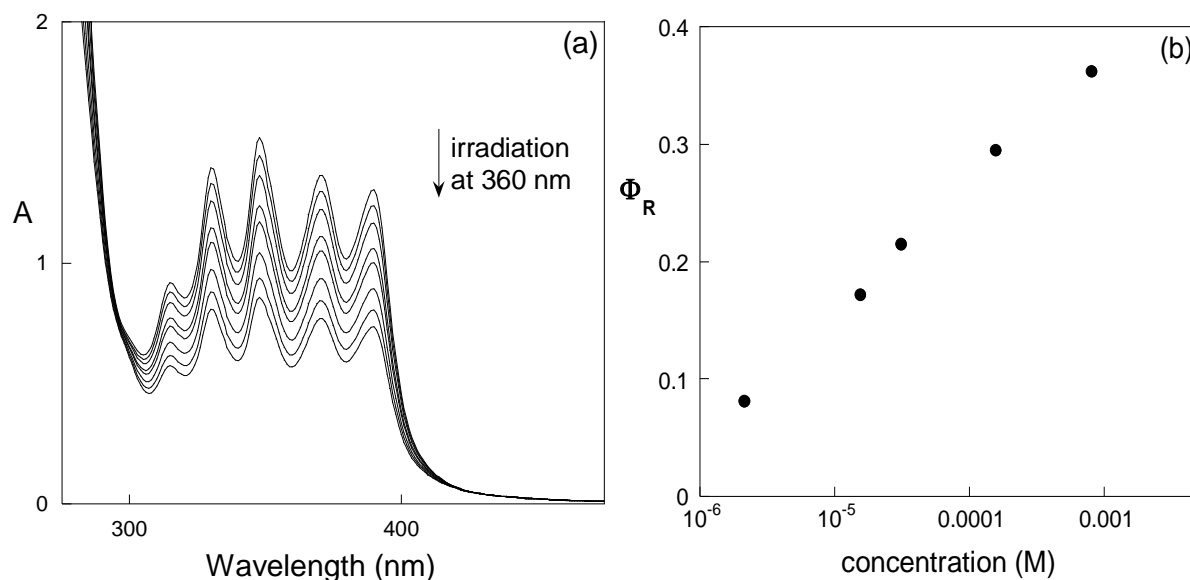


Figure II. 15 – (a) UV-Vis spectral modification of a chloroform deaerated solution of **36** at 3.0×10^{-5} M upon irradiation at 360 nm. Total irradiation time is 10 min; (b) Photochemical quantum yield dependence on the concentration of **39**

It was observed that, at the photostationary state, the proton peaks in the obtained ^1H NMR spectrum were rather broad with low resolution, whereas the peak on the spectrum acquired before irradiation were narrow with well-defined multiplicity. Nonetheless, proton peaks were detected between 6.2 and 7.0 ppm, which are consistent with the formation of benzenic moieties in anthracene dimers. It was hypothesized that the detected peak broadening was caused by polymerization of **36**, since polymer NMR spectra are typically defined by broad, poorly defined peak areas and resolution, due to chain entanglement.^{107,108}

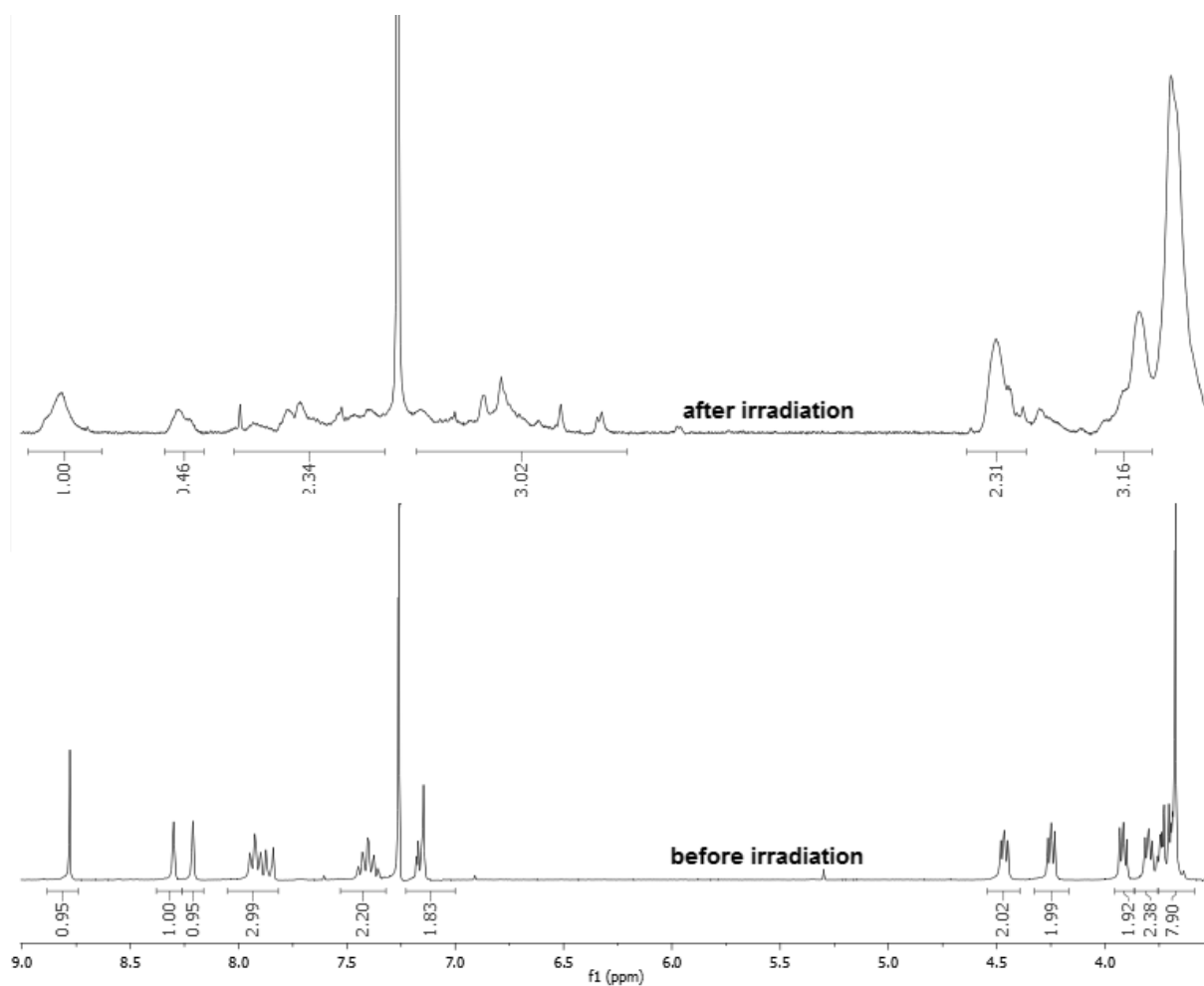


Figure II. 16 – ^1H NMR spectra of **36** in chloroform obtained before and after irradiation at 360nm. Total irradiation time is 60 min.

In order to evaluate the rheological effect of the photochemical polymerization of **36** in organic solutions, viscosity measurements were attempted. Although the low overall reaction yield did not allow the preparation of significant amounts of **36**, necessary for direct viscosity measurements in conventional rheometers, it was envisioned that indirect viscosity determination could be possible using dynamic light scattering spectroscopy. It was demonstrated in chapter II.1 that the Stokes-Einstein equation (equation II.1), relates the diffusion coefficient of a suspended particle with the viscosity of the solvent. Thus, using a suspension of particles with a known size, it is possible, in principle, to determine fluid viscosity from the variations of the correlation curve obtained in DLS experiments (equation II.5).

$$\eta = \frac{kT}{3\pi D_h D_t} \quad \text{II.5}$$

In order to validate this method, silica nanoparticles with diameters of 100 nm were suspended in binary mixtures of water and acetonitrile, and the corresponding correlation curves were obtained. The calculated viscosity values for the mixture correlate well with the results obtained by direct viscometry (Figure II. 17).

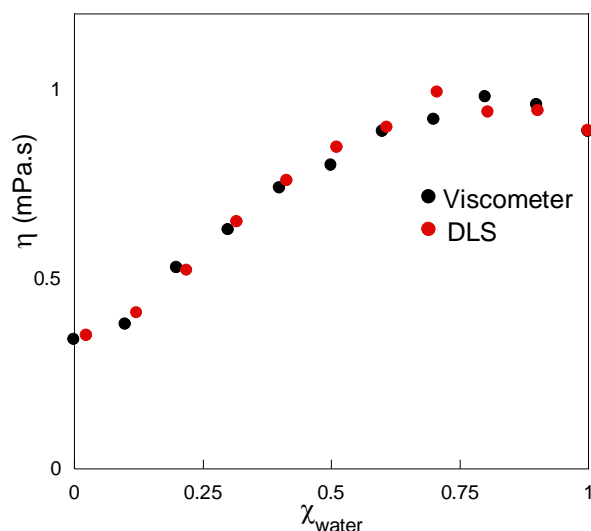
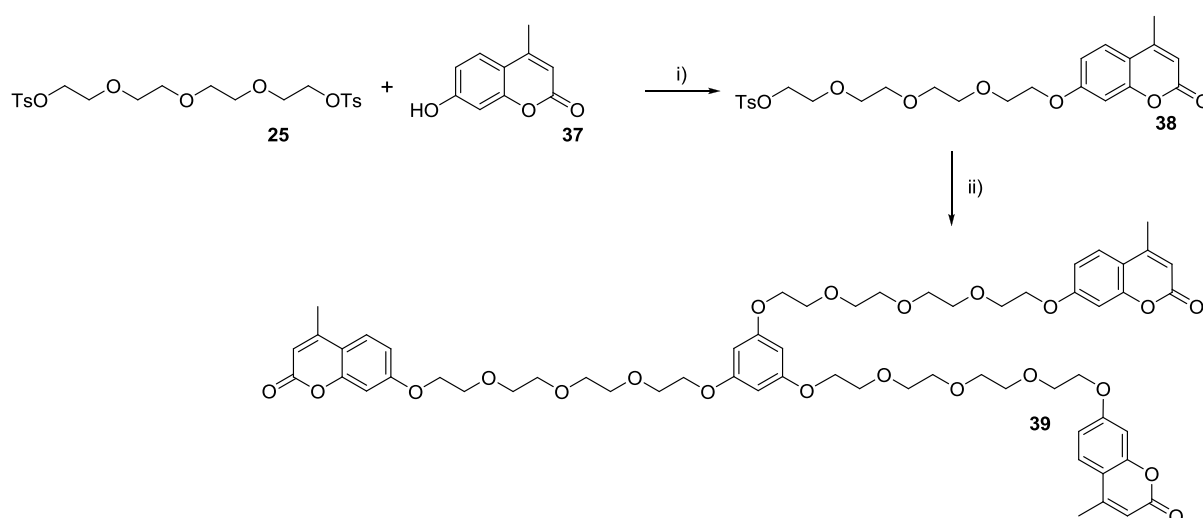


Figure II. 17 – Viscosity of binary mixtures of water and acetonitrile at different ratios, determined by direct measurement with conventional viscometer (black dots) and calculated indirectly from DLS data (red dots).

However, when this method was applied for the determination of viscosity values of solutions of **36**, before and after irradiation, no variations were detected. These results can be justified by the difference between microscopic and macroscopic viscosity. The first is related with the immediate environment surrounding the solute, and has a direct effect on diffusion processes. The macroscopic viscosity is related to the resistance to flow and, therefore, is what is measured in conventional viscometers. In simple liquids, the macroscopic and microscopic viscosities are the same, but differ significantly in systems such as macromolecule solutions, gels and polymer films. This is due to the fact that long polymer chains form crosslinks between different parts of solution, which does not affect solute diffusion but significantly increases flow resistance. For example, this difference has been demonstrated in aqueous solutions of sucrose and poly(vinyl pyrrolidone), in which a change in polymer concentration from 0 to 20% led to a viscosity several orders of magnitude higher, while the sucrose diffusion coefficient changed only by a factor of four.¹⁰⁹

In order to demonstrate by conventional viscometric techniques that the photopolymerization of polyethyleneglycol-based tripodal derivatives would give rise to an increase in viscosity upon irradiation, it was necessary to improve the synthetic method and prepare larger amounts of the desired compound. In chapter II.1 it was demonstrated that coumarin moieties are adequate to induce

photopolymerization of tripodal compounds, albeit with a low quantum yield. Thus, the anthracene moiety was replaced with commercially available 4-methyl-7-hydroxycoumarin **37** for the preparation of tripodal analog **39**. This strategy led to a significant improvement of the overall reaction yield allowing the preparation of larger amounts of tripodal coumarin derivative. Furthermore, due to the difference in polarity between coumarin and coumarate moieties, preparation and purification of tosylate derivative **38** was possible, which in turn led to a significant improvement in final step reaction yield, due to the higher reactivity of tosylate as a leaving group (Scheme II. 7).



Scheme II. 7 – Synthetic pathway for the preparation of tripodal coumarin derivative **39: i) K_2CO_3 , acetone, 60%; ii) phloroglucinol, K_2CO_3 , acetonitrile, 63%.**

The photochemical properties of **39** were investigated in solution, and its ability to undergo photopolymerization was tested. The obtained UV spectrum and molar absorptivity, ϵ , values are in agreement with the expected results for coumarin derivatives, exhibiting two bands without vibrational structure at approximately 220 and 320 nm, corresponding to π - π^* transitions from HOMO-1 and HOMO to LUMO, respectively (Figure II.18a).¹⁰⁴ In addition, the distance between the two absorption bands is decreased and the ratio of their intensities is changed, when compared to the spectrum of **22**. This is due to the electron-donating nature of the alkoxy substituent in position 7, opposed to the electron-withdrawing effect of the amide substituent in position 3 of **22**. Upon irradiation of chloroform solutions of **39** at 320 nm, transformations in the UV spectrum were observed (Figure II.18a). The decrease in absorbance at absorption maximum and a slight increase at shorter wavelengths are consistent with previous results for tripodal coumarin derivative **39**, which undergoes photodimerization upon irradiation. In addition, calculations of Φ_R show that the reaction rate increases with increasing concentration of **39** suggesting that an intermolecular process takes place upon irradiation (Figure II.18b).

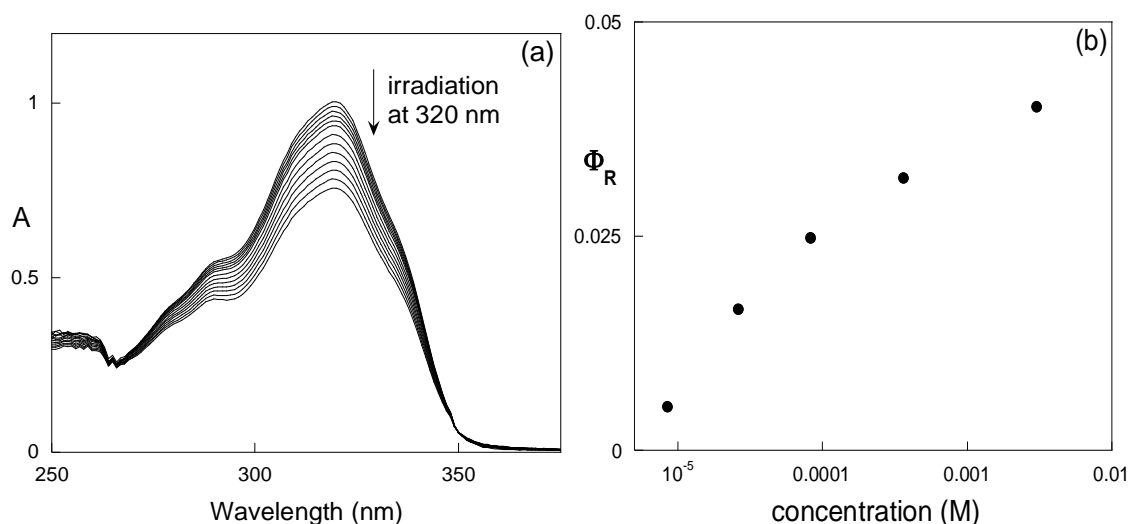


Figure II.18 - (a) UV-Vis spectral modification of a solution of **39 at 1.1×10^{-5} M in chloroform upon irradiation at 320 nm. Total irradiation time is 60 min; (b) Photochemical quantum yield dependence on concentration of **39**.**

Irradiated solutions were analyzed through NMR spectroscopy to confirm that **39** undergoes photochemical dimerization. ^1H NMR spectra, depicted in Figure II. 19, acquired before and after irradiation, are consistent with the formation of coumarin dimers. This conclusion is supported by the reduction of singlet intensity at 6.10 ppm, corresponding to the proton at position 3 and the appearance of a singlet at 3.45 ppm and doublets at 6.60 and 7.20 ppm corresponding to the cyclobutane and benzenic rings formed upon dimerization, respectively. Furthermore, the broadening of the signals at low chemical shift is consistent with the formation of polymers.^{107,108}

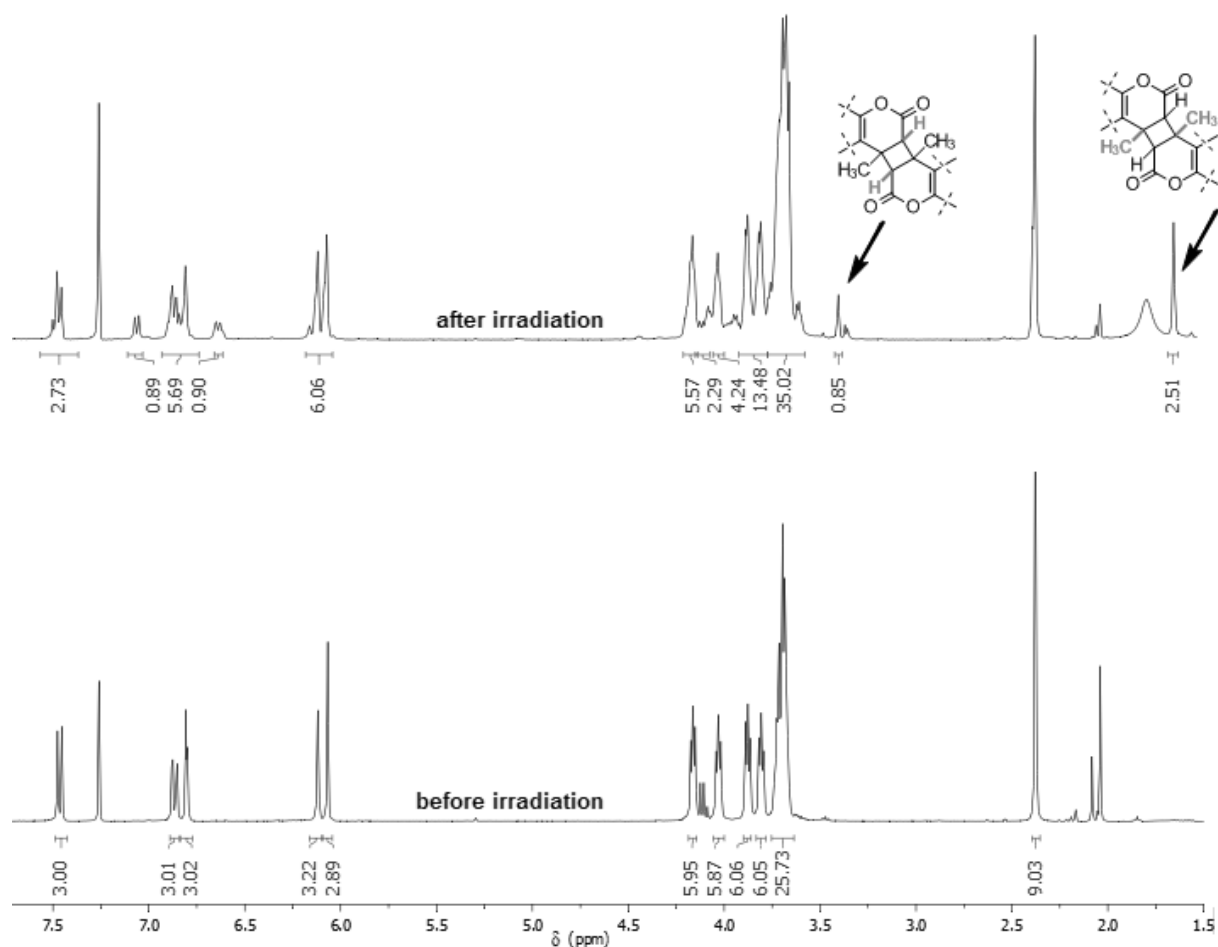


Figure II. 19 – ^1H NMR spectra of **39** in chloroform obtained before and after irradiation.

It was also observed that the irradiated solutions remained clear even at higher concentrations of **39** as opposed to what was detected for coumarin derivative **22**, demonstrating that the introduction of polyether linkers led to higher solubility of the photoproducts. The reversibility of the photochemistry of **39** was also evaluated. However, it was observed that irradiation at shorter wavelengths (< 250 nm) did not result in spectral transformations, followed by UV-Vis or NMR spectroscopy.

With the confirmation that **39** undergoes intermolecular photodimerization, the effect of this reaction on the rheological properties of organic solutions was evaluated through determination of the corresponding viscosity curves, before and after irradiation.

The viscosity curve of a fluid is usually the first and most important rheological measurement as it demonstrates the interdependency of the shear rate applied to it and its viscosity. It is used to determine the physical and mechanical properties of a variety of materials, and provides valuable information required to define their flow behavior and applicability (Figure II. 20). For instance, in lubricant industry it is desired that a fluid retains its viscosity in a wide range of shear rate, which is known as Newtonian behavior. However, most fluids do not exhibit Newtonian behavior and have

viscosity dependent on the applied shear. In cosmetic and paint industries materials are often shear-thinning fluids, i.e., their viscosity decreases with increasing shear rate, which is useful to spread evenly when pressure is applied and remain in place when shear forces are removed after application. On the other hand, for some fluids, known as shear-thickening fluids, the viscosity increases with increased shearing.

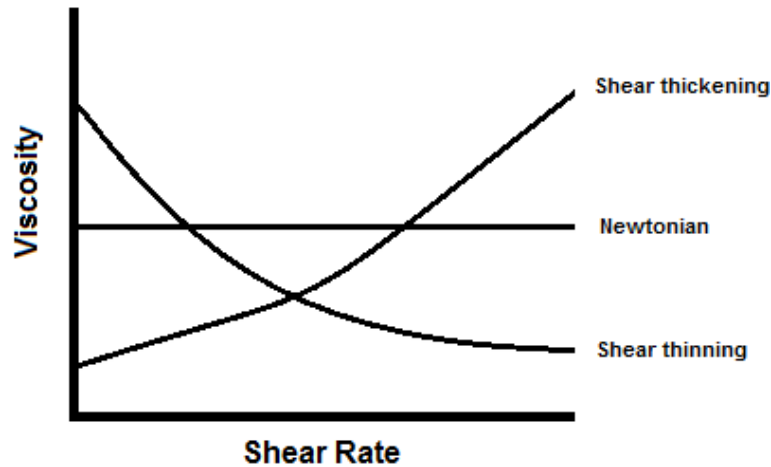


Figure II. 20 – Representation of the three main rheological behaviors exhibited by fluids

This type of measurements is often conducted on rotational rheometers which are based on the principle that the torque required to turn an object in a fluid is a function of its viscosity. The rheometer is a constant speed motor with a torque detection system which is typically a suspended torsion bar. When the drive system turns, the sample resistance, i.e., its viscosity, gives rise to a twist in the torsion bar which is used to calculate the torque. In this case, a cone and plate rheometer was used. This equipment consists of a shallow cone (angles in the order of 1°) which is placed with a known gap into a liquid standing on a horizontal plate (Figure II. 21). Typically, the plate is rotated while the force on the cone, dependent on the liquid viscosity, is measured.

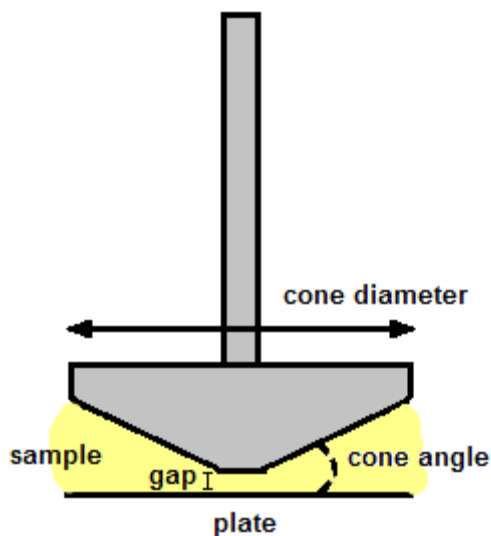


Figure II. 21 – Schematic representation of the typical components of a rotational rheometer

In order to avoid concentration variations during rheological experiments, which could, in principle, occur with volatile solvents due to evaporation in an open system, chloroform was replaced with dimethylformamide (DMF). It was confirmed that this solvent did not significantly affect the photopolymerization reaction of **39** and the same photostationary state was achieved, although with a lower Φ_R (from 0.035 to 0.010 at $10^{-3}M$). This effect was attributed to DMF viscosity (0.920 mPa s at 20 °C) being considerably higher than chloroform viscosity (0.563 mPa·s at 20 °C), which, in principle, affects diffusion of molecules in solution. The rheometry results obtained for **39** in DMF solution are depicted in Figure II. 22.

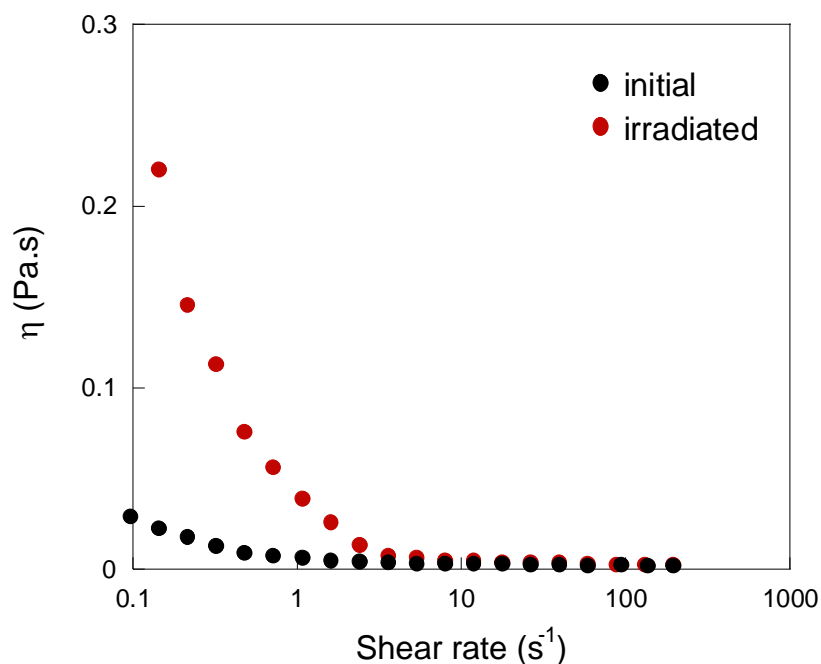


Figure II. 22 – Viscosity curve of a DMF solution of **39** at 10% (w/v) before (black dots) and after (red dots) irradiation at 320 nm. Total irradiation time is 120 min.

It is observed that before and after irradiation, the organic solution of **39** exhibits shear-thinning behavior, which is often associated with polymer solutions.¹¹⁰ However, the zero-shear viscosity is significantly different in both states. Non-irradiated solutions have a zero-shear viscosity of ca. 0.03 Pa.s⁻¹, which is approximately 30 times higher than DMF viscosity, evidencing the thickening effect of ethylene glycol-based polymers.¹¹¹ Upon irradiation, the solution viscosity increases significantly to ca. 0.27 Pa.s⁻¹. This effect is expectable due to the increase in molecular weight of the solute resulting from the photopolymerization of **39**.¹¹² In fact, the relation between solution viscosity, η , and the molecular weight of the polymer solute, M , is described by the Mark-Houwink-Sakurada equation (II.3) where η_s is the solvent viscosity, c the polymer concentration and k' is the proportionality constant, specific for each solvent-polymer system.

$$\frac{\eta}{\eta_s} = k' M c \quad \text{II.3}$$

Since polymer concentration is constant before and after irradiation and if k' remains constant, it can be assumed that photopolymerization of **39** led to a ca. 9-fold increase in molecular weight of the dissolved monomers, since the final viscosity, η_f , is approximately 9 times higher than the initial viscosity, η_i :

$$\left\{ \begin{array}{l} \frac{n_i}{n_s} = k' M_i c \\ \frac{9n_i}{n_s} = k' M_f c \end{array} \right. \Leftrightarrow \left\{ \begin{array}{l} \frac{n_i}{n_s} = k' M_i c \\ 9(k' M_i c) = k' M_f c \end{array} \right. \Leftrightarrow \left\{ \begin{array}{l} \frac{n_i}{n_s} = k' M_i c \\ 9M_i = M_f \end{array} \right. \quad \text{II.4}$$

It is possible to do this approximation since the intrinsic viscosity of a polymer solution does not depend on conversion. In fact, this method is frequently used for the in-line monitoring of average molecular weight in polymerization reactions.^{113,114,115,116,117,118} From the viscosity curves depicted in Figure II. 22, it is also demonstrated that as the shear rate increases, the solution viscosity tends to a value very close to that of pure DMF, which can be explained by the reduction of entanglement between polyether chains as well as other secondary intermolecular interactions when high shear is applied.^{113,116}

Viscosity measurements demonstrate that photopolymerization of tripodal coumarin derivative **39** gave rise to changes in the rheological properties of DMF solutions, essentially on their viscosity, due to the increase of molecular weight of the solute.

Conclusions

The results obtained for high-molecular weight compounds **31**, **36** and **39** show that the careful design and selection of photoresponsive moieties led to a significant improvement in rheological effect over their low-molecular weight counterparts. It was evidenced that compounds bearing anthracene and coumarin moieties underwent photopolymerization upon irradiation, unlike the cinnamic acid derivative, which exhibited only a photoisomerization process. In addition, the selected tetraethylene glycol spacer led to a marked increase in photoproduct solubility over the ethylene spacer of compound **22**. Therefore, it was possible to photopolymerize coumarin derivative **39** in organic solution, which led to a 9-fold viscosity increase upon irradiation. However, due to the low viscosity of the solution prior to irradiation, the overall rheological effect did not yield significant results. In order to render this type of compounds more applicable as photorheological systems, it would be necessary to prepare solutions with much higher viscosity prior to irradiation, which could be achieved by increasing the length of the polyethylene glycol spacers.

Chapter III

Parts of this Chapter have been published:

J. Gordo, J. Avó, A. J. Parola, J. C. Lima, A. Pereira, P. S. Branco, *Org. Lett.* **2011**, *13*, 5112

J. Avó, S. Martins, A. J. Parola, J. C. Lima, P. S. Branco, J. P. P. Ramalho, A. Pereira, *Chem. Plus Chem.* **2013**, *78*, 789

J. Avó, L. Cunha-Silva, J. C. Lima, A. J. Parola, *Org. Lett.* **2014**, *16*, 2582

III. Photoactive ionic liquids

III.1 - Introduction

During the past forty years, ionic liquids (ILs) attracted considerable attention and their research became one of the most rapidly developing areas of modern physical chemistry, technologies and engineering. This class of compounds is defined as salts whose melting temperature is below 100 °C. Therefore, they are composed predominantly of ions and ionic pairs which lead to interesting properties such as negligible vapor pressure at room temperatures, high ionic conductivity, wide liquid temperature range or high thermal stability. Due to their unique characteristics, ILs have been used in a variety of applications, for instance, in electrochemical processes, purification and storage of gases, highly conductive materials, lubricants and propellants or extraction and synthetic solvents.¹¹⁹ The beginning of the history of ionic liquids is subject of controversy, although it is most commonly dated back to 1888, when Gabriel and Weiner reported the synthesis of ethanolammonium nitrate (Figure III.1a), with a melting point of 52-54 °C.¹²⁰ However, the first account of synthesis of an ionic liquid is often attributed to Walden, for his preparation of the first room temperature ionic liquid (m.p. 12 °C), ethylammonium nitrate (Figure III.1b).¹²¹

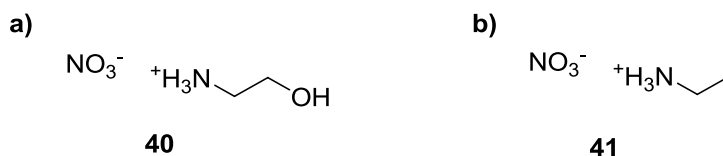


Figure III.1 - Molecular structure of the first synthesized ionic liquids; a) ethanolammonium nitrate 40; b) ethylammonium nitrate 41

After these initial reports, the interest in this class of salts increased, especially with the discovery of chloroaluminates, formed by combining quaternary heterocyclic cations with aluminum chloride. These materials exhibited a great deal of potential for use in a variety of areas, specifically as electrolytes in battery applications, but all suffered from extreme sensitivity to moisture or had high acidity/basicity.¹²² In the early 1990s, a major breakthrough was accomplished by Wilkes, with the preparation of moisture stable ionic liquids, achieved by the replacement of the aluminum chloride with other anions, such as tetrafluoroborate or hexafluoroborate.¹¹⁹ Furthermore, it was evidenced that, by varying the size and nature of the cation and/or anion, the properties of ILs can be tailored to meet the requirements of specific applications to create an almost infinite set of “designer solvents”.¹²³ Thus, a large variety of anions and cations (Figure III. 2) have been used and the number of available ILs and the range of possible applications have grown exponentially.¹²⁴

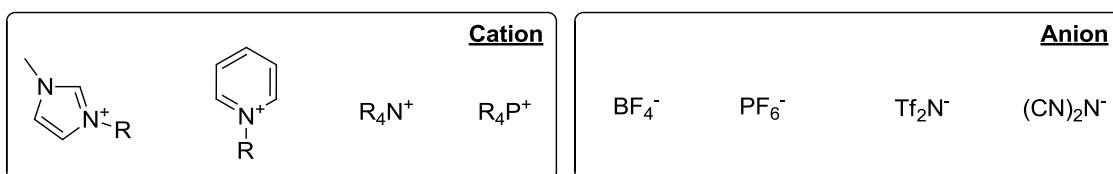


Figure III. 2 - Representative ionic liquid components

The first commercial use of task-specific ionic liquids was developed by BASF on the production of alkoxyphenylphosphines, using *N*-methylimidazole to scavenge acid in a process named BASIL (biphasic acid scavenging utilizing ionic liquids). The reaction results in the formation of *N*-methylimidazolium which separates from the pure product to be recycled.¹²⁵ Expectedly, the scientific and technological interest in ionic liquids for task-specific applications increased significantly and many reports followed. Presently, most of these ionic liquids are employed as catalysts for organic reactions, components in electronic devices, stabilizers in nanomaterials, solvents for analytical and purification methods or lubricants.¹¹⁹ For example, butylmethylimidazolium hydrogenosulfate has been used to overcome problems often associated with cellulose hydrolysis, acting as both solvent and catalyst for the process, resulting in lower overall cost and higher purity of products.¹²⁴ A large variety of ionic liquids based on tetralkylammonium and alkyl imidazolium halides were employed as stabilizing media in metal nanoparticle suspensions.^{126,127} As a result of their high concentration in weak coordinating anions and high viscosity, these ILs prevent particle sedimentation and oxidation, without compromising their activity. Ionic liquids have also shown great potential for application in separation techniques, due to tunable properties such as thermal stability, viscosity and extractability for organic and inorganic ions. In particular, special attention has been devoted to application of ILs as matrixes in MALDI-MS, for the quantification of biomolecules and synthetic polymers.^{128,129} Lubricant industry also turned attention towards ILs applying them both in neat state or as additives to existing base oils, owing to their good adsorbability to metal surfaces and good high pressure performance.¹³⁰ In addition, conventional lubricants may also be modified with ionic moieties to create ionic liquid lubricants with higher durability and stability, lower toxicity, flammability and volatility.¹³¹

Ionic liquids in smart material systems

With new frontiers in materials science opened by the unique properties of ionic liquids, attention was drawn to the application of these compounds in smart systems which undergo a change in their molecular configuration in response to an externally applied stimulus. With high ionic conductivity, large electrochemical window, excellent thermal and chemical stability and low vapor pressure, ionic liquids exhibit the properties required for a good electrolyte. Therefore, this class of

compounds has been used extensively in electrochemical cells and batteries.^{132,133} In fact, several alkylpyrrolidinium based ILs (Figure III. 3a) are currently being used as an alternative to conventional electrolytes in lithium-ion batteries, due to their high thermal stability and low flammability, improving lithium-ion battery security and durability.¹³⁴ In addition, ILs can be polymerized or incorporated in polymeric structures to provide solid-state support broadening their applicability as ionic gels, membranes or films.¹³⁵ For example, tetraalkylammonium cations were modified with acrylate moieties (Figure III. 3b) and polymerized to yield electrolyte gel membranes with enhanced performance and stability.¹³⁶

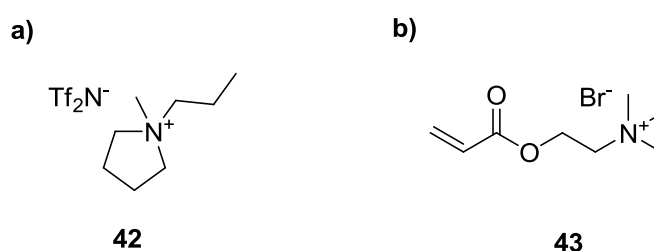


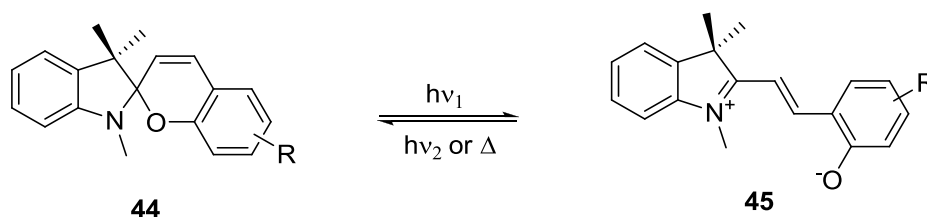
Figure III. 3 - Molecular structure of ionic liquids used as electrolytes; (a) methylpropylpyrrolidinium bis(trifluoromethyl-sulfonyl)imide 42; (b) polymerizable 2-(dimethylethylamino)ethylmethacrylate bromide 43

Phosphonium ILs have been used in ion-selective electrodes with poly(vinylchloride) and poly(methylmethacrylate), with a dual role of both plasticizer and electrolyte for the detection of biomolecules with improved sensitivity.¹³⁷ ILs also have gained momentum in bio applications. It was found that some biomolecules, such as proteins have enhanced solubility and stability when dissolved in biocompatible ILs.^{138,139} In addition, phosphonium ILs mimic moieties commonly found in living organisms and provide a good environment for enzyme interaction, being used in enzyme-IL complex systems for the fabrication of biosensors for several organic molecules.¹⁴⁰ This family of ILs have also been used as a plasticizer for poly(*N*-isopropylacrylamide) based colorimetric wearable pH sensor for real-time health monitoring (Figure III. 4).¹⁴¹



Figure III. 4 – Ionogel based wearable pH sensor for the analysis of human sweat [141]

A system with similar composition was coupled with the photochemical properties of spiropyrans to create a photo-controlled valve for microfluidics systems.¹⁴² Due to the mechanism of the photochemical reaction of these compounds (Scheme III. 1), which involves the formation of a zwitterionic merocyanine **45**, it was possible to control the photochemical reaction kinetics and consequently the rate of contraction of the valves through the application of a phosphonium IL.¹⁴³



Scheme III. 1 – Photochemical reaction of generic spiropyran compounds

The high applicability of ionic liquids in smart material formulation led to an explosion of interest of developing new methods for the synthesis of intrinsically stimuli-responsive ionic liquids (SRILs), and many reports followed.¹¹⁹ Combining the excellent properties of conventional ILs for electrochemical applications with the redox properties of organic and inorganic compounds, electroresponsive ionic liquids became a representative class of SRILs. One of the first reports of this type of ILs was made by Kavanagh and co-workers in which phosphonium ILs were derivatized with viologen moieties in the organic cation to yield electrochromic ILs with fast switching kinetics¹⁴⁴. Alternatively, similar electrochromic responses can be achieved with metal complexes. Branco *et al.* prepared ionic liquids sensitive to both electric and magnetic fields, by using ethylenediaminetetraacetate (EDTA) metal complexes of iron(III), cobalt(III) and chromium(III) which were combined with several organic cations.¹⁴⁵ The resulting compounds display many advantages over conventional systems for electrochromic cells and present a potential alternative to

common magnetic fluids used in magnetic resonance imaging, with tunable magnetic properties and reduced toxicity. Other electrochromic ionic liquids were synthesized by the same group taking advantage of the redox properties of vanadium, using vanadium (V) oxide as the counterion in imidazolium, tetraalkylammonium and tetraalkylphosphonium ILs (Figure III. 5).¹⁴⁶

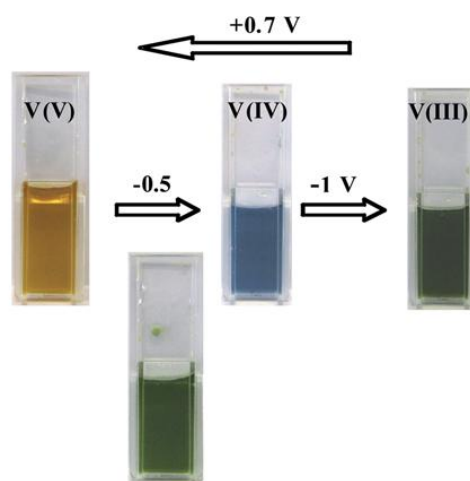


Figure III. 5 – Reversible color switching between three oxidation states of pure ethylmethylimidazolium vanadium (V) oxide IL upon electrolysis (adapted from [146])

Additional chromogenic ionic liquids, which were sensitive to different stimuli, have been synthesized for a variety of applications. For instance, Zhang *et al.* developed a pH-sensitive ionic liquid combining a naturally anionic pH indicator, methyl red, with imidazolium and pyrrolidinium cations.¹⁴⁷ The resulting ILs exhibited increased pH responsiveness in comparison with the precursor methyl red sodium salt due to increased solubility in water, resulting in a selective response in a wider pH range (Figure III. 6).

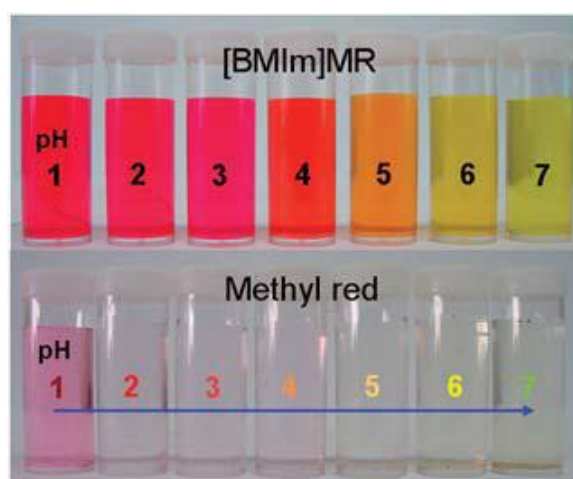


Figure III. 6 – Increased selectivity of methylred based IL over conventional sodium salt from pH 1 to 7 (adapted from [147])

The same chromophore, i.e., an anionic azobenzene, was used by Branco *et al.* for the synthesis of a photoresponsive IL (Figure III. 7a). By reacting methyl orange sodium salt with a

variety of organic cations, several photochromic ionic liquids were obtained. The compounds retained the typical photochemical behavior of azobenzenes, i.e., *trans-cis* isomerization with concomitant change of color, although with slower kinetics due to their rather high viscosity.¹⁴⁸ The same photosensitive unit was also used to create a photoresponsive ILs with conductivity addressable with visible light.¹⁴⁹ However, in this report the azobenzene moiety was covalently bound to an imidazolium cation (Figure III. 7b), resulting in faster isomerization kinetics. In organic solution, ILs exhibited photoinduced variation in conductivity attributed to changes in aggregation state of ionic clusters due to photoisomerization in the organic cation.

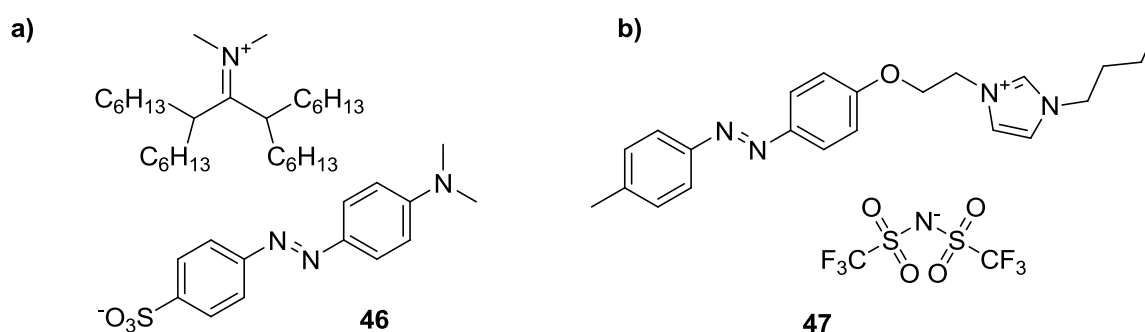
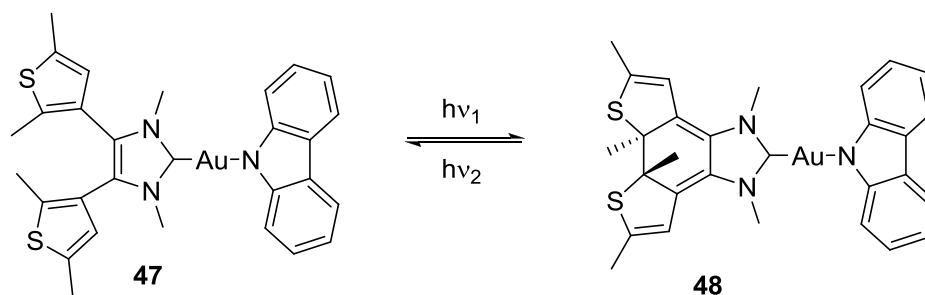


Figure III. 7 – Molecular structures of azobenzene based photochromic ionic liquids (from [148] and [149])

In addition to azobenzenes, other photoresponsive moieties have also been used for the derivatization of cations and anions in ionic liquid synthesis. For example, 1,2-diphenylethene, which is known to undergo reversible *trans-cis* isomerization upon light irradiation, has been functionalized with imidazolium cations for the preparation of several photoresponsive ILs.¹⁵⁰ The resulting compounds were photoresponsive, with melting points and fluorescence quantum yields significantly reduced upon *trans-to-cis* isomerization, a behavior similar to unsubstituted 1,2-diphenylethene.^{151, 152} Moreover, Yam *et al.* have synthesized photochromic ionic liquids based on the photochemistry of other 1,2-diarylethene moieties.¹⁵³ However, instead of *trans-cis* isomerization, these ionic liquids exhibited reversible photocyclization (Scheme III. 2). The compounds were complexed with transition metals and their photochemical properties were exploited for the switching of catalytic or enantioselective activities.



Scheme III. 2 - Ring-closing and ring-opening of photosensitive diarylethene-containing ionic liquids 153

In parallel with the trend followed in the field of photorheological materials (chapter I), attention is shifting towards applying naturally occurring photoresponsive molecules in the preparation of photoresponsive ionic liquids. For instance, Salum and co-workers have used cinnamic acid derivatives for the preparation of photoresponsive ionic liquids.¹⁵⁴ These molecules occur naturally in a number of plants and are extracted from plant-derived products, such as foods, cosmetics or medicines.^{155,156} Besides, the carboxylic acid moiety makes them widely applicable as counter-ions for organic cations.¹⁵⁴ Thus, several ILs were prepared combining commercially available *trans*-cinnamic acids and organic bases (Figure III. 8). Irradiation of the obtained compounds in organic solution allowed the isolation of *cis*-cinnamate ILs with high purity, providing a highly efficient method for preparation and isolation of *cis*-cinnamic acids.

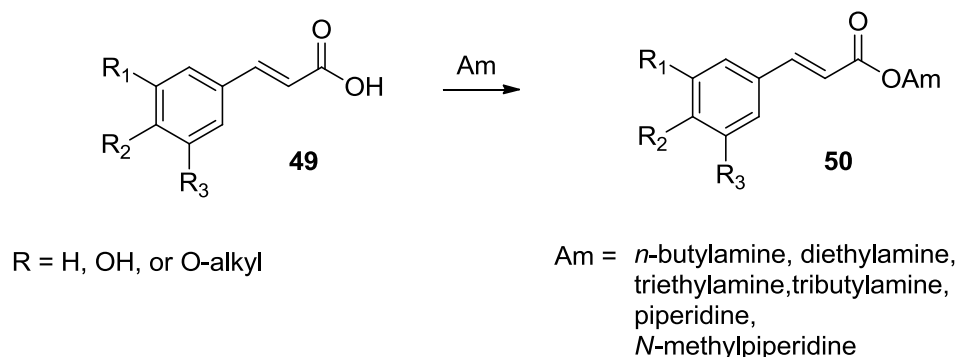


Figure III. 8 – Cinnamate-based photoresponsive ionic liquids (from [154])

Viscosity of ionic liquids

Ionic liquids are increasingly gaining relevance as “green” alternatives for traditional organic solvents, mainly due to their extremely low vapor pressure and volatility, significantly reducing solvent loss, environment pollution and safety hazard.¹¹⁹ Thus, ILs have been subject of a great number of studies on the determination of thermodynamic and thermophysical properties in the past decade, especially their viscosity. The knowledge of the viscosity of ILs is of major importance from an engineering point of view as it plays a major role in stirring, mixing and pumping operations.¹⁵⁷ Additionally, it also affects other transport properties such as diffusion. Therefore, the viscosity values of a particular IL will greatly influence in its applicability. While highly viscous ILs do not make for good solvents in chemical processing, due to negative effects on handling and power requirements or reduction of heat and/or heat transfer in reaction and extraction processes, they are favored in applications such as stationary phases for gas-liquid chromatography.¹⁵⁸ Also, fixed viscosity ranges are a requirement for the application of ILs as lubricants.¹⁵⁹ As a result, a fundamental understanding of the relationship between viscosity and ionic structure is necessary for the rational design and synthesis of ILs with desired viscosity value.¹⁵⁷ Several approaches were used to determine the correlation between structure of ionic liquids and their viscosity, from quantitative structure-property relationship (QSPR) correlations to qualitative analysis based on direct observation, which evidence that viscosity is governed by structural characteristics of ionic pairs, such as cation size, length of substituted group, flexible ether oxygen on alkyl chain, and anion shape.^{160,161} Dzyuba and Bartsch studied a series of alkylimidazolium hexafluorophosphates and bis(trifluoromethyl-sulfonyl)imides regarding the influence of the alkyl chain size on density, surface tension and viscosity.¹⁶⁰ It was shown that the increase in the number of carbons of the alkyl group leads to a general increase of viscosity, which was attributed to van der Waals interactions (Figure III. 9). Furthermore, hexafluorophosphate containing ILs exhibited higher viscosity values than their bis(trifluoromethyl-sulfonyl)imide analogs, which was attributed to the higher symmetry of the anion (less conformational degrees of freedom). In fact, this was later demonstrated in a systematic QSPR study on imidazolium based ILs, in which highly symmetric or almost spherical anions gave rise to the highest viscosity values (Figure III. 9).¹⁶¹

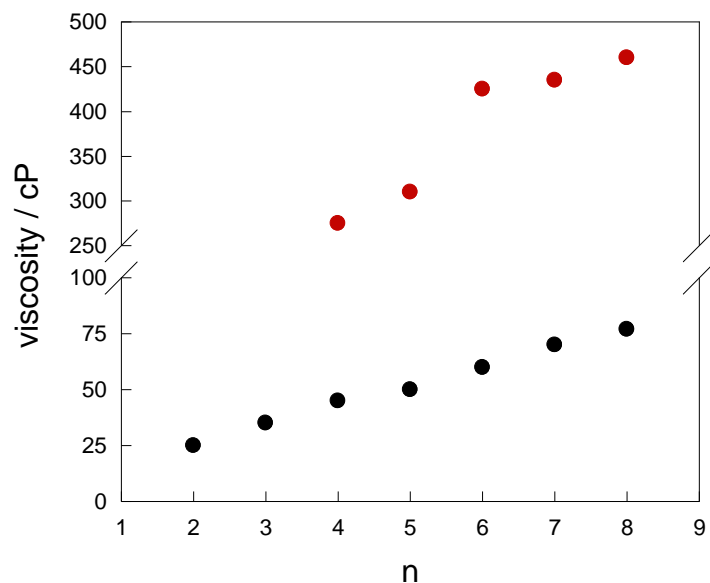
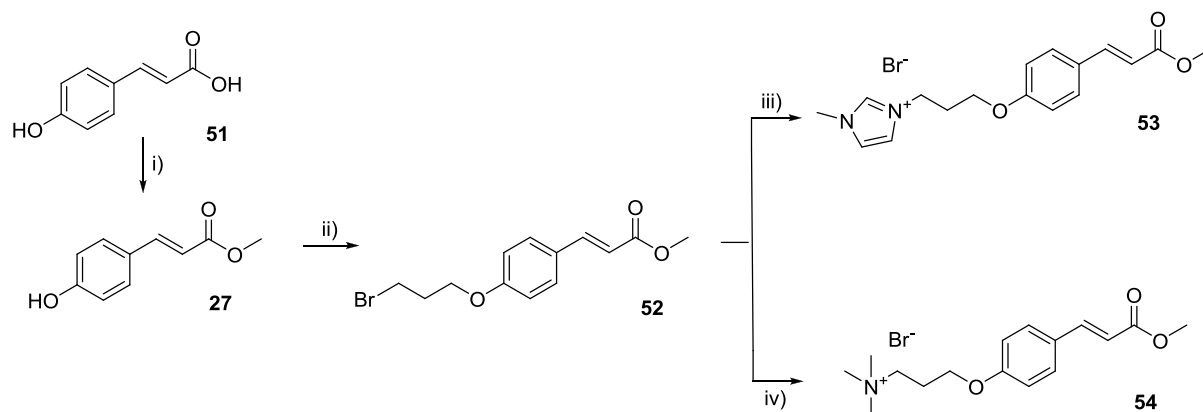


Figure III. 9 – Effect of cation alkyl chain length and counterion on hexafluorophosphate (red dots) and bis(trifluoromethyl-sulfonyl)imide (black dots) alkylmethylimidazolium ILs (from [161])

In a study involving ILs prepared from a variety of cations and anions, Seki *et al.* demonstrated that the viscosity of ILs is affected by molecular shape rather than the molecular weight of their components.¹⁶² In particular, molecular structural changes on the cation species had a stronger effect on the physical properties of ILs than that of anion species, with main influence from conjugation (bond saturation, chainlike or cyclic) and conformation (planar or non-planar). Cations with higher positive charge delocalization, e.g. aromatic vs saturated or phosphorous- vs nitrogen-containing cationic center, lead to less viscous ILs due to weaker cation-anion interaction.¹⁶³ In addition, hydrogen bond interaction through characteristic moieties between cation and anion can also dramatically affect IL viscosity as demonstrated by computational studies.¹⁶⁴ It was also demonstrated that the formation of ionic clusters in ILs, e.g. due to addition of salts, results in increased viscosity.¹⁶⁵ These studies shed light on the relationship between molecular structure and macro-viscosity of ILs, allowing for the rational design and synthesis of ionic liquids with desired viscosity.¹⁶⁶ Furthermore, it was evidenced that conformational changes on cation and anion molecular structure affect dramatically IL physical properties. In this light, several photosensitive ionic liquids were designed and synthesized through functionalization of organic cations with photoresponsive moieties.

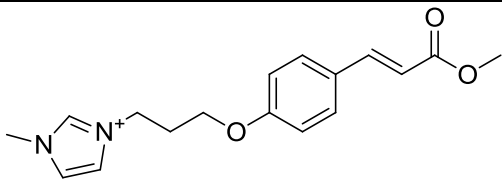
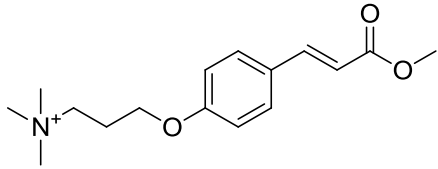
III.2 – Cinnamic acid based ionic liquids

For the design of photoresponsive ionic liquids based on cinnamic acid photochemistry, it was envisioned that the photosensitive moiety should be appended on the cationic component. This can be justified by several QSPR studies evidencing that structural changes occurring in IL cations have stronger effect on physical properties than those occurring on anions.¹⁶⁰⁻¹⁶⁶ Moreover, although carboxylic acids are often used as anion precursors in IL synthesis,^{154,167} they often give rise to unstable ILs due to thermal decomposition of carboxylate moieties via decarboxylation or S_N2-type nucleophilic substitution with cations.¹⁶⁸ Therefore, *p*-coumaric acid **51** was selected as cinnamic acid derivative due to its phenolic moiety, which offers the possibility to append a variety of substituents through S_N-type nucleophilic substitution reactions. In this light, methyl *p*-coumarate **27** was synthesized through acid catalyzed esterification and further derivatized with 1,3-dibromopropane to yield compound **52**. Trimethylamine and *N*-methylimidazole were reacted to give rise to two ionic organic compounds, **53** and **54** (Scheme III. 3), and their melting points were determined (Table III. 1). As expected, compound **53** with a methylimidazolium cation had a lower melting point than its trimethylammonium counterpart **54**, due to lower symmetry and higher charge delocalization.¹⁶³ Therefore, *N*-methylimidazole was selected as cation precursor for the synthesis of photoresponsive ionic liquids.



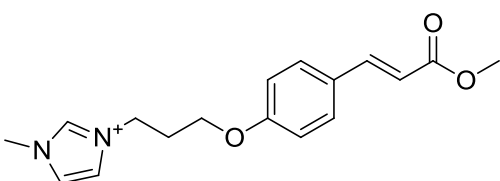
Scheme III. 3 – Synthetic pathway for the preparation of cinnamate organic cations: i) methanol/H₂SO₄, 94%; ii) 1,3-dibromopropane, K₂CO₃, acetone, 94%; iii) *N*-methylimidazole, acetonitrile, 76%; iv) trimethylamine, acetonitrile, 66%

Table III. 1 – Melting points of ionic cinnamate derivatives 53 and 54

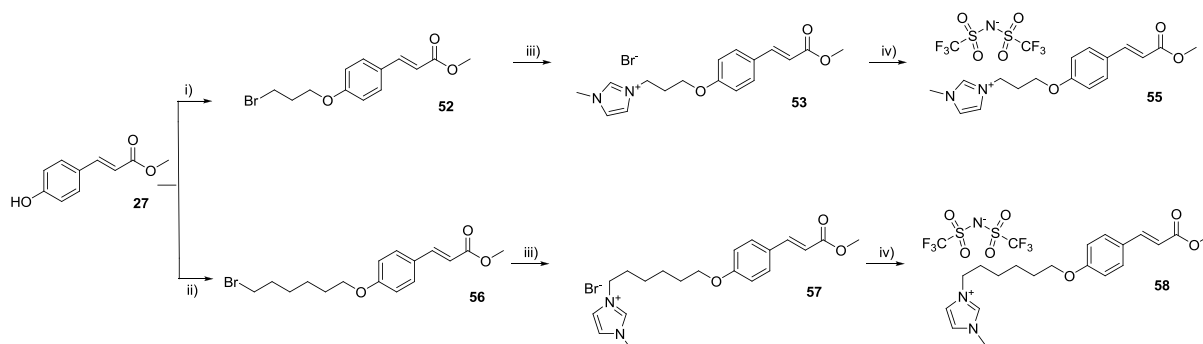
Compound	Cation	Anion	Melting point
53		Br ⁻	143-145 °C
54		Br ⁻	211-213 °C

QSPR studies referred previously show that anion symmetry and charge delocalization have a marked effect on IL melting points.¹⁶¹⁻¹⁶⁶ Thus, rational anion metathesis was performed for compound **53** with several counterions in order to reduce the melting point to below 100 °C. The results are summarized in Table III. 2.

Table III. 2 - Melting points of ionic cinnamate derivative 53 with different counterions

Cation	Anion	Melting point
	Br ⁻	143-145 °C
	MeOSO ₃ ⁻	121-123 °C
	TsO ⁻	115-117 °C
	TfO ⁻	90-92 °C
	Tf ₂ N ⁻	80-82 °C

It is evidenced that an increase in charge delocalization (due to conjugated aromatic rings or electron-withdrawing CF₃ moieties) leads to a decrease in melting temperature. Additionally, a reduction of anion symmetry has a similar effect, except for the case of bis(trifluoromethanesulfonyl)imide (Tf₂N⁻), which gave rise to the lowest melting temperature of all anions. This result can be justified by the fact that this anion may give rise to conformational isomers, increasing the number of degrees of freedom and enhancing the melting point reduction effect.^{169,170,171} From this perspective, the synthetic strategy formerly described was followed with an additional anion metathesis step (Scheme III. 4), to yield ionic liquids **55** and **58** with melting points below 100 °C.



Scheme III. 4 - Synthetic pathway for the preparation of cinnamate photoresponsive ionic liquids: i) 1,3-dibromopropane, K_2CO_3 , acetone, 94%; ii) 1,6-dibromohexane, K_2CO_3 , acetone, 89%; iii) *N*-methylimidazole, acetonitrile, 76%; iv) LiNTf_2 , dichloromethane, 70-76%.

In order to confirm the formation of the obtained ionic liquids **55** and **58**, X-ray diffraction analysis was performed. Both compounds were dissolved in a mixture of CHCl_3 and MeOH 1:1 and the solution was allowed to be in contact with a slow diffusion of Et_2O leading to the formation of colorless single-crystals. The crystal structures (Figure III. 10) of the two compounds were determined in the triclinic space group $P\bar{1}$ with both asymmetric units revealing only one respective organic cation and one Tf_2N^- anion. The organic cation in compound **55** reveals considerable planarity with the phenyl and the imidazolium rings practically in the same plane (the dihedral angle between the average planes of these two aromatic groups is ca. 3.563°), while the structural arrangement of the organic cation in **58** is significantly distinct, showing the imidazolium ring almost perpendicular to the phenyl group (the dihedral angle between the planes is ca. 79.341°). This structural difference is certainly related with the size of the alkylic chain between the cinnamate moieties and the imidazolium groups, as well as with the numerous $\text{C-H}\cdots\text{X}$ ($\text{X} = \text{F}, \text{N}$ or O) intermolecular interactions involving adjacent Tf_2N^- anions.

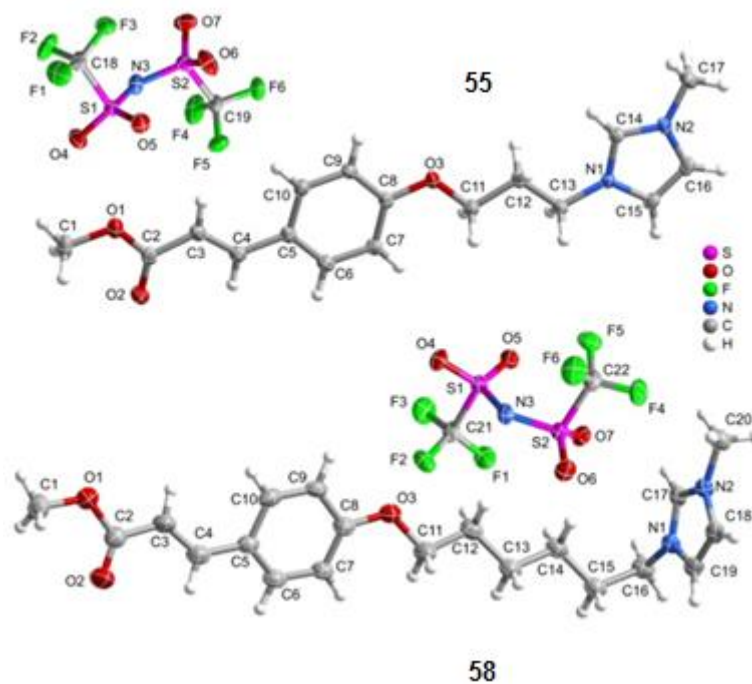


Figure III. 10 - Crystal structures of the compounds **5a** (top) and **5b** (bottom), showing the label scheme for all non-H-atoms which are represented as thermal ellipsoids drawn at the 50% probability

Furthermore, the crystal packing arrangement in both **55** and **58** is strongly influenced by an extensive network of C–H \cdots O weak hydrogen bonds involving neighboring organic cations, as well as C–H \cdots F, C–H \cdots N and C–H \cdots O hydrogen bonding between the organic moieties and the inorganic Tf₂N[−] anions (Figure III. 11). In compound **55** the adjacent organic cations interact via the C₄–H₄ \cdots O₂, C₁₃–H_{13B} \cdots O₂ and C₁₇–H_{17A} \cdots O₃ with H \cdots O distances of 2.547, 2.553 and 2.480 Å, respectively (Figure III. 11a). Furthermore, the inorganic anions establish various C–H \cdots O C₇–H₇ \cdots O₄ (2.661 Å), C₁₄–H₁₄ \cdots O₅ (2.597 Å), C₁₄–H₁₄ \cdots O₆ (2.440 Å), C₁₆–H₁₆ \cdots O₇ (2.519 Å) and C₁₇–H_{17B} \cdots O₆ (2.536 Å) and C–H \cdots F C₁₁–H_{11B} \cdots F₂ (2.657 Å), C₁₃–H_{13A} \cdots F₂ (2.566 Å) and C₁₇–H_{17C} \cdots F₃ (2.379 Å), as well as C₁₅–H₁₅ \cdots N₃ (2.474 Å) weak hydrogen bond interactions with contiguous organic molecules leading to a 3D supramolecular structure (Figure III. 11b). The same type of interactions is observed in the crystal packing of **58** ultimately originating a 3D supramolecular network: C₁₁–H_{11B} \cdots O₂ (2.691 Å) interact neighboring organic cations, while the weak hydrogen bond interactions between the inorganic and the organic species are also C–H \cdots O C₁₆–H_{16A} \cdots O₇ (2.616 Å), C₁₇–H₁₇ \cdots O₅ (2.573 Å), C₁₇–H₁₇ \cdots O₇ (2.256 Å), C₂₀–H_{20A} \cdots O₅ (2.707 Å) and C₂₀–H_{20B} \cdots O₄ (2.590 Å), C–H \cdots F C₁₄–H_{14B} \cdots F₅ (2.509 Å) and C₁₈–H₁₈ \cdots F₂ (2.541 Å) and C₁₉–H₁₉ \cdots N₃ (2.628 Å) (Figure III. 11c).

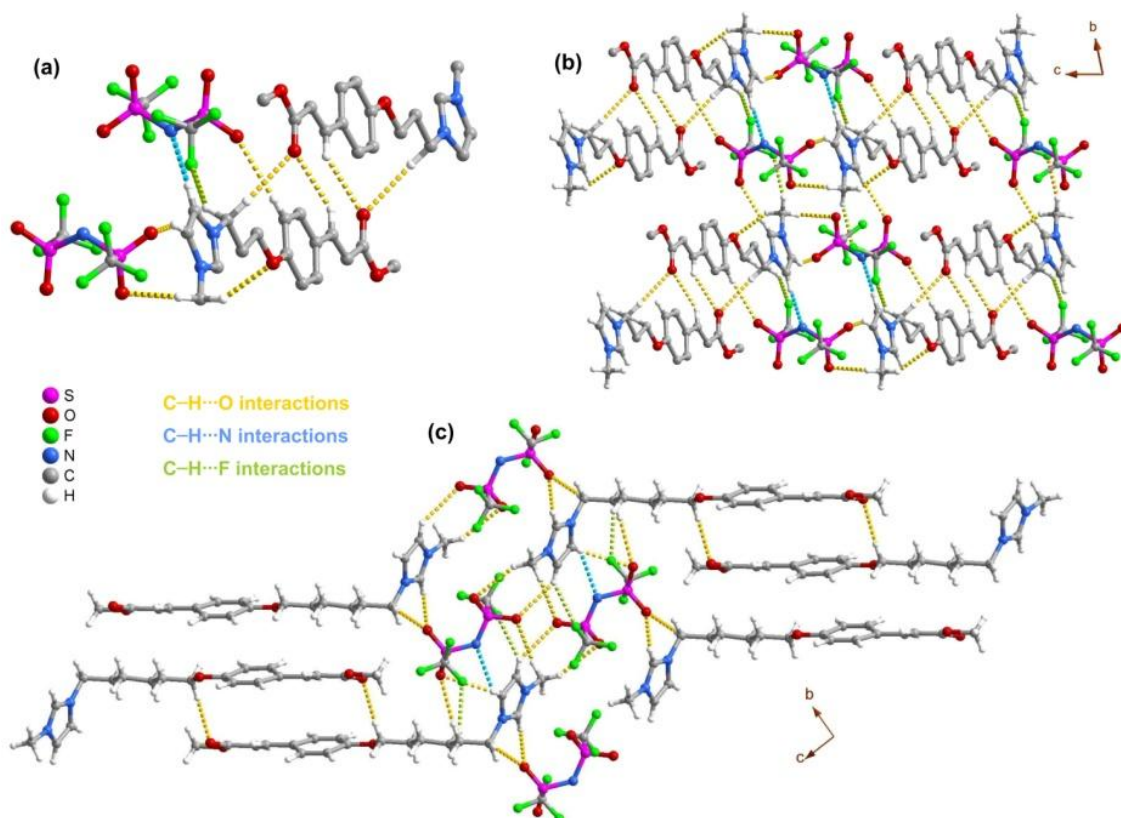


Figure III. 11 - Representation of the diverse C-H...O (yellow dashed lines), C-H...N (blue dashed lines) and C-H...F (green dashed lines) weak hydrogen bonds found in the crystal structures of the compounds **55** and **58**: (a) highlight of the interactions between adjacent cationic and anionic species in **55**; (b) crystal packing of **55** viewed in the [1 0 0] direction of the unit cell; (c) crystal packing of **58** viewed in the [1 0 0] direction of the unit cell

Irradiation of the obtained ionic liquids should, in principle, affect the intricate network of intermolecular interactions in crystal packing, due to photochemical reactions of isomerization and/or dimerization, and ultimately induce changes in their physical properties. Thus, the photochemical behavior of ionic liquids **55** and **58** was investigated. In acetonitrile solution, both compounds underwent photochemical reactions when irradiated at their absorption maxima (Figure III. 12a). The decrease in absorbance around 300 nm and a slight increase in absorbance at lower wavelengths are consistent with the expected photoreactivity of cinnamic acid derivatives, leading to species with blue-shifted maxima. In order to determine whether the photochemical reaction consists of photodimerization or photoisomerization, irradiations were carried out for acetonitrile solutions over a wide range of concentration and photochemical quantum yields (Φ_R) were calculated (results summarized in Table III. 3). For both compounds, Φ_R values did not vary within the selected concentration range, which led to the conclusion that an intramolecular reaction occurs upon irradiation, since the reaction rate does not depend on the concentration of the ionic liquid. Furthermore, the existence of an isosbestic point at 265 nm indicates that no secondary reactions occur during irradiation.¹⁷²

Table III. 3 - Absorption Maxima (λ_{max}), Photochemical Quantum Yields (Φ_{R}), and Cis Isomer Fraction before Irradiation and at the Photostationary State (PSS) of Ionic Liquids **55 and **58** in Acetonitrile**

compound	λ_{abs} (nm)	conc. (M)	Φ_{R}	initial <i>cis</i> fraction	PSS <i>cis</i> fraction
55	304	10^{-2}	0.12	0.0	0.47
		10^{-3}	0.11		
		10^{-4}	0.11		
		10^{-5}	0.12		
58	304	10^{-2}	0.11	0.0	0.48
		10^{-3}	0.10		
		10^{-4}	0.12		
		10^{-5}	0.11		

To corroborate these results, ^1H NMR spectra were obtained for the irradiated solutions of both ionic liquids and it was evidenced that photoisomerization was the only photochemical reaction taking place upon irradiation and photostationary states (PSS) were composed only of *trans* and *cis* isomers in similar proportions (Figure III. 13 and 14). This conclusion is supported by the doublet at 5.84 ppm, corresponding to the β -proton of (*Z*)-isomer of species **55** and **58**. Also, the intensities of (*E*)- H_{β} and (*Z*)- H_{β} peaks add to the same value of H_{A} peaks (imidazolium ring protons, with chemical shifts of 8.73 ppm), indicating that (*E*) and (*Z*) isomers are the only species bearing an imidazolium cation. In addition, the occurrence of photodecarboxylation or photodimerization would give rise to additional doublets at 5.00-5.50 ppm (styrene moiety) or multiplets at 3.50-4.50 ppm (cyclobutane moiety), respectively, which were not detected. For both compounds, further conversion from *trans* to *cis* isomer was not possible, due to the similar absorbance of both isomers at the excitation wavelength.¹⁷³ The reversibility of the system was evaluated both thermally and photochemically, followed by UV-Vis and ^1H NMR spectroscopy. Irradiated solutions were allowed to stand overnight at 50 °C and thermal recovery was not detected, as expected for room temperatures.¹⁷⁴ The photochemical reversibility was evaluated by irradiation at 240 nm. The spectral modifications observed by UV-Vis show full recovery of the initial spectrum (Figure III. 12b). The degree of reversibility from isomer mixture to pure *trans*-**55** was further corroborated by NMR data (Figure III. 15). Full conversion to the *trans*-isomer was achieved after long irradiation times due to the low absorption at selected wavelength and lower *cis*-to-*trans* isomerization quantum yield (0.015).

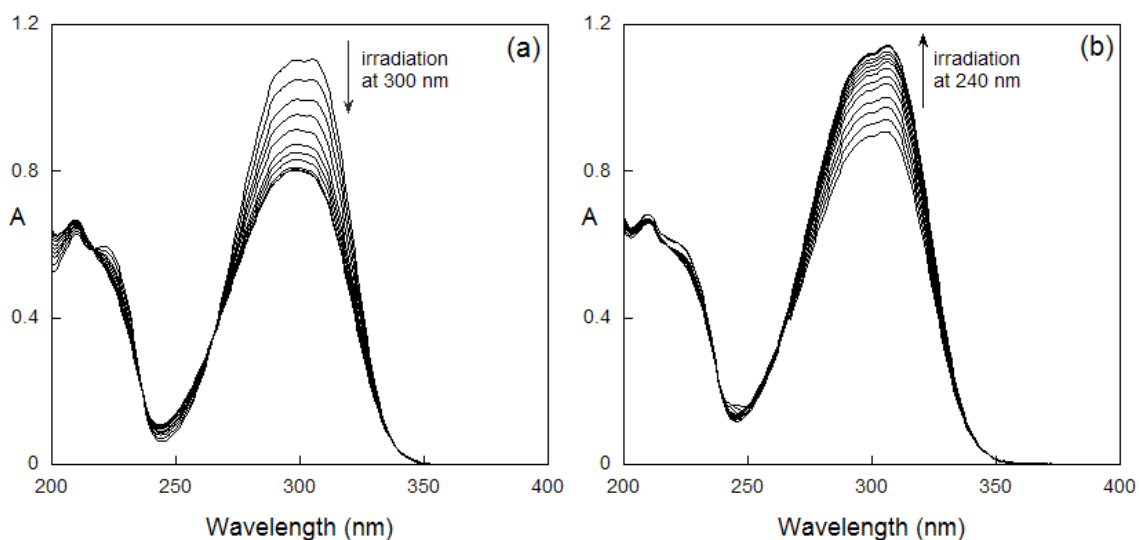


Figure III. 12 - Spectral modifications of 55 at 5.4×10^{-5} M in acetonitrile upon irradiation at 300 nm (a) and 240 nm (b). Under the used experimental setup, PSS was reached after 10 min irradiation at 300 nm while the recovery by irradiating at 240 nm required ca. 600 min.

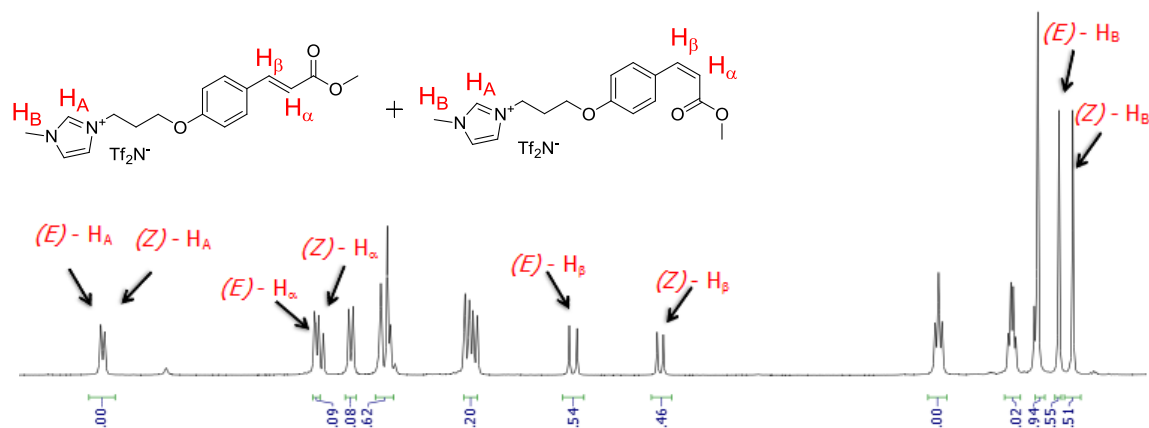


Figure III. 13 - ¹H NMR spectrum of irradiated solution of ionic liquid 55 at the photostationary state

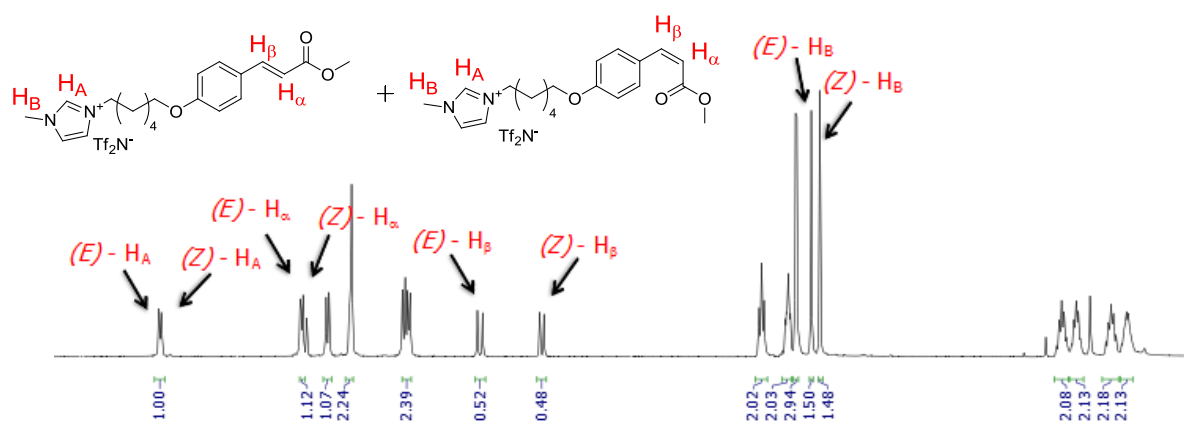


Figure III. 14 - ¹H NMR spectrum of irradiated solution of ionic liquid 58 at the photostationary state

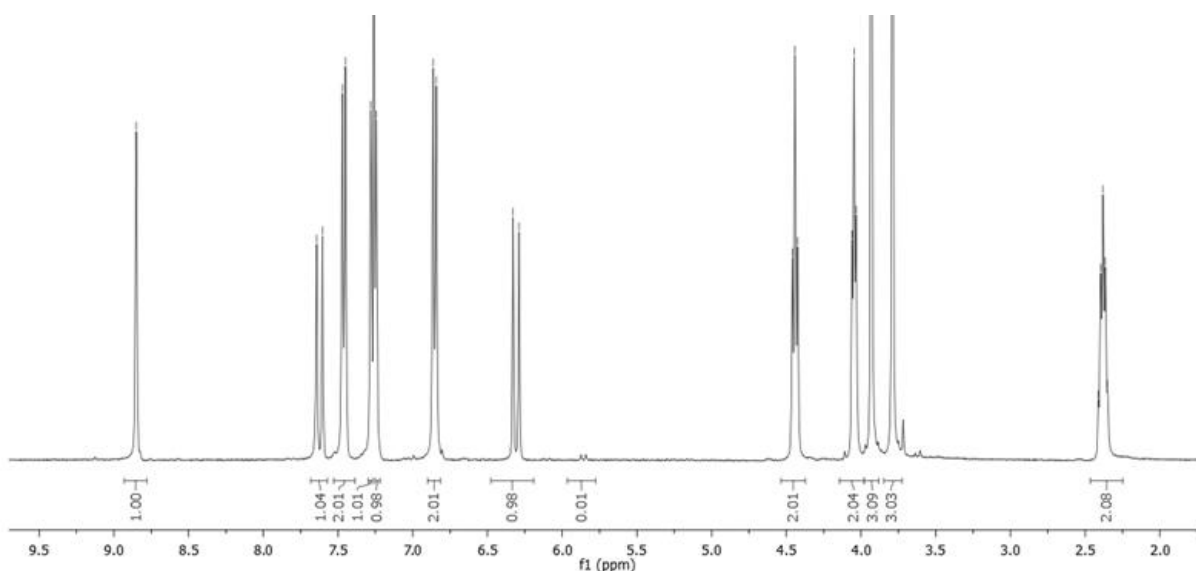


Figure III. 15 - ^1H NMR spectrum of a solution of ionic liquid **55** after irradiation at 240 nm (55_{rec})

Therefore, the occurrence of photodimerization of cinnamate moieties was excluded for this concentration range, in accordance with previously described results for cinnamate ILs.¹⁵⁴

The melting point (T_m) and enthalpies of melting (ΔH_m) of the ionic liquids were determined by differential scanning calorimetry (DSC). The obtained curves are depicted in Figure III. 16 and the corresponding values are summarized in Table III. 4. Both **55** and **58** showed significantly lower melting points (onset temperatures) and ΔH_m after irradiation (photostationary state). While pure *trans*-**55** (55_i) isomer had an initial melting point of 83 °C, its photostationary state (55_{PSS}) composed by both *cis* and *trans* isomers melted at 55 °C. Moreover, its lower enthalpy of melting and larger difference between onset (T_m) and peak (T_p) temperatures indicates that the structural order is reduced after irradiation, due to the presence of both isomers.^{175,176} For ionic liquid **58** the changes in physical properties were even more significant.

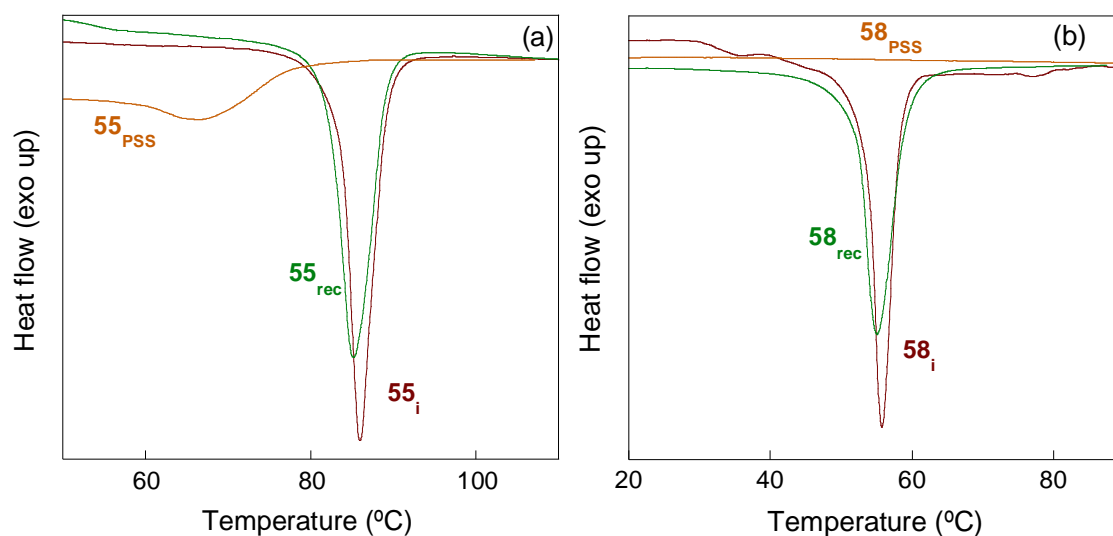


Figure III. 16 – DSC thermograms of ionic liquids **55** (a) and **58** (b) before irradiation (i), at the PSS (PSS) and after photochemical recovery (rec).

Table III. 4 - Melting (T_m) and Peak (T_p) Temperatures and Melting Enthalpies (ΔH_m) of ILs **55 and **58** before Irradiation at 300 nm (i), after the PSS Has Been Reached ($_{PSS}$) and after Recovery upon Irradiation at 240 nm ($_{rec}$)**

compound	55			58		
	55 _i	55 _{PSS}	55 _{rec}	58 _i	58 _{PSS}	58 _{rec}
T_m (°C)	83.4	54.9	82.2	53.4		51.8
T_p (°C)	86.0	66.1	85.4	55.8	n.d.	55.1
ΔH_m (Jg ⁻¹)	63.8	20.9	63.3	62.3		62.2

Upon irradiation at 240 nm to achieve complete recovery of *trans* isomers (**55_{rec}** and **58_{rec}**), both T_m and ΔH_m were measured by DSC. The values obtained are very close to those of non-irradiated samples (**55**, **58**), showing that chemical and physical transformations are reversibly adjustable. After characterization of the photochemical behavior of ionic liquids **55** and **58** in solution, their photochemistry and resulting physical properties modifications were investigated in neat conditions. Both compounds were irradiated at 300 nm at their melting temperature as thin films, and the photochemical transformations were followed by ¹H NMR spectroscopy. NMR data show that, although **55** and **58** also undergo *trans*-to-*cis* isomerization upon irradiation under these conditions, other photochemical reactions take place with significant quantum yields, as indicated by the presence of several proton peaks with high chemical shifts (Figure III. 17). Photostationary states were achieved after one hour of irradiation and were composed of a mixture of *trans*-**55** (ca. 45%), *cis*-**55** (ca. 30%) and other new compounds (ca. 25%).

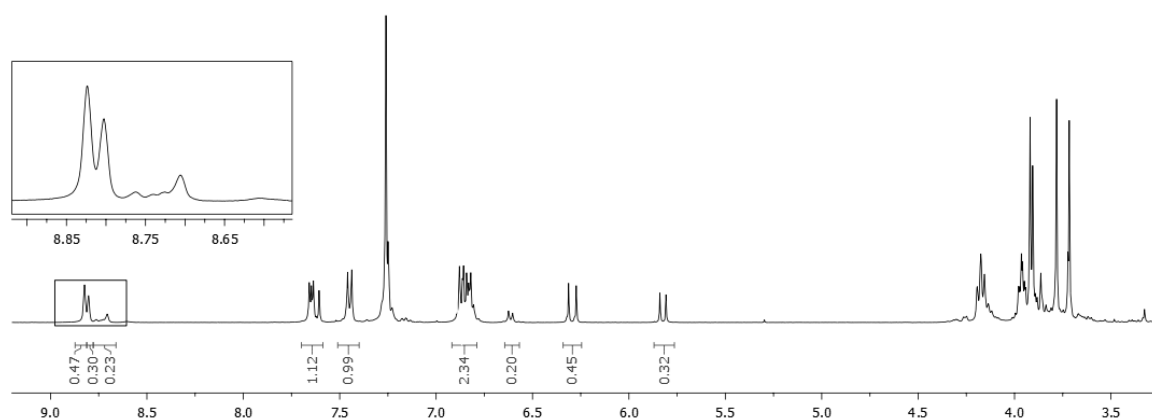


Figure III. 17 – ¹H NMR spectrum of **55 in chloroform after irradiation at 300 nm in neat conditions. Total irradiation time is 120 min.**

Although the complexity of the obtained NMR spectra does not allow the identification of the new species, it is estimated that photo-oxidative processes occurring in cinnamate moieties may give rise to different imidazolium salts. To test this hypothesis, ionic liquids **55** and **58** were melted,

deaired *in vacuo* and irradiated under inert atmosphere. NMR data show that under these conditions, both compounds undergo photochemical *trans*-to-*cis* isomerization upon irradiation, while other photochemical processes are significantly reduced (from ca. 25% to <3%) (Figure III. 18). These experiments had to be carried out in closed quartz tubes to achieve inert atmosphere, and thus, ionic liquid samples had low surface-to-volume ratio which in turn led to heterogeneous mixtures of isomers during irradiation. Therefore, photochemical quantum yields could not be determined and photostationary states were not achieved. However, melting points were still lowered after partial *trans*-to-*cis* isomerization of compounds **55** and **58** (Table III. 5). Moreover, it appears that melting temperature depression (ΔT_m) is directly proportional to the fraction of *cis*-isomer in the irradiated sample (Figure III. 19) and extrapolates to the values of irradiated solution samples with equal fractions of both isomers. These results suggest that irradiation of thin films of **55** and **58** under inert atmosphere would yield similar ΔT_m values to those obtained for irradiated solutions, if the same isomerization rate was achieved. The reversibility in neat conditions was also investigated. Samples were irradiated in solution in order to achieve 1:1 *trans*-*cis* isomer ratio of the photostationary state, dried *in vacuo* and allowed to stand at 90 °C overnight and no changes in ^1H NMR spectra were observed. Equally, irradiation of thin films of **55** and **58** did not yield any changes. These results can be justified by the low absorptivity at the selected wavelength and low quantum yield of *cis*-to-*trans* isomerization. Moreover, photoisomerization kinetics can be significantly reduced in highly viscous media, which is the case of these molten ILs.^{177, 178}

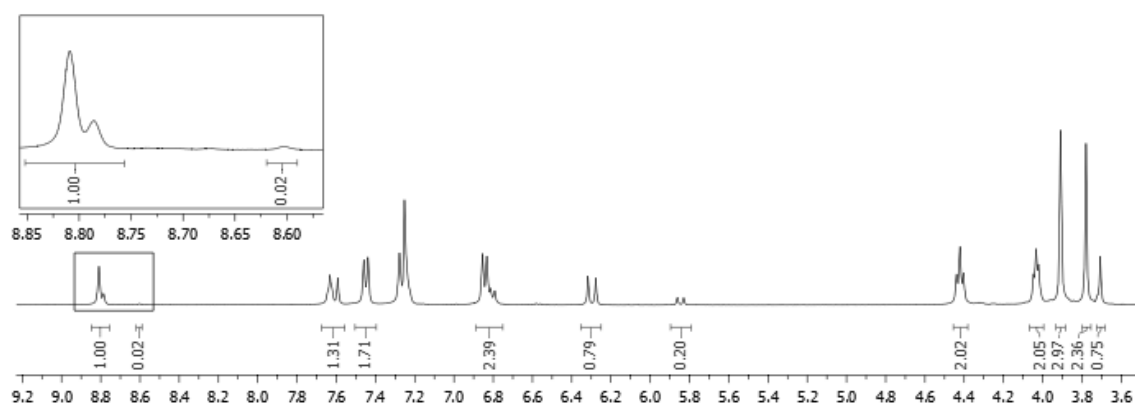


Figure III. 18 - ^1H NMR spectrum of **55** in chloroform after irradiation at 300 nm in neat conditions under inert atmosphere. Total irradiation time is 120 min.

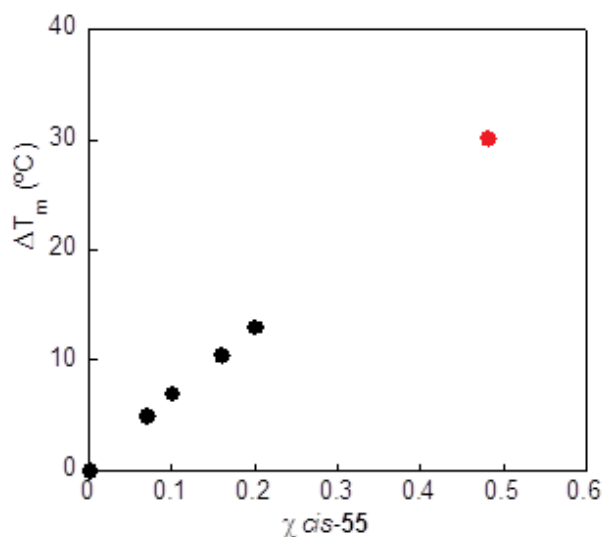
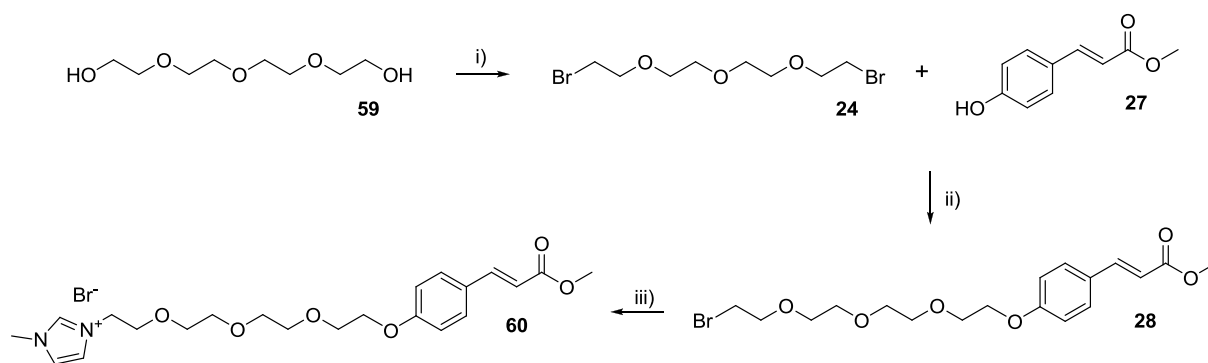


Figure III. 19 - Isomer fraction dependency of melting temperature depression of irradiated neat samples (black dots) and acetonitrile solution (red dot) of 55.

Table III. 5 - Time dependent *cis* isomer ratio and melting point depression (ΔT_m) of irradiated neat samples of ionic liquids 55 and 58

compound	irradiation time (hours)	<i>cis</i> isomer fraction	ΔT_m (°C)
55	1	0.10	7
	3	0.16	11
	6	0.20	14
58	4	0.10	7

After these results, it was anticipated that a room temperature ionic liquid bearing cinnamate moieties would exhibit light-controllable rheological properties, such as viscosity. As demonstrated by numerous QSPR studies on the structure of ionic liquids, flexible ether oxygens on alkyl chains of organic cations affect cation-anion interaction by increasing the number of conformational degrees of freedom, thus, influencing properties such as viscosity and melting points.¹⁶² In this light, an imidazolium ionic liquid bearing cinnamate moiety and a tetraethyleneglycol spacer was synthesized (Scheme III. 5). Following a similar strategy to that previously described, a room temperature ionic liquid, **60**, was obtained by replacing the alkane chain spacer with tetraethylene glycol moiety. DSC data showed that compound **60** remains liquid at temperatures as low as -42 °C, evidencing the notable effect of the polyether chain on the melting point. Thus, anion metathesis was not performed.



Scheme III. 5 – Synthetic pathway for the preparation of room temperature cinnamate ionic liquids: i) triphenylphosphine, Br_2 , acetonitrile, 87%; ii) K_2CO_3 , acetone, 91%; iii) *N*-methylimidazole, acetonitrile, 91%.

In a similar approach to previously described ionic liquids **55** and **58**, the photochemical behavior of IL **60** was studied both in solution and neat conditions. Upon irradiation at absorption maxima, photochemical processes took place as indicated by a decrease in absorbance around 300 nm and a slight increase in absorbance at lower wavelengths, which are consistent with the photoisomerization processes occurring in analogs **55** and **58** (Figure III. 20a). Quantum yield (Φ_R) calculation also show that the photochemical reaction rate is not affected by concentration, indicating that it has an intramolecular nature, in parallel with the behavior of compounds **55** and **58** (Table III. 6). These data were corroborated by ^1H NMR spectra of irradiated samples (Figure III. 21), evidencing that only *trans*-to-*cis* photoisomerization takes places upon irradiation. This conclusion is supported by the doublet at 5.84 ppm, corresponding to the β -proton of (*Z*)-isomer of **60** and by the two singlets around 10.2 ppm, which indicate that (*E*) and (*Z*) isomers are the only species bearing an imidazolium cation. In addition, species resulting from photodecarboxylation or photodimerization reactions would give rise to additional doublets at 5.00-5.50 ppm (styrene moiety) or multiplets at 3.50-4.50 ppm (cyclobutane moiety), respectively, which were not detected. The obtained photostationary state was composed by both isomers in equal proportions, comparable to the behavior of previously studied ILs. Furthermore, the system also showed to be fully reversible when irradiated at lower wavelengths (Figure III. 20b).

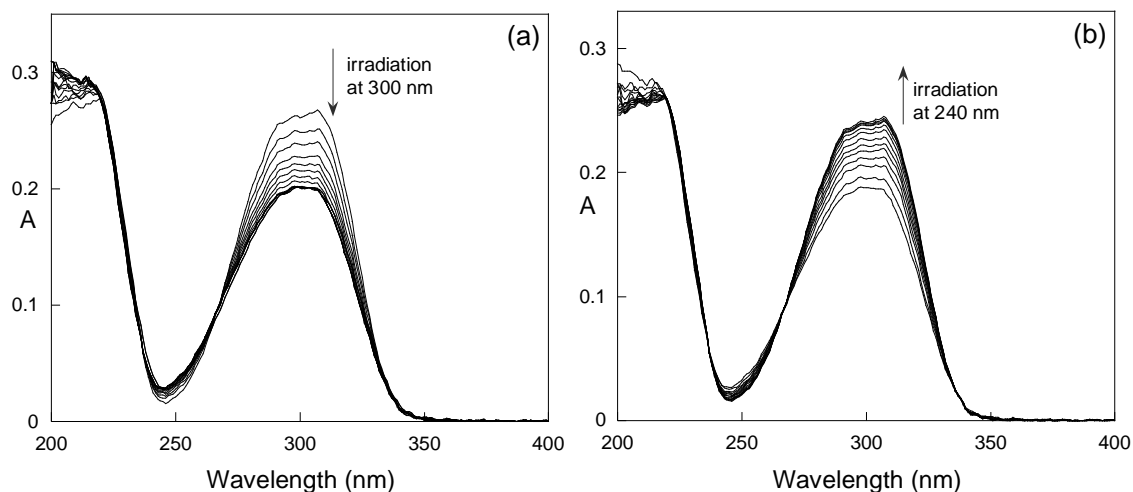


Figure III. 20 - Spectral modifications of **60** at 1.2×10^{-5} M in acetonitrile upon irradiation at 300 nm (a) and 240 nm (b). Under the used experimental setup, PSS was reached after 15 min irradiation at 300 nm while the recovery by irradiating at 240 nm required ca. 600 min

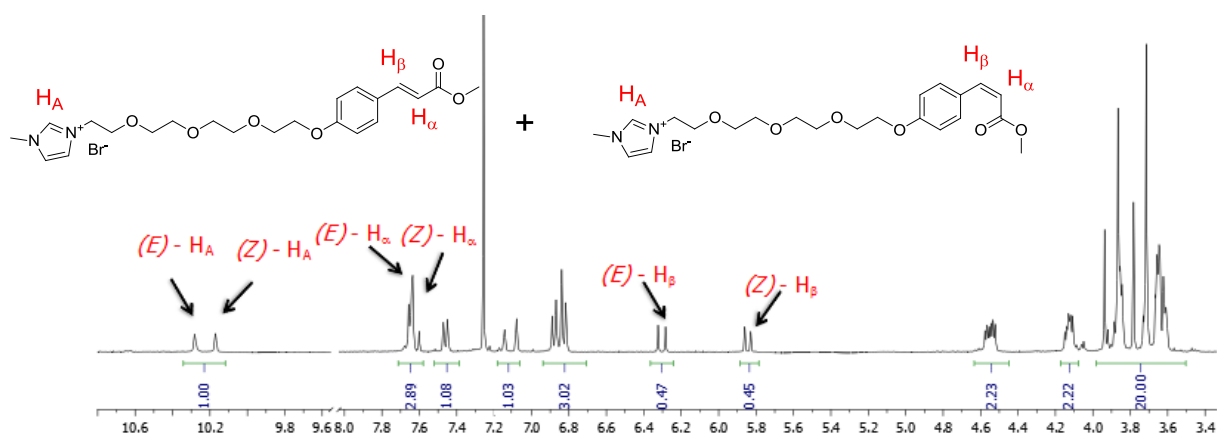


Figure III. 21 – ^1H NMR spectrum of **60** irradiated in chloroform at 300 nm. Total irradiation time is 120 min.

Table III. 6 - Absorption Maxima (λ_{max}), Photochemical Quantum Yields (Φ_{R}), and Cis Isomer Fraction before Irradiation and at the Photostationary State (PSS) of IL **60**

compound	λ_{abs} (nm)	conc. (M)	Φ_{R}	initial <i>cis</i> fraction	PSS <i>cis</i> fraction
60	305	10^{-3}	0.11	0.0	0.49
		10^{-4}	0.10		
		10^{-5}	0.12		
		10^{-6}	0.11		

Compound **60** has also shown to undergo degradation when irradiated in neat conditions, as evidenced by ^1H NMR data depicted in Figure III. 22. The irradiated sample gave rise to a complex spectrum with a high number of peaks around 10.0 ppm corresponding to different imidazolium

bearing species, as well as several new signals at 7.8, 6.6 and 4.5-4.0 ppm (Figure III. 22). Irradiation of **60** in controlled non-oxidative atmosphere did not cause degradation, and the obtained ^1H NMR spectrum was similar to that obtained for irradiation in acetonitrile solution. However, in this case the composition of the photostationary state was different than those of compounds **55** and **58**, with a higher fraction of *cis* isomer (Figure III. 23).

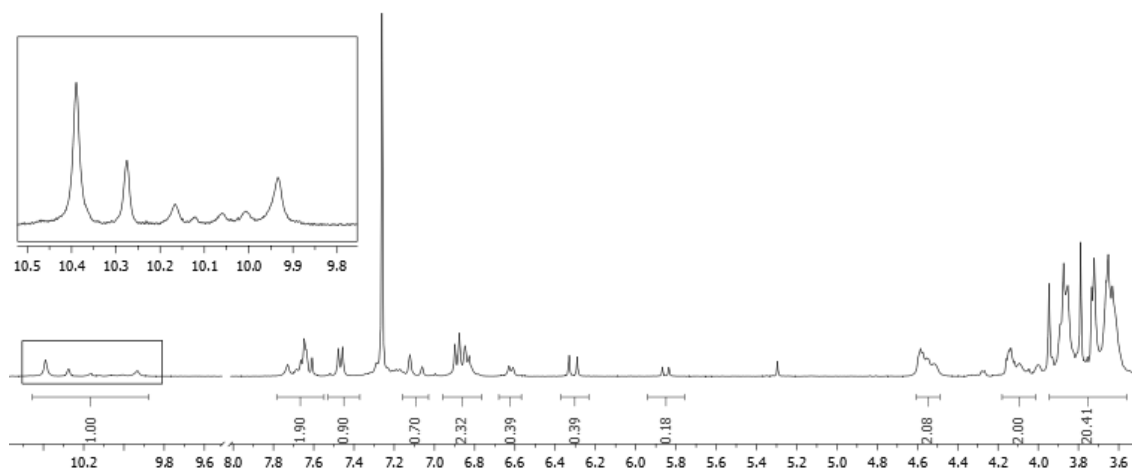


Figure III. 22 – ^1H NMR spectrum of **60** in chloroform after irradiated at 300 nm in neat conditions. Total irradiation time is 120 min.

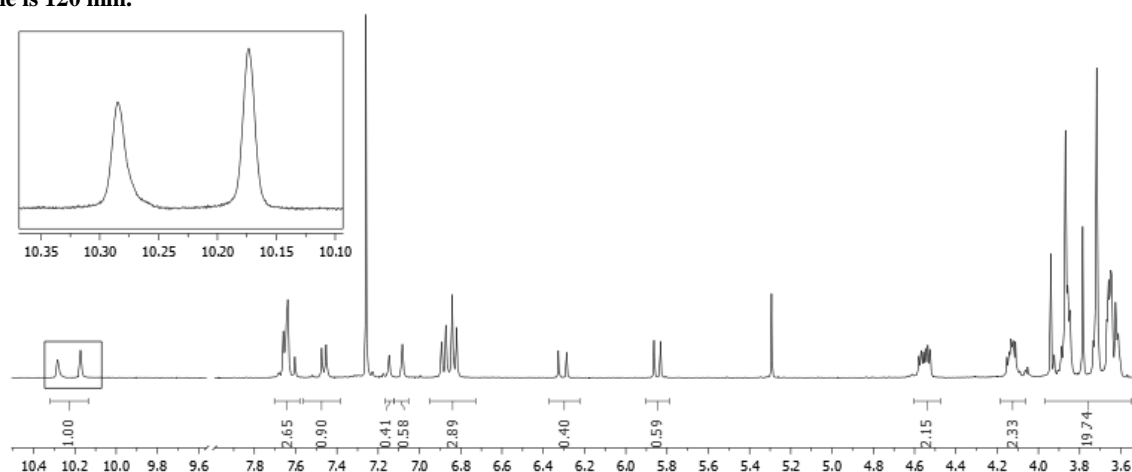


Figure III. 23 - ^1H NMR spectrum of **60** in chloroform after irradiated at 300 nm in neat conditions under inert atmosphere. Total irradiation time is 120 min.

The effect of these transformations on the physical properties of **60** was investigated. In this case, changes in viscosity rather than melting point were tested. Several QSPR studies have shown that the factors that govern melting point in ILs also affect viscosity, such as cation size, shape and symmetry or cation-anion interactions.¹⁶¹⁻¹⁶⁶ It was evidenced that *trans*-to-*cis* isomerization induced significant melting point reduction in ILs **55** and **58**, probably due to disruption in van der Waals and hydrogen bond interaction established between the organic cations and Tf_2N^- anions. It is then expectable that the same photochemical reaction would lead to a decrease in IL viscosity after irradiation. Therefore, the viscosity of neat samples of **60** was measured before and after irradiation at

300 nm, and the results are depicted in Figure III. 24. The same experimental apparatus used for the characterization of the rheological properties of compound **39**, described in the previous chapter, was employed to evaluate the photorheological effect displayed by IL **60**. The flow curve associated with the non-irradiated state exhibits a Newtonian plateau of the shear rate at low shear rates followed by a shear thinning regime at high shear rates. This flow behavior is characteristic of thixotropic fluids which are usually composed of molecules that have a longer range structure that can be altered when a certain level of mechanical shearing is reached. Moreover, it has been demonstrated that ILs with nanostructures composed of aggregates due to intermolecular hydrogen bond networks form liquid crystalline phases and exhibit this rheological behavior. It is then expected that, upon a certain shear level is achieved, intermolecular interactions between cation chains are disrupted, breaking IL nanostructure and consequently decreasing viscosity.^{179,180,181,182} The rather long transition between Newtonian and shear-thinning behaviors can be explained by the diverse intermolecular interaction types that can form in **60**. Upon irradiation into the photostationary state, these rheological properties are significantly changed. The zero-shear viscosity is lower in the irradiated form which can be explained by a weakening in IL nanostructure due to an increase in disorder arising from the mixture of *cis* and *trans* isomers. In addition, the Newtonian region of the flow curve extends to higher shear rates, indicating that weaker intermolecular interactions are established in the photostationary state of **60**.

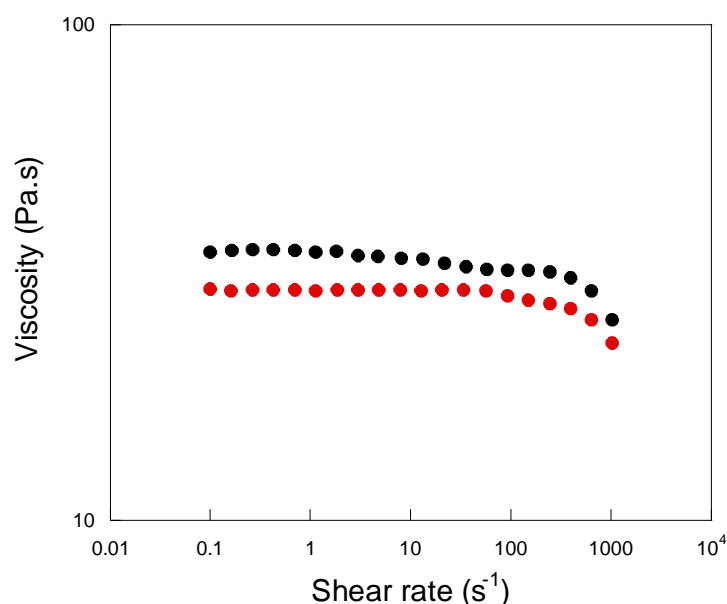


Figure III. 24 - Viscosity curve of pure **60** before (black dots) and after (red dots) irradiation at 300 nm. Total irradiation time is 120 min.

This behavior follows the same trend of melting point depression exhibited by **55** and **58** upon irradiation. It is then proposed that *trans*-to-*cis* isomerizations weakens cation-anion and cation-cation supramolecular interactions leading to a decrease in viscosity, probably due to a reduction in cation

planarity. In order to shed light on the effect of isomerization on intermolecular interactions on the liquid state, Hyper-Rayleigh scattering (HRS) spectroscopy was conducted on neat samples of **60**, before and after irradiation. HRS is a spontaneous process in which a system illuminated with photons with a given frequency ω scatters photons of frequency 2ω . HRS spectroscopy allows the determination of the system hyperpolarizability (β_{HRS}), i.e., the ability to scatter light at the second harmonic frequency, which is a function of size, shape and nature of scatters.^{183,184} The HRS hyperpolarizability, as well as its dipolar ($\beta_{J=1}$) and octupolar ($\beta_{J=3}$) tensorial components, associated depolarization (DR) and anisotropy (ρ) ratios for compound **60** before and after irradiation are summarized in Table III.7, and the associated variation of HRS response is shown in Figure III. 25.

Table III. 7 - β_{HRS} , $\beta_{J=1}$ (dipolar) and $\beta_{J=3}$ (octupolar) values (in atomic units*, using Convention T) and depolarization ratios, DR, and anisotropies, ρ , deduced from HRS measurements at 1064 nm for compound **60, before and after irradiation**

compound	β_{HRS}	DR	ρ	$\beta_{J=1}$	$\beta_{J=3}$
60	506	5.1	0.80	950	760
60_{irrad}	433	5.1	0.80	830	670

* 1 atomic unit of $\beta = 3.62 \times 10^{-42} \text{ m}^4 \text{ V}^{-1} = 8.641 \times 10^{-33} \text{ esu}$.

Before irradiation, the amplitude of β_{HRS} (503 at. units) is considerably high, c.a. ten to twenty times stronger than that reported for other imidazolium based ILs.¹⁸⁵ In principle, no dynamical enhancement of that hyperpolarizability is expected since the absorption band at 300 nm is far from the harmonic response at 532 nm. The depolarization ratio (DR) is approximately 5, which is typical of a two-state model (HOMO-LUMO) where the hyperpolarizability has a strong 1-D character.¹⁸⁶ In addition, the multipolar analysis of the HRS measurements in **60** clearly reveals a dominant dipolar character ($\beta_{J=1} > \beta_{J=3}$) of its hyperpolarizability in contrast again with imidazolium (and even pyridinium, pyrrolidinium or alkylammonium) based ILs where the octupolar character strongly dominates the second order nonlinear optical response. These results indicate that such HRS response excludes a simple molecular cluster in favor of a nanocluster whose organization is probably very close to a crystal packing with a dominant dipolar response, as demonstrated for analogs **55** and **58**.¹⁸⁷ After irradiation (**60_{irrad}**), the HRS parameters are quite identical in proportion except that their respective amplitudes are 12% lower which is in agreement with the weak loss of viscosity observed for the irradiated sample, and correlates well with the melting point depression exhibited by **55** and **58** due to weakening of intermolecular interactions.

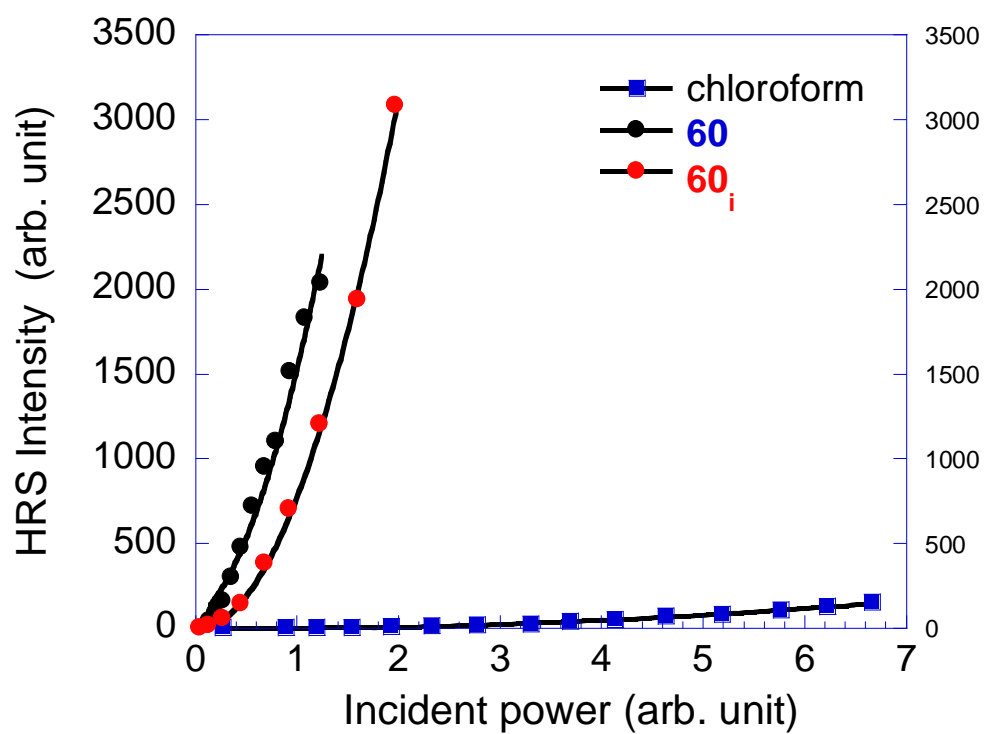
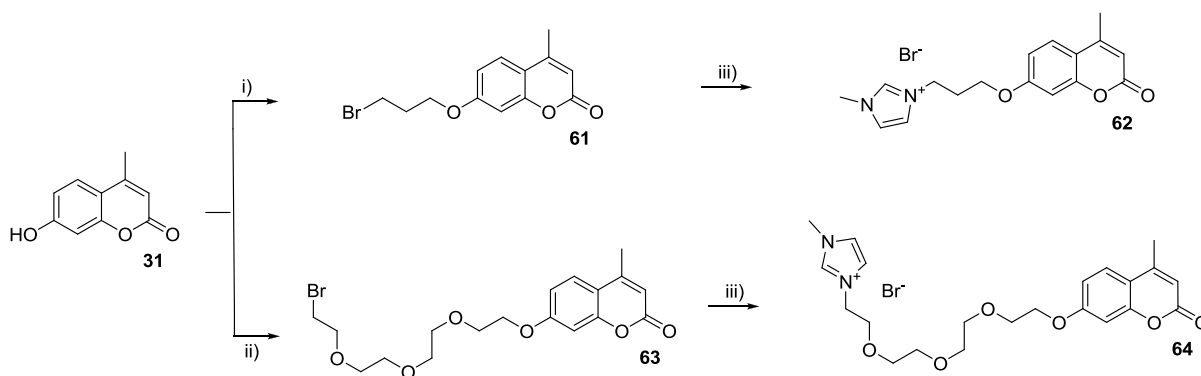


Figure III. 25 – Quadratic dependence of the scattered intensity in IL 60 before (black circles) and after (red circles) irradiation compared with that obtained in the reference solvent (chloroform, blue squares)

III.3 – Coumarin based ionic liquids

In previously described systems (chapter II), coumarin derivatives have shown to undergo photochemical dimerization upon irradiation which was explored to induce photocontrolled polymerization-scission of branched compounds. Thus, it was envisioned that organic cations of ILs bearing coumarin moieties could undergo photodimerization, and the subsequent changes in physical properties should be more significant than those resulting from *trans*-to-*cis* isomerization of cinnamate moieties. In effect, photodimerization would yield dicationic dimers, whose high symmetry and long alkylic chain lengths have shown to give rise to strong supramolecular interactions leading to highly viscous ILs.^{163,164}

For the design of photoresponsive ionic liquids based on coumarin photochemistry, the same synthetic strategy used for the preparation of ILs **55**, **58** and **60** was employed. Instead of *p*-coumaric acid **51**, 4-methyl-7-hydroxy-coumarin **31** was used as photosensitive moiety and linked to *N*-methylimidazolium cation through a alkylic chain and a polyether spacer (Scheme III. 6)



Scheme III. 6 - Synthetic pathway for the preparation of coumarin photoresponsive ionic liquids: i) 1,3-dibromopropane, K_2CO_3 , acetone, 92%; ii) 1,13-dibromotetraethylene glycol, K_2CO_3 , acetone, 86%; iii) *N*-methylimidazole, acetonitrile, 75-91%.

DSC data confirmed that both compounds melted below 100 °C and therefore no anion metathesis was performed. Similarly to IL **60**, the tetraethylene glycol moiety in the molecular structure of compound **64** had a marked effect on its melting temperature and it remained liquid up to -37 °C.

The photochemical behavior of compound **62** was initially investigated in solution. Figure III. 26a depict the spectral transformations of acetonitrile solutions of **62** upon irradiation at absorption maxima. It is evidenced that the compound undergoes photochemical transformations when irradiated, with a decrease in absorption around ca. 330 nm and a slight increase at lower wavelengths. These results are consistent with the expected photodimerization reaction of coumarin moieties and are comparable to the spectral transformations exhibited by compound **39** (chapter II.2). However, although the determined Φ_R values were similar to those calculated for **39**, there was no variation with

increasing concentration, suggesting that an intramolecular photochemical reaction took place upon irradiation (Figure III. 26b).

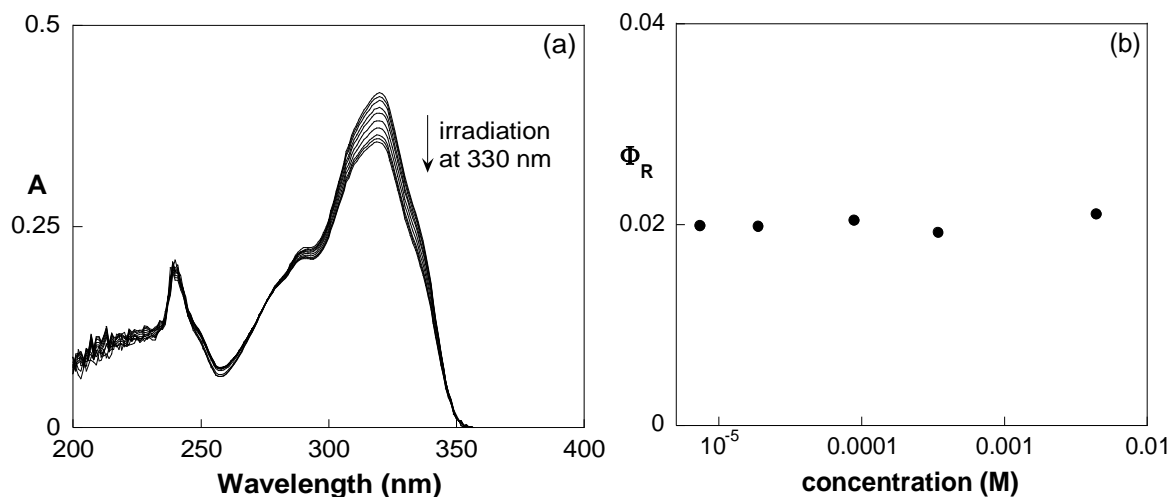


Figure III. 26 – (a) Spectral modifications of **62** at 1.7×10^{-5} M in acetonitrile upon irradiation at 300 nm. Total irradiation time is 60 min. (b) Photochemical quantum yield dependence with concentration of **62**.

Thus, ^1H NMR spectra were acquired for solutions of **62** before and after irradiation. The results, depicted in Figure III. 27, show that after irradiation only two imidazolium containing species are present in solution, indicated by the two singlets at ca. 10.3 and 10.8 ppm, which correspond to the $\text{C}_2\text{-H}$ proton of imidazolium moieties. However, when compared to the ^1H NMR spectra of 4-methyl-7-hydroxy-coumarin before and after dimerization (Figure III. 28), it is evidenced that **62** does not undergo [2+2]-cycloaddition. Although there is a reduction in peak intensity at 6.0 ppm, corresponding to proton $\text{C}_3\text{-H}$ of coumarin moiety, there is no concomitant increase in peak intensity at 3.5 ppm corresponding to the cyclobutane counterpart. Instead, a singlet at a slightly lower chemical shift at 5.8 ppm is detected, suggesting that $\text{C}=\text{C}$ double bond remains after irradiation. Furthermore, a singlet at ca. 1.3 ppm corresponding to the methyl protons of cyclobutane ring is not detected. Thus, it is anticipated that the photochemistry of coumarin moiety in **62** does not follow a conventional pathway.

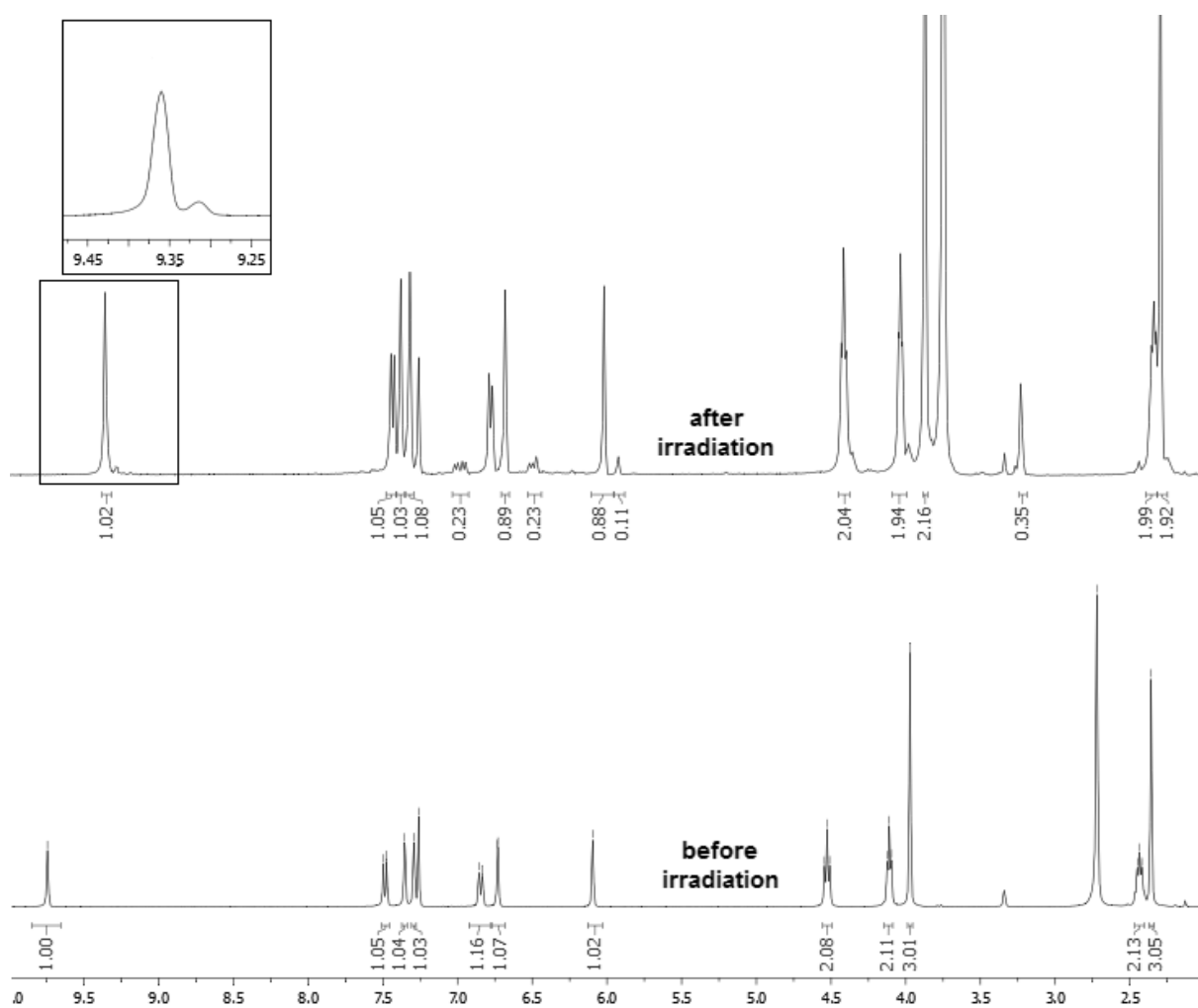


Figure III. 27 - ^1H NMR spectrum of 62 in chloroform before and after irradiation at 330 nm. Total irradiation time is 120 min.

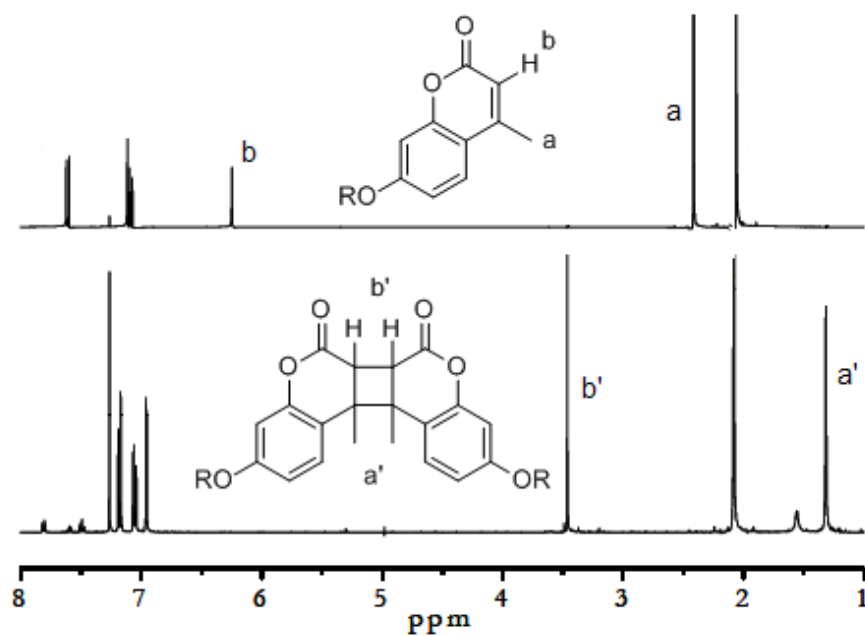
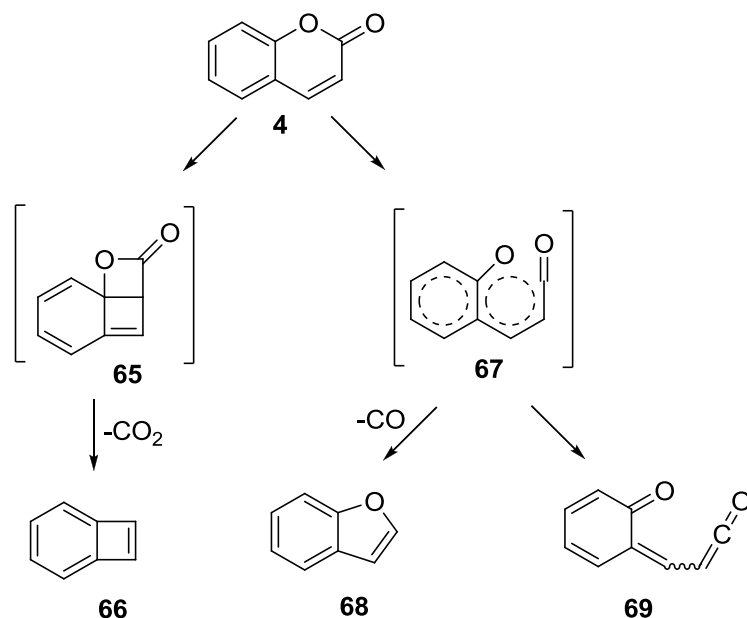
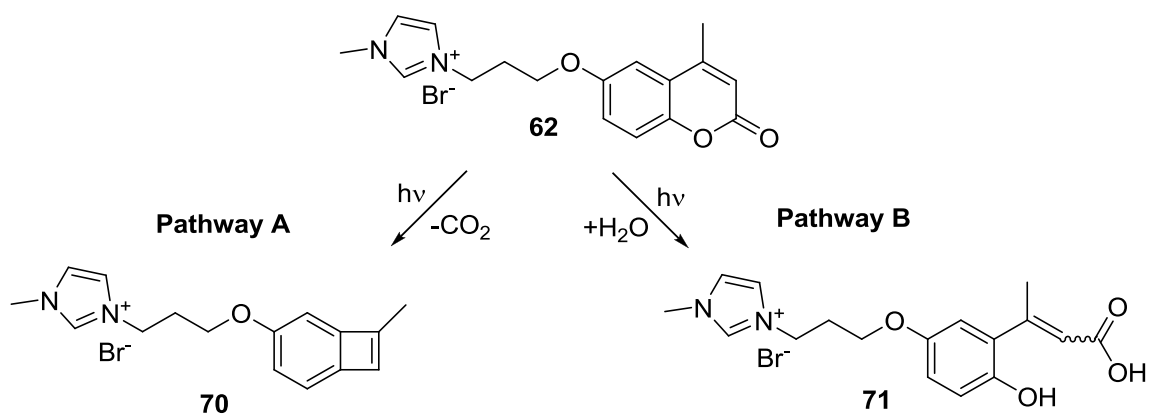


Figure III. 28 - ^1H NMR spectra of 4-methyl-7-alkoxy coumarin derivative in chloroform before and after photoinduced dimerization.

It has been demonstrated that unsubstituted coumarin in gaseous state and isolated in cryogenic matrixes media can give rise to photolytical reactions upon irradiation (Scheme III. 7).^{188,189} Ring-contraction into the Dewar isomer **65** and subsequent decarboxylation to yield benzocyclobutadiene **66** has been detected in cryogenic argon. In principle, this photochemical pathway (Scheme III. 8, pathway A) would yield a photoproduct with a ¹H NMR spectrum consistent with the one obtained after irradiation of **62**. It has also been shown that coumarin derivatives can give rise to Norrish Type I reactions, i.e., homolytical photocleavage of lactone moiety.¹⁸⁸ In gaseous state, this reaction leads to decarbonylation into benzofuran **68**, whilst in solid media results in the formation of aldehyde-ketene **69**. However, both of these compounds would give rise to proton peaks with higher chemical shift, and thus, are not consistent with the obtained results.¹⁸⁹ Furthermore, lactone ring opening is known to occur in the ground state in the presence of mild and strong nucleophiles.¹⁹⁰ Since the irradiation was not carried out in inert atmosphere, it is hypothesized that hydration into cinnamic acid derivative **71** could take place (Scheme III. 8, Pathway B).



Scheme III. 7 – Alternative photochemical reactions taken by coumarin derivatives



Scheme III. 8 – Suggested alternative photochemical reactions taken by compounds 62

It was also observed that the photochemistry of **62** does not change in neat conditions. Upon irradiation of a melted sample a very similar ^1H NMR spectrum was obtained (Figure III. 29), demonstrating that the photochemical reaction does not depend on the solvent.

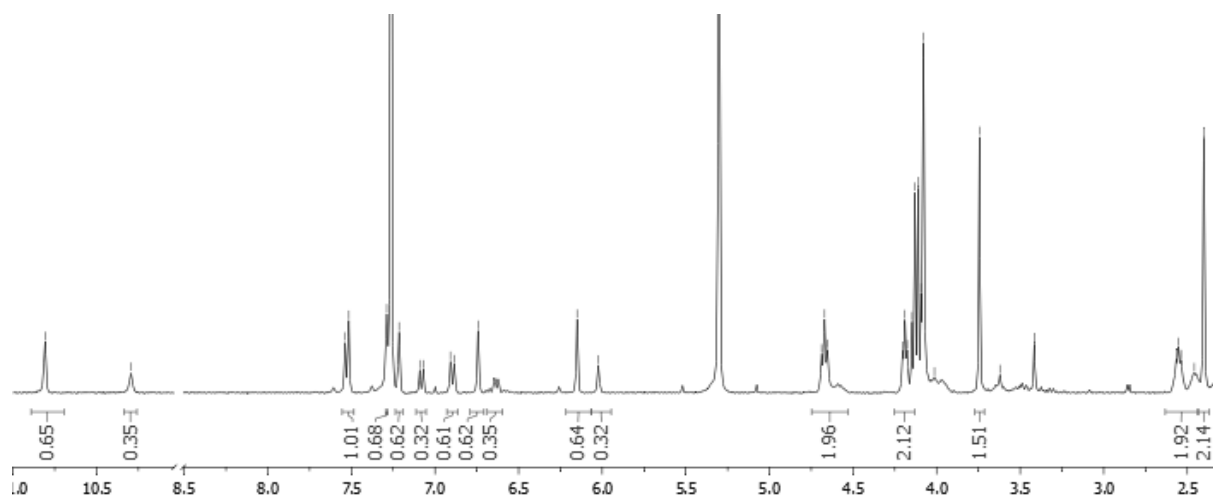


Figure III. 29 - ^1H NMR spectrum of **62** in chloroform after irradiation at 330 nm in neat conditions. Total irradiation time is 120 min.

Thus, in order to shed light on the mechanism of the photochemical reaction of **62**, irradiation of neat anhydrous samples was carried out under inert atmosphere. In principle, in the absence of water and other nucleophiles, **62** cannot undergo ring-opening of lactone moiety, whereas decarboxylation may still occur. The ^1H NMR spectrum acquired after irradiation under these conditions show that, indeed, **62** did not undergo any photochemical transformation, suggesting that the previously detected reaction occurred through ring-opening and concomitant hydration mechanism, resulting in the formation of cinnamic acid **71** (Figure III. 30). It is expected that the *cis*-isomer is primarily formed, due to the decrease in absorption observed in UV-Vis spectra (Figure III. 26a).

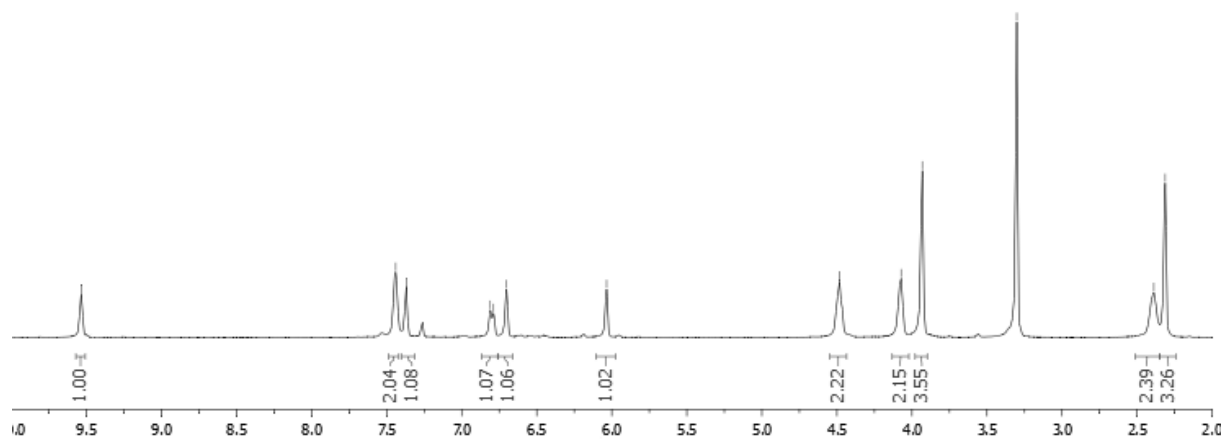


Figure III. 30 - ^1H NMR spectrum of **62** in chloroform after irradiation at 330 nm in neat conditions under inert atmosphere. Total irradiation time is 120 min.

Similarly to what was conducted for cinnamate ionic liquids **55** and **58**, the effect the photochemical reaction of **62** on its melting point was also investigated by differential scanning calorimetry. The thermograms obtained before and after irradiation (Figure III. 31), show that the melting point (onset temperature, T_m) is lower in the irradiated sample. Furthermore, the melting enthalpy (ΔH_m) is also significantly reduced, suggesting that, in parallel to what was observed for compounds **55** and **58**, that the structural order is reduced after irradiation, due to the presence of molecules of both **62** and photoproduct **71**.

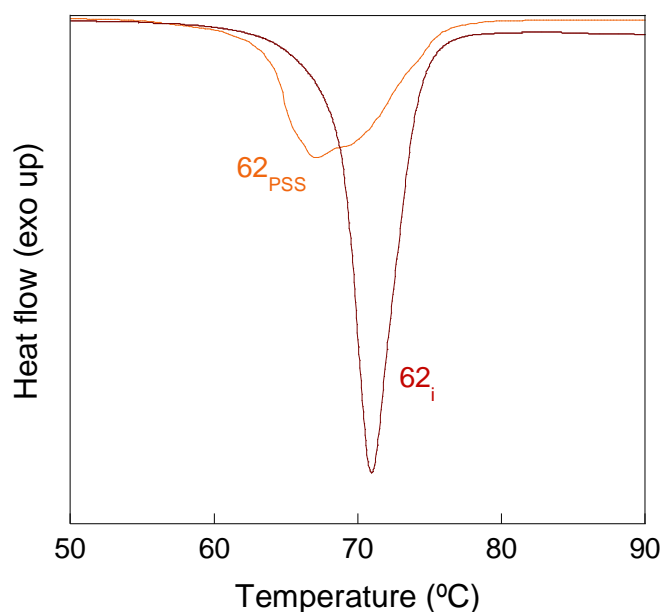


Figure III. 31 - DSC thermograms of ionic liquid **62** before (i) and after (PSS) irradiation at 330 nm.

Table III. 8 - Melting (T_m) and Peak (T_p) Temperatures and Melting Enthalpies (ΔH_m) of IL **62** before (i) and after (PSS) irradiation at 330 nm

compound	62_i	62_{PSS}
T_m (°C)	68.7	64.9
T_p (°C)	71.4	67.1
ΔH_m (Jg ⁻¹)	59.8	40.9

The photochemistry of **64** was also studied both in solution and neat conditions and followed by UV-Vis and NMR spectroscopy. It was observed that irradiation gave rise to spectral changes similar to those exhibited by compound **62** (Figure III. 32a). Although the photochemical quantum yield did not vary with concentration of **64**, its values were lower than those calculated for analog **62** (Figure III. 32b). ¹H NMR spectra obtained after irradiation (Figure III. 33) demonstrate that a similar

photochemical reaction occurs upon irradiation of **64**. Therefore, it is shown that, in parallel to what was observed for cinnamate-based ionic liquids, the tetraethylene glycol spacer had no significant effect on the photochemical properties of the synthesized ionic liquids.

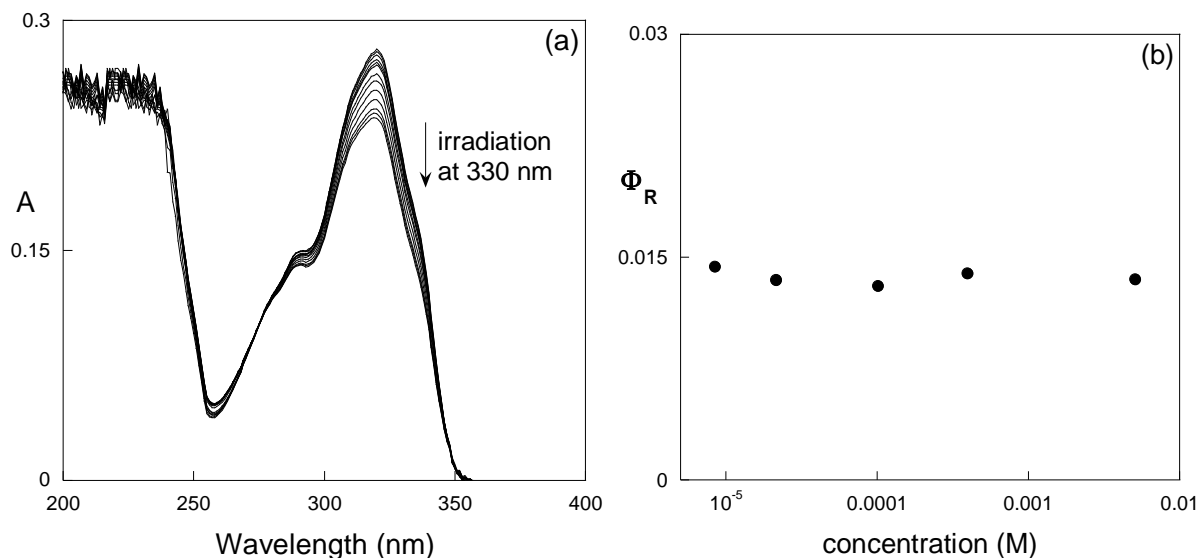


Figure III. 32 - (a) Spectral modifications of **64 at 1.1×10^{-5} M in acetonitrile upon irradiation at 330 nm. Total irradiation time is 60 min. (b) Photochemical quantum yield dependence with concentration of **64**.**

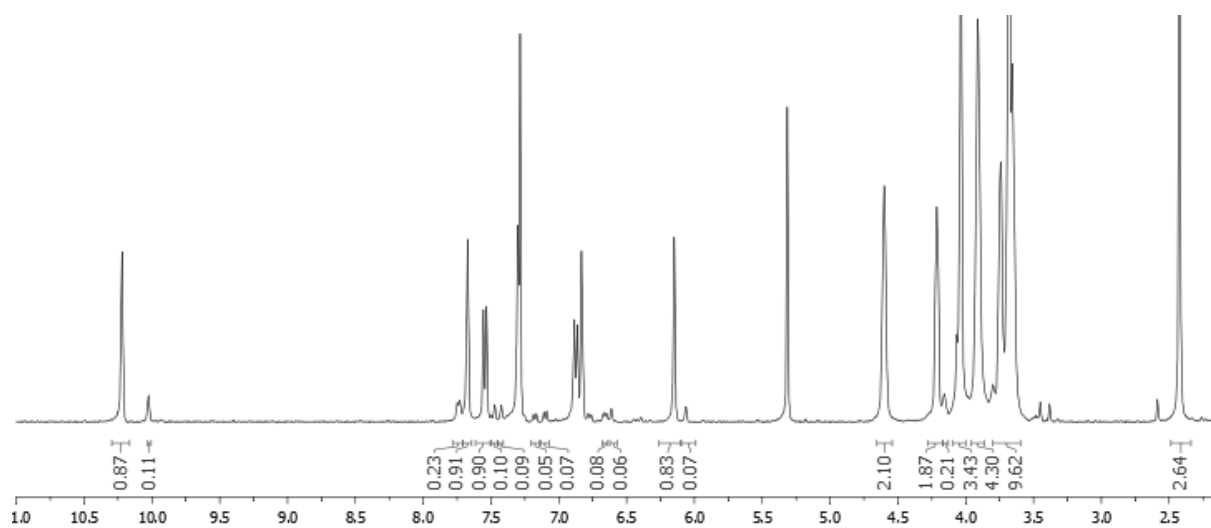


Figure III. 33 - ^1H NMR spectrum of **64 in chloroform obtained after irradiation at 330 nm. Total irradiation time is 120 min.**

The effect of the photochemical reaction on the physical properties of **64** was followed by viscosity measurements. Several QSPR studies have shown that the nature of intermolecular interactions established between cations and anions have a marked effect on IL viscosity. Thus, although **64** does not undergo the expected photodimerization reaction with concomitant increase in cation size and symmetry, it is anticipated that ring-opening of the lactone moiety gives rise to a

carboxylic acid function, which can give rise to hydrogen bond type interaction and increase viscosity.¹⁶⁴ Therefore, the viscosity of neat samples of **64** was measured before and after irradiation at 330 nm, and the results are depicted in Figure III. 34. The same experimental apparatus used for the characterization of the rheological properties of compound **60**, described in chapter III.1, was employed to evaluate the photorheological effect displayed by IL **64**. The flow curve associated with the non-irradiated state exhibits a Newtonian behavior with a constant viscosity at the selected shear rate range. This behavior is significantly different from what was observed for cinnamate analog **60**, suggesting that no liquid crystalline phases are formed in the presence of the coumarin moiety. However, upon irradiation, the rheological properties of **64** are markedly changed.

The zero-shear viscosity is significantly higher in the irradiated form (from ca. 7 to 90 Pa.s) which can be explained by a strengthening of intermolecular interactions arising from the formation of carboxylic acid moieties. In addition, instead of displaying a Newtonian behavior, a shear thinning effect is observed at high shear rates, suggesting that formation of liquid crystalline phases occur at the irradiated state.

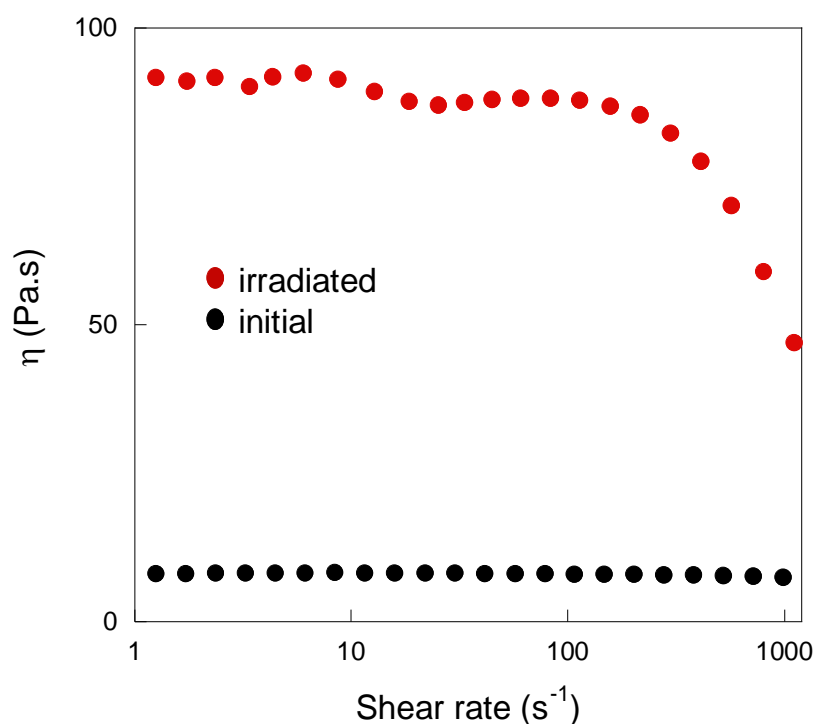


Figure III. 34 - Viscosity curve of pure **64** before (black dots) and after (red dots) irradiation at 330 nm. Total irradiation time is 120 min

In order to shed light on the effect of the photochemical reaction on intermolecular interactions on the liquid state, Hyper-Rayleigh scattering (HRS) spectroscopy was conducted on neat samples of **64**, before and after irradiation. Analogously to what was carried out for compound **60**, the hyperpolarizability, as well as its dipolar ($\beta_{J=1}$) and octupolar ($\beta_{J=3}$) tensorial components, associated depolarization (DR) and anisotropy (ρ) ratios were determined for **64** before and after irradiation and

the results are summarized in Table III.9 and the associated variation of HRS response is shown in Figure III. 35.

Table III. 9 - β_{HRS} , $\beta_{\text{J=1}}$ (dipolar) and $\beta_{\text{J=3}}$ (octupolar) values (in atomic units*, using Convention T) and depolarization ratios, DR, and anisotropies, ρ , deduced from HRS measurements at 1064 nm for compound **64, before and after irradiation**

compound	β_{HRS}	DR	ρ	$\beta_{\text{J=1}}$	$\beta_{\text{J=3}}$
64	227	4.8	0.86	420	360
64_{irrad}	423	5.1	0.80	790	640

* 1 atomic unit of $\beta = 3.62 \times 10^{-42} \text{ m}^4 \text{ V}^{-1} = 8.641 \times 10^{-33} \text{ esu}$.

In parallel to what was observed for compound **60**, the amplitude of β_{HRS} (227 at. units) determined for **64** is considerably high when compared to other imidazolium ionic liquids, which, in combination with the values determined for DR, ρ , $\beta_{\text{J=1}}$ and $\beta_{\text{J=3}}$, indicates that the supramolecular structure of this PRIL is organized as a nanocluster with a dominant dipolar response. However, the HRS response is weaker than that of the cinnamate analog, suggesting that the size of the nanocluster is smaller. These results are in good agreement with the observed values for the zero-shear viscosity of **64**, which is significantly lower than those determined for cinnamate IL **60**.

After irradiation, the HRS response of **64** increases significantly, indicating that the ionic nanocluster grows upon the photochemical reaction of the coumarin moiety. These results correlate well with those obtained in rheological experiments, where a significant increase in viscosity was observed upon irradiation. These results further support the formation of photoproduct **71**, whose carboxylic acid moiety should lead to the formation of strong intermolecular hydrogen-bonding type interactions and, consequently, in large ionic clusters.

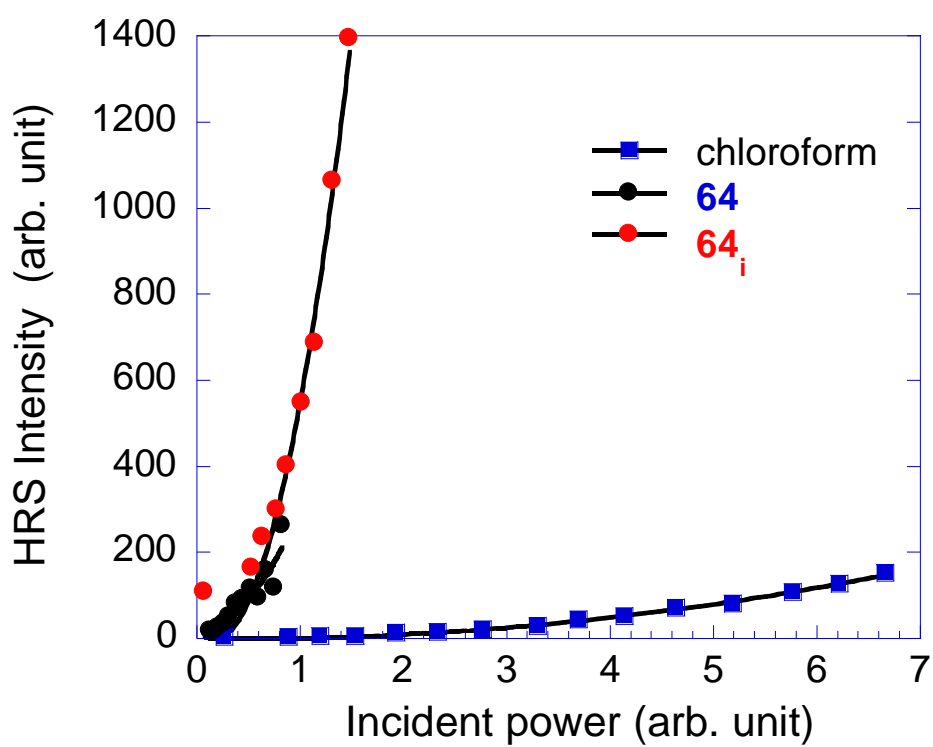
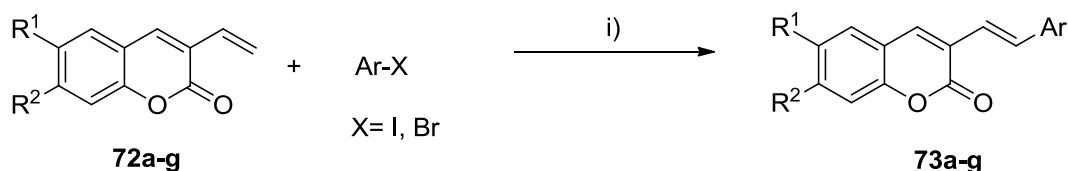


Figure III. 35 - Quadratic dependence of the scattered intensity in IL 64 before (black circles) and after (red circles) irradiation compared with that obtained in the reference solvent (chloroform, blue squares)

III.3.1 – Novel coumarin chromophores for the preparation of photoresponsive ionic liquids

Coumarin-based ionic liquids **62** and **64** exhibited photosensitivity which was applied to induce transformations at the molecular level, leading to changes in physical properties. These transformations were attributed to photochemical ring opening of the lactone moiety of the coumarin chromophore, since photochemical [2+2]-cycloaddition did not occur. Similarly, compounds **55**, **58** and **60** did not undergo photodimerization, and only *trans*-to-*cis* isomerization resulted upon irradiation, which also resulted in modification of physical properties. However, compound **39**, with the same coumarin moiety as ILs **62** and **64** exhibited the anticipated photochemical [2+2]-cycloaddition. Thus, it was hypothesized that dimerization of coumarin derivatives could not be achieved in electrically charged molecules, such as ionic liquids. Nevertheless, coumarins are versatile chromophores with outstanding photophysical properties that find application in a wide variety of systems such as organic light-emitting diodes, optical brighteners and fluorescent sensors.^{191,192,193,194,195,196,197} In addition, they are a common motif in a variety of naturally occurring compounds and display diverse pharmacological activity, namely as anticoagulant, antimicrobial, antibacterial, anticancer, anti-HIV, and antioxidant.^{198,199,200,201} Therefore, it was envisioned that new coumarin-based chromophores could be developed and functionalized with imidazolium cations to give rise to novel photoresponsive ionic liquids. Due to the high fluorescence quantum yield (Φ_F) of coumarin dyes, this strategy can, in principle, be employed to prepare fluorescent ionic liquids, expanding their applicability to luminescent materials. This class of compounds has gathered much attention in recent years, and efforts are made towards the development of ionic liquids with ever increasing fluorescence quantum yields, in particular in the visible region.²⁰²

In this chapter, the preparation of novel coumarin chromophores with extended π -electron system conjugation is described, and their photophysical and photochemical properties are studied. The preparation of 3-aryl coumarin moieties was previously reported using Heck coupling reactions between coumarin and aryl iodides in good yields. Following the same synthetic strategy a series of 3-styryl coumarins were prepared from their 3-vinyl analogs (Scheme III. 9) and their photophysical and photochemical properties were studied.



72a: R¹ = H ; R² = H

72b: R¹ = H ; R² = OMe

72c: R¹ = H ; R² = NEt₂

72d: R¹ = H ; R² = OCOPh

72e: R¹ = H ; R² = OCOCH₂CH=CH₂

72f: R¹, R² = -OCH₂O-

73a: R¹ = H ; R² = H ; Ar = Ph

73b: R¹ = H ; R² = OMe ; Ar = Ph

73c: R¹ = H ; R² = NEt₂ ; Ar = Ph

73d: R¹, R² = -OCH₂O- ; Ar = Ph

73e: R¹ = H ; R² = H ; Ar = *p*-NO₂Ph

73f: R¹ = H ; R² = OMe ; Ar = *p*-NO₂Ph

73g: R¹ = H ; R² = NEt₂ ; Ar = *p*-NO₂Ph

Scheme III. 9 – Synthetic pathway for the preparation of 3-styryl coumarins 73: i) Pd(OAc)₂, DMF, 9-98%.

The obtained 3-substituted coumarins were characterized towards their photophysical properties, such as UV-Vis absorption and emission spectra, fluorescence quantum yields (Φ_F) and excited state lifetimes (τ_m) (Table III. 10). It was showed that the nature of the substituent at position 7 and the extension of the conjugation of π -electron system have a marked effect on the absorption spectra of coumarins **72-73**. Introduction of electron-donating moieties gives rise to significant bathochromic shifts in the absorption maxima. This phenomenon is particularly evident for diethylamine substituent in compounds **72c**, **73c** and **73g** that display maximum absorption at wavelengths 70-90 nm higher than the unsubstituted analogs. Conversely, introduction of electron-withdrawing groups results in the coumarin core did not yield significant changes in the UV spectrum when compared to the parent compound. These results are explained by the fact that absorption bands in coumarin derivatives are related to the charge transfer from the benzenic cycle to the pyranone moiety. Inclusion of the aryl moiety in the vinyl substituent at position 3 also resulted in significant bathochromic shifts in the UV spectra of coumarins, due to the extension of the conjugated π -electron system. This effect was particularly pronounced when the aryl moiety contained a nitro group in *para* position due to its electron-withdrawing character. The emission spectra of the obtained compounds were also acquired and the fluorescence quantum yield (Φ_F) and the fluorescence decay times were determined. All coumarins follow a bi-exponential decay law, which reveals the existence of two states. These states could be a locally excited state (Franck-Condon state, longer lived) and a charge transfer state (shorter lived), in accordance with the known behavior of a large diversity of coumarin derivatives.²⁰³

Table III. 10 - Absorption and Emission Maxima, Fluorescence Quantum Yield and Average Fluorescent Lifetime of Selected Coumarins in Acetonitrile Solutions

compound	R ¹	R ²	Ar	λ_{abs} nm	ϵ cm ⁻¹ M ⁻¹	λ_{em} nm	ϕ_{F}	τ_{m} ns
72a	H	H	-	326	23535	413	0.08	0.39
72b	H	OMe	-	333	27607	425	0.99	2.84
72c	H	NEt ₂	-	400	33212	470	0.98	2.84
72d	H	OCOPh	-	328	25044	420	0.23	3.28
72e	H	OCOCH ₂ CH=CH ₂	-	320	23143	430	0.19	2.81
72f		-OCH ₂ O-	-	363	14504	448	0.65	3.68
73a	H	H	H	351	27618	440	0.61	2.48
73b	H	OMe	H	366	27860	464	0.71	2.75
73c	H	NEt ₂	H	421	24682	477	0.85	2.25
73d		-OCH ₂ O-	H	369	18408	469	0.53	2.95
73e	H	H	NO ₂	371	40311	539	0.04	0.08
73f	H	OMe	NO ₂	392	46130	610	0.24	1.23
73g	H	NEt ₂	NO ₂	459	57040	>800	n.d.	n.d.

Except for the unsubstituted compounds **72a** and **73a** all of the 3-styryl coumarins exhibit a lower fluorescence quantum yield than their 3-vinyl counterparts. These results are corroborated by the fluorescence decay times determined for these compounds, with the 3-styryl derivatives having slightly shorter average decay times than the 3-vinyl derivatives (Figure III. 36a). These data suggest that the introduction of an extra phenyl group in the system opens a new nonradiative deactivation pathway. *Trans*-to-*cis* isomerization is a reasonable hypothesis, and it is supported by previous reports.²⁰⁴ The unpredictably low fluorescence quantum yield of **72a**, which cannot undergo *cis-trans* isomerization, can be explained by its high photoreactivity ($\Phi_{\text{R}} \approx 0.20$ at $\lambda_{\text{irr}} = 313$ nm). This behavior is not exhibited by any of the other 3-vinyl coumarin derivatives, suggesting that the addition of an electron donating or withdrawing group at position 7, as well as the presence of a styryl group in position 3, deactivates this photoreaction. The shape of the absorption bands obtained for irradiated solutions of **72a** resembles the UV spectrum of unsubstituted coumarin, suggesting that the photochemical reaction occurs on the vinyl moiety at position 3 (Figure III. 37).

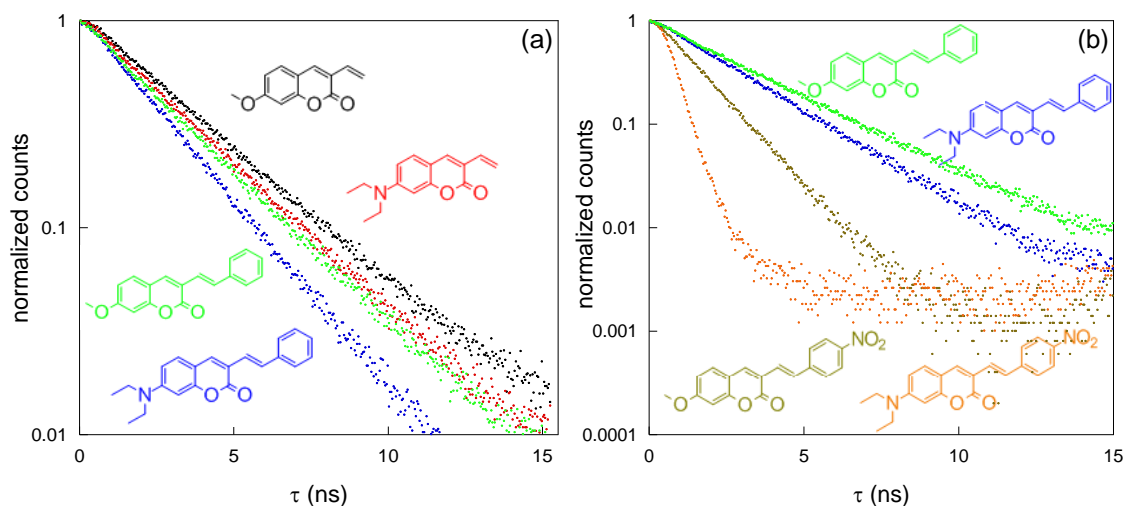


Figure III. 36 – (a) Fluorescence lifetime decays of 3-vinyl coumarins **72b** (black) and **72c** (red) and their respective 3-styryl counterparts **73b** (green) and **73c** (blue); Fluorescence lifetime of 3-styryl coumarins **73b** (green) and **73c** (blue) and their respective nitro derivatives **73f** (brown) and **73g** (orange).

The introduction of a *p*-nitro group in the 3-styryl moiety leads to considerable changes in the fluorescence properties of coumarin derivatives (**73e-g**), evidenced by a decrease in both Φ_F and τ_m . In the case of coumarin **73g**, Φ_F and τ_m are specially low and short, respectively, and the emission maximum occurs above 800 nm (above the instrumental resolution), due to the charge transfer coupling between the electron donating NEt_2 group and electron withdrawing NO_2 group.^{205,206}

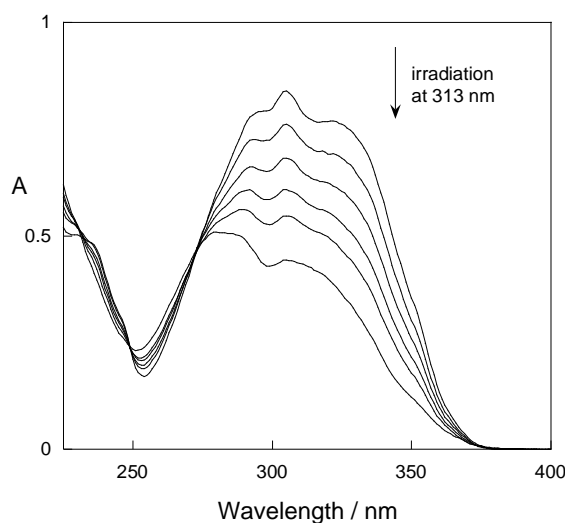
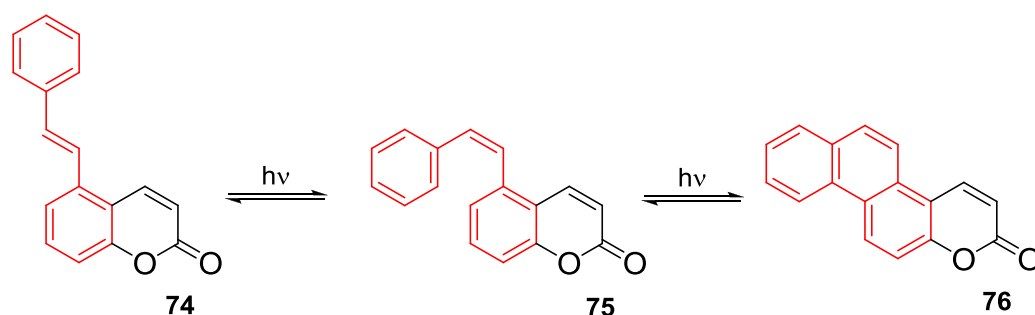


Figure III. 37 – UV-Vis spectral transformation of a solution of **72a** at 2.3 mM in acetonitrile upon irradiation at 313 nm. Total irradiation time is 30 min.

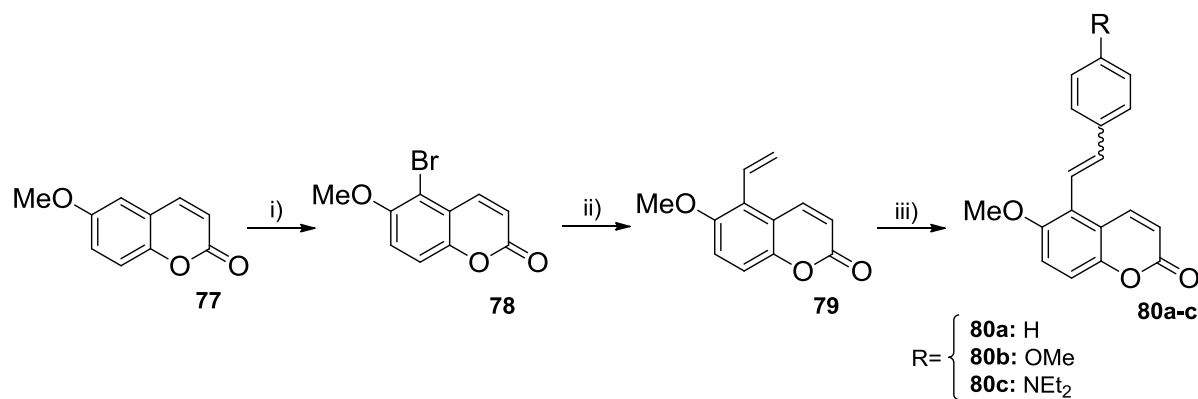
It was demonstrated that extension of the π -electron system conjugation in coumarins, through addition of vinyl or styryl moieties led to compounds with interesting photophysical properties with absorption and emission shifted to longer wavelengths when compared with parent coumarin. In addition, insertion of electron donating groups in the coumarin core led to compounds with very high fluorescence quantum yields, particularly in the case of 3-vinyl derivatives. However, the majority of

these compounds did not exhibit the anticipated photochemical activity required for the development of novel photoresponsive ionic liquids. Nonetheless, it was shown that Heck coupling reactions are convenient for the preparation of new coumarin derivatives. It was envisioned that appending the styryl moiety in the benzenic ring of the coumarin core could yield compounds with photochemical behavior similar to stilbene derivatives, which are known to undergo isomerization and/or oxidative cyclization upon irradiation (Scheme III. 10).



Scheme III. 10 – Suggested photochemical reactions of hypothetical coumarin-based stilbene analog **74**.

Previous reports showed that bromination of coumarin occurred in position 5 when a hydroxyl or alkoxy substituent was present in position 6. Therefore, 5-bromo-6-methoxycoumarin **78**, and subsequently 5-vinyl-6-methoxy coumarin **79**, were obtained from 6-methoxy coumarin **77** through reaction with OXONE/HBr and Suzuki coupling reactions. The extension of the π -electron system to 5-styryl coumarins **80a-c** was achieved by Heck palladium coupling reactions in moderate to high yields (Scheme III. 11 and Table III. 11). As expected, the yield decreases when electron donating groups are present at the iodoaryl substrate which is a consequence of a less favorable palladium insertion step (**80b** vs **80a**). On the other hand, the yield increases with the presence of electron withdrawing groups (**80c** vs **80a**). As opposed to what was observed in the synthesis of 3-styryl coumarins, this reaction was less stereoselective and the 5-styrylcoumarin derivatives **80a-c** were obtained as a mixture of both *E* and *Z* isomers (Table III. 11).



Scheme III. 11 – Synthetic pathway for the preparation of 5-styryl coumarins **80a-c**: i) OXONE®, HBr, dichloromethane, 91%; ii) [PdCl₂(dppf)].CH₂Cl₂, CH₂CHBF₃K, NEt₃, *n*-propanol, 92%; iii) Pd(PPh₃)₄, AgOAc, Ar-I, DMF, 50-90%.

Table III. 11 – Synthetic yields and Z/E ratio of coumarins 80a-c

Compound	R	Yield (%)	Z/E ratio
80a	H	80	32/68
80b	OMe	50	33/67
80c	NO ₂	90	17/83

The photophysics of coumarins **77**, **79** and **80a-c** was studied regarding their absorption and emission properties, as well as fluorescence quantum yield, Φ_F , excited state decay lifetimes, τ , and radiative and apparent non-radiative rate constants, k_r and k_{nr} (Table III. 12).

Table III. 12 - Absorption and Emission Maxima, Molecular Absorptivity, Fluorescence Quantum Yield, Average Fluorescent Lifetime and radiative and apparent nonradiative rate constants of selected coumarins

compound	R	λ_{abs} nm	ϵ cm ⁻¹ M ⁻¹	λ_{em} nm	Φ_F	τ_m ns	τ_1 ns (amp) τ_2 ns (amp)	k_r ns ⁻¹	k_{nr} ns ⁻¹
77	-	275	12890	430	0.02	0.3	0.2 (0.89)	0.06	3.06
		340	4974				2.5 (0.11)		
79	-	287	13619	462	0.03	0.8	0.1 (0.36)	0.04	1.21
		350	3128				1.1 (0.64)		
80a	H	269	19321	512	0.12	3.2	0.8 (0.08)	0.04	0.27
		308	21204				3.5 (0.92)		
		360	6248						
80b	OMe	279	22619	576	0.30	3.9	0.1 (0.08)	0.08	0.18
		317	21689				4.2 (0.92)		
		370	8363						
80c	NO ₂	333	22268	475	<0.01	n.d.*	n.d.*	n.d.*	n.d.*

*not determined due to the very low fluorescence quantum yield

Similarly to what was observed for compounds **73a-g**, the extension of the conjugation of the π -electron system led to bathochromic shifts both in absorption and emission bands of 5-styryl coumarins **80a-c** when compared to compounds **77** or **79**. In addition, the fluorescence lifetime follows a biexponential decay suggesting that the same excited states are formed upon absorption of light. However, introduction of styryl moieties in position 5 increases both fluorescence quantum yields and excited state lifetimes, essentially affecting the long-lived excited state of these coumarins, a behavior contrary to that exhibited by 3-styryl analogs, where more extended conjugation led to a decrease of both photophysical parameter values. In order to shed light on the effect of styryl substituents in the emissive behavior of compounds **80a-c**, the radiative (k_r) and apparent non-radiative rate constants (k_{nr}) were calculated for all compounds (equations III.1-2).

$$\tau_m = \frac{1}{k_r + k_{nr'}} \Leftrightarrow k_{nr'} = \frac{1}{\tau_m} - k_r \quad \text{III.1}$$

$$\Phi_F = k_r \tau_m \quad \text{III.2}$$

Whilst k_r values are similar for all studied coumarins, $k_{nr'}$ values are significantly larger for coumarins **77** and **79**, suggesting that introduction of the 5-styryl moiety affects essentially the non-radiative deactivation process. This could be explained by the anticipated photochemical reactions for these coumarin derivatives. Therefore, the photochemistry of all coumarins was investigated through ^1H NMR spectroscopy. Spectra of irradiated solutions of compounds **77**, **79** and **80a-c** revealed that with the exception of **79**, all the coumarins undergo photochemical reactions upon irradiation at appropriate wavelengths. However, there were two distinct photochemical reactions occurring in these coumarins. Compound **77** underwent photodimerization with a quantum yield of 0.32 (Figure III. 38), which is corroborated by the presence of new multiplets at 3.80 ppm the doublets at 6.60, 6.85 and 7.10 ppm corresponding to the cyclobutane moiety and benzenic ring of coumarin dimers, respectively.

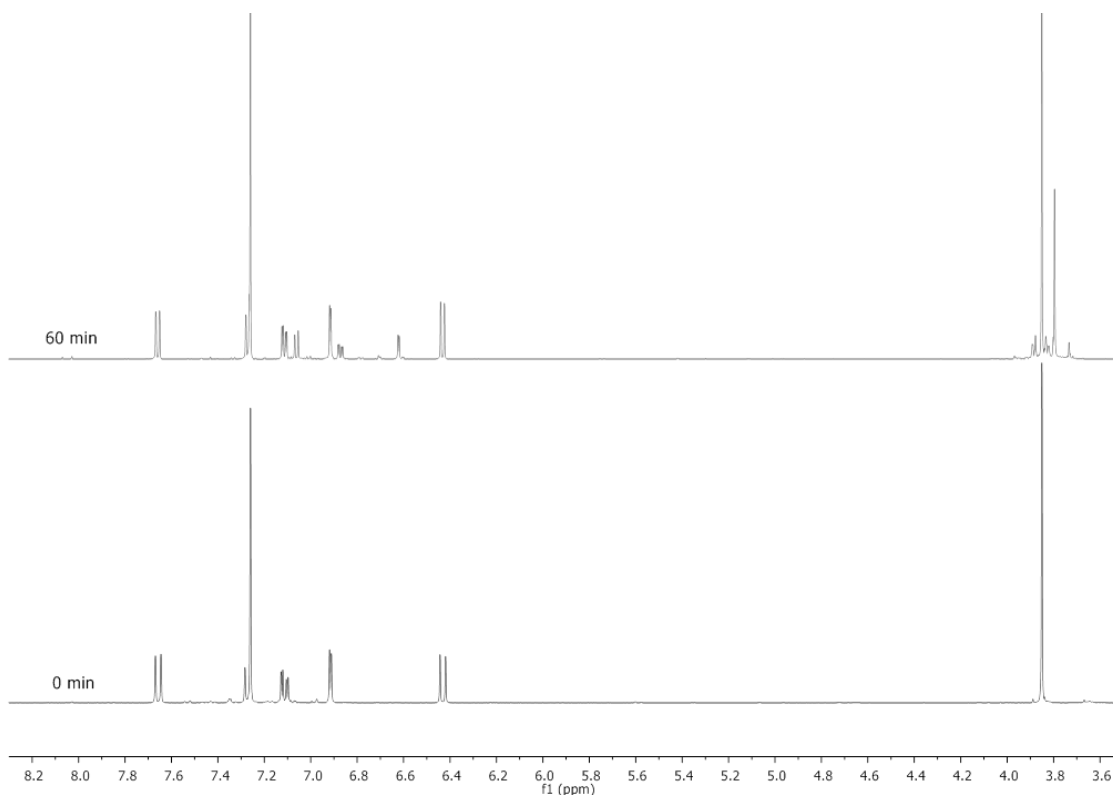


Figure III. 38 - ^1H NMR spectra (400 MHz, CDCl_3) of a solution of coumarin **77** before (red) and after (blue) irradiation for 60 min. $\lambda_{\text{irrad}} = 275 \text{ nm}$

On the other hand, 5-styryl derivatives **80a-c** exhibited *E-Z* isomerization around the exocyclic double bond $C_\alpha-C_\beta$ with relatively high quantum yields Φ_p (from 0.44 to 0.75) (Figure III. 39-41). For compound **80a**, this is evidenced by the intensity increase in doublets at 6.6 and 7.6 ppm, corresponding to the exocyclic double bond protons of the *Z* isomer. Similar results were obtained for compounds **80b** and **80c**, with doublets with increased intensity detected at 6.3 and 7.3 ppm and at 6.2 and 7.8 ppm, respectively in their ^1H NMR spectra.

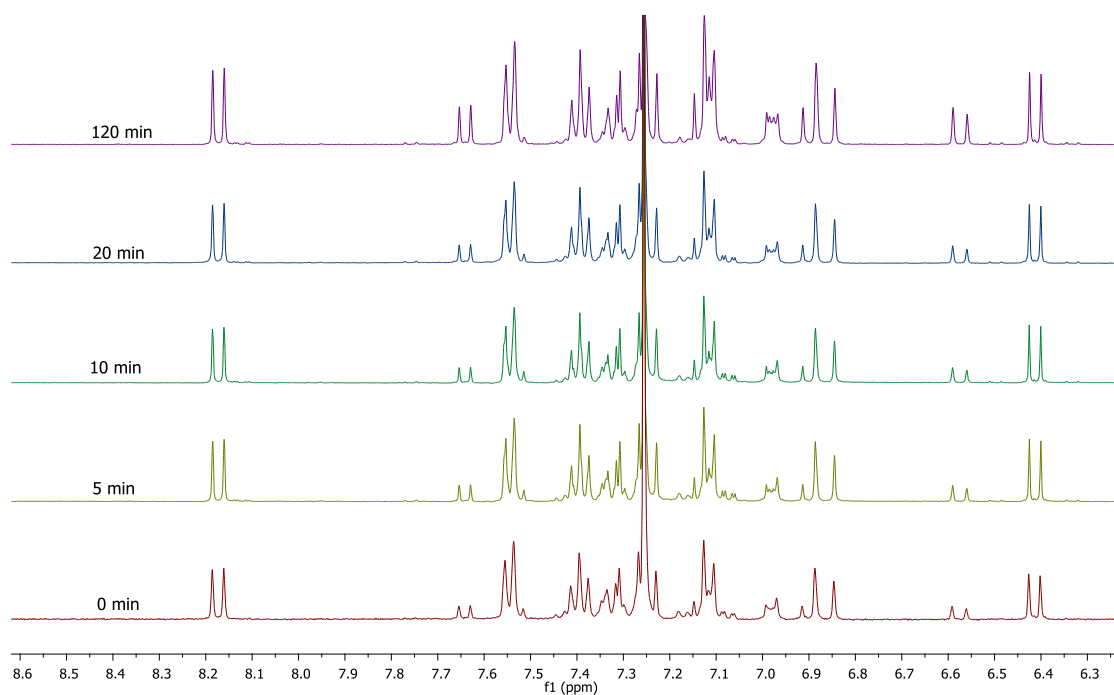


Figure III. 39 - ^1H NMR spectra (400 MHz, CDCl_3) of a solution of coumarin **80a** irradiated at different times: 0 min (red); 5 min (yellow); 10 min (green); 20 min (blue); 120 min (purple). $\lambda_{\text{irrad}} = 360 \text{ nm}$

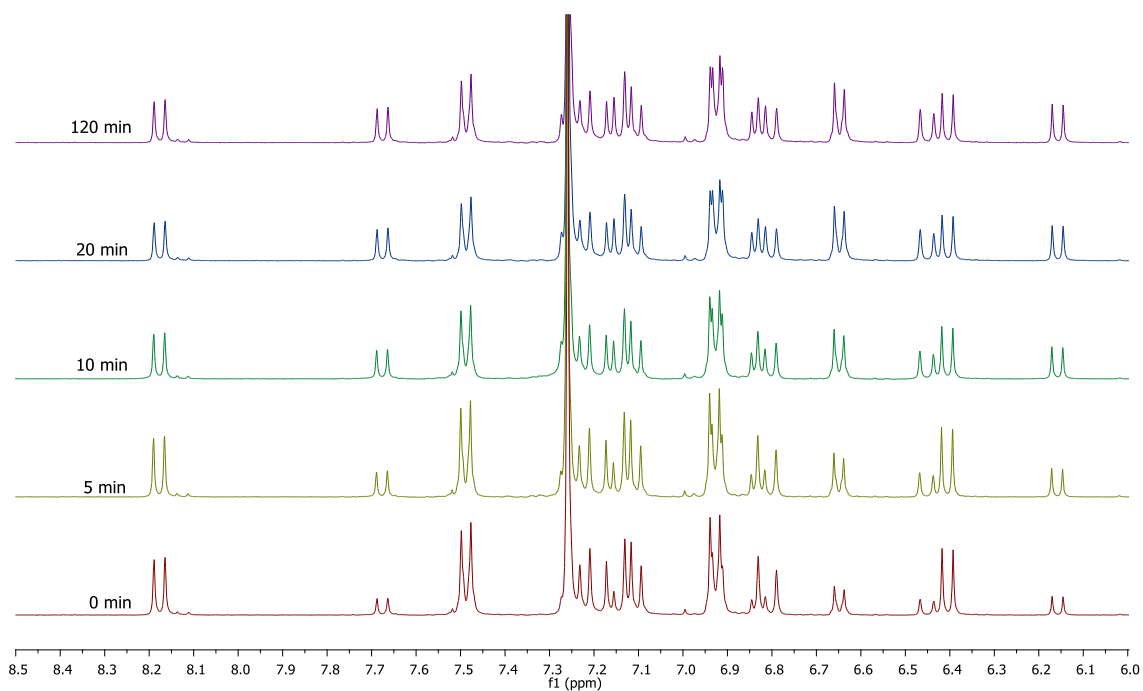


Figure III. 40 - ^1H NMR spectra (400 MHz, CDCl_3) of a solution of coumarin 80b irradiated at different times: 0 min (red); 5 min (yellow); 10 min (green); 20 min (blue); 120 min (purple). $\lambda_{\text{irrad}} = 370 \text{ nm}$

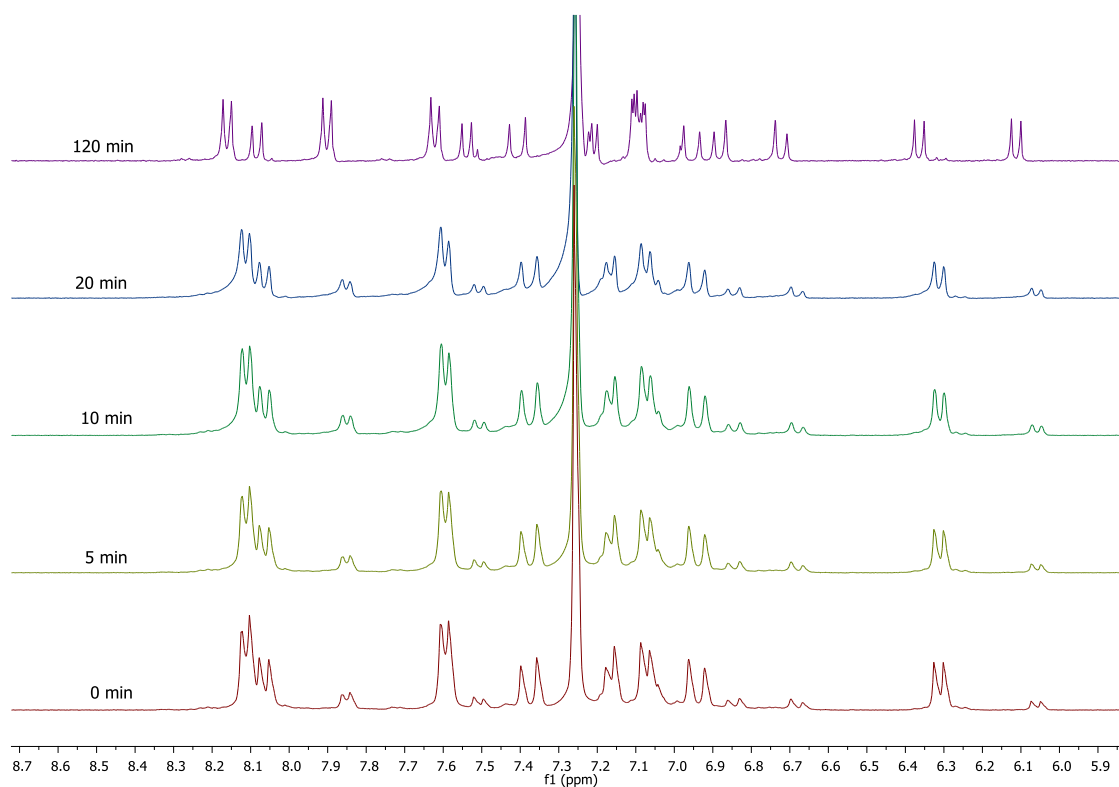


Figure III. 41 - ^1H NMR spectra (400 MHz, CDCl_3) of a solution of coumarin 80c irradiated at different times: 0 min (red); 5 min (yellow); 10 min (green); 20 min (blue); 120 min (purple). $\lambda_{\text{irrad}} = 333 \text{ nm}$

Unlike compound **77** or the 5-styryl derivatives, 5-vinyl coumarin **79** did not evidence photochemical reactivity and changes in ^1H NMR spectra were not detected. However, a relatively

high k_{nr} was determined for this compound, suggesting that it undergoes a significant deactivation process. It was hypothesized that this radiationless deactivation pathway could be similar to the 5-styryl derivatives, going through a rotation around the exocyclic double bond $C_\alpha-C_\beta$ upon irradiation. This hypothesis is compatible with the observed absence of changes in NMR spectra since in compound **79** there are no substituents at the β -position. Furthermore, computational studies show that the exocyclic double bond length of styrene increases in the first excited state, reducing its double bond character and facilitating the rotation.^{207,208} Therefore, it is estimated that an analogous process can occur in 5-vinyl coumarin and to test this theory, similar computational calculations were made for compounds **79** and **80a**.

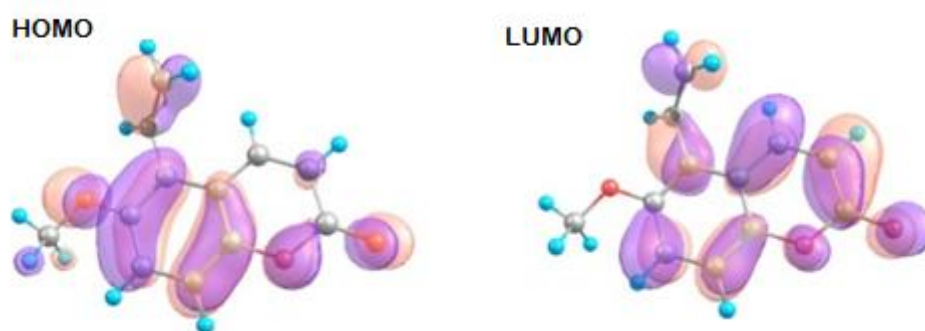


Figure III. 42 - Frontier orbitals for compound **79** obtained from density functional theory (DFT) calculations

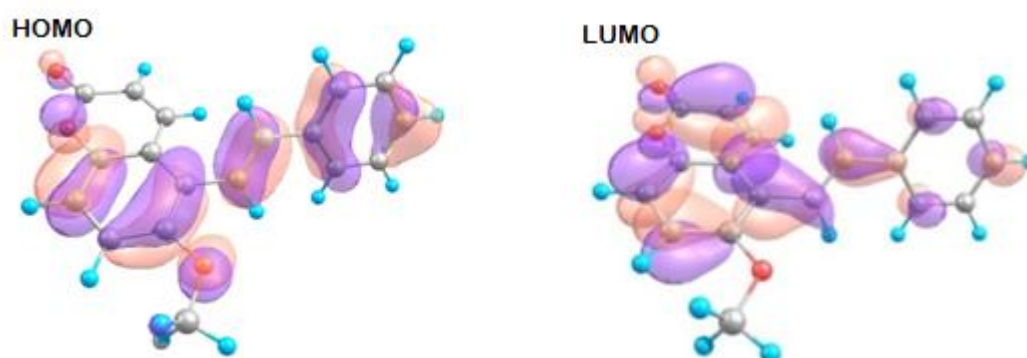


Figure III. 43- Frontier orbitals for compound **80a** obtained from density functional theory (DFT) calculations

Frontier molecular orbitals for these compounds are shown in Figure III. 42-43. For coumarins **79** and **80a** the S_1 state is mainly due to the HOMO-LUMO transition, both for the *E* and *Z* isomers. Excitation of the most abundant *E* isomer to form its first excited state leads to a change in molecular orbital symmetry around $C_\alpha-C_\beta$. Thus an electron excitation from the HOMO to the LUMO leads to a reduction of electronic density around the exocyclic C=C double bond and therefore a decrease of the

rotational barrier in the excited state, for both 5-vinyl coumarin **79** and 5-styryl coumarin **80a**. These results suggest that the main deactivation pathway of **79** could be similar to that of 5-styryl coumarins, i.e., rotation around C=C double bond, and thus, the photodimerization pathway does not occur in coumarins with unsaturated moieties at position 5.

The fact that k_{nr} value is significantly larger for **79** when compared to 5-styryl-coumarins could arise from the lack of substituents at C_β, that may slow down rotation around C=C double bond. With Φ_p values determined for coumarins **77** and **80a-b**, it is possible to calculate reaction rate constant k_p (equation III.3) and non-radiative rate constant k_{nr} (equation III.4).

$$k_p = \frac{\Phi_p}{\tau_m} \quad \text{III.3}$$

$$k_{nr} = k_{nr'} - k_p \quad \text{III.4}$$

The relatively large k_p values calculated for **80a-b** indicate that photoisomerization is the main non-radiative pathway of the deactivation of the excited state for 5-styryl coumarins, and justify the low fluorescence of these derivatives (Table III. 13). The difference in the isomerization quantum yields between coumarins **80a-c** can be justified by the nature of the substituent at the *para* position of the styryl group. In principle, electron-donating groups such as the methoxy group should increase the double bond character of the exocyclic double bond rendering the isomerization less effective, whilst electron-withdrawing groups such as the nitro moiety should have the opposite effect.

Table III. 13 - Fluorescence and Reaction Quantum Yield, Average Fluorescent Lifetime and radiative, nonradiative and reactive rate constants of selected coumarins

compd	R	Φ_F	τ_m ns	k_r ns ⁻¹	k_{nr} ns ⁻¹	PSS	Φ_p	k_p ns ⁻¹
						isomer ratio		
75	-	0.02	0.3	0.06	3.06	-	0.32	1.00
77	-	0.03	0.8	0.04	1.21	-	-	-
80a	H	0.12	3.2	0.04	0.27	55/45	0.59	0.18
80b	OMe	0.30	3.9	0.08	0.18	45/55	0.44	0.11
80c	NO ₂	<0.01	n/d*	n/d*	n/d*	49/51	0.75	n/d*

*not determined due to the very low fluorescence quantum yield

In order to evaluate the applicability of these 5-styryl coumarin derivatives as photochromic dyes, *E-Z* isomerization was also followed by UV-Vis spectroscopy. Table III. 13 shows the initial and photostationary state mole fractions of both isomers, as well as photoreaction quantum yield, Φ_p , (dimerization for **79**, and isomerization for **80a-c**) and respective rate constants. Spectral changes

observed upon irradiation of solutions of **80a-c** in methanol are depicted in Figure III. 44. Because all the compounds were isolated as isomer mixtures, irradiation was carried out at the lowest energy transition, in order to irradiate preferentially the most abundant *E* isomer. The decrease in absorbance at the absorption maximum of 308 nm, concomitant with an increase in absorbance at the lower wavelength part of the spectrum is consistent with *E-Z* photoisomerization, with the *Z*-isomer being less stable due to sterical hindrance that forces the aromatic ring out-of-plane and prevents more extended conjugation.

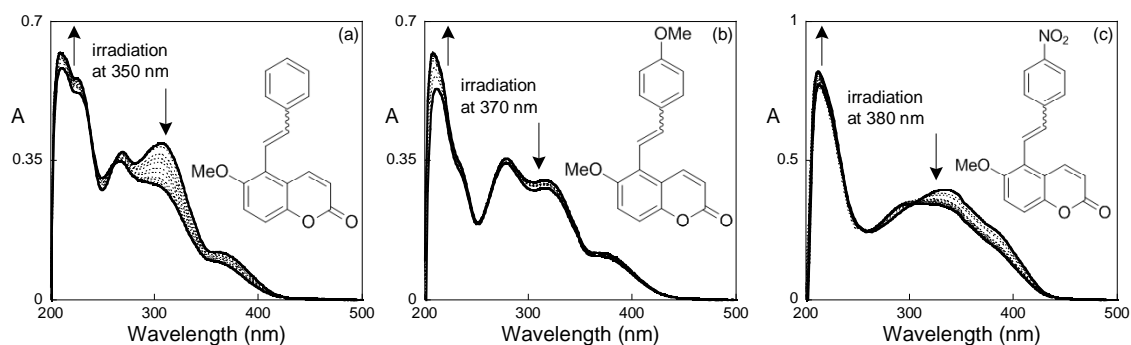


Figure III. 44 – UV-Vis spectral modification of coumarins **80a** (a), **80b** (b) and **80c** (c) in acetonitrile upon irradiation at the longest wavelength transition.

The isomer ratio at the photostationary state was determined by NMR spectroscopy to be ca. 50% for **80a-c** (Table III. 13). Further conversion was not possible probably due to the rather high similarity in the absorbance spectra of both isomers. This was demonstrated by TDDFT calculations for lowest-lying excited singlet states for compound **80a**. Figure III. 45 depicts an overlay of the calculated electronic spectra of both *E* and *Z* isomers, as well as a mixture of the *E* and *Z* spectra with the experimentally (NMR) determined percentages of 0.68 and 0.32 respectively (Table III. 11). It is demonstrated that the observed spectral changes upon irradiation of compound **80a** (Figure III. 46a) are consistent with a decrease in the amount of *E* isomer which is the species that absorbs preferentially in the 300 nm region and an increase of *Z* isomer which is the isomer that absorbs more strongly at longer wavelengths. The determined maxima at 266, 300 and 335 nm are consistent with the maxima observed experimentally at 269, 308 and 360 nm shown in Table III. 12. Furthermore, the predicted spectra for pure *trans* and pure *cis* isomers are show absorption bands at similar wavelength values, justifying the isomer proportion at the photostationary state.

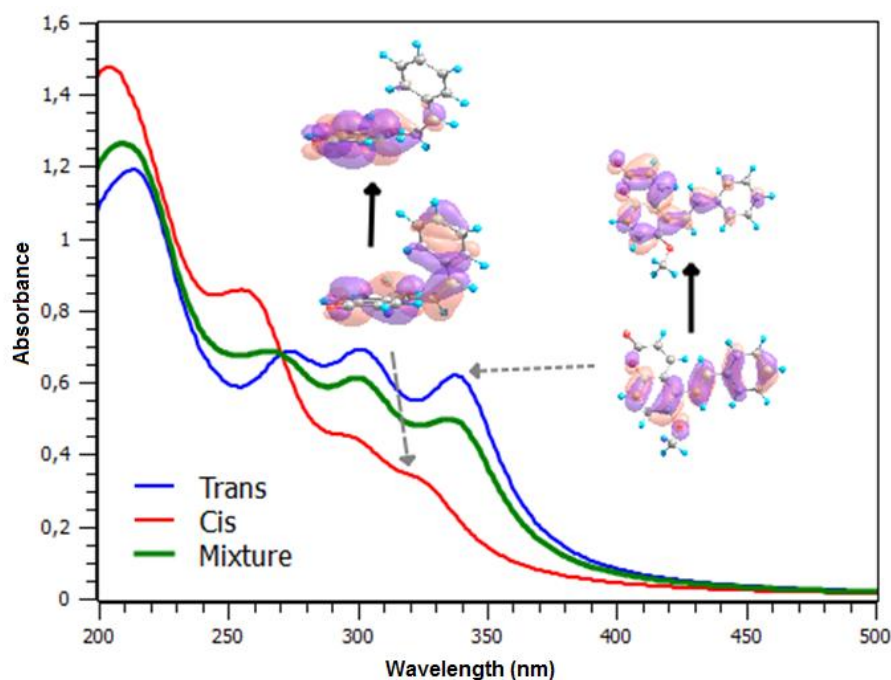


Figure III. 45 - Calculated spectra for the *Z* and *E* isomers of **80a** and the combined spectra of the mixture of isomers with experimental molar fractions

From experimental NMR and UV-Vis spectroscopy data, the difference in molar absorptivities of isomers were determined and the low values further support these results ($\Delta\epsilon=1143 \text{ cm}^{-1} \text{ M}^{-1}$ for **80a** (317 nm); $\Delta\epsilon=703 \text{ cm}^{-1} \text{ M}^{-1}$ for **80b** (317 nm); $\Delta\epsilon=1502 \text{ cm}^{-1} \text{ M}^{-1}$ for **80c** (333 nm)).

The photoswitching of 5-styryl coumarin derivatives was also tested in plastic media. After adsorption in thin N-hydroxyethylacrylamide/poly (ethyleneglycol)dimethacrylate copolymer film, coumarin **80b** was irradiated and its photoreaction followed by fluorescence spectroscopy. The results are depicted in Figure III. 46b.

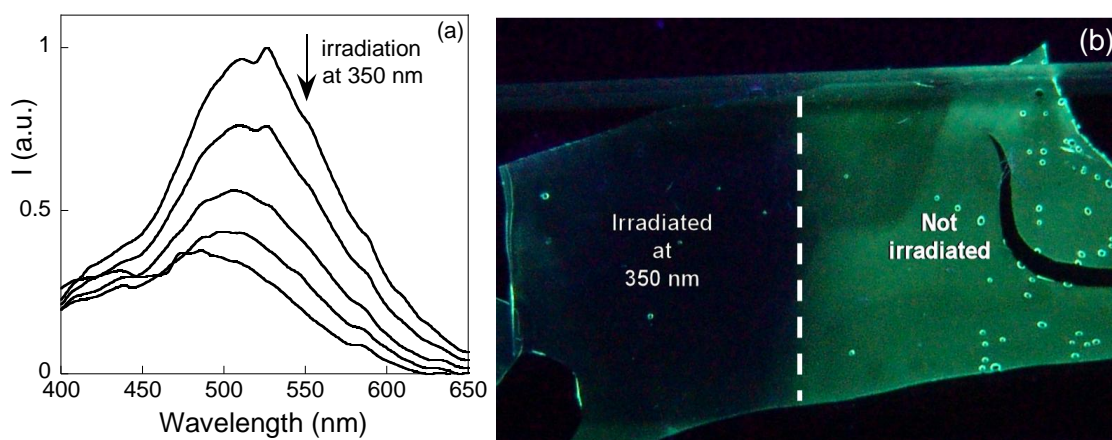


Figure III. 46 – Fluorescence variation of coumarin **80b** adsorbed into hydroxyethylacrylamide/ poly(ethyleneglycol) dimethacrylate copolymer film upon irradiation at 350 nm; (a) followed by fluorescence spectroscopy; (b) photograph under UV light.

From the studies conducted in coumarin derivatives with unsaturated moieties in positions 3 or 5, it is demonstrated that extension of the π -electron system leads to chromophores with different photophysical and photochemical properties. Whereas derivatization with vinyl and styryl moieties at position 3 affects mainly the absorption and emission properties of coumarins, resulting in highly fluorescent compounds that absorb and emit light at longer wavelengths, derivatization at position 5 leads to compounds with different photochemistry from parent compounds. Instead of the typical photodimerization reaction of coumarins, these compounds exhibited a photochemical reaction similar to stilbene derivatives, undergoing photoisomerization around the exocyclic double bond. Although the photochromism evidenced by these compound is negligible, due to the similarity of absorption spectra of both isomers, their emissive properties are distinct and photoswitching from an emissive to a non-emissive state is possible. Thus, 5-styryl coumarin derivatives are interesting chromophores for the development of photoactive ionic liquids. Not only it was previously demonstrated that *trans-to-cis* isomerization may give rise to changes in the physical properties of ILs, the photoswitching of fluorescent properties may extend the applicability of this class of compounds.

III.4 – Conclusions

Through functionalization of organic imidazolium cations with photoresponsive moieties, a new class of stimuli responsive ionic liquids was obtained. By varying the chemical nature of the spacer between the imidazolium moiety and the chromophore, it was possible to tailor the melting point of the prepared ionic liquids. From UV-Vis and NMR spectroscopy data it was demonstrated that cinnamic acid based ionic liquids undergo the anticipated reversible *trans-to-cis* isomerization upon irradiation. Crystallography and Hyper-Rayleigh scattering spectroscopy data showed that this reaction led to a disruption of intermolecular interactions established in the ionic network, which resulted in a decrease in melting point or viscosity. Coumarin based analogs did not give rise to the anticipated photodimerization reaction, which should yield the opposite effect due to the formation of larger and more symmetrical cations. Instead, it was demonstrated that these compounds undergo irreversible lactone ring opening upon irradiation. However, due to the formation of carboxylic acid moieties, the strength of intermolecular interactions in the ionic network increased, resulting in an increase in viscosity. In addition, two families of styryl coumarins were prepared and it was demonstrated that their photochemical and photophysical properties are greatly influenced by the position and nature of the appended substituents. In particular, 5-styryl coumarins exhibited *trans-to-cis* isomerization around the exocyclic double bond upon irradiation with good yields, which expands their applicability and lead to novel photoresponsive ionic liquids with interesting properties.

IV. Conclusions and Future Perspectives

Stimuli-responsive rheological fluids have gained considerable scientific and technological interest over the past decades. They find application in a variety of systems, especially in the domain of clutches, brakes, vibration damping and valves, where magnetic or electric fields are the applied stimuli of choice. However, the development of rheological fluids that respond to irradiation of light offer a third paradigm for rheology modulation and overcomes several issues inherent to magneto- or electrorheological fluids, such as stability and durability problems or the need for complex system assemblies. In addition, photorheological fluids present the advantage of allowing the control of rheology at the microscopic and nanoscale, expanding the applicability of these materials as microvalves for microfluidic systems or photocontrolled carriers for drug delivery. Nonetheless, photorheological fluids still present several drawbacks that need to be addressed and are subject of great attention in scientific research. For example, from the photochemical point of view, these materials are often based on isomerization and dimerization reactions of photoresponsive molecules, which have inherently slow and inefficient or incomplete reversibility. In addition, being usually aqueous or organic solutions, PR fluids can only be applied in pressure and temperature conditions that common solvents can withstand, limiting their application. Thus, the development of novel photorheological fluids presents many challenges and is of great fundamental interest. Under this light, the systems described in this thesis, in particular those based on photoresponsive ionic liquids, present a breakthrough in photorheological fluid research, allowing for the preparation of materials with expanded applicability, due to the high thermal stability and low vapor pressure this class of compounds. In addition, being single component systems, these IL-based PR fluids exhibit the same changes in both microviscosity and macroviscosity, which does not occur in polymer/surfactant based fluids. Albeit these developments, the reversibility is still a factor that requires further attention. One possible strategy to overcome this drawback consists of replacing the naturally occurring photoresponsive moieties of cinnamic acid and coumarin with synthetic derivatives that present different photochemical properties. For instance, the anthracene based compounds evidenced improved photochemical quantum yields over the coumarin counterparts, and are known to exhibit reversible photochemistry. On the other hand, the novel coumarin chromophores with extended conjugation evidenced enhanced photophysical and photochemical properties and can also be exploited for the development of novel PR fluids with greater reversibility and stability, especially if used for the functionalization of organic cation or anions.

It can be concluded that new pathways for the development of photorheological fluid have been opened with this work. However, in parallel with many scientific findings, new strategies pose new problems, and therefore, there is still a lot of effort to be made in this area.

V. Experimental Part

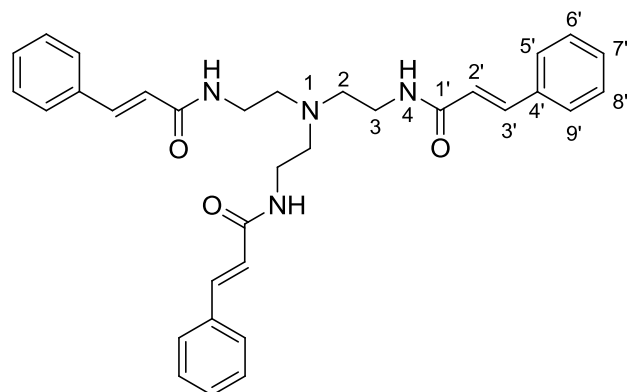
Synthesis

Acetone, acetonitrile, dichloromethane and chloroform were dried by standing 48 hours in 3Å molecular sieves under Argon atmosphere.²⁰⁹ Triethylamine, *N*-methylimidazole and tris(2-aminoethyl)amine were distilled under reduced pressure and stored in 3Å molecular sieves for 24 hours before use. All other chemicals were of analytical grade and used as obtained from the supplier. ¹H and ¹³C NMR spectra were recorded at 400 MHz and 100MHz respectively using a Bruker AMX400 in CDCl₃ referenced to the solvent for both proton and carbon spectra. Elemental analyses (EA) were performed using a Thermofinnigan Flash EA 112 Series.

Procedures

The numbering of the molecular structures of the synthesized compounds did not follow IUPAC rules. Instead, moieties within each compound were numbered separately in order to clarify NMR signal attribution.

Tris(2-(cinnamamide)ethyl)amine (**16**)

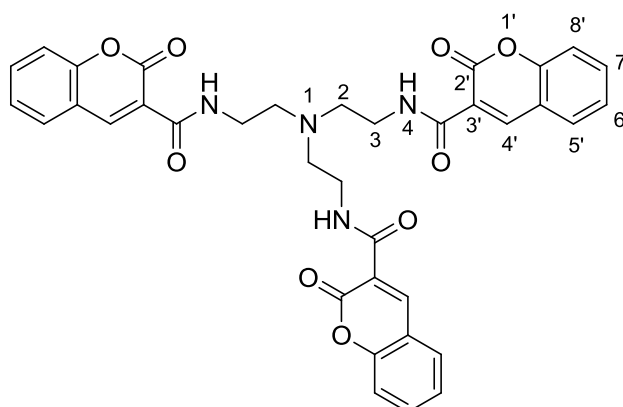


Cinnamic acid **14** (2.0 g, 13.5 mmol) was dissolved in dry chloroform under inert atmosphere and thionyl chloride (3.2 g, 27 mmol) was added dropwise while stirring. The reaction mixture was refluxed for 12 hours and diluted with dichloromethane. The resulting solution was washed with water until gas evolution was not detected. The organic phase was washed with NaHCO₃ 1%, dried (MgSO₄) and evaporated *in vacuo* to yield 2.0 g (89 %) of cinnamoyl chloride **15** as pale brown solid, which was used in subsequent reactions without purification.

Cinnamoyl chloride **15** (2.0 g, 12 mmol) and dry tris(2-aminoethyl)amine **13** (513 mg, 3.5 mmol) were dissolved in dry dichloromethane and dry potassium carbonate (1.8 g, 13 mmol) was added. The

resulting mixture was refluxed while stirring for 12 hours. After cooling down to room temperature, the white solid was filtered off. The filtrate was diluted with 150 mL dichloromethane, washed with saturated NaHCO₃ and brine and dried with anhydrous MgSO₄. The organic phase was concentrated by rotatory evaporation and petroleum ether was added. The resulting precipitate was filtered off and washed with cold diethyl ether, to yield 1.7 g (91%) of compound **16** as a pale yellow solid. For analytical purposes, compound **16** was recrystallized with diethyl ether from chloroform. ¹H RMN (CDCl₃) δ (ppm): 7.53 (d, *J* = 15.6 Hz, 3H, H_{3'}), 7.14-7.20 (m, 9H, H_{5'}, H_{7'}, H_{9'}), 6.99 (t, *J* = 7.6 Hz, 9H, H₄, H_{6'}, H_{8'}), 6.60 (d, *J* = 15.6 Hz, 3H, H_{2'}), 3.47 (m, 6H, H₃), 2.66 (m, 6H, H₄); ¹³C NMR (CDCl₃) δ (ppm): 161.9, 140.9, 134.6, 129.4, 128.6, 127.8, 120.6, 53.2, 37.5; EA calculated for C₃₃H₃₆N₄O₃: C 73.85; H 6.76; N 10.44; found: C 73.93; H 6.84; N 10.32.

Tris(2-(coumarin-3-amide)ethyl)amine (**22**)



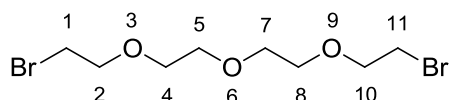
To a stirred solution of 2 g (10.5 mmol) of coumarin-3-carboxylic acid (**20**) in dry chloroform, 2.5 g (21 mmol) of thionyl chloride were added dropwise for 5 min. The resulting mixture was refluxed for 12 hours. After cooling down to room temperature, dichloromethane (150 mL) was added and the solution was washed with water (20 mL) until gas evolution was not detected. The organic phase was then washed with NaHCO₃ 1% and dried with anhydrous MgSO₄. The solvent was removed by rotatory evaporation to yield 2 g (90%) of acyl chloride derivative **21** as a pale yellow solid, which was used in subsequent reactions without purification.

Acyl chloride derivative **21** (2 g, 9.5 mmol) and dry tris(2-aminoethyl)amine **13** (0.44g, 3 mmol) were dissolved in dry dichloromethane and dry potassium carbonate was added (1.38g, 10 mmol). The resulting mixture was refluxed while stirring for 12 hours. After cooling down to room temperature, the white solid was filtered off. The filtrate was diluted with 150 mL dichloromethane, washed with saturated NaHCO₃ and brine and dried with anhydrous MgSO₄. The organic phase was concentrated by rotatory evaporation and petroleum ether was added. The resulting precipitate was filtered off and

washed with cold diethyl ether, to yield 1.9 g (95%) of compound **22** as a pale yellow solid. For analytical purposes, compound **22** was purified from chloroform with diethyl ether.

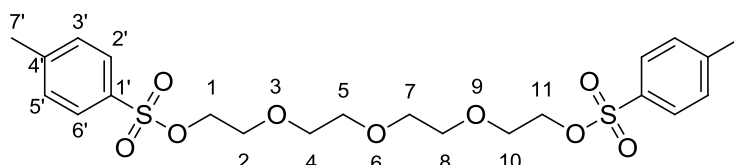
$^1\text{H NMR}$ (CDCl_3) δ (ppm): 8.97 (m, 3H, H_4), 8.75 (s, 3H, H_4'), 7.61-7.54 (m, 6H, H_5 , H_7), 7.31 (t, $J = 7.46$ Hz, 3H, H_6), 7.10 (d, $J = 8.32$ Hz, 3H, H_8), 3.62-3.57 (m, 6H, H_3), 2.86 (t, $J = 5.56$ Hz, 3H, H_2); $^{13}\text{C NMR}$ (CDCl_3) δ (ppm): 161.7, 161.0, 154.3, 147.5, 133.4, 129.7, 124.9, 119.0, 118.7, 116.4, 53.2, 38.2. EA calculated for $\text{C}_{36}\text{H}_{30}\text{N}_4\text{O}_9$: C 65.25; H 4.56; N 8.46; found: C 64.93; H 4.28; N 8.32.

1,11-dibromo-3,6,9-trioxaundecane (**24**)



To a suspension of 15.72 g (62 mmol) of triphenylphosphine in dry acetonitrile at 0°C , 9.6 g (62 mmol) of bromine were added dropwise under inert atmosphere during 30 minutes. To the resulting mixture, a solution of 6.0 g (31 mmol) of tetraethylene glycol (**59**) in acetonitrile was added dropwise. The reaction was allowed to warm up to room temperature and stirred for 48 hours. The white precipitate was removed by filtration and the solvent was removed by rotatory evaporation, resulting in an orange-colored residue, which was extracted several times with hexane. The combined extracts were concentrated *in vacuo* and 8.52 g (87%) of colorless oil were obtained. For analytical purposes, further purification was achieved by silica gel flash column chromatography (dichloromethane as eluent). $^1\text{H NMR}$ (CDCl_3) δ (ppm): 3.82 (t, $J = 6.34$ Hz, 4H, H_2 , H_{10}), 3.68 (s, 8H, H_4 , H_5 , H_7 , H_8), 3.48 (t, $J = 6.34$ Hz, 4H, H_1 , H_{11}); $^{13}\text{C NMR}$ (CDCl_3) δ (ppm): 71.2, 70.7, 70.5, 30.4; EA calculated for $\text{C}_8\text{H}_{16}\text{Br}_2\text{O}_3 \cdot 0.1 \text{CH}_2\text{Cl}_2$: C 29.61; H 4.97; found: C 29.84; H 4.68

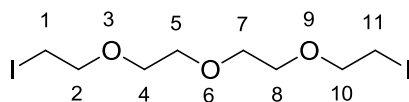
1-11-di-*O*-tosyl-3,6,9-trioxaundecane (**25**)



A solution of 10 g (51.5 mmol) of tetraethylene glycol (**59**) and 19.6 g (103 mmol) of *p*-toluenesulfonyl chloride in dichloromethane was cooled to 0°C with an ice bath. Potassium hydroxide (23 g, 412 mmol) was carefully added in small portions so that the mixture was kept below 5°C . The reaction was left stirring for 5 hours at 0°C and dichloromethane and water were added. The organic

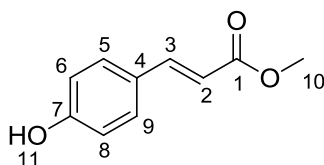
layer was separated and the water layer was extracted with dichloromethane. The combined organic extracts were washed with water and dried with anhydrous magnesium sulfate. The solvent was removed *in vacuo* to yield 25.1 g (97 %) of a colorless oil, requiring no further purification. ^1H NMR (CDCl_3) δ (ppm): 7.77 (d, $J = 7.9$ Hz, 4H, $\text{H}_{2'}$, $\text{H}_{6'}$), 7.32 (d, $J = 7.9$ Hz, 4H, $\text{H}_{3'}$, $\text{H}_{5'}$), 4.13 (t, $J = 4.4$ Hz, 4H, H_1 , H_{11}), 3.66 (t, $J = 4.4$ Hz, 4H, H_2 , H_{10}), 3.54 (s, 8H, $\text{H}_{4,8}$), 2.42 (s, 6H, $\text{H}_{7'}$); ^{13}C NMR (CDCl_3) δ (ppm): 144.9, 133.0, 129.9, 128.0, 70.7, 70.5, 69.3, 68.7, 21.6; EA calculated for $\text{C}_{22}\text{H}_{30}\text{O}_9\text{S}_2$: C 52.57; H 6.02; S 12.76; found: C 52.71; H 6.07; S 11.44.

1,11-diiodo-3,6,9-trioxaundecane (**26**)



To a solution of 10.0 g (20 mmol) of **59** in acetone, sodium iodide 12.0 g (80 mmol) was added and the resulting suspension was refluxed for 8 hours. The white solid was filtered off and the solvent was removed by rotatory evaporation. The residue was redissolved in dichloromethane, washed with brine and dried over potassium sulfate. Removal of the solvent *in vacuo* afforded 7.7 g (94%) of Di-iodo TEG as a pale orange liquid. For analytical purposes, further purification was achieved by silica gel flash column chromatography (hexanes/ethyl acetate eluent). ^1H NMR (CDCl_3) δ (ppm): 3.74 (t, $J = 7.0$ Hz, 4H, H_2 , H_{10}), 3.65 (s, 8H, $\text{H}_{4,8}$), 3.25 (t, $J = 7.0$ Hz, 4H, H_1 , H_{11}); ^{13}C NMR (CDCl_3) δ (ppm): 72.0, 70.7, 70.2, 3.0. EA calculated for $\text{C}_8\text{H}_{16}\text{I}_2\text{O}_3$: C 23.21; H 3.90; found: C 23.50; H 3.88.

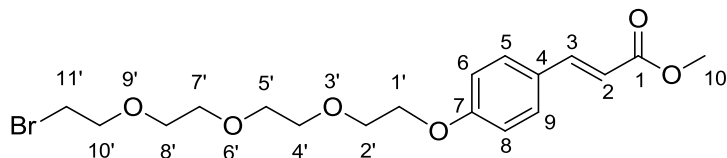
(*E*)-Methyl *p*-(hydroxy)cinnamate (**27**)



To a solution of 5 g (30 mmol) of *p*-hydroxy cinnamic acid (**51**) in methanol (50 mL), a drop of conc. sulfuric acid was added. The resulting mixture was refluxed while stirring for 5 hours. After cooling down to room temperature, dichloromethane (100 mL) and water (100 mL) were added. The organic phase was collected and the aqueous phase washed twice with dichloromethane (100 mL). The combined organic extracts were washed with NaHCO_3 1%, brine and dried with anhydrous MgSO_4 . The solvent was removed by rotatory evaporation to yield 5.0 g (94%) of white solid, requiring no further purification. ^1H NMR (CDCl_3) δ (ppm): 7.64 (d, $J = 15.9$ Hz, 1H, H_3), 7.43 (d, $J = 7.9$ Hz, 2H,

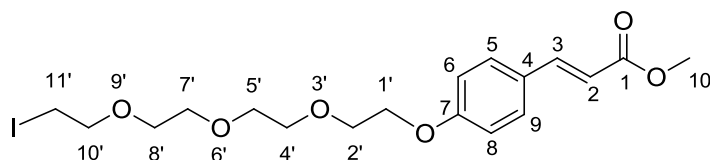
H₅, H₉), 6.85 (d, *J* = 8.0 Hz, 2H, H₆, H₈), 6.30 (d, *J* = 15.9 Hz, 1H, H₂), 5.69 (s, 1H, H₁₁), 3.80 (s, 3H, H₁₀). ¹³C NMR (CDCl₃) δ (ppm): 168.3, 158.0, 144.9, 130.0, 127.0, 115.9, 115.0, 51.8. EA calculated for C₁₀H₁₀O₃: C 67.41; H 5.66; found: C 67.66; H 5.37. m.p. 135-137 °C

(*E*)-Methyl *p*-(11-bromo-3,6,9-trioxaundecanoxy)cinnamate (**28**)



To a solution of 1.0 g (5.6 mmol) of (*E*)-methyl *p*-(hydroxy)cinnamate (**27**) in dry acetone, 5.4 g (16.9 mmol) of 1,11-dibromo-3,6,9-trioxaundecane (**24**) were added. To the resulting mixture, 1.55 g (11.2 mmol) of potassium carbonate were added in one portion and the reaction was refluxed overnight while stirring. The white solid was removed by filtration and the solvent was removed by rotatory evaporation. The residue was purified by silica gel flash column chromatography (hexanes/ethyl acetate eluent) and 2.1 g (91%) of dark yellow oil were obtained. After dissolution in chloroform and filtration through a pad of activated charcoal a pale yellow oil was obtained. ¹H NMR (CDCl₃) δ (ppm): 7.64 (d, *J* = 16.0 Hz, 1H, H₃), 7.46 (d, *J* = 8.6 Hz, 2H, H₅, H₉), 6.92 (d, *J* = 8.7 Hz, 2H, H₆, H₈), 6.31 (d, *J* = 16.0 Hz, 1H, H₂), 4.16 (t, *J* = 4.7 Hz, 2H, H₁), 3.87 (t, *J* = 4.8 Hz, 2H, H₂), 3.79-3.82 (m, 5H, H₁₀, H₁₀'), 3.73 (m, 2H, H₄'), 3.69 (m, 2H, H₅'), 3.67 (s, 4H, H₇, H₈'), 3.46 (t, *J* = 6.3 Hz, 2H, H₁₁); ¹³C NMR (CDCl₃) δ (ppm): 167.8, 160.6, 144.5, 129.7, 127.3, 115.4, 115.0, 71.2, 70.9, 70.7, 70.6, 70.5, 67.6, 51.6, 30.4, 30.3; EA calculated for C₁₈H₂₅BrO₆·0.35 CHCl₃: C 48.01; H 5.57; found: C 48.09; H 5.57

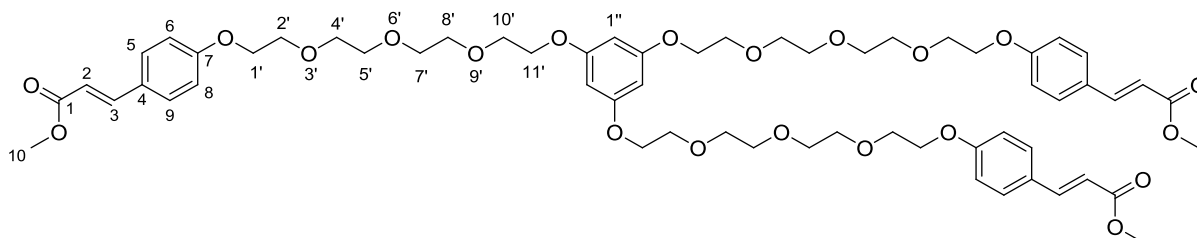
(*E*)-Methyl *p*-(11-iodo-3,6,9-trioxaundecanoxy)cinnamate (**30**)



1,11-diiodo-3,6,9-trioxaundecane (**26**) (5.0 g, 12 mmol) and (*E*)-Methyl *p*-(hydroxy)cinnamate (**27**) (1.07 g, 6 mmol) were dissolved in dry acetonitrile and potassium carbonate (1.24 g, 9 mmol) was added. The reaction was stirred and refluxed overnight under inert atmosphere. The white solid was

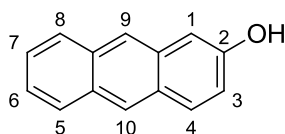
removed by filtration and the filtrate was concentrated *in vacuo*. The residue was redissolved in dichloromethane and washed with saturated sodium bicarbonate, brine, and dried over MgSO₄. Removal of the solvent afforded a brown colored liquid which was purified by silica gel flash column chromatography (hexanes/ethyl acetate eluent), to yield 2.0 g (72%) of Iodo-TEG-Cinnamate as pale yellow oil. ¹H NMR (CDCl₃) δ (ppm): 7.64 (d, *J* = 16.0 Hz, 1H, H₃), 7.46 (d, *J* = 8.8 Hz, 2H, H₅, H₉), 6.92 (d, *J* = 8.8 Hz, 2H, H₆, H₈), 6.31 (d, *J* = 16.0 Hz, 1H, H₂), 4.16 (t, *J* = 4.8 Hz, 2H, H_{1'}), 3.87 (t, *J* = 4.8 Hz, 2H, H_{2'}), 3.79 (s, 3H, H₁₀), 3.66-3.76 (m, 10H, H_{4'-10'}), 3.25 (t, *J* = 7.0 Hz, 2H, H_{11'}); ¹³C NMR (CDCl₃) δ (ppm): 167.6, 160.4, 144.6, 129.9, 127.1, 115.2, 115.0, 71.2, 70.9, 70.8, 70.7, 70.5, 67.6, 51.6, 30.4, 3.0; EA calculated for C₁₈H₂₅IO₆: C 46.56; H 5.43; found: C 46.20; H 5.23.

1,3,5-tris(11-(*p*-(3-methoxy-3-oxoprop-1-enyl)phenoxy)3,6,9-trioxaundecanoxy)benzene (**31**)



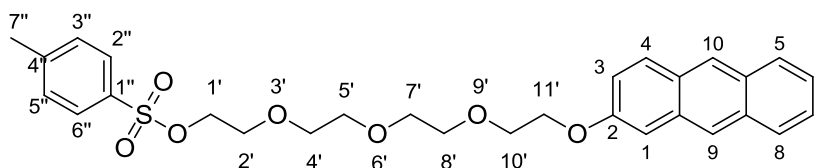
To a solution of 2.0 g (4.3 mmol) of (*E*)-Methyl *p*-(11-iodo-3,6,9-trioxaundecanoxy)cinnamate (**30**) in dry acetonitrile, 155 mg (1.23 mmol) of sublimed phloroglucinol and 690 mg (5.0 mmol) of dry potassium carbonate were added. The reaction mixture was stirred and refluxed overnight under inert atmosphere. The white solid was filtered off and the solvent was removed by rotatory evaporation. The oily residue was purified by silica gel flash column chromatography (hexanes/ethyl acetate eluent) and 120 mg (8.6 %) of pale yellow oil were obtained. ¹H RMN (CDCl₃) δ (ppm): 7.63 (d, *J* = 16.7, 3H, H₃), 7.44 (d, *J* = 8.9 Hz, 6H, H₅, H₉), 6.89 (d, *J* = 8.9 Hz, 6H, H₆, H₈), 6.29 (d, *J* = 16.9 Hz, 3H, H₂), 6.08 (s, 3H, H_{1''}), 4.11-4.14 (m, 6H, H_{1'}), 4.03 (t, *J* = 4.37 Hz, 6H, H_{2'}), 3.85 (t, *J* = 5.1 Hz, 6H, H_{11'}), 3.78-3.81 (m, 15H, H₁₀, H_{10'}), 3.67-3.72 (m, 24H, H_{4'-8'}); ¹³C NMR (CDCl₃) δ (ppm): 167.8, 161.7, 160.6, 144.5, 129.7, 127.3, 115.4, 115.0, 71.2, 70.9, 70.7, 70.6, 70.5, 67.6, 51.6, 30.4, 30.3. EA calculated for C₆₀H₇₈O₂₁·0.2 AcOEt : C 63.34; H 6.96; found: C 63.66; H 6.97.

2-hydroxyanthracene (**34**)



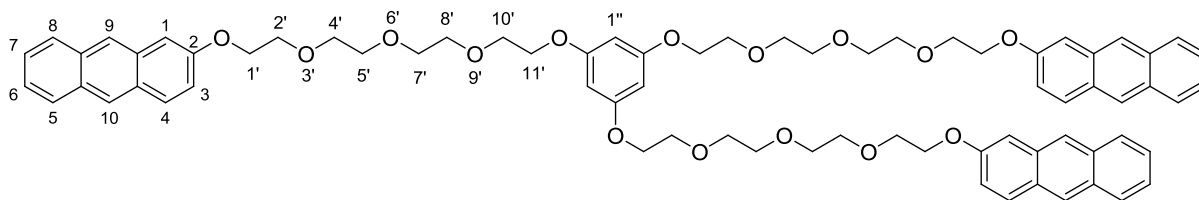
To a solution of 2-aminoanthraquinone (**32**) (1.0 g, 4.5 mmol) in 96% H₂SO₄ (13 mL) at 0°C, sodium nitrite (380 mg, 5.5 mmol) was added while stirring. The solution was stirred at room temperature for 3 hours and the reaction mixture was poured into ice. The resulting slurry was heated to reflux for 30 minutes, during which a dark yellow precipitate was formed. The mixture was cooled to room temperature and the solid was filtered off and washed with cold water. After recrystallization with glacial acetic acid, 520 mg (53%) of **33** were collected. **33** was dissolved in methanol and sodium borohydride (200 mg, 5.3 mmol) was carefully added portionwise to the solution while stirring at 0 °C. The reaction mixture was stirred at room temperature overnight and water was added. The mixture was extracted with dichloromethane and the combined organic extracts were washed with water and brine. After drying with anhydrous MgSO₄ the solvent was removed by rotatory evaporation and the crude product was purified by flash chromatography (dichloromethane as eluent), resulting in 120 mg (24%) of **34** a pale yellow solid. ¹H NMR (CD₃CN) δ (ppm): 8.37 (1H, d, *J* = 2.0 Hz, H₁), 8.25 (1H, s, H₁₀), 8.17 (1H, s, H₉), 7.97 (m, 3H, H₅, H₈, H₄), 7.43 (1H, m, H₆), 7.27 (1H, m, H₇), 7.18 (1H, dd, *J*₁ = 8.9 Hz, *J*₂ = 2.2 Hz, H₃).

2-(11-*O*-tosyl-3,6,9-trioxaundecanoxy)-anthracene (**35**)



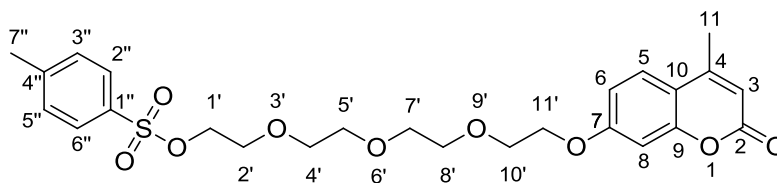
To a solution of **34** in acetone (100 mg, 0.5 mmol), potassium carbonate (138 mg, 1 mmol) and 1-11-di-*O*-tosyl-3,6,9-trioxaundecane (**25**) (502 mg, 1 mmol) were added. The mixture was stirred and heated to reflux for 16 h. After cooling down to room temperature, the solid was removed by filtration and the solvent was evaporated. The crude product was purified by column chromatography with silica gel (ethyl acetate/petroleum ether eluent) to yield 200 mg (76%) of **35** as a pale yellow oil. ¹H NMR (CDCl₃) δ (ppm): 8.77 (s, 3H, H₁), 8.31 (s, 3H, H₁₀), 8.21 (s, 3H, H₉), 7.85-7.95 (m, 9H, H₅, H₈, H₄), 7.77 (d, *J* = 7.9 Hz, 4H, H₂, H₆), 7.35-7.43 (m, 6H, H₆, H₇), 7.30 (d, *J* = 7.9 Hz, 4H, H₃, H₅), 7.15 (m, 3H, H₃), 4.47 (t, *J* = 4.86 Hz, 6H, H₁), 4.25 (t, *J* = 4.76 Hz, 6H, H₂), 3.92 (t, *J* = 4.98 Hz, 6H, H₁₁), 3.80 (t, *J* = 4.98 Hz, 6H, H₁₀), 3.68-3.76 (m, 24H, H₄₋₈), 2.42 (s, 6H, H₇).

1,3,5-tris(11-(anthracene-9-oxy)-3,6,9-trioxaundecanoxy)benzene (**36**)



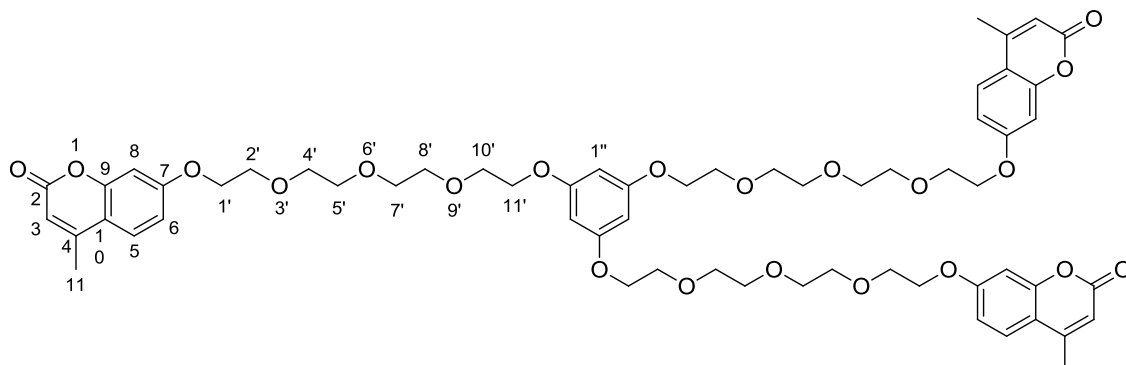
To a solution of 200 mg (0.38 mmol) of **35** in dry acetonitrile, 14 mg (0.11 mmol) of sublimed phloroglucinol and 70 mg (0.5 mmol) of dry potassium carbonate were added. The reaction mixture was stirred and refluxed overnight under inert atmosphere. The white solid was filtered off and the solvent was removed by rotatory evaporation. The oily residue was purified by silica gel flash column chromatography (hexanes/ethyl acetate eluent) and 80 mg (61 %) of dark yellow amorphous solid were obtained. ^1H NMR (CDCl_3) δ (ppm): 8.78 (s, 3H, H_1), 8.30 (s, 3H, H_{10}), 8.21 (s, 3H, H_9), 7.84-7.95 (m, 9H, H_5 , H_8 , H_4), 7.37-7.43 (m, 6H, H_6 , H_7), 7.15-7.18 (m, 6H, H_3 , H_{11}), 4.47 (t, $J = 4.86$ Hz, 6H, $\text{H}_{1'}$), 4.25 (t, $J = 4.76$ Hz, 6H, $\text{H}_{2'}$), 3.92 (t, $J = 4.98$ Hz, 6H, $\text{H}_{11'}$), 3.80 (t, $J = 4.98$ Hz, 6H, $\text{H}_{10'}$), 3.68-3.76 (m, 24H, $\text{H}_{4'-8'}$); ^{13}C NMR (CDCl_3) δ (ppm): 161.7, 146.0, 133.6, 131.9, 128.9, 128.3, 128.0, 127.0, 126.0, 125.7, 125.0, 123.0, 120.9, 120.8, 103.4, 71.2, 70.9, 70.7, 70.6, 70.5, 67.6, 30.4, 30.3

4-methyl-7-(11-*O*-tosyl-3,6,9-trioxaundecanoxy)-coumarin (**38**)



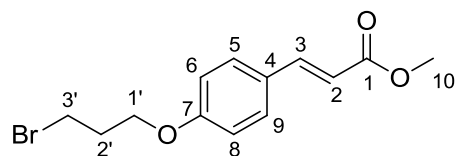
To a solution of 10.0 g (20 mmol) of 1-11-di-*O*-tosyl-3,6,9-trioxaundecane (**25**) and 3.5 g (20 mmol) of 4-methyl-7-hydroxy-coumarin (**31**) in acetonitrile, potassium carbonate (3.45 g, 25 mmol) was added. The mixture was refluxed overnight while stirring and the white solid was removed by filtration. The solvent was removed by rotatory evaporation and the residue was purified by silica gel flash column chromatography (hexanes/ethyl acetate eluent) to yield 6.1 g (60 %) of white solid. ^1H NMR (CDCl_3) δ (ppm): 7.78 (d, $J = 8.3$ Hz, 2H, $\text{H}_{2''}$, $\text{H}_{6''}$), 7.49 (d, $J = 8.8$ Hz, 1H, H_5), 7.33 (d, $J = 8.2$ Hz, 2H, $\text{H}_{3''}$, $\text{H}_{5''}$), 6.88 (dd, $J_1 = 2.4$ Hz, $J_2 = 8.8$ Hz, 1H, H_6), 6.82 (d, $J = 2.4$ Hz, 1H, H_8), 4.12-4.21 (m, 4H, $\text{H}_{1'}$, $\text{H}_{11'}$), 3.88 (t, $J = 4.8$ Hz, 2H, $\text{H}_{10'}$), 3.64-3.72 (m, 6H, $\text{H}_{2'}$, $\text{H}_{4'}$, $\text{H}_{8'}$), 3.59 (s, 4H, $\text{H}_{5'}$, $\text{H}_{7'}$), 2.43 (s, 3H, $\text{H}_{7''}$), 2.39 (s, 3H, H_{11}); ^{13}C NMR (CDCl_3) δ (ppm): 161.9, 161.3, 155.2, 152.6, 144.8, 133.0, 129.8, 128.0, 125.6, 113.7, 112.7, 112.0, 101.6, 70.9, 70.8, 70.7, 70.6, 69.4, 69.2, 68.7, 68.0, 21.6, 18.7; EA calculated for $\text{C}_{25}\text{H}_{30}\text{O}_9\text{S}$: C 59.28; H 5.97; S 6.33; found: C 59.01, H 5.81, S 5.84.

1,3,5-tris(11-(4-methyl-coumarin-7-oxy)-3,6,9-trioxaundecanoxy)benzene (**39**)



To a solution of 2.0 g (3.95 mmol) of **38** in dry acetonitrile, 142 mg (1.13 mmol) of sublimed phloroglucinol and 620 mg (4.5 mmol) of dry potassium carbonate were added. The reaction mixture was stirred and refluxed overnight under inert atmosphere. The white solid was filtered off and the solvent was removed by rotatory evaporation. The oily residue was purified by silica gel flash column chromatography (hexanes/ethyl acetate eluent) and 820 mg (63 %) of pale yellow oil were obtained. $^1\text{H NMR}$ (CDCl_3) δ (ppm): 7.46 (d, $J = 8.8$ Hz, 3H, H_5), 6.87 (dd, $J_1 = 2.4$ Hz, $J_2 = 8.8$ Hz, 3H, H_6), 6.80 (d, $J = 2.4$ Hz, 3H, H_8), 6.11 (d, $J = 0.8$ Hz, 3H, H_3), 6.06 (s, 3H, $\text{H}_{1''}$), 4.16 (t, $J = 4.5$ Hz, 6H, $\text{H}_{1'}$), 4.03 (t, $J = 4.5$ Hz, 6H, H_2), 3.87 (t, $J = 4.9$ Hz, 6H, $\text{H}_{11'}$), 3.80 (t, $J = 4.9$ Hz, 6H, $\text{H}_{10'}$), 3.68-3.73 (m, 24H, $\text{H}_{4'-8'}$), 2.37 (d, $J = 0.8$ Hz, 9H, H_{11}). $^{13}\text{C NMR}$ (CDCl_3) δ (ppm): 161.9, 161.6, 161.3, 155.2, 152.6, 125.6, 113.7, 112.7, 112.0, 101.6, 93.0, 70.9, 70.8, 68.0, 21.6, 18.7; EA calculated for $\text{C}_{60}\text{H}_{72}\text{O}_{21} \cdot 0.18 \text{C}_4\text{H}_8\text{O}_2$: C 63.82; H 6.43; found: C 63.51; H 6.52.

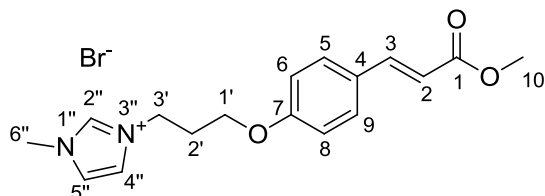
(*E*)-Methyl *p*-(3-bromopropoxy)cinnamate (**52**)



To a solution of 2.5 g (14 mmol) of (*E*)-methyl *p*-(hydroxy)cinnamate (**27**) in dry acetone (50 mL), 8.4 g (42 mmol) of 1,3-dibromopropane, and 4 g (30 mmol) of K_2CO_3 were added. The resulting mixture was refluxed while stirring for 16 h under inert atmosphere. After cooling down to room temperature, the white solid was filtered off and the solvent was removed by rotatory evaporation. The residue was washed with hexanes and filtered to yield 4 g (94%) of a white crystalline solid, requiring no further purification. $^1\text{H NMR}$ (CDCl_3) δ (ppm): 7.65 (d, $J = 16.0$ Hz, 1H, H_3), 7.47 (d, $J = 8.6$ Hz, 2H, H_5 ,

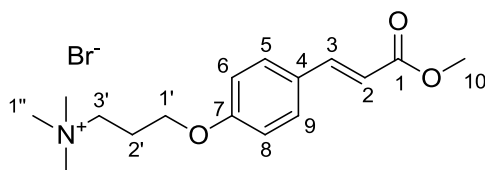
H₉), 6.91 (d, *J* = 8.6 Hz, 2H, H₆, H₈), 6.31 (d, *J* = 16.0 Hz, 1H, H₂), 4.14 (t, *J* = 5.7 Hz, 2H, H_{1'}), 3.79 (s, 3H, H₁₀), 3.60 (t, *J* = 6.3 Hz, 2H, H_{3'}), 2.36 – 2.30 (m, 2H, H_{2'}). ¹³C NMR (CDCl₃) δ (ppm): 167.7, 160.5, 144.4, 129.8, 127.4, 115.4, 114.9, 65.4, 51.6, 32.2, 29.8. EA calculated for C₁₃H₁₅BrO₃: C 52.19; H 5.05; found: C 52.14; H 4.88. m.p. 72-74 °C

(*E*)-3-(3-(*p*-(3-methoxy-3-oxoprop-1-enyl)phenoxy)propyl)-1-*N*-methyl-imidazol-3-ium bromide (**53**)



To a solution of 1 g (3.5 mmol) of (*E*)-Methyl *p*-(3-bromopropoxy)cinnamate (**52**) in dry acetonitrile, 0.287 g (3.5 mmol) of 1-methylimidazole was added. The resulting mixture was refluxed while stirring for 16h under inert atmosphere. The solvent was then removed by rotatory evaporation and the residue was washed with diethyl ether to yield 1.01 g (76%) of a pale yellow solid. For analytical purposes further purification was achieved by recrystallization with chloroform and ether. ¹H NMR (CDCl₃) δ (ppm): 10.60 (s, 1H, H_{2''}), 7.61 (d, *J* = 15.8 Hz, 1H, H₃), 7.45 (d, *J* = 6.2 Hz, 2H, H₅, H₉), 7.33 (s, 1H, H_{4''}), 7.30 (s, 1H, H_{5''}), 6.86 (d, *J* = 6.4 Hz, 2H, H₆, H₈), 6.30 (d, *J* = 15.8 Hz, 1H, H₂), 4.62 (m, 2H, H_{3'}), 4.10 (m, 2H, H_{1'}), 4.06 (s, 3H, H_{6''}), 3.78 (s, 3H, H₁₀), 2.50 (s, 2H, H_{2'}). ¹³C NMR (CDCl₃) δ (ppm): 167.6, 159.8, 144.2, 138.2, 129.8, 127.7, 123.0, 122.4, 115.8, 114.8, 64.2, 51.6, 47.4, 36.8, 29.8. EA calculated for C₁₇H₂₁BrN₂O₃: C 53.55; H 5.55; N 7.35; found: C 53.87; H 5.40; N 7.25. m.p. = 142-145 °C

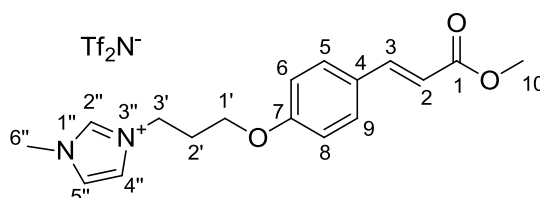
(*E*)-*N*-(3-(*p*-(3-methoxy-3-oxoprop-1-enyl)phenoxy)propyl)-trimethyl-amine bromide (**54**)



To a solution of 1 g (3.5 mmol) of (*E*)-Methyl *p*-(3-bromopropoxy)cinnamate (**52**) in acetonitrile, an ethanolic solution of triethylamine 31% (1.4 mL, 7.0 mmol) was added. The resulting mixture was stirred at room temperature for 48 hours. The solvent was then removed by rotatory evaporation and the residue was washed with diethyl ether to yield 824 mg (66%) of a pale yellow solid. For analytical purposes further purification was achieved by recrystallization with chloroform and ether. ¹H NMR (CDCl₃) δ (ppm): 7.61 (d, *J* = 15.8 Hz, 1H, H₃), 7.45 (d, *J* = 6.2 Hz, 2H, H₅, H₉), 6.86 (d, *J* = 6.4 Hz, 2H, H₆, H₈), 6.30 (d, *J* = 15.8 Hz, 1H, H₂), 4.72 (m, 2H, H_{3'}), 4.10 (m, 2H, H_{1'}), 3.78 (s, 3H, H₁₀), 3.21

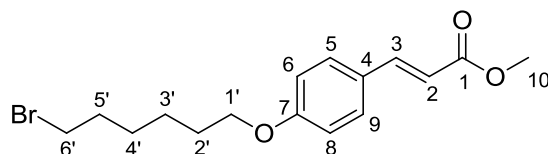
(s, 9H, H_{1''}) 2.50 (s, 2H, H_{2'}). ¹³C NMR (CDCl₃) δ (ppm): 167.6, 159.8, 144.2, 129.8, 127.7, 115.8, 114.8, 64.2, 51.6, 42.3, 38.8, 29.8. EA calculated for C₁₆H₂₄BrNO₃: C 53.64; H 6.75; N 3.91; found: C 53.81; H 6.70; N 3.98. m.p. = 211-213 °C

(*E*)-3-(3-(*p*-(3-methoxy-3-oxoprop-1-enyl)phenoxy)propyl)-1-*N*-methyl-imidazol-3-ium bis(trifluoromethylsulfonyl)amide (**55**).



To a solution of 0.5 g (1.31 mmol) of **53** in dichloromethane (10 mL), 0.76 g (2.62 mmol) of lithium bis(trifluoromethylsulfonyl)amide was added. The suspension was stirred for 16h and then water (25 mL) and dichloromethane (50 mL) were added. The organic extract was dried by filtration through anhydrous MgSO₄ and the solvent was removed by rotatory evaporation to yield a pale yellow viscous liquid. This residue was dissolved in dichloromethane (10 mL) and filtered through activated charcoal (50 mg). The colorless solution was dried under vacuum and 0.53 g (70%) of colorless oil were recovered. This oil solidified after standing 10h protected from light at room temperature. No bromide ion was detected by the silver (I) nitrate titration test. Further purification was achieved by recrystallization from chloroform/methanol with ether. ¹H NMR (CDCl₃) δ (ppm): 8.85 (s, 1H, H_{2''}), 7.62 (d, *J* = 16.0, 1H, H₃), 7.46 (d, *J* = 8.4 Hz, 2H, H₅, H₉), 7.28 (s, 1H, H_{4''}), 7.24 (s, 1H, H_{5''}), 6.85 (d, *J* = 8.5 Hz, 2H, H₆, H₈), 6.31 (d, *J* = 16.0 Hz, 1H, H₂), 4.44 (t, *J* = 7.0 Hz, 2H, H_{3'}), 4.05 (t, *J* = 5.6 Hz, 2H, H_{1'}), 3.93 (s, 3H, H_{6''}), 3.79 (s, 3H, H₁₀), 2.46 – 2.27 (m, 2H, H_{2'}). ¹³C NMR (CDCl₃) δ (ppm): 167.69, 159.74, 144.21, 136.46, 129.84, 127.76, 123.55, 122.66, 115.77, 114.68, 63.88, 51.65, 47.36, 36.43, 29.50. EA calculated for C₁₉H₂₁F₆N₃O₇S₂: C 39.24; H 3.64; N 7.23; S 11.03; found: C 39.18; H 3.72; N 7.38; S 11.09 m.p. 80-82 °C

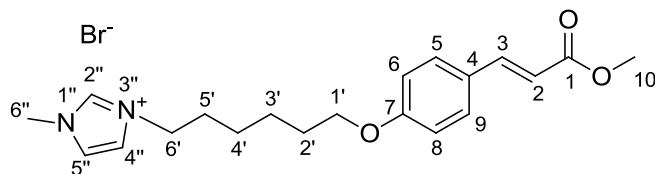
(*E*)-methyl *p*-(6-bromohexyloxy)cinnamate (**56**).



To a solution of 2.5 g (14 mmol) of (*E*)-methyl *p*-(hydroxy)cinnamate (**2**) in dry acetone (50 mL), 10.2 g (42 mmol) of 1,6-dibromohexane, and 4 g (30 mmol) of K₂CO₃ were added. The resulting mixture

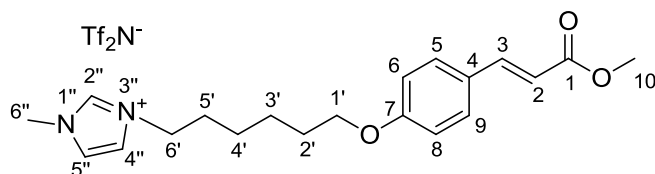
was refluxed while stirring for 16 h under inert atmosphere. After cooling down to room temperature, the white solid was filtered off and the solvent was removed by rotatory evaporation. The residue was washed with hexanes and filtered to yield 4.2 g (89%) of a white crystalline solid, requiring no further purification. ^1H NMR (CDCl_3) δ (ppm): 7.65 (d, $J = 16.0$ Hz, 1H, H_3), 7.46 (d, $J = 8.4$ Hz, 2H, H_5 , H_9), 6.89 (d, $J = 8.5$ Hz, 2H, H_6 , H_8), 6.30 (d, $J = 15.9$ Hz, 1H, H_2), 3.99 (t, $J = 6.2$ Hz, 2H, $\text{H}_{1'}$), 3.79 (s, 3H, H_{10}), 3.43 (t, $J = 6.7$ Hz, 2H, $\text{H}_{6'}$), 1.90 (m, 2H, H_2), 1.81 (m, 2H, H_5), 1.54 (m, 4H, H_3 , H_4). ^{13}C NMR (CDCl_3) δ (ppm): 167.80, 160.9, 144.6, 129.7, 127.0, 115.2, 114.8, 67.9, 51.6, 33.8, 32.7, 29.0, 27.9, 25.3. EA calculated for $\text{C}_{16}\text{H}_{21}\text{BrO}_3$: C 56.32; H 6.20; found: C 56.31; H 6.12. m.p. 74-76 $^\circ\text{C}$

(*E*)-3-(6-(*p*-(3-methoxy-3-oxoprop-1-enyl)phenoxy)hexyl)-1-*N*-methyl-imidazol-3-ium bromide (**57**).



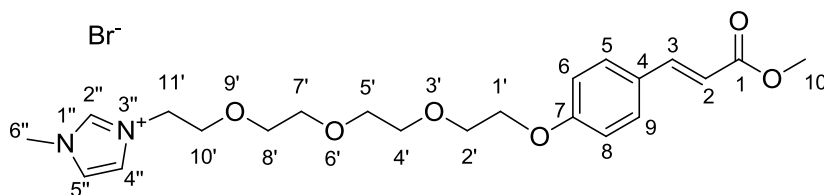
To a solution of 1 g (2.91 mmol) of (*E*)-methyl *p*-(6-bromohexyloxy)cinnamate (**56**) in dry acetonitrile, 0.238 g (2.91 mmol) of 1-methylimidazole was added. The resulting mixture was refluxed while stirring for 16h under inert atmosphere. The solvent was then removed by rotatory evaporation and the remaining residue was washed with diethyl ether to yield 0.99 g (79%) of a pale yellow solid. For analytical purposes further purification was achieved by recrystallization with chloroform and ether. ^1H NMR (CDCl_3) δ (ppm): 10.49 (s, 1H, $\text{H}_{2''}$), 7.62 (d, $J = 16.0$ Hz, 1H, H_3), 7.44 (d, $J = 8.78$ Hz, 2H, H_5 , H_9), 7.39 (s, 1H, $\text{H}_{4''}$), 7.34 (s, 1H, $\text{H}_{5''}$), 6.86 (d, $J = 8.77$ Hz, 2H, H_6 , H_8), 6.28 (d, $J = 16.0$ Hz, 1H, H_2), 4.34 (t, $J = 7.4$ Hz, 2H, $\text{H}_{6'}$), 4.09 (s, 3H, $\text{H}_{6''}$), 3.96 (t, $J = 6.3$ Hz, 2H, $\text{H}_{1'}$), 3.77 (s, 3H, H_{10}), 2.01 – 1.90 (m, 2H, H_5), 1.81 – 1.74 (m, 2H, H_2), 1.54-1.49 (m, 2H, H_4), 1.46-1.40 (m, 2H, H_3). ^{13}C NMR (101 MHz, CDCl_3) δ 167.80, 160.81, 144.53, 140.07, 136.78, 129.75, 127.02, 123.02, 121.54, 115.21, 114.83, 67.67, 51.59, 50.10, 36.78, 30.20, 28.83, 25.92, 25.45. EA calculated for $\text{C}_{20}\text{H}_{27}\text{Br}_2\text{N}_2\text{O}_3 \cdot 0.14 \text{CHCl}_3$: C 54.97; H 6.22; N 6.37; found: C 54.80; H 6.37; N 6.41. m.p. = 153-155 $^\circ\text{C}$

(*E*)-3-(6-(*p*-(3-methoxy-3-oxoprop-1-enyl)phenoxy)hexyl)-1-*N*-methyl-imidazol-3-ium bis(trifluoromethylsulfonyl)amide (**58**).



To a solution of 0.5 g (1.18 mmol) of **57** in dichloromethane (10 mL), 0.68 g (2.36 mmol) of lithium bis(trifluoromethylsulfonyl)amide was added. The suspension was stirred for 16h and then water (25 mL) and dichloromethane (50 mL) were added. The organic extract was dried by filtration through anhydrous MgSO_4 and the solvent was removed by rotatory evaporation to yield a pale yellow viscous liquid. This residue was dissolved in dichloromethane (10 mL) and filtered through activated charcoal (50 mg). The colorless solution was dried under vacuum and 0.56 g (76%) of colorless oil were recovered. This oil solidified after standing 10h protected from light at room temperature. No bromide ion was detected by the silver (I) nitrate titration test. Further purification was achieved by recrystallization from chloroform/methanol with ether. ^1H NMR (CDCl_3) δ (ppm): 8.76 (s, 1H, $\text{H}_{2''}$), 7.62 (d, $J = 16.0$ Hz, 1H, H_3), 7.44 (d, $J = 8.7$ Hz, 1H, H_5 , H_9), 7.27 (s, 2H), 6.86 (d, $J = 8.8$ Hz, 1H, H_6 , H_8), 6.29 (d, $J = 16.0$ Hz, 1H, H_2), 4.19 (t, $J = 7.5$ Hz, 1H, $\text{H}_{6''}$), 3.96 (t, $J = 6.3$ Hz, 1H, $\text{H}_{1'}$), 3.92 (s, 1H, $\text{H}_{4''}$), 3.78 (s, 1H, $\text{H}_{5''}$), 1.93-1.86 (m, 2H, $\text{H}_{5'}$), 1.81-1.74 (m, 2H, $\text{H}_{2'}$), 1.55-1.48 (m, 2H, $\text{H}_{4'}$), 1.43-1.36 (m, 2H, $\text{H}_{3'}$); ^{13}C NMR (CDCl_3) δ (ppm): 167.8, 160.9, 144.5, 136.2, 129.7, 127.0, 123.6, 122.2, 121.4, 119.0, 115.2, 114.8, 67.6, 51.6, 50.1, 36.4, 30.0, 28.7, 25.8, 25.3. EA calculated for $\text{C}_{22}\text{H}_{27}\text{F}_6\text{N}_3\text{O}_7\text{S}_2$: C 42.37; H 4.36; N 6.74; S 10.28; found: C 42.40; H 4.62; N 6.94; S 10.20 m.p. 52-54 °C

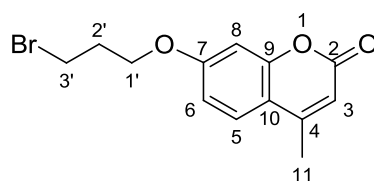
(*E*)-3-(11-(*p*-(3-methoxy-3-oxoprop-1-enyl)phenoxy)3,6,9-trioxaundecanoxy)-1-*N*-methyl-imidazol-3-ium bromide (**60**)



To a solution of 1.0 g (2.4 mmol) of (*E*)-Methyl *p*-(11-bromo-3,6,9-trioxaundecanoxy)cinnamate (**28**) in acetonitrile, 197 mg (2.4 mmol) of *N*-methylimidazole were added dropwise. The reaction was refluxed overnight and allowed to cool down to room temperature. The solvent was removed by rotatory evaporation and the residue was washed with boiling diethyl ether, yielding 1.1 g (91%) of a pale yellow oil. For analytical purposes further purification was achieved by filtration in chloroform solution through a pad of activated charcoal and removal of solvent *in vacuo*. ^1H NMR (CDCl_3) δ

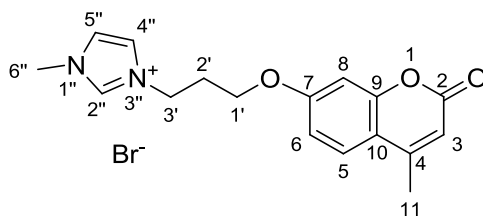
(ppm): 10.37 (s, 1H, H_{2''}), 7.61-7.65 (m, 2H, H₃, H_{4''}), 7.47 (d, *J* = 8.7 Hz, 2H, H₅, H₉), 7.13 (t, *J* = 1.7 Hz, 1H, H_{5''}), 6.88 (d, *J* = 8.7 Hz, 2H, H₆, H₈), 6.31 (d, *J* = 16.4 Hz, 1H, H₂), 4.58 (t, *J* = 4.5 Hz, 2H, H_{11'}), 4.14 (t, *J* = 4.4 Hz, 2H, H_{1'}), 3.95 (s, 3H, H_{6''}), 3.85-3.90 (m, 4H, H_{2'}, H_{10'}), 3.79 (s, 3H, H₁₀), 3.71-3.73 (m, 2H, H_{8'}), 3.60-3.67 (m, 6H, H_{4'}, H_{5'}, H_{7'}); ¹³C NMR (CDCl₃) δ (ppm): 167.5, 160.3, 144.1, 137.3, 129.7, 127.2, 123.4, 123.2, 122.7, 115.4, 114.8, 70.6, 70.3, 70.2, 70.1, 69.4, 68.8, 67.5, 51.5, 49.6, 36.4. EA calculated for C₂₂H₃₁BrN₂O₆·0.2 CHCl₃: C 50.96; H 6.01, N 5.35; found: C 50.71, H 5.96, N 5.43

4-methyl-7-(3-bromopropoxy)-coumarin (**61**)



To a solution of 2.0 g (11.3 mmol) of 4-methyl-7-hydroxycoumarin (**31**) in dry acetone (50 mL), 6.8 g (34 mmol) of 1,3-dibromopropane, and 3.2 g (23 mmol) of K₂CO₃ were added. The resulting mixture was refluxed while stirring for 16 h under inert atmosphere. After cooling down to room temperature, the white solid was filtered off and the solvent was removed by rotatory evaporation. The residue was washed with hexanes and filtered to yield 3.08 g (92%) of a white crystalline solid, requiring no further purification. ¹H NMR (CDCl₃) δ (ppm): 7.48 (d, *J* = 8.6 Hz, 1H, H₅), 6.85 (d, *J* = 8.6 Hz, 1H, H₆), 6.80 (s, 1H, H₈), 6.12 (s, 1H, H₃), 4.16 (t, *J* = 5.6 Hz, 2H, H_{1'}), 3.60 (t, *J* = 6.3 Hz, 2H, H_{3'}), 2.38 (s, 3H, H₁₁), 2.33-2.36 (m, 2H, H_{2'}); ¹³C NMR (CDCl₃) δ (ppm): 161.6, 161.1, 155.2, 152.4, 125.6, 113.7, 112.3, 112.0, 101.5, 65.8, 31.9, 29.5, 18.6; EA calculated for C₁₃H₁₃BrO₃: C 52.55; H 4.41; found: C 52.81; H 4.33. m.p. 78-80 °C

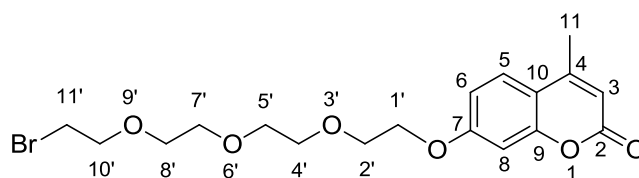
3-(3-(4-methyl-7-coumarinoxy)propyl)-1-*N*-methylimidazol-3-ium bromide (**62**)



To a solution of 1.0 g (3.4 mmol) of 4-methyl-7-(3-bromopropoxy)-coumarin (**61**) in dry acetonitrile, 0.277 g (3.4 mmol) of *N*-methylimidazole was added. The resulting mixture was refluxed while stirring for 16h under inert atmosphere. The solvent was then removed by rotatory evaporation and the

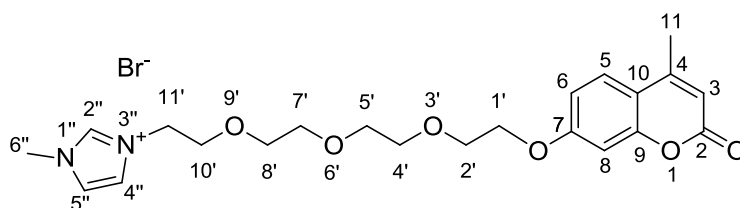
residue was washed with diethyl ether to yield 0.99 g (75%) of a pale yellow solid. For analytical purposes further purification was achieved by recrystallization with chloroform and ether. ^1H NMR (CDCl_3) δ (ppm): 10.62 (s, 1H, $\text{H}_{2''}$), 7.50 (d, $J = 8.6$ Hz, 1H, H_5), 7.38 (s, 1H, $\text{H}_{4''}$), 7.29 (s, 1H, $\text{H}_{5''}$), 6.88 (dd, $J_1 = 2.2$ Hz, $J_2 = 8.6$ Hz, 1H, H_6), 6.75 (d, $J = 2.2$ Hz, 1H, H_8), 6.12 (s, 1H, H_3), 4.67 (t, $J = 7.0$ Hz, 2H, $\text{H}_{3'}$), 4.18 (t, $J = 5.8$ Hz, 2H, $\text{H}_{1'}$), 4.08 (s, 3H, $\text{H}_{6''}$), 2.54 (m, 2H, $\text{H}_{2'}$), 2.39 (s, 3H, H_{11}). ^{13}C NMR (CDCl_3) δ (ppm): 161.5, 161.1, 154.8, 153.0, 137.1, 125.8, 123.4, 122.4, 113.8, 112.1, 111.7, 101.6, 65.7, 47.0, 36.4, 29.5, 18.5. EA calculated for $\text{C}_{17}\text{H}_{19}\text{BrN}_2\text{O}_3$: C 53.84; H 5.05; N 7.39; found: C 53.60; H 5.00; N 7.45. m.p. = 142-145 °C

4-methyl-7-(11-bromo-3,6,9-trioxaundecanoxy)coumarin (**63**)



4-methyl-7-hydroxy coumarin (**31**) (1.0 g, 5.7 mmol) and 1,11-dibromo-3,6,9-trioxaundecane (**24**) (5.5 g, 17.1 mmol) were dissolved in dry acetonitrile. Potassium carbonate (1.6 g, 11.4 mmol) was added in one portion and the reaction mixture was heated to reflux overnight while stirring. The white solid was removed by filtration and the solvent was removed by rotatory evaporation. The residue was purified by silica gel flash column chromatography (hexanes/ethyl acetate eluent) to yield 2.0 g (86%) of pale yellow oil. ^1H NMR (CDCl_3) δ (ppm): 7.48 (d, $J = 8.8$ Hz, 1H, H_5), 6.88 (dd, $J_1 = 2.2$ Hz, $J_2 = 8.8$ Hz, 1H, H_6), 6.82 (d, $J = 2.2$ Hz, 1H, H_8), 6.12 (s, 1H, H_3), 4.18 (t, $J = 4.7$ Hz, 2H, $\text{H}_{1'}$), 3.89 (t, $J = 4.6$ Hz, 2H, $\text{H}_{2'}$), 3.80 (t, $J = 6.3$ Hz, 2H, $\text{H}_{10'}$), 3.67-3.73 (m, 8H, $\text{H}_{4'-8'}$), 3.46 (t, $J = 6.2$ Hz, 2H, $\text{H}_{11'}$), 2.39 (s, 3H, H_{11}); ^{13}C NMR (CDCl_3) δ (ppm): 161.6, 161.1, 155.2, 152.4, 125.6, 113.7, 112.3, 112.0, 101.5, 71.2, 70.7, 70.5, 30.4, 18.6; EA calculated for $\text{C}_{18}\text{H}_{23}\text{BrO}_6$: C 52.06; H 5.58; found: C 52.13; H 5.50

3-(11-(4-methyl-7-coumarinoxy)-3,6,9-trioxaundecanoxy)-1-*N*-methylimidazol-3-ium bromide (**64**)



Compound **63** (1.0 g, 2.4 mmol) and *N*-methylimidazole (197 mg, 2.4 mmol) were dissolved in dry acetonitrile. The reaction was refluxed overnight and allowed to cool down to room temperature. The solvent was removed by rotatory evaporation and the residue was washed with boiling diethyl ether, yielding 1.1 g (91%) of pale yellow oil. For analytical purposes further purification was achieved by filtration in chloroform solution through a pad of activated charcoal and removal of solvent *in vacuo*. ¹H NMR (CDCl₃) δ (ppm): 10.17 (s, 1H, H_{2''}), 7.67 (s, 1H, H_{4''}), 7.50 (d, *J* = 8.8 Hz, 1H, H₅), 7.37 (s, 1H, H_{5''}), 6.83 (dd, *J*₁ = 2.4 Hz, *J*₂ = 8.8 Hz, 1H, H₆), 6.78 (d, *J* = 2.4 Hz, 1H, H₈), 6.10 (s, 1H, H₃), 4.57 (t, *J* = 4.4 Hz, 2H, H_{11'}), 4.18 (t, *J* = 4.4 Hz, 2H, H_{1'}), 4.01 (s, 3H, H_{6''}), 3.85-3.88 (m, 4H, H₂, H₁₀), 3.70-3.72 (m, 2H, H₈), 3.60-3.65 (m, 6H, H_{4'-7'}), 2.38 (s, 3H, H₁₁); ¹³C NMR (CDCl₃) δ (ppm): 161.6, 161.1, 155.2, 152.4, 137.3, 125.6, 123.4, 123.2, 122.7, 113.7, 112.3, 112.0, 101.5, 70.6, 70.3, 70.2, 70.1, 69.4, 68.8, 67.5, 18.6

EA calculated for C₂₂H₂₉BrN₂O₆: C 53.13; H 5.88; N 5.63; found: C 53.25; H 5.82; N 5.85.

Coumarins **72**, **73** and **77-80** were synthesized as described in chapter III.2.1 and obtained from Prof. Dr. Paula de Sérgio Branco, FCT-UNL and Prof. Dr. António Pereira, University of Évora.

Photochemistry

All solvents used for spectroscopic characterization were of analytical grade and used as obtained from the supplier. UV-Vis absorption spectra were acquired using a Cary Varian 100 spectrophotometer using 1 nm slits. Fluorescence spectra were obtained using a Horiba Jobin Yvon SPEX 212 I Fluorolog spectrofluorimeter using 1 nm slits and 1 s integration time. All irradiations of photoresponsive compound solutions were carried out in quartz 1 cm path length cells in a 200 W Xe/Hg Arc lamp coupled with a ThorLabs UG11 Colored Glass UV-Passing Filter, 275 - 375 nm for concentrated solutions (*A*>1) or in Horiba Jobin Yvon spectrofluorimeter (*A*≤1) for dilute solutions. Photochemical quantum yields were determined from NMR data collected for irradiated 3 mL deuterated chloroform solutions of the selected compound. Aliquots of 0.5 mL were taken at each time interval.

Actinometry of the lamps used for irradiation was carried out using the conventional ferrioxalate actinometer.

Neat ionic liquid samples were irradiated in the liquid state in thin films spread over 1 cm quartz plates (under open atmosphere) or in 0.2 cm wide quartz tubes (under inert atmosphere). For compounds **53**, **58** and **62** the temperature was kept above the melting point during irradiation. For compounds **60** and **64** the irradiation was conducted at room temperature.

Dynamic Light Scattering

DLS spectroscopy experiments were conducted on laser light scattering instrument (SZ-100 nanopartica, Horiba) at a 90° scattering angle on quartz cuvettes at 25 °C. All tests were run six times during 30 seconds and the average values were presented. Particle size was calculated by fitting the correlation curves using solver mathematical software.

Atomic Force Microscopy

AFM images were taken by the vibrating mode in air on an AFM Workshop TT-AFM instrument. For the imaging of nanoparticles of compound **22** the samples were prepared by depositing 20 uL of an irradiated solution at 1 mg.mL⁻¹ onto a freshly cleaved mica lamella which was dried overnight under reduced pressure.

Viscometry

Rheological measurements were performed in a TA Instruments AR500 stress-controlled rheometer, using a standard cone and plate geometry. For compound **39** a cone with diameter of 40 mm, angle of 2°, and a gap of 57 µm was used. The viscosity curves were recorded for a single 2 mL solution of **39** in DMF at 10% (w/v) was measured at 20 °C before and after irradiation. For ionic liquid neat samples of compounds **60** and **64**, a cone with diameter of 20 mm, angle of 1°, and a gap of 57 µm was used. The viscosity curves of both samples were recorded prior and after to irradiation at 20 °C.

Photophysics

For fluorescence experiments coumarin solutions were prepared in analytical grade acetonitrile or methanol and respective spectra were recorded directly. Previously the coumarin samples were purified by high performance liquid chromatography using a Macherey-Nagel Nucleosil 300-7 C-18 column with isocratic methanol as eluent. Purified fractions were concentrated in vacuo and absorbance was adjusted below 0.1, to avoid re-absorption of emitted light.²¹⁰ Fluorescence measurements were performed on a SPEX 212 I Fluorolog Spectrofluorimeter. All emission spectra were collected with 3 nm slit bandwidth for excitation and emission, with correction files. Fluorescence quantum yields of compounds **72**, **73**, **77**, **79** and **80** were calculated using a Jobin-Yvon integrating sphere for SPEX 212 I Fluorolog Spectrofluorimeter or by comparison with a solution of diphenylhexatriene in deaerated cyclohexanol as standard.²¹¹

Time-resolved fluorescence measurements were carried out by the single photon counting technique, using picosecond laser excitation. The fluorescence was selected by a monochromator (Jobin-Yvon, with a grating of 100 lines mm^{-1} (20 nm bandwidth)) and detected by a microchannel plate photomultiplier (Hamamatsu 2809U-01). Fluorescence decays were deconvoluted from the excitation pulse using Striker's Sand program, which uses the improved modulating functions method that is then refined using a non-linear least-square analysis.²¹²

Computational calculations

Computational studies were performed by Prof. J.P. Prates Ramalho, University of Évora.

VI. References

- ¹ J.M. Jani, M. Leary, A. Subic, M.A. Gibson, *Mater. Des.* **2014**, *56*, 1078-1113
- ² Newnham, R.E.; Cross, L. Eric (November 2005). "Ferroelectricity: The Foundation of a Field from Form to Function". *MRS Bulletin* 30: pp. 845–846
- ³ Webster, John G (1999). *The measurement, instrumentation, and sensors handbook*. pp. 32–113. ISBN 978-0-8493-8347-2.
- ⁴ Holler, F. James; Skoog, Douglas A; Crouch, Stanley R (2007). "Chapter 1". *Principles of Instrumental Analysis* (6th ed.). Cengage Learning. p. 9
- ⁵ R. Lane, B. Craig, *AMPTIAC Quat.*, **2003**, *7*, 9-14
- ⁶ C.M. Lampert *Mater. Today*, **2004**, *7*, 28-35
- ⁷ *Handbook of Materials Selection*, Edited by Myer Kutz ISBN 0-471-35924-6 2002 John Wiley & Sons, Inc., New York - James A. Harvey pp 401-418
- ⁸ T. Dürrschmidt, H. Hoffmann, *Coll. Surf. A*, **1999**, *156*, 257-269
- ⁹ J.W. Goodwin, G.M. Markham, B. Vincent, *J. Phys. Chem.* **1997**, *101*, 1961-1967
- ¹⁰ T. Hao, *Adv. Mater.*, **2001**, *13*, 1847-1857
- ¹¹ M. Kciuk, R. Turczyn, *J. Achiv. Mat. Manuf. Eng.*, **2006**, *18*, 127-130
- ¹² I. B. Jang, H. B. Kim, J. Y. Lee, J. L. You, and H. J. Choi, *J. Appl. Phys.*, **2005**, *97*, 10Q912
- ¹³ X.D. Pan, G.H. McKinley, *J. Colloid Interface Sci.*, **1997**, *195*, 101-113
- ¹⁴ A.M. Ketner, R. Kumar, T.S. Davies, P.W. Elder, S.R. Raghavan, *J. Am. Chem. Soc.*, **2007**, *129*, 1553-1559
- ¹⁵ K. Sun, R. Kumar, D.E. Falvey, S.R. Raghavan, *J. Am. Chem. Soc.*, **2009**, *131*, 7135-7141
- ¹⁶ C.B. Gong, M.H.W. Lam, H.X. Yu, *Adv. Funct. Mater.*, **2006**, *16*, 1759–1767
- ¹⁷ Y. Li, X.R. Jia, M. Gao, H. He, G.C. Kuang, Y. Wei, *J. Polym. Sci. A*, **2010**, *148*, 551–557.
- ¹⁸ T. Wolff, N. Müller, *J. Photochem.* **1983**, *23*, 131-140
- ¹⁹ N. Müller, T. Wolff, G. von Büнау, *J. Photochem.* **1984**, *24*, 37-43
- ²⁰ T. Wolff, C.S. Emming, T.A. Suck, G. von Büнау, *J. Phys. Chem.*, **1989**, *93*, 4894-4898
- ²¹ M. Doi, S.F. Edwards, *J. Chem. Soc. Faraday Trans. 2*, **1978**, *78*, 560-918.
- ²² T. Wolff, K.J. Kerperin, *J. Colloid Interface Sci.*, **1993**, *157*, 185-195.
- ²³ J. Frömmel, T. Wolff, *J. Colloid Interface Sci.*, **1998**, *201*, 86-92.
- ²⁴ H. Ihmels, J. Luo, *J. Photochem. Photobiol. A*, **2008**, *200*, 3-9.
- ²⁵ C. Lehnberger, T. Wolff, *J. Colloid Interface Sci.*, **1999**, *213*, 187-192.
- ²⁶ N.A. Kuznetsova, O.L. Kaliya, *Usp. Khimii.*, **1992**, *61*, 1243.
- ²⁷ X. Yu, T. Wolff, *Langmuir*, **2003**, *19*, 9672-9679.
- ²⁸ A.M. Ketner, R. Kumar, T.S. Davies, P.W. Elder, S.R. Raghavan, *J. Am. Chem. Soc.*, **2007**, *129*, 1553-1559.
- ²⁹ R. Kumar, S.R. Raghavan, *Soft Matter*, **2009**, *5*, 797-803.
- ³⁰ R. Kumar, A.M. Ketner, S.R. Raghavan, *Langmuir*, **2010**, *26*, 5405-5411.
- ³¹ M. Pereira, C.R. Leal, A.J. Parola, U.M. Schevens, *Langmuir*, **2010**, *26*, 16715-16721.
- ³² T. Shikata, H. Hirata, T. Kotaka, *Langmuir* **1987**, *3*, 1081–1086
- ³³ T. Shikata, H. Hirata, T. Kotaka, *Langmuir* **1989**, *5*, 398-405
- ³⁴ H. Sakai, Y. Orihara, H. Kodashima, A. Matumura, T. Ohkubo, K. Tsuchiya, M. Abe, *J. Am. Chem. Soc.* **2005**, *127*, 13454-13455.
- ³⁵ T. Hayashita, T. Kurosawas, T. Miyata, K. Tanaka, M. Igawa, *Colloid Polym. Sci.* **1994**, *272*, 1611.
- ³⁶ Y.J. Shin, L.N. Abbott, *Langmuir* **1999**, *15*, 4404.
- ³⁷ J. Eastoe, M.S. Dominguez, P. Wyatt, A. Beeby, R.K. Heenan, *Langmuir* **2002**, *18*, 7837.
- ³⁸ J. Eastoe, M. Sanchez-Dominguez, H. Cumber, G. Burnett, P. Wyatt, R.K. Heenan, *Langmuir* **2003**, *19*, 6579.
- ³⁹ T. Shang, K.A. Smith, T.A. Hatton, *Langmuir* **2003**, *19*, 10764.
- ⁴⁰ R. Nagarajan, C.C. Wang, *Langmuir* **1995**, *11*, 4673.
- ⁴¹ R. Nagarajan, *Langmuir* **2002**, *18*, 31.
- ⁴² C.T. Lee, Jr., K.A. Smith, T.A. Hatton, *Macromolecules*, **2004**, *37*, 5397-5405.
- ⁴³ R.K. Ahmad, D. Faure, P. Goddard, R. Oda, D.M. Bassani, *Org. Biomol. Chem.*, **2009**, *7*, 3173-3178.
- ⁴⁴ M. Kroon, W.L. Vos, G.H. Wegdam, *Phys. Rev. E*, **1998**, *57*, 1962–1970.
- ⁴⁵ Van Olphen, H. 1977 *An introduction to clay colloid chemistry*. New York, NY: Wiley
- ⁴⁶ J. Zebrowski, V. Prasad, W. Zhang, L.M. Walker, D.A. Weitz., *Colloids Surf. A*, **2003**, *213*, 189-197.
- ⁴⁷ K. Sun, R. Kumar, D.E. Falvey, S.R. Raghavan, *J. Am. Chem. Soc.*, **2009**, 7135-7141.
- ⁴⁸ K.A. Juggernaut, A.E. Gros, N.A.K. Mezmarich, B.J. Love, *Soft Matter*, **2011**, *7*, 10108-10115.
- ⁴⁹ A. Nelson, T. Cosgrove, *Langmuir*, **2005**, *21*, 9176–9182.
- ⁵⁰ E. Reichmanis, F.M. Houlihan, O. Nalamasu, T.X. Neenan, *Chem. Mater.*, **1991**, *3*, 394–407.
- ⁵¹ J.L. Dektar, N.P. Hacker, *J. Org. Chem.*, **1990**, *55*, 639–647.

-
- ⁵² H.Y. Gu, W.Q. Zhang, K.S. Feng, D.C. Neckers, *J. Org. Chem.*, **2000**, *65*, 3484–3488.
- ⁵³ X. Yuan, M. Schnell, S. Muth, W. Schärtl, *Langmuir*, **2008**, *24*, 5299-5305.
- ⁵⁴ T. Frecska, *J. Rad. Curing*, **1987**, *14*, 26.
- ⁵⁵ C. Carlini, L. Angiolini, D. Caretti, E. Corelli, *J. Appl. Polym. Sci.*, **1997**, *64*, 2237-2246.
- ⁵⁶ Y.W. Chen-Yang, J.R. Chuang, Y.C. Yang, C.Y. Li, Y.S. Chiu, *J. Appl. Polym. Sci.*, **1998**, *69*, 115-122.
- ⁵⁷ N.B. Cramer, J.W. Stansbury, C.N. Bowman, *J. Dent. Res.*, **2011**, *90*, 402-416.
- ⁵⁸ Y. Zheng, M. Mimic, S.V. Mello, M. Mabrouki, F.M. Andreopoulos, V. Konka, S.M. Pham, R.M. Leblanc, *Macromolecules*, **2002**, *35*, 5228-5234.
- ⁵⁹ L. M. Minsk, J. G. Smith, W. P. Van Deusen, J. F. Wright, *J. Appl. Polym. Sci.* **1959**, *11*, 302
- ⁶⁰ E. M. Robertson, W. P. Van Deusen, L. M. Minsk, *J. Appl. Polym. Sci.* **1959**, *11*, 308.
- ⁶¹ F. D. Lewis, S. L. Quillen, P. D. Hale, J. D. Oxman, *J. Am. Chem. Soc.* **1988**, *110*, 1261.
- ⁶² Y. Zheng, F.M. Andreopoulos, M. Mimic, Q. Huo, S.M. Pham, R.M. Leblanc, *Adv. Func. Mater.* **2001**, *11*, 37-40.
- ⁶³ F.M. Andreopoulos, I. Persaud, *Biomaterials*, **2006**, *27*, 2468-2476.
- ⁶⁴ F.M. Andreopoulos, C.R. Deible, M.T. Stauffer, S.G. Weber, W.R. Wagner, E.J. Beckman, A.J. Russel, *J. Am. Chem. Soc.* **1996**, *118*, 6235-6240.
- ⁶⁵ Y. Chen, K.H. Chen, *J. Polym Sci. A*, **1997**, *35*, 613-624.
- ⁶⁶ L.A. Wells, M.A. Brook, H. Sheardown, *Macromol. Biosci.* **2011**, *11*, 988-998.
- ⁶⁷ G. Bergmann, P. O. Jackson, J. H. C. Hogg, T. Stirner, M. O'Neill, W. L. Duffy S. M. Kelly, G. F. Clark, *Appl. Phys. Lett.*, **2005**, *87*, 061914.
- ⁶⁸ J. Dai, J.C. Kim, *Korean J. Chem. Eng.*, **2012**, *29*, 323-328.
- ⁶⁹ J. Yamaguchi, J. Watanabe, M. Takai, K. Ishihara, *J. Appl. Polym. Sci.*, **2007**, *104*, 44-50.
- ⁷⁰ K.M. Gattás-Asfura, E. Weisman, F.M. Andreopoulos, M. Mimic, B. Muller, S. Sirpal, S.M. Pham, R.M. Leblanc, *Biomacromolecules*, **2005**, *6*, 1503-1509.
- ⁷¹ L. A. Estroff, A.D. Hamilton, *Chem. Rev.*, **2004**, *104*, 1201-1217.
- ⁷² M. Loos, B.L. Feringa, J.H. van Esch, *Eur. J. Org. Chem.* **2005**, 3615-3631.
- ⁷³ I. Tomatsu, K. Peng, A. Kros, *Adv. Drug Deliv. Rev.*, **2011**, *63*, 1257-1266.
- ⁷⁴ L. Frkanec, M. Jovic, J. Makarevic, K. Wolsperger, M. Zinic, *J. Am. Chem. Soc.*, **2002**, *124*, 9716-9717.
- ⁷⁵ Z.J. Qiu, H.T. Yu, J.B. Li, Y. Wang, Y. Zhang, *Chem. Commun.*, **2009**, 3342–3344.
- ⁷⁶ G.C. Kuang, Y. Ji, X.R. Jia, Y. Li, E.Q. Chen, Z.X. Zhang, Y. Wei, *Tetrahedron*, **2009**, *65*, 3496-3501.
- ⁷⁷ Pfeiffer, R. in *Photopolymerization Fundamentals and applications*; ACS: Washington D.C., 1997, vol 673
- ⁷⁸ P.G. Bahn, *Nature* **1992**, *356*, 109
- ⁷⁹ E. Reichmanis, J. Crivello, *Chem. Mater.* **2014**, *26*, 533-548.
- ⁸⁰ R. Phillips, *J. Photopolym.*, **1984**, *25*, 79-82.
- ⁸¹ B. Baroli, *J. Chem. Technol. Biotechnol.*, **2006**, *81*, 491–499.
- ⁸² K. Matyjaszewski, J. Spanswick, *Mater. Today*, **2005**, *8*, 26-33.
- ⁸³ M.C. Davies, J.V. Dawkins, D.J. Hourston, *Polymer*, **2005**, 1739-1753.
- ⁸⁴ W.L. Dilling, *Chem. Rev.*, **1983**, *83*, 1-47.
- ⁸⁵ V.A. Bhanu, K. Kishore, *Chem. Rev.*, **1991**, *91*, 99-117.
- ⁸⁶ O. Diels, K. Alder, *Ber. Dtsch. Chem. Ges.*, **1929**, *62*, 554-562.
- ⁸⁷ O. Diels, K. Alder, *Ber. Dtsch. Chem. Ges.*, **1929**, *62*, 2081-2087.
- ⁸⁸ O. Diels, K. Alder, *Liebigs Ann. Chem.*, **1928**, *460*, 98-122.
- ⁸⁹ O. Diels, K. Alder, *Liebigs Ann. Chem.*, **1929**, *470*, 62-103.
- ⁹⁰ S. Laschat, *Angew. Chem., Int. Ed.*, **1996**, *35*, 289-291.
- ⁹¹ S. Kotha, M. Meshram, A. Tiwari, *Chem. Soc. Rev.*, **2009**, *38*, 2065-2092.
- ⁹² K. Hanabusa, J. Tange, Y. Taguchi, T. Koyama, H. Shirai, *J. Chem. Soc. Commun.*, **1993**, 390.
- ⁹³ F. Fages, F. Vögtle, M. Žinic, *Top. Curr. Chem.* **2005**, *256*, 77-131
- ⁹⁴ S. Wawzonek, S.C. Wang, P. Lyons, *J. Org. Chem.*, **1950**, *15*, 593-599.
- ⁹⁵ J. Santamaria, R. Ouchabane, J. Rigaudy, *Tetrahedron Lett.*, **1989**, *30*, 3977-3980.
- ⁹⁶ A. Nakamura, Y. Inoue, *J. Am. Chem. Soc.* **2003**, *125*, 966-972.
- ⁹⁷ H. Dürr, H. Bouas-Laurent, *Photochromism: Molecules and Systems*, Gulf Professional Publishing, 12/03/2003
- ⁹⁸ R. Ghazy, S.A. Zim, M. Shaheen, F. El-Mekawey, *Opt. Laser Technol.*, **2004**, *36*, 463-469.
- ⁹⁹ G. Jones II, W.R. Jackson, C. Choi, *J. Phys. Chem.* **1985**, *89*, 294-300.
- ¹⁰⁰ S. Karthikeyan, V. Ramamurthy, *J. Org. Chem.* **2007**, *72*, 452-458.
- ¹⁰¹ D. Shimada, R. Kusaka, Y. Inokuchi, M. Ehara, T. Ebata, *Phys. Chem. Chem. Phys.*, **2012**, *14*, 8999-9005.
- ¹⁰² T. Hoyer, W. Tuszynski, C. Lineau, *Chem. Phys. Lett.*, **2007**, *443*, 107-112.
- ¹⁰³ J. Donovalova, M. Cigan, H. Stankovicova, J. Gaspar, M. Danko, A. Gaplovsky, P. Hrdlovic, *Molecules*, **2002**, *17*, 3259-3276.

- ¹⁰⁴ R.H. Abu-Eittah, B.A.H. El-Tawil, *Can. J. Chem.*, **1985**, *63*, 1173-1179.
- ¹⁰⁵ F.J. Giessibl, *Rev. Mod. Phys.*, **2003**, *75*, 949-1034.
- ¹⁰⁶ R.N. Jones, *Chem. Rev.*, **1947**, *41*, 353-371.
- ¹⁰⁷ K.J. Liu, W. Burlant, *J. Polym. Sci. A.*, **1967**, *5*, 1407-1413.
- ¹⁰⁸ P. Klemarczyk, *Polymer*, **2001**, *42*, 2837-2848.
- ¹⁰⁹ Y. Nishijima, G. Oster, *J. Polym. Sci.* **1956**, *19*, 337.
- ¹¹⁰ V.N. Kalashnikov, *J. Rheol.*, 1994, *38*, 1385-1403.
- ¹¹¹ S. Thomas, W. Yang, *Advances in Polymer Processing: From Macro- To Nano- Scales*. **2009**, Elsevier
- ¹¹² M.R. Kasaai, *Carbohydr. Polym.* **2007**, *68*, 477-488.
- ¹¹³ M.P. Vega, E.L. Lima, J.C. Pinto, *Polymer*, **2001**, *42*, 3909-3914.
- ¹¹⁴ A. Penlidis, D.C.H. Chien, *J. Macromol. Sci. Rev. Macromol. Chem. Phys.*, **1990**, *30*, 1-42.
- ¹¹⁵ O. Kammona, E.G. Chatzi, C. Kiparissides, *J. Macromol. Sci. Rev. Macromol. Chem. Phys.*, **1999**, *39*, 57-134.
- ¹¹⁶ S.R. Ponnuswam, S.L. Saha, *J. Appl. Polym. Sci.*, **1986**, *32*, 3239.
- ¹¹⁷ S.R. Ponnuswam, S.L. Saha, C. Kiparissides, *Ind. Engng. Chem. Res.*, **1987**, *26*, 229.
- ¹¹⁸ M. Zisenis, *Eur. Polym. J.*, **1997**, *33*, 773-780.
- ¹¹⁹ S.T. Handy, *Applications of Ionic Liquids in Science and Technology*, **2011**, Intech
- ¹²⁰ S. Gabriel, J. Weiner, *Chem. Ber.*, **1888**, *21*, 2669-2679.
- ¹²¹ Paul Walden (1914), *Bull. Acad. Sci. St. Petersburg*, pages 405-422.
- ¹²² H.L. Chum, V.R. Koch, L.L. Miller, R.A. Osteryoung, *J. Am. Chem. Soc.*, **1975**, *97*, 3264-3265.
- ¹²³ M. Freemantle, *Chem. Eng. News*, **1998**, *76*, 32.
- ¹²⁴ H. Olivier-Bourbigou, L. Magna, D. Morvan, *Appl. Catal. A.*, **2010**, *373*, 1-56.
- ¹²⁵ M. Freemantle, *Chem. Eng. News*, **2003**, *81*, 9.
- ¹²⁶ L.S. Ott, R.G. Finke, *Coord. Chem. Rev.*, **2007**, *251*, 1075.
- ¹²⁷ E. Redel, R. Thomann, C. Janiak, *Chem. Commun.*, **2008**, 1789.
- ¹²⁸ A. Berthod, J.A. Crank, K.I. Rundlett, D.W. Armstrong, *Rapid Commun. Mass Spectrom.*, **2009**, *23*, 3409-3422.
- ¹²⁹ M. Zabet-Moghaddam, E. Heinzle, A. Tholey, *Rapid Commun. Mass Spectrom.*, **2004**, *18*, 141-148.
- ¹³⁰ A.E. Somers, P.C. Howlett, D.R. MacFarlane, M. Forsyth, *Lubricants*, **2013**, *1*, 3-21.
- ¹³¹ H. Kondo, *Tribology Lett.*, **2008**, *31*, 211-218.
- ¹³² D. Monti, E. Jonsson, M.R. Palacin, P. Johansson, *J. Pow. Sour.* **2014**, *245*, 630-636.
- ¹³³ A. Deshpande, L. Kariyawasam, P. Dutta, S. Banerjee, *J. Phys. Chem. C*, **2013**, *117*, 25343-25351.
- ¹³⁴ G.B. Appetecchi, G.T. Kim, M. Montanino, F. Alessandrini, S. Passerini, *ECS Trans.*, **2008**, *11*, 119-129.
- ¹³⁵ M.A. Susan, T. Kaneko, A. Nosa, M. Watanabe, *J. Am. Chem. Soc.* **2005**, *127*, 4976-4983.
- ¹³⁶ M. Li, B. Yang, L. Wang, Y. Zhang, Z. Zhang, F. Fang, Z. Zhang, *J. Membr. Sci.*, **2013**, *447*, 222-227.
- ¹³⁷ D.V. Chernyshov, N.V. Shuedene, E.R. Antipova, I.V. Pletnev, *Anal. Chim. Acta*, **2008**, *621*, 178-184.
- ¹³⁸ K. Fujita, D.R. MacFarlane, M. Forsyth, *Chem. Commun.* **2005**, 4804-4806.
- ¹³⁹ S.N. Baker, T.M. McCleskey, S. Pandey, G.A. Baker, *Chem. Commun.* **2004**, 940-941.
- ¹⁴⁰ J. Zhang, J. Lei, Y. Liu, J. Zhao, H. Ju, *Biosens. Bioelectron.* **2009**, *24*, 1858-1863.
- ¹⁴¹ F. Benito-Lopez, S. Coyle, R. Byrne, C. O'Toole, C. Barry, D. Diamond, *Body Sensor Networks*, **2010**, 291-296.
- ¹⁴² F. Benito-Lopez, R. Byrne, A.M. Raduta, N.E. Vrana, G. McGuinness, D. Diamond, *Lab Chip*, **2010**, *10*, 195-201.
- ¹⁴³ R. Byrne, S. Coleman, K.J. Fraser, A. Raduta, D.R. MacFarlane, D. Diamond, *Phys. Chem. Chem. Phys.* **2009**, *11*, 7286-7291.
- ¹⁴⁴ A. Kavanagh, K.J. Fraser, R. Byrne, D. Diamond, *Appl. Mater. Interfaces*, **2013**, *5*, 55-62.
- ¹⁴⁵ A. Branco, L.C. Branco, F. Pina, *Chem. Commun.*, **2011**, *47*, 2300-2302.
- ¹⁴⁶ A. Branco, J. Belchior, L.C. Branco, F. Pina, *RSC Adv.*, **2013**, *3*, 25627-25630.
- ¹⁴⁷ Q. Zhang, S. Zhang, S. Liu, X. Ma, L. Lu, Y. Deng, *Analyst*, **2011**, *136*, 1302-1304.
- ¹⁴⁸ L.C. Branco, F. Pina, *Chem. Commun.*, **2009**, 6204-6206.
- ¹⁴⁹ S. Zhang, S. Liu, Q. Zhang, Y. Deng, *Chem. Commun.*, **2011**, *47*, 6641-6643.
- ¹⁵⁰ H. Tamura, Y. Shinohara, T. Arai, *Chem. Lett.*, **2010**, *39*, 240-241.
- ¹⁵¹ N. DiCesare, J. R. Lakowicz, *J. Phys. Chem. A* **2001**, *105*, 6834-6840.
- ¹⁵² A. Kvaran, Á.E. Konradsson, C. Evans, J.K.F. Geirsson, *J. Mol. Str.* **2000**, *553*, 79-90.
- ¹⁵³ V.W.W. Yam, J.K.W. Lee, C.C. Ko, N. Zhu, *J. Am. Chem. Soc.*, **2009**, *131*, 912-913.
- ¹⁵⁴ M.L. Salum, C.J. Robles, R. Erra-Balsells, *Org. Lett.*, **2010**, *12*, 4808-4811.
- ¹⁵⁵ S. Caccamese, R. Azzolina, *Chromatographia*, **1979**, *12*, 545.
- ¹⁵⁶ W.S. Wong, D. Guo, X.L. Wang, Z.Q. Yin, B. Xia, N. Li, *Plant Physiol. Biochem.* **2005**, *43*, 929.
- ¹⁵⁷ J. Jacquemin, P. Husson, A.A.H. Padua, V. Majer, *Green Chem.*, **2006**, *8*, 172-180.

- ¹⁵⁸ J.L. Anderson, D.W. Armstrong, *Anal. Chem.* **2003**, *75*, 4851-4858.
- ¹⁵⁹ Z. Mu, W. Liu, S. Zhang, F. Zhou, *Chem. Lett.* **2004**, *33*, 524-525.
- ¹⁶⁰ S.V. Dzyuba, R.A. Bartsch, *Chem. Phys. Chem.*, **2002**, *3*, 161-166.
- ¹⁶¹ B.K. Chen, M.J. Lianga, T.Y. Wu, H.P. Wang, *Fluid Phase Equil.* **2013**, *350*, 37-42.
- ¹⁶² S. Seki, T. Kobayashi, Y. Kobayashi, K. Takei, H. Miyashiro, K. Hayamizu, S. Tsuzuki, T. Mitsugi, Y. Umebayashi, *J. Mol. Liquids*, **2010**, *152*, 9-13.
- ¹⁶³ Z.B. Zhou, H. Matsumoto, K. Tatsumi, *Chem. Eur. J.* **2006**, *12*, 2196-2212.
- ¹⁶⁴ G.R. Yu, S.J. Zhang, G.H. Zhou, X.M. Liu, X.C. Chen *AIChE J.* **2007**, *53*, 3210-3221.
- ¹⁶⁵ M.L.P. Le, F. Alloin, P. Strobel, J.C. Lepretre, C.P. del Valle, P. Judeinstein, *J. Phys. Chem. B*, **2010**, *114*, 894-903
- ¹⁶⁶ G. Yu, L. Wen, D. Zhao, C. Asumana, X. Chen, *J. Mol. Liquids*, **2013**, *184*, 51-59.
- ¹⁶⁷ R.L. Gardas, Rile Ge, P. Goodrich, C. Hardacre, A. Hussain, D.W. Rooney, *J. Chem. Eng. Data* **2010**, *55*, 1505-1515
- ¹⁶⁸ M.T. Clough, K. Geyer, P.A. Hunt, J. Mertes, T. Welton *Phys. Chem. Chem. Phys.*, **2013**, *15*, 20480-20495.
- ¹⁶⁹ M. Herstedt, W.A. Henderson, M. Smirnov, L. Ducasse, L. Servant, D. Talaga, J.C. Lassegues, *J. Mol. Struct.* **2006**, *783*, 145-156.
- ¹⁷⁰ P. Johansson, S.P. Gejji, J. Tegenfeldt, J. Lindgren, *Electrochim. Acta*, **1998**, *43*, 1375.
- ¹⁷¹ M. Herstedt, M. Smirnov, P. Johansson, M. Chami, J. Grondin, L. Servant, J.C. Lassegues, *J. Raman Spectrosc.*, **2005**, *36*, 762.
- ¹⁷² S.E. Braslavsky, *Pure Appl. Chem.*, **2007**, *79*, 293-465.
- ¹⁷³ G. S. Hu, J.M. Jia, Y.S. Chung, J.H. Lee, D.J. Yun, W.S. Chung, G.H. Yi, T. H. Kim, D. H. Kim, *Mol. Biol. Rep.* **2011**, *38*, 3741-3750.
- ¹⁷⁴ M.B. Hocking, *Can. J. Chem.*, **1969**, *47*, 4567-4576.
- ¹⁷⁵ J. Ahmed, J.X. Zhang, Z. Song, S.K. Varshney, *J. Therm. Anal. Calorim.*, **2009**, *95*, 957-964.
- ¹⁷⁶ K. Inoue, S. Hoshino, *J. Polym. Sci., Part B: Polym. Phys.*, 1984, *22*, 1969-1977.
- ¹⁷⁷ F. Serra, E.M. Terentjev, *Macromol.* **2008**, *41*, 981-986.
- ¹⁷⁸ D. Hadzi, *J. Chem Soc* **1956**, 2143
- ¹⁷⁹ H.J. Castejón, T.J. Wynn, Z.M. Marcin, *J. Phys. Chem. B*, **2014**, *118*, 3661-3668.
- ¹⁸⁰ J.A. Smith, G.B. Webber, G.G. Warr, R. Atkin, *J. Phys. Chem. B*, **2013**, *117*, 13930-13935.
- ¹⁸¹ S.N. Butler, F. Müller-Plathe, *J. Mol. Liquids*, **2013**, *192*, 114-117.
- ¹⁸² G.L. Burrell, N.F. Dunlop, F. Separovic, *Soft Matter*, **2010**, *6*, 2080-2086.
- ¹⁸³ T. Verbiest, L. Derhaeg, E. Kelderman, J.F.J. Engbersen, W. Verboom, D.N. Reinhoudt, K. Clays, A. Persoons, In: *Organic Materials for non-linear optics III*. Royal Society of Chemistry, Cambridge, 326-331.
- ¹⁸⁴ P. Kaatz, D.P. Shelton, *Mol. Phys.* **1996**, *88*, 683-691.
- ¹⁸⁵ V. Rodriguez, *J. Raman Spectrosc.* **2012**, *43*, 627-636.
- ¹⁸⁶ F. Castet, E. Bogdan, A. Plaquet, L. Ducasse, B. Champagne, V. Rodriguez, *J. Chem. Phys.* **2012**, *136*, 024506
- ¹⁸⁷ V. Rodriguez, J. Grondin, F. Adamietz, Y. Danten, *J. Phys. Chem. B*, **2010**, *114*, 15057-15065.
- ¹⁸⁸ N. Kus, S. Breda, I. Reva, E. Tasal, C. Ogretir, R. Fausto, *Photochem. Photobiol.*, **2007**, *83*, 1237-1253.
- ¹⁸⁹ T. Yatsushashi, N. Nakashima, *J. Phys. Chem. A*, **2000**, *104*, 1095-1099.
- ¹⁹⁰ N.N. López-Castillo, A.D. Rojas-Rodriguez, B.M. Porta, M.J. Cruz-Gomez, *Adv. Chem. Eng. Sci.* **2013**, *3*, 195-201
- ¹⁹¹ a) R.S. Koefo, K.R. Mann, *Inorg. Chem.* **1989**, *28*, 2285; b) A.R. Jagtap, V.S. Satam, R.N. Rajule, V.R. Kanetkar, *Dyes Pigm.* **2009**, *82*, 84.
- ¹⁹² a) C.H. Chang, H.C. Cheng, Y.J. Lu, K.C. Tien, H.W. Lin, C.L. Lin, C.J. Yang; C.C. Wu, *Org. Electron.* **2010**, *11*, 247; b) T.Z. Yu, P. Zhang, Y.L. Zhao, H. Zhang, J. Meng, D.W. Fan, *Org. Electron.* **2009**, *10*, 653.
- ¹⁹³ a) A. Dorlars, C.W. Schellhammer, J. Schroeder, *Angew. Chem., Int. Ed. Engl.* **1975**, *14*, 665; b) S.S. Keskin, N. Aslan, N. Bayrakceken, *Spectrochim. Acta, Part A* **2009**, *72*, 254; c) J. Kido, Y. Iizumi, *Appl. Phys. Lett.* **1998**, *73*, 2721.
- ¹⁹⁴ a) C.R. Moylan, *J. Phys. Chem.*, **1994**, *98*, 13513; b) A. Painelli, F. Terenziani, *Synth. Met.* **2001**, *124*, 171.
- ¹⁹⁵ J.H. Kim, H.J. Kim, S.H. Kim, J.H. Lee, J.H. Do, H.J. Kim, *Tetrahedron Lett.* **2009**, *50*, 5958
- ¹⁹⁶ R.L. Sheng, P.F. Wang, Y.H. Gao, Y. Wu, W.M. Liu, J.J. Ma, H.P. Li, S.K. Wu, *Org. Lett.*, **2008**, *10*, 5015
- ¹⁹⁷ W.Y. Lin, L. Yuan, X.W. Cao, W. Tan, Y.M. Feng, *Eur. J. Org. Chem.* **2008**, 4981
- ¹⁹⁸ J.R.S. Hoult, M. Paya, *Gen. Pharmacol.*, **1996**, *27*, 713.
- ¹⁹⁹ I. Kostova, *Curr. Med. Chem.*, **2005**, *5*, 29.
- ²⁰⁰ R. Dayam, R. Gundla, L.Q. Al-Mawsawi, N. Neamati, *Med. Res. Rev.*, **2008**, *28*, 118.
- ²⁰¹ P.T. Thuong, T.M. Hung, T.M. Ngoc, D.T. Ha, B.S. Min, S.J. Kwack, T.S. Kang, J.S. Choi, K. Bae, *Phytother. Res.* **2010**, *24*, 101.
- ²⁰² X.W. Chen, J.W. Liu, J.H. Wang, *J. Phys. Chem. B*, **2011**, *115*, 1524

-
- ²⁰³ C.Ranjitha, K.K. Vijayana, V.K. Praveena, N.S.S. Kumar, *Spectrochimica Acta Part A*, **2010**, 75, 1610–1616;
M. Kaholek, P. Hrdlovic, *J. Photochem. Photobiol. A*, **1997**, 108, 283-288.
- ²⁰⁴ J.N. Moorthy, P. Venkatakrishnan, G. Savitha, R.G. Weiss, *Photochem. Photobiol. Sci.* **2006**, 5, 903
- ²⁰⁵ M. Suresh, A. Das, *Tetrahedron Lett.* **2009**, 50, 5808.
- ²⁰⁶ B. Valeur, I. Leray, *Coord. Chem. Rev.*, **2000**, 205, 3.
- ²⁰⁷ J. Del Nero, C. P. De Melo, *Int. J. Quantum Chem.*, **2003**, 95, 213-218.
- ²⁰⁸ J.M. Smith, J.L. Knee, *Laser Chem.*, **1994**, 14, 131-141.
- ²⁰⁹ D.B.G. Williams, M. Lawton, *J. Org. Chem.* **2010**, 75, 8351-8354.
- ²¹⁰ I.L. Arbela, *J. Photochem.* **1980**, 14, 97-105.
- ²¹¹ A.T.R. Williams, S.A. Winfield, J.N. Miller, *Analyst*, **1983**, 108, 1067-1071.
- ²¹² G. Striker, V. Subramaniam, C.A.M. Seidel, A. Volkmer, *J. Phys. Chem.* **1999**, 103, 8612-8617